UNIVERSIDAD COMPLUTENSE DE MADRID

FACULTAD DE CIENCIAS QUÍMICAS
DEPARTAMENTO DE QUÍMICA FÍSICA I

TESIS DOCTORAL

Simulación y control de la dinámica electrónica y nuclear con pulsos láser intensos y ultracortos

Simulation and control of electron and nuclear dynamics with strong and ultrashort laser pulses

MEMORIA PARA OPTAR AL GRADO DE DOCTORA

PRESENTADA POR

Patricia Vindel Zandbergen

DIRECTOR

Ignacio Solá Reija

Madrid, 2017

UNIVERSIDAD COMPLUTENSE DE MADRID
FACULTAD DE CIENCIAS QUÍMICAS
DEPARTAMENTO DE QUÍMICA FÍSICA I

Simulación y control de la dinámica electrónica y nuclear con pulsos láser intensos y ultracortos

Simulation and control of electron and nuclear dynamics with strong and ultrashort laser pulses

Memoria presentada por
Patricia Vindel Zandbergen

para optar al grado de
Doctor en Ciencias Químicas

Director:
Dr. Ignacio Solá Reija

Madrid, Septiembre de 2016

Contents

List of Figures

Resumen

Comprender la estructura y la dinámica de los procesos químicos a nivel molecular es un paso clave para el diseño de materiales con propiedades deseadas o para el control de las reacciones químicas. Desde los inicios de la mecánica cuática, el control de los fénomenos cuánticos ha sido uno de los principales objetivos en el campo de la física y la química. El desarrollo de los láseres ultrarrápidos y ultraintensos ha permitido el uso de pulsos externos, no sólo para seguir el movimiento nuclear y electrónico [1–3], sino también para controlarlo de forma activa, es decir, manipular la dinámica molecular en la escala de tiempos en la que ocurren los procesos físicos y químicos, así como resolver las ecuaciones dinámicas que los gobiernan, de forma que pueda favorecerse un tipo de proceso en particular [4]. De esta forma, el campo de Control Cuántico (o coherente) se ha desarrollado conjuntamente con la Femtoquímica y la Attofísica.

Las primeras propuestas de control surgieron independientemente con dos escenarios. Por un lado, Tannor y Rice propusieron un mecanismo de control en la variable temporal: el esquema pump-dump [5, 6], que es un precursor de lo que se llamaría control óptimo. Por otro lado, Brumer y Shapiro [7,8] propusieron un esquema de control coherente o resuelto en frecuencias. Sin embargo, estos esquemas sólo permiten el control de forma eficiente cuando se conocen el Hamiltoniano molecular y las superficies de energía potencial. Por ejemplo, en el esquema de Brumer y Shapiro, el mismo estado intermedio puede dar lugar a diferentes productos de reacción. En el esquema pump-dump, sólo es posible el control de transiciones verticales (ventana Frank-Condon) entre estados

electrónicos. Resolviendo este problema, se formularon esquemas que permitían controlar la dinámica del paquete de ondas en cada potencial. Utilizando la teoría matemática de control óptimo, Rabitz y colaboradores [9] (e independientemente Kosloff y col. [10]) generalizaron la búsqueda del esquema apropiado para manipular la dinámica del sistema como un problema de cálculo de variaciones, donde la incógnita es el pulso óptimo que se quiere obtener, mientras que la dinámica del sistema se describe mediante de la ecuación de Schrödinger dependiente del tiempo. Esta generalización trasladó el problema a términos matemáticos, y los siguientes desarrollos se centraron en la búsqueda de métodos numéricos que solucionasen de la manera más eficaz la ecuación de Euler-Schrödinger correspondiente.

En esta tesis se emplea la Teoría de Control Local (LCT) [11, 12]. La idea de esta teoría apareció inicialmente en la formulación de la Teoría de Control Óptimo Cuántica [10]. Básicamente, consiste en elegir un campo láser de control de forma que se consiga un incremento o disminución del valor medio de un observable ($< x >$,$< H >$) durante un cierto intervalo de tiempo en el que actúa el campo externo. De esta forma, las metodologías empleadas son más simples comparadas con aquelas utilizadas en control óptimo.

El objetivo de la presente tesis es la simulación de la dinámica de moléculas excitadas por pulsos láseres intensos y ultracortos, en la escala de femto y attosegundos, y el control de distintos procesos moleculares como ionización, disociación, interferencia, transferencia eléctronica, estado de espín, propiciados por la preparación de estados electrónicos en superposición cuántica bajo el campo láser. Estudiando dichos procesos, se exploran las limitaciones del control de la dinámica electrónica y los efectos de la interacción entre los movimientos nucleares y electrónicos.

En este trabajo se combinan técnicas de control cuántico y los procesos de femto y attofísica, simulados mediante solución de la ecuación de Schrödinger dependiente del tiempo por métodos de propagación en malla (grid-based methods). Se emplean modelos de potencial muy simplificados (y generales) que nos permiten comprender cualitativamente la naturaleza de los procesos, su posible control y la validez de las aproximaciones más habituales (Born-Oppenheimer, único electrón activo, etc.). Pretendemos predecir qué capacidad de control existe en procesos de attofísica (ionización, disociación, alteración de las propiedades electrónicas) cuando las técnicas de modulación de pulsos puedan extenderse al dominio de attosegundo, de manera que esta investigación pueda servir de estímulo a su desarrollo incipiente. Dado que la tecnología aún no está disponible, y por tanto sus alcances o limitaciones no se conocen con precisión, nos centramos en modelos generales para intentar responder a cuestiones como las siguientes:

¿cómo afectan los procesos ionizantes con láseres de baja frecuencia en el rendimiento de muchos métodos de control?, ¿cómo pueden evitarse?, ¿es posible controlar la transferencia espín-órbita?, ¿pueden un láser conducir electrones entre átomos distantes?

En anteriores trabajos del grupo de investigación se propusieron diversas estrategias para controlar la transición espín-órbita mediante pulsos fuertes no resonantes. En esta tesis se comprueban los límites de validez de dichos esquemas y la búsqueda de posibles correcciones, incorporando efectos que no se observan en la aproximación Born-Oppenheimer. Utilizando una extensión del modelo de potencial de Shin y Metiu se describe la dinámica electrónica (los efectos de ionización y la violación de la aproximación Born-Oppenheimer). También, se pretenden controlar procesos que implican transiciones reversibles entre estados ligados y estados ionizantes (del continuo). Esto es, queremos maximizar la probabilidad de que los electrones, cuando son excitados al continuo, se vuelvan a atrapar al volver al núcleo, cuando la fase del pulso cambia.

En los primeros trabajos de esta tesis, se pretende manipular las transiciones singlete-triplete en cadenas de iones utilizando una extensión del modelo de potencial de Shin-Metiu (modelo SME) [13,14]. Mediante este modelo, es posible caracterizar simultáneamente el movimiento nuclear y electrónico acoplados. El acoplamiento espín-órbta se introduce de un modo heurístico de forma que puedan producirse transiciones entre los componentes singlete-triplete de la función de onda. Para controlar la dinámica del sistema se emplea el efecto Stark Dinámico No Resonante [15]. Este mecanismo se basa en la utilizaión de campos intensos que cambian el espectro de energías de los estados singlete y triplete de manera independiente. Así, simplemente variando la intensidad y frecuencia del campo láser, es posible encontrar los parametros óptimos que nos permiten controlar con éxito la evolución del sistema y poder evitar o inducir una transición de espín.

Inicialmente, se consiguió el desacoplamiento de la transición singlete-triplete en el límite adiabático (incluyendo diferentes grupos de estados singlete y triplete) y en el modelo completo de potencial de Shin-Metiu (dinámica de paquetes de onda vibrónicos). En ausencia de un pulso láser se produce la transferencia completa de población en ambos casos. Sin embargo, bajo el efecto de un campo láser intenso no resonante, se varía la energía de los estados electrónicos y se consigue mantener de forma eficiente la población en los estados singlete. Cuando se consideran todos los estados electrónicos en el modelo (dinámica en 3 dimensiones), se logra igualmente evitar la transferencia a los estados triplete, aunque aumenta la dispersión de la población entre los diferentes estados singlete, siendo la absorción multifotónica el efecto predominante, dando lugar a la ionización completa del sistema. En este trabajo, también variamos diferentes parámetros del pulso láser, empleando la aproximación de Born-Oppenheimer en el

modelo SME para elegir los valores óptimos con los que obtuvimos los mejores resultados, evitando la transferencia de población entre estados singlete y triplete. Finalmente, se estudió la relación entre el acoplamiento de espín y el grado de ionización en un modelo analítico de Hamiltoniano de dos estados, para identificar bajo qué condiciones se consigue un control eficiente de las transiciones espín-órbita.

En la segunda parte de resultados, se simula y controla la transferencia de un electrón en la escala de femto y attosegundos mediante pulsos láser intensos, haciendo uso de la Teoría de Control Local. Para describir nuestro sistema (las moléculas H_2^+ y HeH^{2+}), se utiliza el potencial soft-core de Coulomb. Trabajando bajo la aproximación de Born-Oppenheimer, nuestro objetivo era excitar el electrón inicialmente localizado en uno de los núcleos para, a continuación, atraparlo en el otro átomo. Se emplearon dos formulaciones distintas de la Teoría de Control Local. En la primera, el campo láser es proporcional al valor medio del momento del electrón y el objetivo es disminuir la energía del sistema. En el segundo caso, el láser depende de la proyección de la función de onda sobre un estado objetivo (el autoestado de menor energía del núcleo objetivo). El mecanismo por el que ocurre la transferencia del electrón es distinto según la escala de tiempos en la que ésta tiene lugar. En la escala de femtosegundos, la energía del electrón nunca supera la barrera interna entre los núcleos, por lo que la transferencia ocurre por túnel, mientras que en la escala de attosegundos, se observa un mecanismo impulsivo, es decir, el electrón es excitado al continuo y, a contrinuación, es reatrapado en el núcleo objetivo. Además, comprobamos la validez de los resultados obtenidos considerando los núcleos fijos, y cómo la energía cinética inicial influye en la transferencia electrónica al aplicar los pulsos láser encontrados en los cálculos 1D en una simulación completa 2D (1+1D).

En definitiva, el trabajo realizado en esta tesis aúna dos campos de investigación actualmente en auge, el Control Cuántico y los procesos ultrarrápidos (escala de femto y attosegundos). Podemos concluir que, mediante la aplicación de diferentes métodos de control a varios procesos físicos relevantes, se ha conseguido influir de forma satisfactoria sobre la dinámica nuclear y electrónica en diversos sistemas.

Introduction

Introduction

Understanding the structure and dynamics of chemical processes at the molecular level is a key step toward the design of materials with the desired properties, or the efficient control of chemical reactions. Many subtleties involving basic quantum properties, such as superposition of states and interfering pathways allow to highly increase the yield of a specific process, far beyond what the probability distribution would suggest, should it follow the classical rules of motion. The spectra of molecules is one of the strongest evidence of this phenomena. Rather than distributing its energy in a continuous way along the molecule, one can find resonances that relate to particular structures. The playground of quantum dynamics offers more spectacular predictions. Using the quantum correlations at our advantage, one can externally drive a molecule toward selecting specific states or chemical processes from the huge pool of competing processes that are energetically available.

Much of the history of the probe and control of chemical processes has come side-by-side with the development of lasers. As we will see, one can arguably relate this history as a process. The laser was first used as a tool to ignite and selectively probe specific states and processes given its fine-tunability and intensity. With ultrashort laser pulses came the first probe and control of the dynamics. Pulse shaping then allowed to promote the laser to the role of a chemical agent, using Rabitz's terminology [16]. Finally, the use of very strong non-resonant pulses is promoting the laser to the role of a catalyst. Obviously, all the different roles are still being enacted by the laser depending on the particular use we need. We will now review in more detail what particular features of lasers are mainly used and how they were developed in order to fullfil the different roles of igniting, probing, "reacting" with molecules, and "catalyzing" chemical processes.

In this thesis we are mainly interested in the nuclear and electronic motion that are

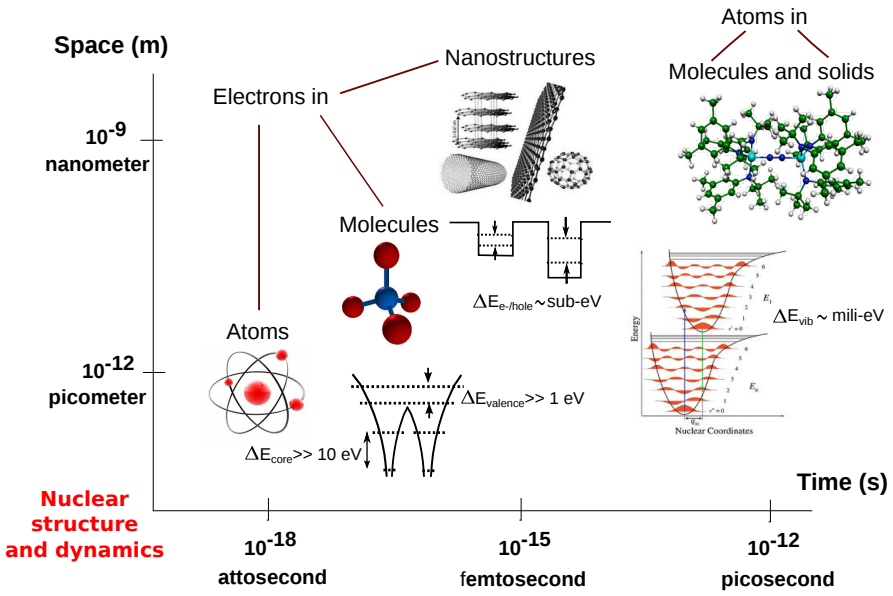

Figure 1: Characteristic length and time scales for structure and dynamics in the microcosm, respectively [17]

fundamental steps underlying most chemical processes. The control of these processes, however, often requires manipulating the systems in the time-scale where they occur. The phenomena that give rise to the formation of new materials and chemical and biological transformations consist of elementary physical steps that occur on the femtosecond (1 fs= 10^{-15} s), or in the sub-femtosecond (attosecond, 1 as = $10^{-}18$ s), timescale (fig. 1). One can easily predict why we need to delve into such ultrashort limits. Regarding the formation and breaking of chemical bonds, they occur in the timescale of the vibrational period of a molecule. As the spacing of vibrational energy levels is in the sub-electronvolt scale ($\sim$ 0.1 eV), it implies that molecular vibrations correspond to the femtosecond domain. This is consistent with the fact that atoms at thermal velocities ($\sim$ 1000 m/s) travel the distance over which a chemical bond changes character (1 Åor $\sim 10^{-10}$ m) in approximately 100 fs. On the other hand, if we consider the electronic motion inside atoms, the typical timescale is the atomic unit of time (1 au = 0.024 fs = 24 as). A simple calculation shows that the characteristic transition period from the ground state (1s) to the first excited state (2p) of hydrogen is $T = 2\pi/\omega_{1s-2p} = 24$ attoseconds. The electron dynamics on the molecular scale is behind the emission of ultraviolet and x-ray radiation. All the processes that we will describe on this thesis involve the ultrafast motion of electrons or nuclei, so how can we observe the molecular

dynamics in real time and moreover, would it be even possible to influence and control the incredibly quick phenomena that occur at the atomic scale?

Ultrafast spectroscopy

In the past few decades, the increasingly shorter (in time) light sources and faster detection schemes, have lead to constant improvement in the temporal resolution of chemical and biological processes. In the 1980s the experimental advances in spectroscopy culminated in the birth of a new scientific field called *Femtosecond Chemistry* or *Femtochemistry* [18–21]. The first great success of Femtochemistry (deserving the Nobel Prize of Ahmed Zewail in 1999) [1], was the use of a pair of femtosecond pulses (a pump and probe pulses) to resolve the nuclear dynamics. In the femtosecond laser experiments, the pump pulse either initiates a chemical reaction or creates a non-stationary state. Due to the broad spectrum of the femtosecond pulse, several vibrational levels from that particular state are coherently excited. This coherent superposition is also known as a *wave packet*. The propagation of the wave packet corresponds to the movement of the nuclei. An oscillation is described by the periodical (classical) motion of the wave packet back and forth in the molecular potential well. The probe pulse then is shot at a series of well-timed intervals after the pump pulse excited the molecule and is chosen to generate an observable that will provide information about the evolution of the system. This pulse allows us to "freeze" the nuclear motion with the necessary spatial resolution, owing to the localized nature of the wave packet. The next question is: could we go further and observe and control in real time the electron dynamics on the atomic scale? Electrons played an important role in the scientific and technological revolution of the 20th century [22], such as superconductivity, particle accelerators, electron microscopes, magnetism, nanostructures, quantum information... However, the insight and influence into the electron motion at the atomic scale is still a challenge for the future.

More recently, further advances in laser technology allowed the production of ultrastrong radiation fields with frequencies in the XUV regime, paving the way to the development of a new scientific domain, called *Attosecond Physics*. These sub-femtosecond (hence attosecond) pulses are so short that in principle, ionization or Auger processes can be resolved in real time [2,23]. The studies can then again give input to the control of chemical processes, because in chemical reactions the nuclei move in a potential surface set by the electrons, the attosecond electron dynamics indirectly governs the nuclear dynamics. The most important idea behind the technique is a sort of two-step procedure: first to ignite the dynamics by means of UV (or XUV) or IR ultrashort pulses or even a

combination of both; then to "probe" the electronic motion, and the effect induced on it by the molecular structure, using ultrashort ionization [24]. In the case of very strong fields, the recollision of the ionized electron with the parent molecular ion can occur, leading to high harmonic generation, which was also shown to be a interferometric way of probing the structure. The pursuit of attosecond pulses dates back to 1979 when Agostini *et al.* discovered the above threshold ionization (ATI) [25], a process in which the electron could absorb more photons than the minimum required for ionization after its ejection from an atom. A typical ATI photo-electron energy spectrum consists of several peaks, separated by the photon energy $\hbar\omega$. Shortly after, in the late 1980s researchers discovered high-harmonic generation (HHG) in noble gases [26–28]: the conversion of a near-infared (NIR) field into extreme ultraviolet (XUV) radiation. The HHG spectrum consists of discrete peaks located at odd integer multiples of the fundamental NIR harmonic frequency. The spectrum initially falls off with energy, but then remains constant, forming a plateau which ends at an energy of about $I_p + 3.17U_p$ [29, 30], I_p being the ionization energy of the gas-phase medium and U_p the ponderomotive energy. This is a clear signature of non-perturbative effects, which scale at powers of the intensity. The physical mechanism of HHG is explained by a three-step semi-classical model, where the electron is first ionized by tunneling from the atom,then accelerated in the laser field back towards the parent ion, and finally recaptured by the core [31, 32]. The most intriguing property of the HHG process, however, is its ultrashort, sub-laser-cycle time scale. The continuum electron is in fact a wave packet of attosecond duration. Since the three-step process is repeated in each half-cycle of the driving laser field, the XUV pulses produced by HHG with femtosecond laser pulses consequently have features both on the femtosecond and the attosecond time scales. On the femtosecond scale, they are conveniently described as high-order harmonics of the fundamental driving laser frequency, while on the attosecond scale, the picture of a recolliding electron wave-packet, emitting a short burst of XUV light every half-cycle of the driving field, is more appropriate. The short duration of the XUV pulses is not only interesting for time resolved studies, but it also concentrates the pulse energy in an extremely short time, allowing to combine high photon energies with high peak intensities, hardly available otherwise. The temporal characterization of attosecond pulse trains, techniques such as frequency resolved optical gating (FROG) [33, 34] and reconstruction of attosecond beating by interference of two photon transitions (RABITT) [35, 36] were proposed. This latter technique proved useful not only to characterize high harmonic radiation, but also to study the electron dynamics.

Along with the birth of attosecond pulses came many novel technologies and appli-

cations. Initially, the use of attosecond pulses focused on the generation of attosecond electron wave packets for real time observation of tunneling [37] or the interference of wave packets using attosecond trains [38]. In addition, these ultrafast pulses have been used for obtaining ionization widths [39], for imaging molecular orbitals [40] or to achieve electron localization in simple molecules [41]. Attosecond techniques have been also applied in the field of ultrafast solid-state physics (condensed phase) [42, 43], and they have already been used to control the collective electron motion in plasmas [44] and in protein crystallography by so called "diffraction before destruction" techniques [45, 46]. Recently, by using attosecond pulse trains it has been possible to control the photoionization in small molecules such as D_2 and H_2 [47, 48] or the outcome of a simple chemical reaction [49]. Moreover, although the study of more complex molecules is challenging, the direct measurement of the change of the electronic structure in an amino-acid, initiated by attosecond pulses, has been achieved [50].

Quantum Dynamics and Quantum Control

Accompanying these advances, the theoretical calculations and computer simulations have the advantage to overcome experimental restrictions and have access to the whole dynamics, allowing further insight and also providing new ideas in designing future experiments. The advances have occurred both in concepts and methodology. Both Femtochemistry and Attophysics have greatly benefited from the different efforts put into solving the time dependent Schrödinger equation (TDSE). Although early attempts remount to the sixties [51, 52], the development of grid-based methods by R. Kosloff and coworkers, and M. D. Feit and J. A. Fleck in the mid eighties [6, 53], allowed to simulate the essential steps in the time-evolution of nuclear wave packets, illuminating the first experimental results of Zewail [54–56]. Although the simulation of electronic processes adds more difficulties, owing to the divergence of the Coulomb potential and the high increase in dimensionality even for the smallest molecules, it is interesting to observe that the first applications to understand attophysical processes, ionization and high-harmonic generations, were already explored in the 80s [57, 58].

The attempt to control quantum phenomena has been an implicit goal in physics and chemistry since the early days of quantum mechanics [59, 60]. The development of the ultrafast science allowed the use of external pulses not only to detect nuclear and electron motion, but also to control it actively: to manipulate the molecular dynamics in its proper time scale in order to enhance a particular process. This was the birth of the field of *Quantum (or coherent) control* [4]. Recent years have witnessed the rapid

development of this new field [16, 61–65], in which the coherence properties of applied laser fields and/or matter are employed to steer a given quantum dynamical process in a desired direction.

Many of the theoretical basis of the field were established in the process of designing effective strategies to use lasers to actively manipulate chemical reactions at the single-molecule level. Nowadays, a growing number of theoretical and experimental studies have reported laser control of molecular dynamics and other physical processes. Furthermore, the fundamental ideas of coherent control are pervading into different branches of science (quantum optics, quantum information...) and are expected to foster substantial developments.

Quantum Control deals with the manipulation of the Hamiltonian dynamics by exerting an external action on the system. The operation is necessarily unitary in the framework of coherent control. Thus one gets a modified, appropriately called controlled time-evolution of the system dynamics which helps steer the system in the desired pathway towards some predetermined goal with high selectivity and high efficiency. Then, provided that the coherence of the laser and of matter is preserved in each quantum pathway, interference effects are expected in the final state wave function and exploited to produce the control. Properly, quantum control is always about selecting or enhancing a particular molecular processes from the set of all possible outcomes through constructive or destructive quantum interference effects. Based on this principle, and closely related ideas, several basic control scenarios have been proposed.

But control with light requires control of the light itself. An ultrashort pulse has a shape, a temporal phase and a polarization state and all of them need to be controlled and measured accurately. Several methods have been used to shape femtosecond pulses. Most of these techniques involve devices such as liquid-crystal spatial light modulators, acousto-optic modulators, or deformable mirrors, that are designed to modulate the phase and/or amplitude of the dispersed spectral components of a femtosecond pulse [59, 66, 67]. It is routinely possible to generate user-defined waveforms for coherent control with these pulse shapers and characterize them using a variety of ultrafast measuring techniques.

In addition to the technological advances, it is of utmost importance to have powerful theoretical methods available. Theoretically, there are three big questions related to the control problem. The first one is that of *controllability* [68] or in other words, if indeed there exists a "controller" (e.g. laser field), that brings the quantum system (e.g. molecule) from an initial state, to a given target state (a certain reaction product) exactly or differentially close. The second question concerns the problem of finding the

best way to achieve a given control objective, e.g., calculating the optimal laser pulse for breaking a particular bond in a molecule or to induce population transfer to a particular quantum state. This problem is called the *Quantum Optimal Control* problem and the algorithms necessary to solve it are called quantumoptimal control algorithms. The third one involves the properties of the space of all possible solutions, that is, how many different solutions exist and their properties, what are the main control knobs in the laser field, what are the characteristics of the dynamics, etc. These questions are very dependent on the Hamiltonian and the optimal field. This is called the *Landscape* or *Quantum Control Landscape* problem.

Quantum Control schemes

One can classify the Quantum Control schemes according to those that operate under an iterative scheme, and those that do not. Within the latter ones, Tannor, Kosloff and Rice introduced in the 1980s a method for selective control in a photo-induced reaction based on the precise timing between sequential pulses of an applied electric field to guide the temporal evolution of a wave packet [5, 6]. This scheme is known as *pump-dump* or *Tannor-Rice* control scheme. The model system is best visualized using two electronic surfaces of a linear triatomic molecule: a model ABC molecule, with a stable configuration in its ground state and two possible fragmentation channels on the ground state potential energy surface: AB+C and A+BC (two dissociative reaction pathways), see fig. 2 (a). The control problem reduces itself to finding the time dependent electric field, which starting from the initial state (ground state, $v = 0$) sends the wave packet to the desired channel.

This control mechanism will be discussed in terms of a two-level model system. The first laser pulse, the pump pulse, transfers population from the ground state to the excited electronic state ($ABC^{\ddagger}$), where the wave function is no longer a stationary state. Thus the wave packet moves along the excited state surface and its shape changes because of dephasing. At some time after the excitation, there will be more wave packet amplitude over the ABC $\rightarrow$ AB + C channel. A second ultrashort laser pulse is used to dump the wave packet from the excited state to the ground state, whereby mostly AB + C are formed. At some other time after excitation, there might be more amplitude over the ABC$\rightarrow$ A + BC channel; then the dump pulse will form predominantly A + BC products. Hence the selectivity in the product formation is achieved by the different transfer of wave packet amplitudes into one of the two channels of the ground state. The scheme relies on the Ehrenfest theorem by associating the wave packet dynamics

with classical trajectories [69]. The time delay Δt between the two pulses is the time in which the wave packet propagates on the excited state potential surface and represents the "control knob".

The Tannor-Rice control scheme has been demonstrated experimentally on the Na_2 molecule in which the branching ratio of $Na^+ + Na$ to Na_2^+ was modified [70], as well as in the K_2 dimer, to induce efficient population transfer to a predefined electronic state [71]. Zewail's group also applied the concept to the reaction $Xe+I_2 \rightarrow XeI + I$ where an extra pump pulse was applied instead of a dump pulse, in a pump-pump approach [72]. The pump-dump control scheme is an appropriate method for increasing the selectivity of a chemical reaction by employing specially designed laser pulses [5]. The optimal form of the dump-pulse was calculated as a convolution of the pump pulse with the molecular dynamics on the excited state.

Another extension of the Tannor-Rice control method is a pump-pump via an infrared (IR) and an ultraviolet (UV) laser pulses. This scheme has been applied to control selective dissociation of several systems, including the symmetric ozone molecule [73], the symmetric FHF^- molecule [74], and extended to asymmetric molecules HOD [75] and OHF^- [76].

A year after the Tannor-Rice method was introduced, Brumer and Shapiro elaborated on a scheme based on phase control, where the coherence of a laser field is exploited to control population transfer as well as the branching ratio for dissociation of small molecules [61]. The original scheme showed that the variation of the relative phase between two phase-locked CW lasers with different frequencies opened two pathways to a final state allowing the control of reaction yields [7,8,78]. The two independent pathways can be two different dissociative final states which can be resonantly excited by one or three photons (or two and four, respectively) of the same total energy: $E = \hbar\omega_1 = 3\hbar\omega_3$ (or $E = 2\hbar\omega_2 = 4\hbar\omega_4$). One laser field is resonant with the transition between the ground state ψ_g and the final electronic state ψ_f, with a frequency ω_1; the other has a frequency ω_3, such that $\omega_1 = 3\omega_3$, induces a multiphoton transition [see fig. 2 (b)]. The application of these two lasers leads to an interference term in the quantum mechanical description of the probability amplitudes of the wave function. By changing the relative phase between the two lasers ϕ, constructive or destructive interferences between the two possible pathways occur, thereby controlling the branching ratio of different products. The principle of this method is similar to a diffraction pattern observed in a double-slit experiment, where the diffraction pattern originating from two waves which interfere after crossing the two slits is measured. This theoretical scheme was experimentally verified by Gordon and co-workers in small molecules such as HCl, HI, DI, H_2S or

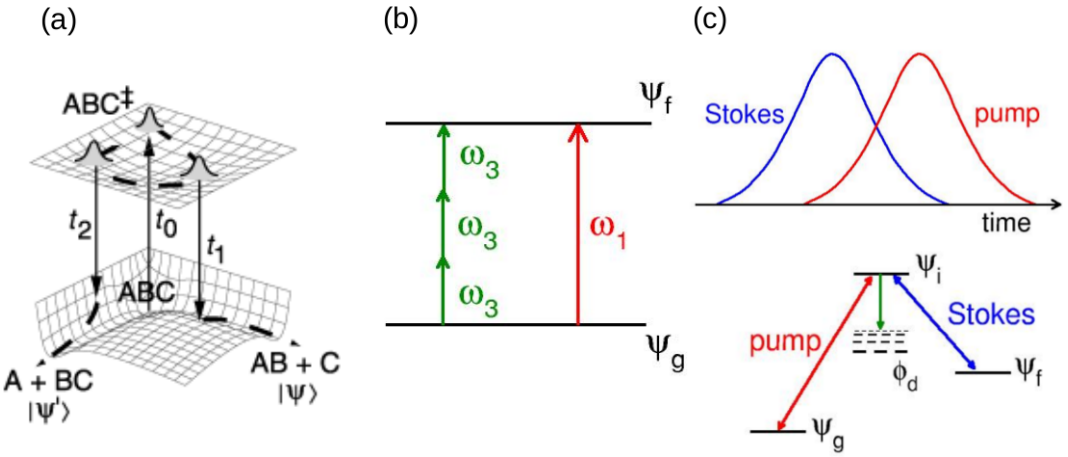

Figure 2: (a) The Tannor-Kosloff-Rice scheme uses an ultrashort laser pulse to initiate coherent wavepacket motion on an electronically excited state potential energy surface. After a suitable time delay, the population is dumped back to the ground state into the desired dissociation channel. (b) The Brumer-Shapiro phase-control technique exploits constructive versus destructive interference of two different excitation pathways via one-photon and three-photon absorption. By tuning the relative phase between the two CW laser fields with different frequencies, the population in the final states can be modulated. (c) The STIRAP scheme uses two time-delayed nanosecond laser pulses in a counter-intuitive sequence to induce adiabatic population transfer with nearly 100% efficiency from the ground state ψ_g to the final state ψ_f. The two levels are coupled via an intermediate state ψ_i of which the transient population, however, remains zero and dissipative losses to levels ϕ_d are avoided [77]

CH_3I [79–84].

Another control strategy based on the coherent adiabatic excitation, is the STImulated Raman Adiabatic Passage (STIRAP) scheme, developed by Bergmann and collaborators [85, 86] and Eberly *et al* [87]. This control scheme is designed to achieve full population transfer between specified quantum states, and is very robust to variations in the laser parameters once the proper operating regime, called adiabatic regime, is achieved [88–90] [the mechanism will be detailed in sec. 3.1]. The basic version of the approach is shown in fig. 2 (c), in which the inversion of population from the ground state ψ_g to the final state ψ_f is accomplished with the support of an intermediate state ψ_i. The scheme employs two intense laser pulses in a counter-intuitive sequence in order to achieve population inversion. Sequentially, the first pulse, the Stokes pulse, is resonant with the energy difference between the final state ψ_f and the intermediate state ψ_i. The second pulse is the pump pulse which couples the ground state ψ_g with the intermediate state ψ_i. This counter-intuitive sequence of pulses is designed such that when the pump pulse is switched while the Stokes pulse is still acting, a dark or trapped state is prepared which prevents populating the intermediate state, ψ_i, that is, the transient population in this state remains zero, and possible dissipative population losses into states ϕ_d by radiative decay, for example, are avoided. The population is considered to be virtually confined to the two states, ψ_g or ψ_f. The complete transfer from the ground to the final state occurs when the pump pulse is applied at the tail of the Stokes pulse. The phenomenon of trapping is a consequence of quantum interference between the two pathways leading to state ψ_i in fig. 2 (c). This technique of control has been experimentally verified for atoms and small molecules [91, 92]. The STIRAP scheme has also been extended to N-level systems [87, 93].

It is interesting to note that these control schemes are not necessarily mutually exclusive, but part of the principles of some of these schemes can be combined to generate hybrid schemes. For instance, it was shown that it is possible to combine the selectivity of coherent control and the robustness of adiabatic passage in a new control scheme sometimes referred to as Coherent Controlled Adiabatic Passage. This scheme has been used to prepare arbitrary superposition states [94] or to control the double proton transfer in a model nucleotide base-pair with the goal of detecting and automatically repairing base-pair mutations [95].

Another control strategy exploits the resulting Stark shifts of non-adiabatic potential energy curves due to intense nonresonant IR laser pulses as a means to control molecular reactions [15]. The Dynamic Stark Control method has been tested theoretically and experimentally influencing the outcome of photodissociation reactions at conical

intersections [96], in bond softening or hardening [97–100], selectively driving population to excited states [101–103], changing the molecular structure [104–106], squeezing wave packets [107, 108] or stopping or inducing a spin-orbit coupling [109–112]. In this work, a control scheme based on the dynamic Stark effect is employed to influence the population transfer between singlet and triplet states (see sec. 3.3).

Quantum Control algorithms

The presented control strategies can be tuned to operate efficiently when the molecular Hamiltonian and the potential energy surfaces are well known. For example, the Brumer-Shapiro scheme faces the problem that the same intermediate state leads to different reaction products. In the Tannor-Rice method it is only possible to control the vertical transitions between electronic states. But, due to the anharmonicity of the excited state PES, the evolution of the wave packet will, in most cases, spread out, preventing a clean dump into the desired dissociation channel. A necessary improvement required to control the wave packet dynamics within each electronic potential. This became possible with the development of Quantum Optimal Control Theory (QOCT). QOCT was first developed by Rabitz and co-workers [9,113–115] and, independently, by Kosloff *et al.* [10]. The Tannor-Rice pump-dump scheme for controlling the selectivity of product formation in a chemical reaction is improved by the development of a method for optimizing the field of a particular product with respect to the shapes of the pump and dump pulses. QOCT was generalized using the mathematical theory of Optimal Control, where the shape of the dump pulse (and finally of a single pulse) is determined by maximizing the desired yield, given the Hamiltonian and the final time at which the yield is calculated. Thus, the development of QOCT became a mathematical problem, and the following advances were focused on the search of the most efficient numerical methods to solve the corresponding Euler-Schrödinger equation. Aside the methodological advances and all different QOCT methods [5, 10, 114, 116–122], the idea was applied to control many different systems [114, 116, 123–129].

However, the tailored electric fields that are produced from QOCT simulations tend to be rather complex, and therefore difficult to reproduce experimentally, hiding the control mechanism in their intrincate pulse shapes. Finding this so-called optimal laser field is not trivial, since, as mentioned before, the approximations made in the theoretical calculations do not always correspond to the real Hamiltonian. For polyatomic molecules there is an amount of uncertainty in the Hamiltonian and developing QOCT for these systems is a challenging task. Additionally, it is clear that for large molecules, by

increasing the density of accessible quantum states, the QOCT iterative schemes quickly become computationally very demanding.

Some theoretical efforts were developed to bridge the gap between QOCT and experiment by introducing new functionals and optimization strategies. It is possible to restrict the optimal pulse complexity to a minimum, thereby achieving robust pulses, whose spectra are a direct signature of the control mechanism.

Experimentally, the difficulty is to find the optimal tailored pulse that leads to the wanted outcome of the experiment by the correct interference of the multiple light-induced pathways. Consequently, a more practical approach lead to the adaptive learning or Quantum Optimal Control Experiments (QOCE) [130], adapted to the experimental techniques used in ultrafast laser pulse control, to solve this search problem.

In QOCE a closed-loop algorithm iteratively modifies the laser pulse until the experimental observable (representing the desired target state) is maximized or minimized. This is achieved by feeding the pulse shaper with information about the measured signal so that the electric field pattern is modified until the response signal does not significantly change using a learning algorithm like, e.g., an evolutionary algorithm (convergence is achieved). In this way the algorithm learns the optimal sequence for the investigated system, i.e., the best pulse for a desired process in a particular molecule. All of this is achieved without an a priori knowledge of the molecular Hamiltonian during the optimal path towards the selected target state.

Many groups applied the adaptive control in the laboratory. Processes like population transfer to excited states [131], fragmentation of organometallic molecules [132], ionization [133], impulsive stimulated Raman scattering (ISRS) [134], and high harmonic generation [135] were objectives of the optimization.

In this thesis, the approach of Local Control Theory (LCT) [11, 12], is followed. The idea first appeared in the formulation of QOCT introduced by Kosloff, Rice, and Tannor [10] and has been extensively developed since then [11, 93, 121, 136–139]. In contrast with optimal control, which involves an iterative forward- backward procedure, in local optimization the pulse shape is optimized at every instant in time and immediately fed back into the dynamics. The basic idea is to choose a control field in order to ensure an increase or decrease of the expectation value of an observable, e.g., $\langle x \rangle$, $\langle H \rangle$, etc. during a certain period of time where the external field is acting. This involves less detailed target states and the use of simpler methodologies.

The local control concept was used to model laser cooling or heating (in the sense of adding or taking away internal energy) of molecular vibrational motion on the electronic ground state, in which an excited state is used by changing the phase of the

laser field [121,137]. This method has also been applied to control the photodissociation of small molecules [140, 141] or charge transfer processes [138, 139, 142]. Furthermore, this approach has been used for a generalization of stimulated Raman adiabatic passage (STIRAP) [143] to an N-level quantum system [93]. In all these applications, the heating/cooling or population transfer were achieved by locally designing external fields under certain constraints like, for example, the locking of population in specific electronic states.

Further developments include the treatment of multiple objectives leading to possibly force the system dynamics along a predescribed path through Hilbert space [144–147]. From the viewpoint of global optimization, a different theory of local control has been derived, applied to finite time intervals [118,148,149]. This approach can also be applied within a classical context, and local control fields from classical dynamics have been used in quantum problems [150]. In parallel, Rabitz and coworkers developed a method called "*tracking control*", in which Ehrenfest's equations [151] for an observable are used to derive an explicit expression for the electric field that forces the system dynamics to reproduce a predefined temporal evolution of the control observable [120,152]. Quantum computing has also taken advantage from this theory [153, 154].

In addition to the examples already mentioned, the different local control schemes have found many applications in molecular physics, like population control [155–158], selective mode excitation in biological systems [159], control of molecular photoassociation [160], wave packet control [161–163], control within a dissipative environment [164, 165], selective vibrational excitation or dissociation [166, 167] and selective rotational molecular fragmentation [168]. Other examples include isomerization control [148, 169], control of predissociation [170], or enantiomer control [171, 172]. Local control has also been applied to control particle transfer in the case of coupled electronic and nuclear motion [173]. A further application of this theory is the so called optical paralysis scheme [136, 151, 174]. The basic idea is to manipulate ground state properties while suppressing unwanted excitations to high-lying states, an important issue for strong field coherent control.

Considering the general formulation of LCT, it is interesting to note that there exist similarities between monotonically convergent algorithms for optimal control and local control methods [175]. An additional important point that is worth mentioning, is that the control fields constructed within the LCT scheme can be interpreted in a straightforward way. This is not always possible for fields derived from other control theories.

Regarding the attosecond time domain, quantum control of electron dynamics was

established based on advances in the field of control of nuclear dynamics, but in the case of sub-fs pulses, pulse shaping is at the moment technically not developed. However, the theoretical anticipation is timely, and might foster the development of pulse shaping techniques in the attosecond domain [2]. In the last years, the attention has shifted from the creation of new ways to obtain and characterize attosecond pulses towards the use of these pulses to monitor and control electron dynamics, following the path of what was done with reaction dynamics in molecules with femtosecond lasers [47, 176, 177].

Many control schemes to directly manipulate the electronic motion have been already devised, for example dipole switching control in molecules and in open systems [178,179], stereocontrol of electron dynamics in polyatomic molecules [180], magnetization switching control in quantum rings [181], optimal control of population transfer in polyatomic molecules [182], attosecond control of charge migration in small peptides [183], coherent control of electric currents in superlattices and molecular wires [184, 185], chiral control of electron transmission (current transfer) through molecules [186], and coherent spin control of matrix isolated molecules by IR+UV laser pulses [187]. Quantum control of HHG [188] includes restricted optimal control of attosecond laser pulse synthesis from HHG using chirped driven laser pulses [189], IR+UV control of HHG [190] and optimal control of HHG by pulse-shaped laser pulses [191, 192] and by intense few-cycle pulses [193]. Finally, quantum control of ionization and dissociation includes strong field control of landscapes involving multiphoton ionization using pulse-shaped laser pulses [194], optimal control of multiphoton ionization by ultrafast polarization shaping [195], IR+UV control of electron localization in dissociation of H^{2+} [196], IR+UV control of photoelectron spectroscopy of electron tunneling in H_2 [197], laser control of symmetry breaking of dissociation of H_2 [198].

Besides the time or frequency domain features of the spectra, the laser intensity constitutes another essential feature of control techniques. Beyond intensities of the order or higher than the TW/cm^2, many nonlinear multi-photon transitions occur that may allow to excite highly inaccessible regions of the electronic potentials. Additionally, Autler-Townes splittings and strong Stark shifts modify the electronic forces and reshape the potential energy surface [199]. At this intensities, static phenomena as bond hardening or bond softening [98,200], as well as dynamical processes that will be studied in this project, can be controlled. At even higher intensities, multi-photon ionization and Coulomb explosion destroy the molecule, but can be used to gather information about the wave function prior to the molecule's breakdown [201]. In a recent future, perhaps shaping laser pulses in the attosecond regime it will become feasible to stabilize the molecule and control the electronic motion [202, 203].

Considering this new time domain in chemistry and biology, the question arises of whether femto- and attosecond probing of molecular dynamics just represents a benchmark in an observation window, or whether it reveals new phenomena and new frontiers. Along the years, it has been clearly shown that the ultrafast regime does not simply provide more time resolution for a better observation of the processes but also opens new ways to manipulate matter.

The research attempting to control quantum phenomena has been advancing for some 50 years, but in many aspects the field could be viewed as a few years young with the basic physical principles only now beginning to reveal themselves. Despite the evident limitations of currently available laser resources, they have already enabled the successful control of many types of quantum phenomena. Each advance in control resources is expected to reveal significant new domains for quantum control and enhance the quality of the achieved results. The prospect of simultaneously observing nuclear and electronic motion in molecules may make non-Born-Oppenheimer processes like the dynamics at conical intersections accessible to direct observation for the first time. The recent advances in the quantum control field emerged through joint efforts from the theoretical and experimental communities, and this cooperation is expected to be crucial to the future development of the field.

Motivation of the thesis

The main goal of this thesis is the simulation of the dynamics of molecules excited by intense ultrashort pulses in the femto and attosecond scale, and the control of different molecular processes such as ionization, dissociation, interference, spin and electron transfer, facilitated by the preparation of electronic states in a quantum superposition under laser fields. Using model systems, we will explore what are the main sources that limit our ability to control the electron dynamics and the role of the interaction between the nuclear and electronic degrees of freedom.

We combine quantum control techniques with femto and attophysics processes, working with highly simplified (but generic) potential models for qualitatively understanding the nature of the processes, its controllability and the validity of the usual approximations that give rise to important physical representations of the systems under study. We intend to predict the degree of control that can be achieved in attophysics processes (ionization, dissociation, change of electronic properties) when pulse modulation techniques are extended to the attosecond domain, so that this research can serve as an incitement to its development. Since the technology is not yet available, and therefore

its range and limitations are not known precisely, we will focus on general models trying to answer questions such as: How do ionizing processes with low-frequency lasers affect the efficiency of many control methods? Is it possible to avoid the ionization and to control the spin-orbit transfer? Can one use the external fields as drivers for electrons between distant atoms?

The two main results developed in this thesis are:

- The test of the limits of validity of controlling the spin-orbit transitions through nonresonant strong pulses, when the effects of ionization by tunneling or multi-photon absorption and the violation of the Born-Oppenheimer approximation are incorporated in the electron dynamics.

- The control of processes involving reversible transitions between bound states and ionizing states (continuum). That is, we want to maximize the probability that the electrons, after being transported through the continuum, will be re-trapped when they return to the core, after the phase of the pulse changes, or to a different ion.

Work Plan

We conclude this chapter laying out the organization of the remaining of this thesis.

In Chapter 2 we review the most important theoretical ideas that are central to the studies of this thesis. Our main object of study is the evolving wave function of the system. We start by analyzing the time dependent Schrödinger equation and the different approximations we embrace to describe the molecular dynamics under the effect of a laser field. In particular, we discuss the Born-Oppenheimer approximation (sec. 1.1). In sec. 1.2 we introduce the equations that define the laser-matter interaction, as well as the approximations made to simplify our Hamiltonian when the coupling with the laser field is included. We restrict ourselves to the non-relativistic regime for the electron dynamics, and we will always assume the dipole approximation. This means that the laser–molecule interaction is theoretically described by the time dependent Schrödinger equation where the magnetic field of the laser pulse is neglected. The laser acts merely via the electric field, which is (as seen from the viewpoint of the molecule) time dependent but homogeneous in space.

In the rotating wave approximation (sec. 1.2.1) the fast oscillating terms are removed, i.e., we neglect the instantaneous effect of very non-resonant frequency components of the field. This approximation is valid when the interaction energy is lower than

the energy of the photon and when the pulse duration is larger than the inverse of its frequency. Under the adiabatic approximation (sec. 1.2.2) we describe our system in terms of *adiabatic* or *dressed states*, which are the instantaneous eigenfunctions of the complete Hamiltonian, including the coupling with the laser field. The adiabatic regime defines the evolution of a system in an environment characterized by a slowly varying time dependent Hamiltonian, which implies that there are no transitions between the adiabatic states and their populations are conserved. Within this representation one typically neglects the non-adiabatic couplings (off-diagonal elements in the Hamiltonian), greatly simplifying the Hamiltonian. The adiabatic evolution requires a smooth pulse, long interaction time and large Rabi frequency and/or large detuning.

We continue with the description of the spin-orbit coupling (sec. 1.3). In this thesis we are interested in the control of the spin-orbit transitions working in the ultaintense regime, where second order effects must be considered carefully and the Born-Oppenheimer approximation fails to account for important physical processes. Therefore, new terms must be included in the Hamiltonian, since these effects produce significant variations in the energy of the states and induce dynamical processes. Once we have imposed these approximations, we obtain the complete time dependent Schrödinger equation (TDSE) describing the evolution of our molecular system. Chapter 2 reveals the mathematical methods applied to numerically solve this equation and to follow the system dynamics "steered" by a laser field. The Fourier Grid Hamiltonian (FGH) method [204] is used (sec. 2.2) to calculate the eigenstates of the Hamiltonian in a grid (sec. 2.1). The TDSE is solved as a propagator by using the Split Operator method [205], which approximates the Hamiltonian as a product of kinetic energy and potential energy propagators over short time intervals, which can be each efficiently evaluated in different representations.

In sec. 2.6 we describe the specific Hamiltonian models that we employ to describe the electronic and nuclear dynamics. Normally, the TDSE approach is restricted to model systems, since already the dynamics of two electron molecules (without approximations) in a strong pulse is too demanding for present-day computers. Therefore it is popular to employ the single-active-electron approximation (SAE) and/or reduced dimensionality of the molecular system of interest. Rather than using a realistic Hamiltonian, we extend the Shin-Metiu model [206, 207] to include non adiabatic couplings which allow us to explore the degree of control over the spin-orbit transitions. In addition, a soft-core Coulomb potential [208] is used to control charge transfer processes in small molecules (H_2 and HeH^{2+}).

In chapter 3 different quantum control schemes are described. The nonresonant

dynamic Stark effect is used as a strategy to influence the spin-orbit transitions (sec. 3.3.2). By means of strong laser fields one can modify the molecular potentials, creating new non adiabatic couplings, thus changing the wave packet evolution along the potential energy curves and stopping or inducing a singlet-triplet transition. In chapter 4 we introduce the Quantum Control Algorithms, focusing on the description of Local Control Theory (sec. 4.2). We derive the different control equations to obtain the laser control fields that maximize the electron transfer between separated nuclei.

The following sections present the results of this thesis. The original results are divided in two different chapters consisting in a brief summary describing the theoretical work and then we include the articles as they are published.

In chapter 5 we explain in detail the results obtained in this thesis. Section 5.1 concerns the control of the spin of the wave function via the nonresonant dynamic Stark effect in a model system and analyzes under which conditions this control is possible. It consists of the results of three different articles: "*Quantum wave packet dynamics in spin-coupled vibronic states*" (*J. Phys. Chem. A*, **116**, *11427-11433*, 2012), "*Manipulating the singlet-triplet transition in ion strings by nonresonant dynamic Stark effect*" (*Theor. Chem. Acc.*, **132**, *1359*, 2013) and "*The time-scale of non linear events driven by strong fields: can one control the spin coupling before ionization runs over?*" (*J. Phys. B*, **47**, *124027*, 2014).

Section 5.2 deals with the laser control of the electron transfer between nuclei when long internuclear distances are considered. Different formulations of the Local Control theory are applied working under two different time scales: femto and atto. The results are presented in two articles: "*Local Control approach to ultrafast electron transfer*" (*Chem. Phys.*, *In press*, 2016) and "*Slow electron transfer between separated nuclei*" (*In preparation*).

Finally chapter 7 is the summary and conclusions.

Theoretical background

Atoms and molecules in strong fields

Along this chapter we deal with the Hamiltonian describing the physics behind the different phenomena investigated in this thesis. In general, we study the evolution of the system by solving the *time dependent Schrödinger equation* (TDSE)

$$\frac{\partial}{\partial t}|\Psi(R,x,t)\rangle = -\frac{i}{\hbar}\hat{H}|\Psi(R,x,t)\rangle \tag{1.1}$$

where t is the time, $|\Psi(R,x,t)\rangle$ represents the global wave function of the system, $\hat{H}$ is the Hamiltonian, and R and x represent the nuclear and electron coordinates, respectively.

Initially, in section 1.1, we introduce the Born-Oppenheimer approximation, which separates the electron and nuclear motion. We follow with the description of the molecular dynamics in the presence of a laser assuming a classical behaviour of the external field (1.2). Right after, we explain the rotating wave approximation (RWA) and the adiabatic approximation, which allow us to simplify the equations characterizing our system dynamics. In section 1.3, we finally end up describing the effects that force us to go beyond the Born-Oppenheimer approximation with the new terms that must be included in the Hamiltonian defining the system.

1.1 The molecular Hamiltonian under the Born-Oppenheimer approximation

The Born-Oppenheimer approximation is one of the basic concepts underlying the description of the quantum states of the molecule. It separates the electron and nuclear motion based on the idea that the nuclear mass is so much larger than the electron mass.

From where the next assumptions follow:

1. The electronic wave function depends upon the nuclear positions, but not upon

their velocities, i.e., the nuclear motion is so much slower than the electron motion, that the nuclei can be considered to be fixed.

2. The nuclear motion (e.g. rotation,vibration) sees a smeared out potential from the speedy electrons.

Due to their smaller mass, electrons bounded in the nuclear potential move more rapidly than the heavy nuclei themselves and, on average, follow their motion. The physical result is that the electronic motions are instantaneously "adapted" at each nuclear position. Therefore we can solve the electronic Schrödinger equation at each nuclear configuration which is much more computationally affordable.

In general, the Hamiltonian can be written as

$$\hat{H} = \hat{T}_N(R) + \hat{H}_e(R, x) \tag{1.2}$$

where $\hat{T}_N(R)$ is the nuclear kinetic energy operator and $\hat{H}_e(R, x)$ is called "*electronic Hamiltonian*".

Considering a diatomic molecule **AB**, disregarding the rotation and translation of the center of mass, the nuclear kinetic term is

$$\hat{T}(R) = -\frac{\hbar^2}{2\mu}\frac{\partial^2}{\partial R^2} \tag{1.3}$$

where $\mu = m_A m_B/(m_A + m_B)$ is the reduced mass of the nuclei **A** and **B**, and R the internuclear distance.

Concerning the electronic Hamiltonian $\hat{H}_e(R, x)$, this term includes the kinetic energy of the electrons, the nuclear repulsion, the attraction between the electron and nuclei and the electronic repulsion. Thus, we can express the electronic Hamiltonian as

$$\hat{H}_e(R,x) = \overbrace{-\frac{\hbar^2}{2m_e}\sum_i^{n_e}\frac{\partial^2}{\partial x_i^2}}^{\text{kinetic}} + \frac{1}{4\pi\epsilon_0}\overbrace{\left(\underbrace{\frac{Z_A Z_B e^2}{R}}_{n-n} \underbrace{-\sum_i^{n_e}\frac{Z_A e^2}{D_{Ai}} - \sum_i^{n_e}\frac{Z_B e^2}{D_{Bi}}}_{e^- - n} + \underbrace{\sum_i^{n_e}\sum_{j\neq i}^{n_e}\frac{e^2}{d_{ij}}}_{e^- - e^-}\right)}^{\text{potential}} \tag{1.4}$$

where n_e is the number of electrons in the diatomic molecule, x_i represents the electronic coordinates i with respect to the center of mass defined by the nuclei, m_e and e are the electronic mass and charge respectively, Z_A y Z_B are the number of protons in the nuclei **A** and **B**, d_{ij} is the interelectronic distance between the electrons i and j,

whereas D_{Ai} and D_{Bi} are the distances between electron i and the nuclei **A** and **B**.

Considering this separation of the Hamiltonian, one can propose the following expansion of the wave function

$$\hat{H}_e(R;x)|\chi_\alpha(R;x)\rangle = V_\alpha(R)|\chi_\alpha(R;x)\rangle \tag{1.5}$$

Equation (1.5) is the electronic *time independent Schrödinger equation* (TISE). This equation can be solved by standard ab initio methods [209, 210].

From these electronic wave functions it is possible to evaluate the total Hamiltonian over the total wave function, which is a linear combination of products of nuclear and electronic wave functions [see eq. (1.12)].

Applying $\hat{H}_e(R;x)$ to this linear combination results in

$$\hat{H}_e(R;x)\sum_\alpha^N |\psi_\alpha(R,t)\rangle|\chi_\alpha(R;x)\rangle = \sum_\alpha^N |\psi_\alpha(R,t)\rangle\hat{H}_e(R;x)|\chi_\alpha(R;x)\rangle \tag{1.6}$$

given that there is no derivative with respect to the coordinates of the nuclear wave function in $\hat{H}_e(R;x)$. From this result we obtain,

$$\hat{H}_e(R;x)|\Psi(R,x,t)\rangle = \sum_\alpha^N |\chi_\alpha(R;x)\rangle V_\alpha(R)|\psi_\alpha(R,t)\rangle \tag{1.7}$$

Besides, when applying the nuclear kinetic term we have to derive with respect to the internuclear distance R. Operating sequentially, the first derivative is

$$\frac{\partial}{\partial R}\sum_\alpha^N |\psi_\alpha(R,t)\rangle|\chi_\alpha(R;x)\rangle = \sum_\alpha^N |\chi_\alpha(R;x)\rangle\frac{\partial|\psi_\alpha(R,t)\rangle}{\partial R} + \sum_\alpha^N \frac{\partial|\chi_\alpha(R;x)\rangle}{\partial R}|\psi_\alpha(R,t)\rangle \tag{1.8}$$

and the second derivative results in

$$\begin{aligned}\frac{\partial^2}{\partial R^2}\sum_\alpha^N |\psi_\alpha(R,t)\rangle|\chi_\alpha(R;x)\rangle = &\sum_\alpha^N |\chi_\alpha(R;x)\rangle\frac{\partial^2|\psi_\alpha(R,t)\rangle}{\partial R^2} + \\ &\sum_\alpha^N \frac{\partial^2|\chi_\alpha(R;x)\rangle}{\partial R^2}|\psi_\alpha(R,t)\rangle + \sum_\alpha^N 2\frac{\partial|\chi_\alpha(R,t)\rangle}{\partial R}\frac{\partial|\psi_\alpha(R;x\rangle}{\partial R}\end{aligned} \tag{1.9}$$

Lastly, we can integrate with respect the whole electronic coordinates to follow the

nuclear motion. Applying eq. (1.5) and considering that the electronic wave functions are orthonormal ($\langle\chi_\alpha(R;x)|\chi_\beta(R;x)\rangle = \delta_{\alpha\beta}$), we obtain for $\hat{H}_e(R;x)$

$$\langle\chi_\beta(R;x)|\hat{H}_e(R;x)|\sum_\alpha^N \chi_\alpha(R;x)\psi_\alpha(R,t)\rangle = V_\beta(R)|\psi_\beta(R,t)\rangle \tag{1.10}$$

and the global Hamiltonian $\hat{H}$ results in

$$\overbrace{\langle\chi_\beta(R;x)|\hat{H}|\sum_\alpha^N|\chi_\alpha(R;x)\rangle|\psi_\alpha(R,t\rangle\rangle}^{\text{BO approx.}} = \overbrace{\underbrace{V_\beta(R)|\psi_\beta(R,t)\rangle}_{\boxed{\text{eq. (1.10)}}} + \underbrace{-\frac{\hbar^2}{2\mu}\frac{\partial^2}{\partial R^2}|\psi_\beta(R,t)\rangle}_{\boxed{\text{eq. (1.9)}}}}^{\boxed{\text{eq. (1.9)}}}$$

$$\underbrace{-\frac{\hbar^2}{2\mu}\sum_\alpha^N \underbrace{\langle\chi_\beta(R;x)|\frac{\partial^2}{\partial R^2}|\chi_\alpha(R;x)\rangle}_{T^{RR}_{\beta\alpha}(R)}|\psi_\alpha(R,t)\rangle - \frac{\hbar^2}{\mu}\sum_\alpha^N \underbrace{\langle\chi_\beta(R;x)|\frac{\partial}{\partial R}|\chi_\alpha(R;x)\rangle}_{T^{R}_{\beta\alpha}(R)}\frac{\partial}{\partial R}|\psi_\alpha(R,t)\rangle}_{\boxed{\text{eq. (1.9)}}} \tag{1.11}$$

where $T^{RR}_{\beta\alpha}(R)$ y $T^{R}_{\beta\alpha}(R)$ represent the derivatives with respect to the internuclear distance of the electronic wave function.

Within the adiabatic approximation [211] the probability of transition between the electronic wave functions of the same basis set can be neglected, and only the terms in the diagonal remain in the Hamiltonian. Dismissing also the kinetic terms $T^{RR}_{\beta\beta}(R)$ and $T^{R}_{\beta\beta}(R)$ with respect to $V_\beta(R)$ in the Born-Oppenheimer approximation, the TDSE for the molecular motion reads

$$\frac{\partial}{\partial t}|\psi_\beta(R,t)\rangle = -\frac{i}{\hbar}\left(\overbrace{-\frac{\hbar^2}{2\mu}\frac{\partial^2}{\partial R^2}}^{\hat{T}(R)}|\psi_\beta(R,t)\rangle + V_\beta(R)|\psi_\beta(R,t)\rangle\right) \tag{1.12}$$

The $V_\beta(r)$ terms are usually known as *potential energy curves*, and can be calculated, within the Born-Oppenheimer approximation, as the sum of the kinetic and potential energy of the electrons in a quantum state β with the internuclear repulsion for each nuclear position R.

Summarizing, once the Hamiltonian is integrated, a nuclear potential is created in which the electrostatic energy (repulsions and attractions) of the system and the kinetic energy of the electrons are included.

1.2 Light and matter interaction

Throughout this thesis, we are interested in the processes triggered by the interaction between molecules and a coherent external pulse of electromagnetic radiation. In this section we describe the fundamentals of the molecular dynamics in the presence of a laser field with a coherent interaction with the system, under a semiclassical approach, in which the field is treated classically while the molecule-laser interaction is quantized. We assume that the characteristic time of the decoherence processes is much larger than those we are interested in, and they lie beyond the scope of this work. In general, neglecting the multipolar terms and the effects of the magnetic field, we can write the Hamiltonian of the system, including the interaction between the laser field and the molecule, as

$$\hat{H}(R,x,t) = \hat{T}(r) + \hat{H}_e(R;x) - \hat{\mu}(R;x)\mathcal{E}(t) \tag{1.13}$$

where $\mathcal{E}(t)$ is the amplitude of the electric field (disregarding its spatial dependence) and $\mu(R;x)$ is the dipolar moment operator, oriented in some direction of the polarization of the laser field.

We can define again as in sec. 1.1 the global wave function $|\Psi(R,x,t)\rangle$ as a linear combination of products of $|\chi_\alpha(x;R)\rangle|\psi_\alpha(R,x)\rangle$. If we project over the electronic wave functions $\langle\chi_\beta(R;x)|$ and we integrate with respect to the electronic coordinates (x) we obtain a set of coupled equations very similar to eq. (1.12)

$$\frac{\partial}{\partial t}|\psi_\beta(R,t)\rangle = -\frac{i}{\hbar}\left(\hat{T}(R)|\psi_\beta(R,t)\rangle + V_\beta(R)|\psi_\beta(R,t)\rangle - \sum_\alpha^N \mu_{\beta\alpha}(R)\mathcal{E}(t)|\psi_\alpha(R,t)\rangle\right) \tag{1.14}$$

where $\mu_{\beta\alpha}(R)$ is the transition dipole moment between the electronic wave functions β and α, $\mu_{\beta\alpha}(R) = \langle\chi_\beta(R;x)|\mu(R;x)|\chi_\alpha(R;x)\rangle$. The electric field is represented by its envelope $\mathcal{E}_0(t)$, its frequency ω and a phase φ

$$\mathcal{E}(t) = \mathcal{E}_0(t)\cos(\omega t + \varphi) \tag{1.15}$$

In this thesis we employ the laser field as a tool to control the system dynamics, but before delving into the study of the control mechanisms we applied to influence its evolution, we will enquire into the study of how the electric field can produce transitions between different quantum levels, in particular between vibrational and electronic levels (rotational levels are not considered). Usually, in spectroscopy, the transition probability is calculated by the time dependent perturbation theory [151], where the Hamiltonian matrix is defined in the basis of the Hamiltonian eigenfunctions of the system in the absence of radiation. But when the intensity of the radiation exceeds the acceptable limits to be treated as a perturbation (in our case the electric field can induce population inversion), we must solve the TDSE exactly, as it happens in different control mechanism as the π-*pulses* model, the STIRAP mechanism (*Stimulated Raman Adiabatic Passage*) or other control schemes based on ultrashort and strong laser fields.

To this aim, in the next section we first introduce the *rotating wave approximation* (RWA) so one can simplify the Hamiltonian term with the coupling to the electric field. Right after, we will define the system in the basis of the *dressed states* or *adiabatic states*, which are the instantaneous "eigenfunctions" of the time dependent Hamiltonian including the coupling with the laser field.

1.2.1 Rotating wave approximation (RWA)

Let us consider the simplest situation of two potentials [V_α and V_β] coupled by a laser of frequency ω which acts directly over the transition, disregarding the permanent dipole moments [$\mu_\alpha(R) = 0$] (diatomic homonuclear molecules).

From eq. (1.14), the TDSE is

$$\begin{aligned} -\frac{\hbar}{i}\frac{\partial}{\partial t}|\psi_\alpha(R,t)\rangle &= T(R)|\psi_\alpha(R,t)\rangle + V_\alpha(R)|\psi_\alpha(R,t)\rangle - \mu_{\alpha\beta}(R)\mathcal{E}_0(t)\cos(\omega t)|\psi_\beta(R,t)\rangle \\ -\frac{\hbar}{i}\frac{\partial}{\partial t}|\psi_\beta(R,t)\rangle &= T(R)|\psi_\beta(R,t)\rangle + V_\beta(R)|\psi_\beta(R,t)\rangle - \mu_{\beta\alpha}(R)\mathcal{E}_0(t)\cos(\omega t)|\psi_\alpha(R,t)\rangle \end{aligned} \tag{1.16}$$

If we change the representation as

$$\begin{gathered} |\psi'_\beta(R,t)\rangle = |\psi'_\beta(R,t)\rangle e^{+i\omega t} \Rightarrow |\psi_\beta(R,t)\rangle = |\psi'_\beta(R,t)\rangle e^{-i\omega t} \\ |\psi'_\alpha(R,t)\rangle = |\psi_\alpha(R,t)\rangle \end{gathered} \tag{1.17}$$

we obtain

$$-\frac{\hbar}{i}\frac{\partial}{\partial t}|\psi_\beta(R,t)\rangle = -\frac{\hbar}{i}\mathrm{e}^{-i\omega t}\frac{\partial}{\partial t}|\psi_\beta(R,t)\rangle + \hbar\omega|\psi_\beta(R,t)\rangle\mathrm{e}^{-i\omega t} \tag{1.18}$$

and the TDSE transforms in

$$\begin{array}{cc} -\frac{\hbar}{i}\frac{\partial}{\partial t} & \begin{array}{c}|\psi_\alpha(R,t)\rangle\\|\psi_\beta(R,t)\rangle\end{array} \\ \begin{array}{c}T(R)+V_\alpha(R)\\-\mu_{\beta\alpha}(R)\mathcal{E}_0(t)\cos(\omega t)\mathrm{e}^{+i\omega t}\end{array} & \begin{array}{c}-\mu_{\alpha\beta}(R)\mathcal{E}_0(t)\cos(\omega t)\mathrm{e}^{-i\omega t}\\T(R)+V_\beta(R)-\hbar\omega\end{array} \end{array} \begin{array}{c}|\psi_\alpha(R,t)\rangle\\|\psi_\beta(R,t)\rangle\end{array} = \tag{1.19}$$

With $cos(\omega t) = (\mathrm{e}^{+i\omega t} + \mathrm{e}^{-i\omega t})/2$, we can write

$$\begin{array}{cc} -\frac{\hbar}{i}\frac{\partial}{\partial t} & \begin{array}{c}|\psi_\alpha(R,t)\rangle\\|\psi_\beta(R,t)\rangle\end{array} \\ \begin{array}{c}T(R)+V_\alpha(R)\\-\mu_{\beta\alpha}(R)\mathcal{E}_0(t)(\mathrm{e}^{+2i\omega t}+1)/2\end{array} & \begin{array}{c}-\mu_{\alpha\beta}(R)\mathcal{E}_0(t)(\mathrm{e}^{-2i\omega t}+1)/2\\T(R)+V_\beta(R)-\hbar\omega\end{array} \end{array} \begin{array}{c}|\psi_\alpha(R,t)\rangle\\|\psi_\beta(R,t)\rangle\end{array} = \tag{1.20}$$

At this point the rotating wave approximation is introduced, which amounts to considering $1 + \mathrm{e}^{\pm 2i\omega t} \approx 1$, neglecting the transition probability due to $\mathrm{e}^{\pm 2i\omega t}$. This is because this term oscillates faster than $\mathcal{E}_0(t)$ and the wave function and therefore its accumulated effect rapidly averages zero. With this approximation we neglect the transition probability coming from processes out of resonance: excitation from state $|\psi_\alpha\rangle$ to $|\psi_\beta\rangle$ by stimulated emission of a photon, and decay from state $|\psi_\beta\rangle$ to $|\psi_\alpha\rangle$ by the absorption of a photon. This approximation is fulfilled when the coupling radiation energy $V_{\alpha\beta} = \mu_{\alpha\beta}\mathcal{E}(t)$, is lower than the energy of the photon, $\hbar\omega$, and when the pulse duration is greater than the inverse of the frequency.

In the RWA, the resulting TDSE is:

$$-\frac{\hbar}{i}\frac{\partial}{\partial t}\begin{array}{c}|\psi_\alpha(R,t)\rangle\\|\psi_\beta(R,t)\rangle\end{array} = \begin{array}{ccc}T(R)+V_\alpha(R) & -\mu_{\alpha\beta}(R)\mathcal{E}_0(t)/2 & |\psi_\alpha(R,t)\rangle\\-\mu_{\beta\alpha}(R)\mathcal{E}_0(t)/2 & T(R)+V_\beta(R) & |\psi_\beta(R,t)\rangle\end{array} \tag{1.21}$$

where $V_\beta(R) = V_B(R) - \hbar\omega$.

It is easy to demonstrate that this change in the representation does not modify the observables. For instance, neither the norm

$$\left\langle \psi_\beta(R,t)|\psi_\beta(R,t)\right\rangle = \left\langle \psi_\beta(R,t)|\mathrm{e}^{-i\omega t}\mathrm{e}^{+i\omega t}|\psi_\beta(R,t)\right\rangle = \left\langle \psi_\beta(R,t)|\psi_\beta(R,t)\right\rangle \tag{1.22}$$

nor the relative average position change

$$\left\langle R\right| \equiv \left\langle \psi_\alpha(R,t)|r|\psi_\alpha(R,t)\right\rangle = \left\langle \psi_\alpha(R,t)|R|\psi_\alpha(R,t)\right\rangle \tag{1.23}$$

as well as the kinetic energy $[T(R)]$.

1.2.2 The adiabatic approximation: dressed states

When the laser field does not exceed the acceptable limits of intensity to be treated as a perturbation, the Hamiltonian matrix can be expressed in the basis of the eigenstates of the system in the absence of radiation. On the contrary, we can define the system in terms of *adiabatic states* or *semiclassical dressed states* or *dressed states*, which are the instantaneous eigenfunctions of the complete Hamiltonian, including the coupling with the laser pulse.[1]

When the system evolves under the adiabatic approximation, it can be correctly described in terms of dressed states. Let us suppose that $\{\Phi_i(t)\}$ is the set of wave functions that diagonalize the Hamiltonian in the RWA ($H_{\mathrm{RWA}}(t)$) at each time step (the basis constitutes a uniparametric family of orthonormal functions). In this case, $H(t)|\Phi_i(t)\rangle = \omega_i^A(t)|\Phi_i(t)\rangle$, where $\omega_i^A(t)$ are the eigenvalues of the dressed states and are usually called *quasi-energies*. Either the eigenstates of the isolated Hamiltonian $\hat{H}_0$, $\{\psi_i\}$, and the dressed states are complete representations of the Hilbert space, there exist a lineal transformation between both basis, which has to be defined for each time: $\phi = R(t)\Phi$. Therefore making

$$|\psi(t)\rangle = \sum_{i=1}^{N} a_i(t)|\Phi_i(t)\rangle,$$

the Schrödinger equation for the wave function defined in the new basis will be

$$i\frac{\partial}{\partial t}a(t) = \left(H^A(t) - iR^{-1}\frac{\partial R}{\partial t}\right)a(t), \tag{1.24}$$

[1]The dressed states where firstly introduced in a complete description of the Hamiltonian including the quantized field [212]. Therefore in the semiclassical description of the field the adiabatic states must be properly called semiclassical dressed states

where $a(t)$ is the coefficients vector and $H^A(t) = R^{-1}(t)H_{\mathrm{RWA}}(t)R(t)$ is the Hamiltonian matrix in the dressed states representation, which is diagonal due to the definition of the basis ($H^A_{ij}(t) = \langle\Phi_i(t)|H(t)|\Phi_j(t)\rangle = \omega^A_i(t)\delta_{ij}$). The second term on the right side of the equation (1.24) defines the non-adiabatic couplings, which account for the fact that the Hamiltonian $H^A(t)$ is not self-commuting at different times and therefore the laser can produce transitions between two dressed states at different moments (but it can not couple the two states at the same time, because they are orthogonal).

The adiabatic approximation lies in neglecting the non-adiabatic couplings. This is the same as considering that the temporal variation of the dressed states is much slower than the variation of its eigenvalues, that is, the non-diagonal terms that produces $\partial R/\partial t$ (the breaking of orthogonality at different times) are smaller than the diagonal terms, $\{\omega^A_i(t)\}$. Mathematically, the adiabatic criteria is usually expressed as [213]

$$\left|\langle\Phi(t)_n|\frac{d}{dt}|\Phi_m(t)\rangle\right| \ll |\omega^A_n(t) - \omega^A_m(t)| \tag{1.25}$$

Within this approximation, now the integration of the Schrödinger equation is much easier, as it generates just phase terms (complex exponentials which imply the dynamic phase) that multiply the dressed states

$$|\psi(t)\rangle = \sum_{n=i}^{N} a_n(0)|\Phi_n(t)\rangle \mathrm{e}^{-i\int_0^t dt'\omega^A_n(t')} \tag{1.26}$$

where $a_n(0) = \langle\Phi_n(0)|\psi(0)\rangle$ are the initial probability amplitudes (in the absence of radiation) of the dressed states.

As we are considering the evolution of the system in the Dirac representation, where the temporal dependence of the Hamiltonian is only due to the pulse envelopes, so if the temporal variation is slow enough, the adiabatic approximation is valid. The adiabatic approximation is the same as considering that the radiation does not produce couplings between the dressed states. As an immediate consequence, if the initial state of the system is only a dressed state, this state will not change because of the interaction with the laser. Therefore, the radiation will drive the system from the initial state, to the final states of the system which can be projected over the dressed state when the pulse is turned off.

1.3 Breakdown of the Born-Oppenheimer approximation: spin-orbit coupling

In common molecular electronic structure calculations one employs the Born-Oppenheimer approach, not including the spin-orbit (SO) coupling or internal conversion terms at conical intersections in the electronic Hamiltonian. This is the standard procedure when the initial basis is not fully adiabatic [214].

Despite its great explanatory capabilities, the dynamics of nuclear wave packets generally fail to account for important physical processes in two limits: at short times and at high energies. Then, the breakdown of the Born-Oppenheimer approximation (BOA) and the role of electron dynamics, specially for ionization processes, must be considered carefully.

The spin-orbit coupling is a relativistic effect that mainly affects the Hamiltonian systems with heavy nuclei [215]. In molecules, the breakdown of the Born-Oppenheimer approximation is mainly caused by the spin-orbit transitions in the dynamics of excited states. It induces intersystem crossing (ISC) and has significantly implications in the spectroscopy and predissociation of molecules [216–218] and in the rate of relaxation mechanisms [219]. More importantly for our work, it has immediate use in molecular magnetism. In solids, the spin-coupling can be used to create states of mixed multiplicity and to prepare optical spin-switches [220]. In the field of spintronics [221], spin-orbit effects for electrons in semiconductors and other materials are explored for technical applications such as quantum information storage or quantum information processing devices [222].

The relativistic effects due to the SO coupling provoke significant variations of energy of the states and induce dynamical processes. These effects are usually introduced adding a new term in the Hamiltonian

$$\hat{H} = \hat{T}(R) + \hat{H}_e(R;x) + \hat{H}_{SO}(R;x) \tag{1.27}$$

The spin-orbit coupling Hamiltonian can be written as

$$\hat{H}_{SO}(R;x) = \overbrace{\frac{g_S\mu_B}{c}\left[\sum_i^{n_e}\frac{Z_A e}{D_{Ai}^3}(\vec{X}_{Ai}\times\vec{v}_i/2)\cdot\vec{s}_i + \sum_i^{n_e}\frac{Z_B e}{D_{Bi}^3}(\vec{X}_{Bi}\times\vec{v}_i/2)\cdot\vec{s}_i\right]}^{\text{Direct spin-orbit interaction for each e}^-} \underbrace{-\frac{g_s\mu_B}{c}\sum_{i=j}^{n_e}\left[\frac{e}{d_{ij}^3}(\vec{x}_{ij}\times\frac{\vec{v}_i-\vec{v}_j}{2})\cdot\vec{s}_i\right]}_{\text{Interaction of the spin with another orbit}} \tag{1.28}$$

where c is the velocity of light, Z_A and Z_B the atomic number of A and B nuclei, e is the electron charge, $\vec{X}_{Ai}$, $\vec{X}_{Bi}$, D_{Ai} and D_{Bi} are the relative positions and the distances between the electron and the A nucleus and between the electron and the B nucleus, $\vec{x}_{ij}$ and $d_{ij}$are the relative positions and the distance between the electrons i and j, $\vec{v}_i$ is the electron velocity with respect to the center of mass of the nuclei, $g_s \approx 2$ is the Landé factor, $\vec{s}_i$ is the spin of the electron i and $\mu_B = e\hbar/2m_e c$ is the Bohr magneton, being m_e the mass of the electron. The electron velocity can be replaced by its linear momentum. Then, the vectorial product of the linear momentum and the relative positions is the orbital angular momentum ($\vec{l}_{Ai}$)

$$\vec{l}_{Ai} = \frac{1}{\hbar}(\vec{X}_{Ai}\times\frac{\vec{v}_i}{m_e}) \tag{1.29}$$

Now, the coupling term turns into

$$\hat{H}_{SO} = \frac{\alpha^2}{2}\sum_i^{n_e}\left[\frac{Z_A}{D_{Ai}^3}\vec{l}_{Ai}\cdot\vec{s}_i + \frac{Z_B}{D_{Bi}^3}\vec{l}_{Bi}\cdot\vec{s}_i\right] - \frac{\alpha^2}{2}\sum_{i=j}^{n_e}\left[\frac{1}{d_{ij}^3}\ \vec{x}_{ij}\times\frac{\vec{v}_i}{m_e}\ (\vec{s}_i+2\vec{s}_j)\right] \tag{1.30}$$

where $\alpha = e^2/\hbar c$.

In this equation, two different terms contribute to the spin orbit coupling: an interaction between the spin ($\vec{s}_i$) and the orbital angular momentum ($\vec{l}_{ij}$) , which is a monoelectronic operator, and a bielectronic interaction.

As it follows from this formula, there is a possibility to change the spin state of a molecule and it does not depend on an external field. Applying the same procedure as in the Born-Oppenheimer approximation, we can integrate the new Hamiltonian over the electronic coordinates resulting in

$$\begin{aligned}\left\langle\chi_\beta(R;x)|\hat{H}\sum_\alpha^N|\chi_\alpha(R;x)\right\rangle|\psi_\alpha(R,t)\rangle = \\ -\frac{\hbar^2}{2\mu}\frac{\partial^2}{\partial R^2}|\psi_\beta(R,t)\rangle + V_\beta(R)|\psi_\beta(R,t)\rangle + \sum_\alpha^N V_{\beta\alpha}(R)|\psi_\alpha(R,t)\rangle\end{aligned} \tag{1.31}$$

where the non-adiabatic transitions are neglected due to the variation of the wave function with the internuclear distance, $T^R_{\beta\alpha}(R) = T^{RR}_{\beta\alpha}(R) = 0$. Besides, $V_{\beta\alpha}(R) = \left\langle\chi_\beta(R;x)|\hat{H}_{SO}(R;x)|\chi_\alpha(R;x)\right\rangle$ represents the spin-orbit coupling integrated over the electronic coordinates for each value of the internuclear distance.

1.4 The complete time dependent Schrödinger equation

Once we have described all the individual physical phenomena of our interest, and which terms we must add to our Hamiltonian to study the system dynamics, we can obtain the complete TDSE

$$-\frac{\hbar}{i}\frac{\partial}{\partial t}|\psi_\beta(R,t)\rangle = \underbrace{V_\beta(R) - \frac{\hbar^2}{2\mu}\frac{\partial^2}{\partial r^2}\ |\psi_\beta(R,t)\rangle}_{\text{BO}} + \underbrace{\sum_\alpha^N [V_{\beta\alpha}(R) - \mu_{\beta\alpha}(R)\mathcal{E}(t)]|\psi_\alpha(R,t)\rangle}_{\text{diabatic crosses}} \tag{1.32}$$

Thus, we get a Born-Oppenheimer potentials equation, where the wave functions are eigenfunctions of $\hat{H}_e(R;x)$ for each nuclear configuration. In this equation, the potentials are coupled by two Hamiltonian terms: the external laser field $-\mu_{\beta\alpha}(R)\mathcal{E}(t)$ and the spin-orbit coupling $V_{\beta\alpha}(R)$.

In the next chapter we focus on the mathematical methods that allow us to numerically solve this equation.

Numerical Methods

Numerical tools: unravelling the equations that govern the system dynamics

From a theoretical point of view, the simulation of the control schemes demands solving the TDSE. Different numerical methods have been developped to that end [151]. In this chapter, we describe the numerical methods used in this thesis to characterize the interaction processes between light and matter. But first we have to consider some assumptions:

1. The effects of the matter over the laser are neglected (dispersion, attenuation...), in such manner we just consider the transitions in the molecule
2. The coupling is treated classically, that is, we work under the dipole approximation, which establishes that the wavelength of the type of electromagnetic radiation which induces, or is emitted during transitions between different atomic energy levels is much larger than the typical size of the system
3. The interaction is fully coherent, disregarding fluctuations in the pulse shape and phase and incoherent processes such as fluorescence and collisions.

Under these conditions the intramolecular dynamics is described by the time dependent Schrödinger equation. The way we solve this first order differential equation depends mainly on the basis we choose to represent the Hamiltonian of the system.

2.1 Wave function representation. Discretization on a grid

In this thesis, the wave function of the system is discretized on a grid. When ultrashort and strong pulses are involved, it is most convenient to work in coordinate grids, since

the wave function is typically localized in some vibrational modes. The eigenstates of the laser-free Hamiltonian (or the dressed states of the laser controlled Hamiltonian) are better suited to follow the dynamics of weaker, short-bandwidth pulses. We wish to replace the continuous range of coordinate values x by a grid of discrete values x_i. Using a uniform discrete grid of x values

$$x_i = i\Delta x \tag{2.1}$$

where Δx is the uniform spacing between the grid points. The discretization of the normalization integral for a wave function $\psi(x)$ (where $\psi(x)$ is $\langle x|\psi\rangle = \psi(x)$) on a regular grid of N values of x [eq. (2.1)] leads to

$$\sum_{i=1}^{N} \psi^*(x_i)\psi(x_i)\Delta x = 1, \tag{2.2}$$

or

$$\Delta x \sum_{i=1}^{N} |\psi_i|^2 = 1 \tag{2.3}$$

where $\psi_i = \psi(x_i)$.

The basic bras and kets of our discretized coordinate space give the value of the wave function at the grid points

$$\langle x_i|\psi\rangle = \psi(x_i) = \psi_i \tag{2.4}$$

As we will work also in the momentum representation, the selection of the grid in momentum space is defined by the imposed discretization in the coordinate space. Thus, the distance between grid points in the momentum space Δk is related to the spacing between grid points in the coordinate space Δx. The total length of the coordinate space covered by the grid is $N\Delta x$. This length determines the longest wavelength and therefore the smallest frequency, which occurs in the reciprocal momentum space

$$\Delta k = \frac{2\pi}{\lambda_{max}} = \frac{2\pi}{N\Delta x} \tag{2.5}$$

This relationship gives us the grid spacing in momentum space. The central point in the momentum space grid is taken as $k = 0$, and the grid points are evenly distributed about zero from $-k_{max} = -\frac{N-1}{2\Delta k}$ to $k_{max} = \frac{N-1}{2\Delta k}$.

The two alternative representations of a state function $|\psi\rangle$ on a discretized grid of

points either in coordinate space or in momentum space may be written as

$$|\psi\rangle = \sum_i |x_i\rangle \Delta x \psi(x_i) = \sum_i |x_i\rangle \psi_i^x \tag{2.6}$$

or

$$|\psi\rangle = \sum_i |k_i\rangle \Delta k \psi(k_i) = \sum_i |k_i\rangle \psi_i^k \tag{2.7}$$

The transformation between the two representations is computed efficiently by the fast Fourier transform [223]. This algorithm requires the number of grid points to be powers of 2 ($N = 2^n$) but it reduces the process from $O(N^2)$ (discrete Fourier transform) to $O(Nlog_2N)$ operations, therefore saving a huge computational time[1].

The uncertainty principle is conserved in a discretized grid when the Fourier transform method is applied [224]. Therefore, the minimum spacing between grid points Δx must be chosen in a way that the energy of the wave packet during the evolution remains below the maximum energy that can be represented in the grid. This energy is the sum of the maximum available potential energy, (V_{max}-V_{min}) and the maximum available kinetic energy, $T_{max} = \pi^2\hbar^2(\Delta x)^2/2m$ (being m the reduced mass of the system). On the other hand, the maximum spacing between grid points , $N\Delta x$, must be chosen considering that it provides the wave packet resolution in the momentum space.

2.2 Time independent Schrödinger equation

The need for solving the Schrödinger equation numerically arises from the description of the electronic structure. Conventional methods for determining the eigenvalues and eigenfunctions of the Schrödinger equation rely on the diagonalization of a Hamiltonian matrix or iterative numerical solutions of a time independent wave equation. Usually, a polynomial orthogonal basis is chosen $\phi_i(x)$, that provides a very fast and accurate evaluation of the matrix elements $H_{ij} = \int_{-\infty}^{\infty} \phi_i(x)\hat{H}\phi_j(x)\mathrm{d}x$. As an example, we can mention the FBR-DVR methods [225–228] (*Finite Basis Representation-Discrete Variable Representation*), which divide the Hamiltonian in two, $\hat{H} = \hat{H}_0 + \hat{V}$, so that the matrix elements are diagonal with respect to $\hat{H}_0$, while the integral with respect to $\hat{V}$ can be solved by a Gaussian quadrature [225, 226]. Finally, a standard algorithm [223] (Jacobi, Lanczos...) is used to diagonalize the resulting Hamiltonian matrix, obtaining

[1]There are other less efficient FFT algorithms with $O(NlogN)$ complexity for all N, even for prime N

the eigenvalues and eigenfunctions (over the polynomial basis $\phi_i(x)$).

Although the solution of the Schrödinger equation in the basis of Hamiltonian eigenfunctions is a computationally simple procedure, it is not very efficient when we need to consider a high number of states in the system dynamics, particularly when one works with strong or ultrashort fields, and the probability of dissociation or ionization (accesing the continuum) must be taken into account. In this case, is much more useful to solve the Schrödinger equation in a discretized positional basis, or a grid, where one can evaluate both bound and continuum states.

In this thesis, instead of this procedure, two different algorithms were used: the Fourier Grid Hamiltonian method, derived from the discrete Fourier transform algorithm, and the spectral method, based on the spectral properties of solutions of the time dependent Schrödinger equation.

In any case, once we obtain the Hamiltonian matrix by diagonalization, we need to integrate the Schrödinger equation, which requires the multiple evaluation of the product of the $\hat{H}$ matrix times the state vector. This last operation scales with N_1xN, where N_1 is the number of steps in the temporal integration and N is the basis dimension or spatial points. Furthermore, the first step implies the diagonalization of the matrix, which scales with N^3.

2.2.1 FGH method

The Fourier Grid Hamiltonian (FGH) method [204] is an accurate and simple variational procedure to compute eigenvalues and eigenfunctions of a Schrödinger equation. This method is derived from the discrete Fourier transform algorithm. Its implementation and use is extremely simple, requiring the evaluation of the potential only at equally spaced grid points, and yielding directly the amplitude of the eigenfunctions at the same grid points.

It relies on the fact that the Hamiltonian operator appearing in the Schrödinger equation is composed of the sum of a kinetic energy and a potential energy operator. The kinetic energy operator is best represented in the momentum space, as the basic vectors of this representation are eigenfunctions of both the linear momentum and the kinetic energy operators. On the other hand, the potential is best treated in the coordinate space in which it is diagonal. The transformation between these two representations is by Fourier transforms.

This method has the advantage of simplicity over other techniques. Particularly, the wave functions or eigenfunctions of the Hamiltonian operator are generated directly as

the amplitudes of the wave function on the grid points and they are not given as a linear combination of any set of basis functions. The accuracy of the method depends on the number of grid points and on the maximal radial distance considered to integrate the eigenvalue equation.

The wave function can be expressed in a spatial grid as it was explained in section 2.1. Wave functions of this basis set are not eigenfunctions of the Hamiltonian of the system, thus the evaluation of the Hamiltonian in this basis is not diagonal, though it is possible to obtain a linear combination of functions in this basis set, obtaining the eigenfunctions of the Hamiltonian as linear combination of the $|x\rangle$ basis.

Applying the Hamiltonian to this grid, the eigenfunctions are obtained as linear combinations in this grid just solving the eigenvalue equation. Thus, just evaluating $\langle x|\hat{H}|x\,\rangle$ we obtain the eigenenergies (E_n) as the eigenvalues of this matrix and the eigenvectors are the eigenfunctions expressed in the grid $\langle x|\phi_n\rangle = \phi(x_i) = \psi_i$.

Considering a single particle of mass m moving in one linear direction under the influence of a potential V, the non relativistic Hamiltonian operator $\hat{H}$ may be written as a sum of a kinetic energy and a potential energy operator

$$\hat{H} = \hat{T} + V(\hat{x}) = \frac{\hat{p}^2}{2m} + V(\hat{x}) \tag{2.8}$$

The corresponding coordinate representation of the Hamiltonian operator is given as follows

$$\langle x|\hat{H}|x\,\rangle = \langle x|\hat{T}|x\,\rangle + \langle x|\hat{V}|x\,\rangle \tag{2.9}$$

The basic vectors of this representation, $|x\rangle$, are eigenfunctions of the position or coordinate operator $\hat{x}$:

$$\hat{x}|x\rangle = x|x\rangle \tag{2.10}$$

The eigenfunctions of the momentum operator in the momentum representation are written as

$$\hat{p}|k\rangle = k\hbar|x\rangle \tag{2.11}$$

The orthogonality and completeness relationships in terms of these basic vectors are

$$\langle u|u\,\rangle = \delta(u - u\,) \tag{2.12}$$

and

$$\hat{I} = \int_{-\infty}^{\infty} |u\rangle\langle u| \, dx \tag{2.13}$$

being $u = x, k$, and the transformation matrix between the coordinate and momentum representation is

$$\langle k|x\rangle = \frac{1}{\sqrt{2\pi}} \mathrm{e}^{-ikx} \tag{2.14}$$

.

The potential is diagonal in the coordinate representation

$$\langle x|\hat{V}|x\,\rangle = V(x)\delta(x - x\,) \tag{2.15}$$

and the kinetic energy operator is diagonal in the momentum representation

$$\langle k|\hat{T}|k\,\rangle = T_k\delta(k - k\,) = \frac{\hbar^2 k^2}{2m}\delta(k - k\,) \tag{2.16}$$

.

Armed with this formulas and definitions, the Hamiltonian operator in the coordinate representation [eq. (2.9)] reads

$$\langle x|\hat{H}|x\,\rangle = \langle x|\hat{T}|x\,\rangle + V(x)\delta(x - x\,) \tag{2.17}$$

Inserting the identity operator [eq. (2.13)] to the right of the kinetic energy operator, one obtains

$$\begin{aligned} \langle x|\hat{H}|x\,\rangle &= \langle x|\hat{T}\{\int_{-\infty}^{\infty} |k\rangle\langle k|\}|x\,\rangle \, dk \; + V(x)\delta(x - x\,) \\ = \int_{-\infty}^{\infty} \langle x|k\rangle T_k \langle k|x\,\rangle \, dk \; + V(x)\delta(x - x\,) &= \frac{1}{2\pi}\int_{-\infty}^{\infty} \mathrm{e}^{ik(x-x')} T_k \, dk \; + V(x)\delta(x - x\,) \end{aligned} \tag{2.18}$$

This equation is at the heart of the FGH method. The exponential factor and the integral over k may be regarded as arising from a forward, followed by an inverse Fourier transform (FFT).

The FFT technique may be represented as a unitary matrix transformation between the coordinate and momentum grid representations of the state function (sec. 2.1). Denoting the matrix which represents the forward FFT by F, we can write

$$\psi^k = F\psi^x \tag{2.19}$$

where ψ^k and ψ^x are column vectors.

Defining a column vector ϕ_n which is composed entirely of zeros except for a single element of unity in the nth row

$$\begin{pmatrix} 0 \\ 0 \\ . \\ . \\ 1 \\ . \\ . \\ 0 \end{pmatrix} \leftarrow \text{nth row} \tag{2.20}$$

We may now use this vector, together with a forward and reverse fast Fourier transformation, to obtain the nth column of the Hamiltonian matrix H^0

$$H^0_{in} = [(F^{-1}TF + V)\phi_n]_i, \tag{2.21}$$

where T and V are the diagonal kinetic energy and potential energy $[V(x_i)]$ matrices. By repeating this process for all the possible N vectors ϕ_n, one can generate the complete matrix H_0.

A limitation of this method, specially when its generalization to many mathematical dimensions is considered, is the high order of matrices which must be diagonalized. The FGH method involves the use of matrices of order (N x N), where N is the number of grid points used. In one dimension, this does not constitute a problem, but for $N > 2$ the computational time required increases as N^2.

2.2.2 Spectral Method

The spectral method [229] is based on the spectral properties of solutions to the time dependent Schrödinger equation. It requires computation of the time dependent autocorrelation function

$$\xi(t) = \big\langle \psi(x,0) | \psi(x,t) \big\rangle, \tag{2.22}$$

where $\psi(x,t)$ represents a numerical solution to the time dependent Schrödinger

equation, and $\psi(x,0)$ is the wave function at $t=0$. The solution of $\psi(x,t)$ can be accurately calculated by applying the Split Operator method (see sec. 2.3.1). The numerical Fourier transform of $\xi(t)$, i.e., $\xi(E)$, displays a set of sharp maxima for $E=E_n$, where E_n are the desired eigenvalues. Once the eigenvalues are known, the corresponding eigenfunctions can be computed by numerically evaluating the integrals

$$|\phi_k\rangle = \int_0^t \mathrm{e}^{\frac{iE_k t}{\hbar}} dt |\psi(x,t)\rangle \approx \Delta t \sum_t \mathrm{e}^{\frac{iE_k t}{\hbar}} \sum_j^N \underbrace{\mathrm{e}^{-\frac{i}{\hbar} l\delta t E_j}}_{c_j(t)} |\phi_j\rangle \tag{2.23}$$

With a new propagation, one can filter the desired wave function ϕ_k. Unless there were degenerated wave functions, the components of $\psi(x,t)$ different from ϕ_k quickly disappear, remaining just the desired wave function.

An attractive feature of this method is that it allows the eigenvalue spectrum to be displayed graphically and the energy levels to be identified visually as they would be an experimental spectrum. Since the lineshapes for the theoretical spectrum are known, it is also possible to characterize the spectrum quantitavely.

The spectral method is in principle applicable to any linear eigenvalue problem [230] and to problems involving any number of dimensions. The only requirement is an available numerical solution for the time dependent wave function (or other dependent variable) specified on a suitable coordinate grid. The high accuracy of the Split Operator method [205] makes it particularly attractive for application with the spectral method to the Schrödinger equation in Cartesian coordinates.

Matrix diagonalization is attractive for treating Hamiltonians that do not differ greatly from Hamiltonians with known eigenfunctions or for potentials with simple analytic forms, which permit setting up the Hamiltonian matrix without excessive computation. However, the spectral method becomes essential when a large amount of computation is required to set up the Hamiltonian matrix or, in general, when the required Hamiltonian matrix is of high order. The iterative numerical integration methods are known to give very accurate results for one-dimensional problems. To apply them, it is necessary to home in on the individual eigenvalues before the cycle of iterations is begun, both to reduce the number of iterations and to assure that no eigenvalues are missed [231]. While this poses no problem in principle, it can lower the efficiency in situations where information on the eigenvalue spectrum is limited.

The spectral method is specially advisable when starting from an approximation of the eigenfunctions, for example, an eigenfunctions of H_0 computed by the FGH method, and we want to calculate the solution when a perturbation is included.

2.3 Time dependent Schrödinger equation

Since the main purpose of this thesis is to control the electron dynamics, it is important to perfectly characterize the evolution of the electronic wave packet.

The electron motion is represented by the time dependent Schrödinger equation (TDSE) [eq. (1.1)].

In the coordinates representation and considering one dimension, the Hamiltonian implies second order partial derivatives and a potential that will also depend on time,

$$\hat{H} = -\frac{\hbar^2}{2m}\frac{\partial^2}{\partial x^2} + V(x,t) \tag{2.24}$$

Traditionally, the solution of this equation lies in dividing the differential equation and first solving the time independent Schrödinger equation (sec. 2.2). Once the Hamiltonian eigenvalues are known, the temporal part can be solved immediately. However, when the potential is coupled with a time dependent external field, it is impossible to separate the initial differential equation, except if perturbation theory is applied. Another possibility is to diagonalize the Hamiltonian each time step (so that the basis depends on time) and assume the adiabatic approach [213]. But this method implies excessive computation.

On the other hand, it is possible to start from the general differential equation in the coordinates representation and discretize either the spatial and temporal variable in a grid, and then apply the Crank-Nicholson algorithm [232].

Finally, a third possibility deals with focusing on the temporal variable, so the Schrödinger equation can be solved as a propagator. The use of time dependent methods allows the system to be described by the dynamics of an always-squared-integrable wave packet. Thus problems involving ionization can be studied in the same straightforward manner as problems involving purely bound-state processes.

Regarding this third possibility, it follows from the Schrödinger equation that the evolution of the wave function within an infinitesimal time increment Δt is described by the unitary operator $\mathrm{e}^{(-\frac{i}{}tH(t)\Delta t)}$:

$$\Psi(x, t+\Delta t) = \mathrm{e}^{-\frac{i}{}\hat{H}(t)\Delta t}\Psi(x,t) \tag{2.25}$$

where the exponential term is called *time evolution operator* or *propagator*. Now, the problem becomes that of a differential equation with initial conditions. Starting from $\Psi(x,t_0)$ the propagator lead us to obtain $\Psi(x,t)$ at each differential time step.

We turn now to the question of the numerical implementation of $\mathrm{e}^{-\frac{i}{}\hat{H}(t)\Delta t}$. There

are three basic strategies for doing this. The first is the straightforward method of using the approximate eigenvalues and eigenvectors of $\hat{H}$ to propagate. The main drawback of this approach are that it is limited to time-independent Hamiltonians and it requires the construction and diagonalization of the Hamiltonian matrix, the latter scaling as N^3. The second approach is to retain the exponent structure of the propagator, but to approximate the propagator as a product of a kinetic and potential factor [229]:

$$e^{\hat{H}} = e^{-\frac{i}{}(\frac{\hat{p}^2}{2m}+V(x))\Delta t} \approx e^{-\frac{i}{}\hat{T}\Delta t}e^{-\frac{i}{}\hat{V}\Delta t} \tag{2.26}$$

This approach is called the Split Operator method, and explicitly preserves unitarity.

The third major strategy is to consider $e^{(-\frac{i}{}\hat{H}(t)\Delta t)}$ as a function of the Hamiltonian, that is, $f(H)$, and look for a suitable polynomial approximation to this function [233, 234]:

$$e^{\hat{H}} = \sum_{n=0}^{N} c_n P_n(H) \tag{2.27}$$

where $P_n(H)$ is some polynomial of the Hamiltonian operator. Once a polynomial sequence is chosen, the c_n are uniquely determined. Polynomial methods can be divided into two categories: those that choose the polynomial in advance, such as the Chebyshev method [235] in which the Hamiltonian must be time independent, and those that do not, for example the Short Iterative Lanczos propagator [236].

In this thesis, the TDSE was always solved by the Split Operator method, which will be detailed in the next section.

2.3.1 Split Operator method

The Split-Operator method is one of the simplest and most popular methods for time propagation of wave packets [53, 229, 237].

The method begins by representing the propagator over the global time interval $[0, t]$ as a product of propagators over short time intervals, Δt, where $N\Delta t = t$. Thus,

$$U(t,0) = e^{-\frac{it}{}\hat{H}} = \underbrace{e^{-\frac{i\Delta t}{}\hat{H}}e^{-\frac{i\Delta t}{}\hat{H}}...e^{-\frac{i\Delta t}{}\hat{H}}}_{\text{N times}} \tag{2.28}$$

The strategy is then to approximate each short time propagator as a product of a kinetic factor and a potential factor, according to the Trotter product formula:

$$e^{-\frac{i\Delta t}{}\hat{H}} = e^{-\frac{i\Delta t}{}(\frac{\hat{p}^2}{2m}+V(x))} \approx e^{-\frac{i\Delta t}{}\hat{T}}e^{-\frac{i\Delta t}{}V(x)} + O(\Delta t^2) \tag{2.29}$$

In this way, the kinetic factor is evaluated in the momentum representation where it is diagonal, and the potential exponential is calculated in the coordinates representation, being this factor diagonal in this space as well.

If we define F as a unitary matrix of transformation between the coordinate and momentum representation

$$\mathrm{e}^{-\frac{i\Delta t}{}T}\mathrm{e}^{-\frac{i\Delta t}{}V} = FF^{\dagger}\mathrm{e}^{-\frac{i\Delta t}{}T}FF^{\dagger}\mathrm{e}^{-\frac{i\Delta t}{}V} = F\mathrm{e}^{-\frac{i\Delta t}{}F^{\dagger}TF}F\mathrm{e}^{-\frac{i\Delta t}{}V} \tag{2.30}$$

one can evaluate each exponential in the representation where the operators are diagonal. Therefore, the factorization let us use all the advantages that come from the Fourier method, as it was explained before.

However, note that the product in eq. (2.29) would be exact if T and V commuted; we expected the error, therefore, to be proportional to the commutator $[T, V]$.

It is easily verified that the factorization in two exponentials is a very poor approximation of the propagator. If the exponentials are expanded, with $\alpha = -\frac{i\Delta t}{\hbar}$

$$\begin{aligned}\mathrm{e}^{\alpha H} =& 1 + \alpha(V+T) + \frac{\alpha^2}{2}(V^2 + VT + TV + T^2) + ...\mathrm{e}^{\alpha T}\mathrm{e}^{\alpha V} \\ &= 1 + \alpha(V+T) + \frac{\alpha^2}{2}(V^2 + T^2 + 2TV) + ...\end{aligned} \tag{2.31}$$

where the difference is

$$\zeta(\alpha^2) = \frac{\alpha^2}{2}[V, T] + O(\alpha^3). \tag{2.32}$$

Hence, the error depends on the commutator $[T, V]$ (the potential includes the coupling with the laser field) and it is a second order error in Δt. However, the leading order error can be eliminated by forming a symmetrized product of the kinetic and potential factors:

$$\mathrm{e}^{-\frac{i\Delta t}{}H} \approx \mathrm{e}^{-\frac{i\Delta t}{2}V}\mathrm{e}^{-\frac{i\Delta t}{2}T}\mathrm{e}^{-\frac{i\Delta t}{2}T}\mathrm{e}^{-\frac{i\Delta t}{2}V} + O(\Delta t^3) = \mathrm{e}^{-\frac{i\Delta t}{2}V}\mathrm{e}^{-\frac{i\Delta t}{}T}\mathrm{e}^{-\frac{i\Delta t}{2}V} + O(\Delta t^3) \tag{2.33}$$

where $\zeta = \frac{i^3\Delta t^3}{24\hbar^3}[2T + V, [T, V]] + O(\Delta t^4)$. This third order error depends on a double commutator. This propagator was first introduced by Feit and Fleck [229].

It is worth noting that the Split Operator method is not limited to the Fourier basis, in fact it can be used with other spectral methods provided that the Fourier Transform is replaced by the corresponding pseudospectral $\leftrightarrow$ spectral transformation matrix. The Split Operator method is manifestly unitary, and is recommended whenever

the Hamiltonian can be written as a sum of operators that depend on coordinates and operators that depend on the momenta. However, the method can not handle operators that mix coordinates and momenta, such as an operator of the form $e^{i\hat{p}\hat{x}}$.

As an example, a simple model of spin-orbit coupling (sec. 1.3) is used in order to get a better insight of this method. We start the dynamics from an initially populated singlet potential $[V_1(x)]$ strongly coupled to a triplet potential $[V_2(x)]$. Applying the dynamic Stark effect as a tool to influence the dynamics of the system, we employ a laser pulse $\mathcal{E}(t)$ which couples $V_2(x)$ with another triplet potential $[V_3(x)]$ by means of a non-zero dipole transition moment, $\mu_{23} \neq 0$.

Following this model the wave function can be written as

$$|\psi(x,t)\rangle = \begin{pmatrix} \sum_i^N c_{i,1}(t)|x_i\rangle \\ \sum_i^N c_{i,2}(t)|x_i\rangle \\ \sum_i^N c_{i,3}(t)|x_i\rangle \end{pmatrix} \xrightarrow{FT} \begin{pmatrix} \sum_i^N d_{i,1}(t)|k_i\rangle \\ \sum_i^N d_{i,2}(t)|k_i\rangle \\ \sum_i^N d_{i,3}(t)|k_i\rangle \end{pmatrix} = |\psi(k,t)\rangle \tag{2.34}$$

where the second index is the Born-Oppenheimer potential which the coefficient belongs, as the grid is defined equally for the potentials $V_1(x)$, $V_2(x)$ and $V_3(x)$.

The kinetic term reads

$$\hat{T} = -\frac{\hbar^2}{2\mu} \begin{pmatrix} \partial^2/\partial x^2 & 0 & 0 \\ 0 & \partial^2/\partial x^2 & 0 \\ 0 & 0 & \partial^2/\partial x^2 \end{pmatrix} = \frac{1}{2\mu} \begin{pmatrix} \hat{p}^2 & 0 & 0 \\ 0 & \hat{p}^2 & 0 \\ 0 & 0 & \hat{p}^2 \end{pmatrix} \tag{2.35}$$

and the potential term $V(x,t)$ is

$$V(x,t) = \begin{pmatrix} V_1(x) - \mu_{11}(x)\mathcal{E}(t) & V_{SO} & 0 \\ V_{SO}^* & V_2(x) - \mu_{22}(x)\mathcal{E}(t) & -\mu_{23}(x)\mathcal{E}(t) \\ 0 & -\mu_{23}(x)\mathcal{E}(t) & V_3(x) - \mu_{33}(x)\mathcal{E}(t) \end{pmatrix} \tag{2.36}$$

where the spin-orbit coupling $[V_{SO}(x)]$ allows the population transfer between the singlet and triplet and the transition between the triplets is achieved by means of the laser field.

Evaluation of the potential term

As it was previously described, the potential and kinetic terms are evaluated separately. In the SO method the first and third steps are common, so they are jointly explained.

We need to evaluate the exponential factor

$$\mathrm{e}^{-\frac{i}{2}\frac{\Delta t}{2}V(x,t)}|\psi(x,t)\rangle \tag{2.37}$$

To this aim the potential matrix must be diagonalized

$$\mathrm{e}^{-\frac{i}{2}\frac{\Delta t}{2}W(x,t)} = R(x,t)^{\dagger}\mathrm{e}^{-\frac{i}{2}\frac{\Delta t}{2}V_d(x,t)}R(x,t) \tag{2.38}$$

where $R(x,t)$ is the diagonalization matrix of $V(x,t)$ and $V_d(x,t)$ is the diagonal eigenvalue matrix.

Now one can represent $\mathrm{e}^{-i\Delta t V_d(x,t)/2\hbar}$ as

$$\begin{pmatrix} \mathrm{e}^{-\frac{i}{2}\frac{\Delta t}{2}U_1(x,t)} & 0 & 0 \\ 0 & \mathrm{e}-\frac{i}{\hbar}\frac{\Delta t}{2}U_2(x,t) & 0 \\ 0 & 0 & \mathrm{e}^{-\frac{i}{2}\frac{\Delta t}{2}U_3(x,t)} \end{pmatrix} \tag{2.39}$$

resulting

$$|\psi^V(x,t)\rangle = \underbrace{R(x,t)\mathrm{e}^{-\frac{i}{2}\frac{\Delta t}{2}V_d(x,t)}R^{\dagger}(x,t)}_{U_W(x,t)}|\psi(x,t)\rangle \ , \tag{2.40}$$

where we have defined $U_W(x,t)$ as the propagator corresponding the potential term of the split operator.

Evaluation of the kinetic term

As it was explained in section 2.1, the wave function can be represented in the momentum space applying the Fourier transform, where it is diagonal.

Starting from $|\psi^V(x,t)\rangle$ we obtain $|\psi^V(x,t)\rangle$, which is diagonal in $\hat{p}$:

$$|\psi^V_\alpha(x,t)\rangle \xrightarrow{FT} |\psi^V_\alpha(k,t)\rangle = \sum_i^N d_{i,\alpha}|k_i\rangle \tag{2.41}$$

where α represent the considered potential [eq. (2.34)].

In this representation, it is easy to evaluate the exponential of the kinetic term

$$\underbrace{\mathrm{e}^{\frac{1}{2\mu}\hat{p}^2}\sum_{i}^{N} d_{i,\alpha}|k_i\rangle}_{|\psi_\alpha^V(k,t)\rangle} = \underbrace{\sum_{i}^{N} \mathrm{e}^{\frac{1}{2\mu}\overbrace{i^2\,{}^2\Delta k^2}^{\hat{p}^2}} d_{i,\alpha}|k_i\rangle}_{|\psi_\alpha^{TV}(k,t)\rangle} \tag{2.42}$$

Applying the inverse Fourier transform we obtain again the wave function in the coordinates space

$$|\psi_\alpha^{TV}(k,t)\rangle \xrightarrow{FT^{-1}} |\psi_\alpha^{TV}(x,t)\rangle \tag{2.43}$$

2.4 Absorbing boundaries

In the numerical simulation of wave packet propagation by spatially discrete methods, there is always a need to eliminate artificial events which are generated by the boundaries of the numerical grid. These events arise because the numerical mesh covers a finite region of space. Frequently, the numerical grid can not be made large enough to contain the whole wave function as it spreads over time. In particular, this is so when we deal with ionization in strong fields. Within a few optical cycles, the extension of the electronic wave function easily reaches several hundred atomic units. Numerically, wave packets reaching the grid boundary must be absorbed. Otherwise, a "ghost" wave packet reenters on the opposite side of the grid since the numerical Fourier transformation effectively imposes periodic boundary conditions. In propagation techniques other than the Split-Operator method, one usually has to specify the boundary conditions explicitly. In that case, the absence of an absorber typically leads to reflection. These events are always extraneous to the real physical events under study so that their elimination is desirable.

There exist many absorbing boundaries to choose, to avoid the problem of reflection [238, 239]. In this thesis, we use complex ("optical") potentials.

Absorbing boundaries have been employed by a number of workers, mostly by those carrying out time dependent wave packet calculations on a coordinate grid. Neuhauser and Baer successfully applied a negative imaginary potential (NIP) for enforcing the outgoing boundary condition in the case of reactive scattering [240, 241]. The efficiency of the absorbing potential was found to increase when it was complex rather than imaginary. The complex absorbing potential (CAP) concept draws attention from researchers owing to its very simple implementation. In a grid representation, to generate a CAP,

a complex potential is simply added to the Hamiltonian.

CAP has successfully and efficiently been used for the calculation of the electronic resonances in atomic and molecular systems [242–246] and for wave packet propagation [243, 247]. CAP was also used in the time dependent treatment of reactive scattering to calculate the reaction probabilities [240, 241, 248, 249].

The ideal absorbing potential would absorb perfectly all incident momenta and be numerically robust with respect to the discretization of the coordinates. In practice it is also desirable that its form is either explicit or, at least, easy to obtain, and that the values of the parameters of the functional form are optimized with minimal effort. The absorbing boundaries prevent parts of the wave packet approaching to the edge of a numerical grid from unphysical reflection back toward the interaction region that deteriorate the quality of the computed solution. However, the CAP method, due to its nonphysical nature, leads to artificial perturbations of the system and may cause a shift in the energy [250]. The conditions and limitations are that one wants to turn it on sufficiently rapidly to absorb the flux over in a short distance as possible, but not to turn on sharply enough to cause reflection back toward the physically relevant region or space. In spite of these problems, the CAP method stands out because of its straightforward and simple applicability. The CAP is zero in the interaction region and "turns on" in the region where there is no interaction. The absorbing boundary attenuates the asymptotic part of the wave packet and, hence, suppresses the reflection.

In our calculations, some absorbing boundaries were tested and between the available methods we chose the most efficient one, i.e., the method offering the smallest reflection for the smallest width of the absorption zone. Our complex absorbing potential was selected from a work of Monnerville et al. [251] In a one-dimensional grid extending from $-x_0$ to $+x_0$, this optical potential has the form

$$V(z) = \begin{cases} -i\frac{\eta}{2}\left\{1+\sin\left[\pi\left(-\frac{1}{2}+\frac{x+x_1}{x_1-x_0}\right)\right]\right\} & , \quad -x_0 \le z \le -x_1 \\ 0 & , \quad -x_1 \le x \le +x_1 \\ -i\frac{\eta}{2}\left\{1+\sin\left[\pi\left(-\frac{1}{2}+\frac{x-x_1}{x_0-x_1}\right)\right]\right\} & , \quad x_1 \le x \le x_0 \end{cases} \tag{2.44}$$

where η is a parameter chosen to maximize the absorption for a wave packet. Using eq. (2.44), the wave function in the regions $[-x_0, -x_1]$ and $[x_1, x_0]$ is effectively multiplied by $\mathrm{e}^{(V_{opt}(x))}$ in each time step. This CAP can be also extended to a two-dimensional grid by applying the same function to the second coordinate. Parameters have to be chosen

with care, if not, on one hand, the wave packets could be entirely absorbed before they run into the boundary. On the other hand, a part of the wave function could be reflected.

2.5 Quasiprobability distributions

Quasi-probability distribution functions are known to play an important role in the study of quantum-classical transition properties of quantum dynamical systems [252, 253]. Their usefulness stems from the fact that they provide a re-expression of quantum mechanics in terms of classical concepts so that quantum mechanical expectation values are now expressed as averages over phase-space distribution functions. In other words, statistical information is transferred from the density operator to a quasi-classical (distribution) function. Although it is possible to get all the information about the dynamics of the quantum system by examining its properties in the position or momentum representations, to fully understand the dynamics is often advantageous to use the phase-space information. To this end only the quasi-probability distribution functions are helpful, because the phase space in the quantum approach is constructed through them. The first definition of the quasi-probability distribution functions in the quantum approach was developed in the 1930s, when the Wigner function was proposed to study quantum corrections in classical statistical mechanics [254]. It has been widely used as a tool for analysis [255–257].

The Wigner function in terms of momentum p and position x is determined as follows:

$$F_W(x,p) = \frac{1}{\pi\hbar}\int_{-\infty}^{\infty} \psi^*(x+y)\psi(x-y)\mathrm{e}^{2ipy/\hbar}\mathrm{d}y \tag{2.45}$$

where ψ is the wave function and x and p are the position and momentum, but could be any other conjugate variable pair. It is symmetric in x and p,

$$F_W(x,p) = \frac{1}{\pi\hbar}\int_{-\infty}^{\infty} \phi^*(p+q)\phi(p-q)\mathrm{e}^{-2ixq/\hbar}\mathrm{d}q \tag{2.46}$$

where ψ is the Fourier transform of ϕ. It is bounded by the restriction $|F_W(p,x)| \leq (\pi\hbar)^{-1}$, which means that such a function generally takes both negative and positive values. Because of this one often uses smoothing funtions in order to define some class of completely positive joint probability functions of the following form. Using a Gaussian filter:

$$\bar{F}(p,x) = \frac{1}{\pi\hbar}\int_{-\infty}^{\infty}\int_{-\infty}^{\infty} \exp\ \ -\frac{q^2}{2\Delta_p^2} - \frac{y^2}{2\Delta_x^2}\ \ F_W(p+q, x+y)\mathrm{d}q\mathrm{d}y \geq 0 \tag{2.47}$$

Here, $\Delta_p\Delta_x$ defines a finite region in the phase space. Choosing some value for this definition, one can obtain a Gaussian smoothing of the Wigner function. The simplest way corresponds to the value $\Delta_p\Delta_x = \hbar/2$. Then eq. (2.47) is known as the Husimi function [258] of the form:

$$F_H(p,x) = \frac{1}{(2\pi)^{3/2)}\hbar\Delta_x}\ \left|\int_{-\infty}^{\infty}\psi(y)\mathrm{e}^{-\frac{ipy}{}-\frac{(x-y)^2}{4}\Delta_x^2}\mathrm{d}y\right|^2 \tag{2.48}$$

Unlike the Wigner quasi-distribution function, the Husimi quasi-distribution function is bounded by the restriction $0 \leq F_H(p,x) \leq (\pi\hbar)^{-1}$. In other words, one observes from this restriction that it takes only positive values, therefore it represents a distribution function rather than a quasi-distribution one. The Husimi distribution can be interpreted as the probability distribution obtained from simultaneous optimal measurement of coordinate and momentum, which are canonically conjugated variables. Although it has been demonstrated that the Husimi function can be clearly separated into two measurements of the position and momentum, and these measures can be easily realized in the situation close to the experiment [259], it is well known that the knowledge of the exact quantum mechanical probability distributions both for coordinate and momentum does not supply enough information to determine, in a unique way, a quantum state which has such probability distributions of coordinate and momentum.

The Husimi distribution is employed to describe systems in different areas of physics such as Quantum Mechanics, Quantum Optics, Information Theory [260–264]. Additionally, in nanotechnology it is possible to obtain a clear description of localization –which corresponds to classicality– and is crucial to determine correctly the size of systems when the particle dynamics takes into account mobility boundaries [265].

In this thesis, Husimi distributions are used to provide a two-dimensional picture of a one-dimensional wave function, to compare them directly with classical phase space distributions, and to decide which mechanism provides a better understanding of the behaviour of the studied system.

2.6 Hamiltonian models: reduced dimensionality

The interaction of strong laser pulses with atoms and molecules requires handling of many-body processes and non-perturbative dynamics, which both pose difficult theoretical and computational problems. One of the theoretical approaches to deal with this non-perturbative problem relies on exact numerical solutions of the time dependent Schrödinger equation (TDSE) on available supercomputers [41, 266, 267]. The computational requirements are obviously dependent on the complexity of the model. The use of realistic (e.g. ab initio) electronic potentials is specially difficult because computationally it is very time-consuming to calculate the electronic potentials and dipole moments of excited states, and not many data are available. In many applications, the problem has been simplified by reducing the number of spatial dimensions.

When dealing with the nuclei, if we are primarily interested in the dynamics on the femtosecond and attosecond time scale, we can assume the rotational motion is almost frozen as the molecular rotations occur on the picosecond time scale. This might not be true for small molecules such as H_2, but in this case, experiments and theory indicate that the molecules become aligned with the laser polarization axis [268–271]. If one uses a sufficiently intense laser pulse, it is possible to replace the random angular distribution of a gas-phase molecular sample by a distribution that is strongly aligned, that is, to create a situation where the molecules are oriented in space, with their axes along the polarization vector of the laser. In species with no permanent dipole moment, this effect is mediated by the interaction of the electric field of the laser with the induced dipole in the molecule. Hence, for a diatomic molecules, it seems that a one-dimensional (1D) treatment of the nuclei, including vibration but no rotation, should be able to qualitatively account for the experimental situation.

For electrons we argue differently. As we are interested in strong fields, the electrons are heavily accelerated. If we just employ linearly polarized light, we can expect that the electrons will move along the direction of polarization.

Although the commonly used approach of solving first the electronic problem to obtain the potential energy surfaces (PES) and coupling elements and afterwards treating the nuclear wave packet motion is, in principle, exact (if one also considers scattering states), some information is not easily obtained in such a way. This, in particular, applies to properties of the electronic part of the total wave function. Therefore it is desirable to not only follow the dynamics of the nuclei but, simultaneously, characterize the electronic motion thereby gaining insight into situations where the adiabatic separation either applies or not. This requires solving the TDSE for the complete electronic

and nuclear problem. This task is computationally far too demanding and, for the time being, restricted to the treatment of systems of a few particles only. The problem of how to include non-adiabatic couplings in a numerical scheme, normally carried out through by employing some method of diabatization [272, 273], vanishes completely if the electronic and nuclear degrees of freedom are treated at the same level. Several model studies limited to a co-linear particle configuration and screened Coulomb interactions have been presented, where the quantum mechanical equations of motion are solved numerically for the electrons and nuclei simultaneously to describe multiphoton processes occurring in strong laser field [266, 274–276]. In order to study electronic and nuclear quantum dynamics, treating all particles on the same footing, it is advantageous to find models which are, on one hand, simple enough to be computationally tractable and, on the other hand, contain all the physics of a coupled electronic and nuclear dynamics.

Rather than using a realistic Hamiltonian for a particular system, in our work we use a very generic model based on the Shin-Metiu model (sec. 2.6.2), in such a way that the transition from a Born-Oppenheimer adiabatic dynamics to motions involving strong non adiabatic coupling can be studied systematically [13, 14, 277, 278]. Additionally, to study charge transfer processes in small molecules, the soft-core Coulomb potential is used to describe the system (sec. 2.6.3).

2.6.1 The Shin-Metiu model

The useful two-dimensional model was first introduced by Shin and Metiu to study charge-transfer in solids [206,207]. Within this model system it is possible to characterize the coupled motion of the nucleus and the electrons simultaneously. The electron-nucleus interaction is parameterized in such a way as to allow for an easy transition from an adiabatic (Born-Oppenheimer type) behaviour to a situation where the motion of the particles is strongly coupled.

The Shin-Metiu model system (fig. 2.1) consists of three ions and one electron arranged in a line: two ions are fixed and the third ion and the electron are allowed to move on the internuclear axis. The masses of the ions are chosen to be that of a proton, while all charges are set to $Z = +1$, respectively. The system has two degrees of freedom: the position of the nucleus R and the position of the electron x.

The interaction of the electron with the nuclei is parameterized in the form of "screened" Coulomb interactions. The Hamiltonian of the full system then takes the form (in a.u.)

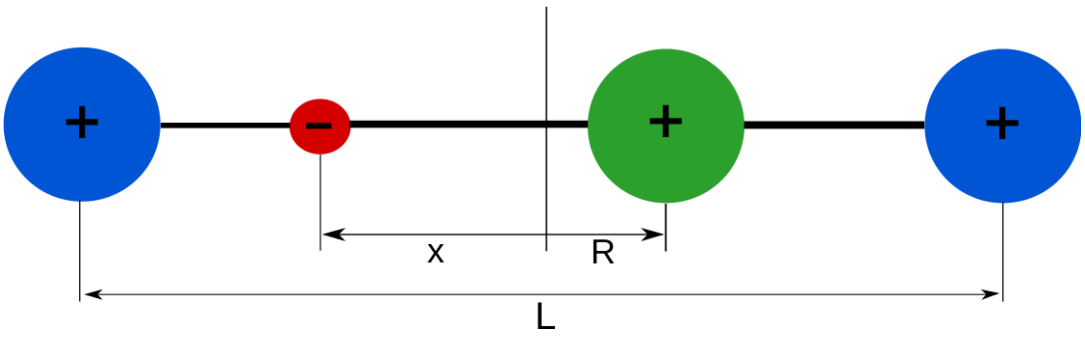

Figure 2.1: A schematic representation of the Shin-Metiu model. An ion (green solid circle) and a electron (in red) are confined to move on the line joining two identical positive ions (blue solid circles) that are held fixed at a distance L [206].

$$\hat{H}(x,R) = -\frac{1}{2}\frac{\partial^2}{\partial x^2} - \frac{1}{2m}\frac{\partial^2}{\partial R^2} + V(x,R) \tag{2.49}$$

with the ion mass m, which is taken as the proton mass. The particle interactions are of the form

$$\begin{aligned} V(x,R) = &\frac{1}{|R_1 - R|} + \frac{1}{|R_2 - R|} + -\frac{\mathrm{erf}(|R_1 - x|/R_f)}{|R_1 - x|} \\ &- \frac{\mathrm{erf}(|R_2 - x|/R_f)}{|R_2 - x|} - \frac{Z\mathrm{erf}(|R - x|/R_c)}{|R - x|} + E_0 \end{aligned} \tag{2.50}$$

In the expression for the potential energy all electron-nuclei interactions are cut off with error functions (erf). The value of E_0 was chosen such that the global minimum of the full potential was zero in all regarded cases. R_1 and R_2 denote the positions of the fixed ions. The parameter R_f which appears in the interaction between the electron and stationary ions was taken to be $1.5\mathring{A}$. The interaction with the moving ion was determined by different values of the parameter R_c, that generates a variety of potential energy surfaces for the moving ion. The system has two wells, one in which the moving ion is bound to the fixed ion on the left (1) and the other in bound to the right. The properties of the system can be varied by changing the energy gap between the electron and the moving ion. This changes the barrier of the lowest adiabatic states and the energy gap between the ground and the first excited adiabatic states. The distance between the fixed ions can be used as an additional parameter.

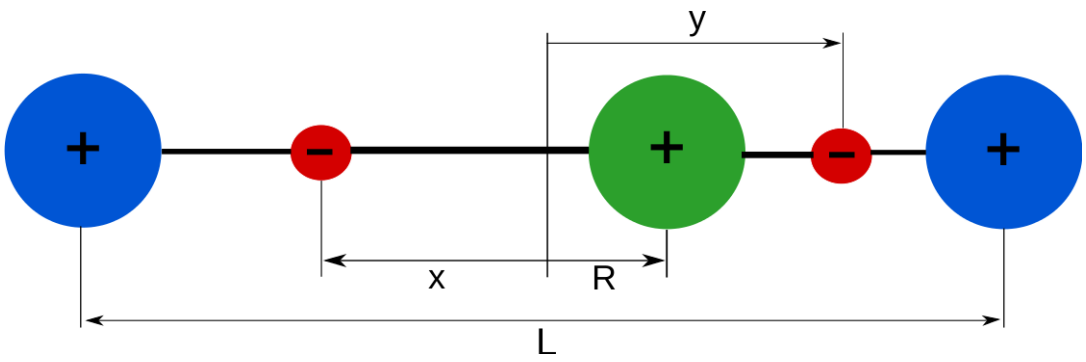

Figure 2.2: Particle configuration in the extended Shin-Metiu model, consisting of a mobile positive ion (green) and two electrons (red) confined to move in a single dimension between two fixed positive ions (in blue). This model allows to characterize the coupled nuclear and electronic motion simultaneously [279].

2.6.2 The extended Shin-Metiu model

Volker Engel proposed the first extension of the original SM model to include three degrees of freedom (3D) for a proton and two collinear electrons moving between two fixed ions [279]. In this work, we further generalize the model to allow transitions between the singlet and triplet components of the electronic wave function.

The extended Shin-Metiu model (ESM) consists of an ion (coordinate R) and two electrons (coordinates x,y) being confined to move in a single dimension. As in the original model these particles interact with each other and two additional fixed ions through screened Coulomb interactions. Figure 2.2 sketches the particle configuration.

The Hamiltonian of the full system now takes the form (in a.u.):

$$\hat{H}(x,y,R) = -\frac{1}{2}\frac{\partial^2}{\partial x^2} - \frac{1}{2}\frac{\partial^2}{\partial y^2} - \frac{1}{2m}\frac{\partial^2}{\partial R^2} + V(x,y,R) \tag{2.51}$$

with the nuclear mass m, which is taken as the proton mass. The potential energy is given as

$$\begin{aligned} V(x,y,R) = {} & \frac{Z_1 Z}{|R_1 - R|} + \frac{Z_2 Z}{|R_2 - R|} + \frac{\mathrm{erf}(|x-y|/R_e)}{|x-y|} \\ & - \frac{Z_1 \mathrm{erf}(|R_1 - x|/R_f)}{|R_1 - x|} - \frac{Z_2 \mathrm{erf}(|R_2 - x|/R_f)}{|R_2 - x|} - \frac{Z \mathrm{erf}(|R - x|/R_c)}{|R - x|} \\ & - \frac{Z_1 \mathrm{erf}(|R_1 - y|/R_f)}{|R_1 - y|} - \frac{Z_2 \mathrm{erf}(|R_2 - y|/R_f)}{|R_2 - y|} - \frac{Z \mathrm{erf}(|R - y|/R_c)}{|R - y|} \end{aligned} \tag{2.52}$$

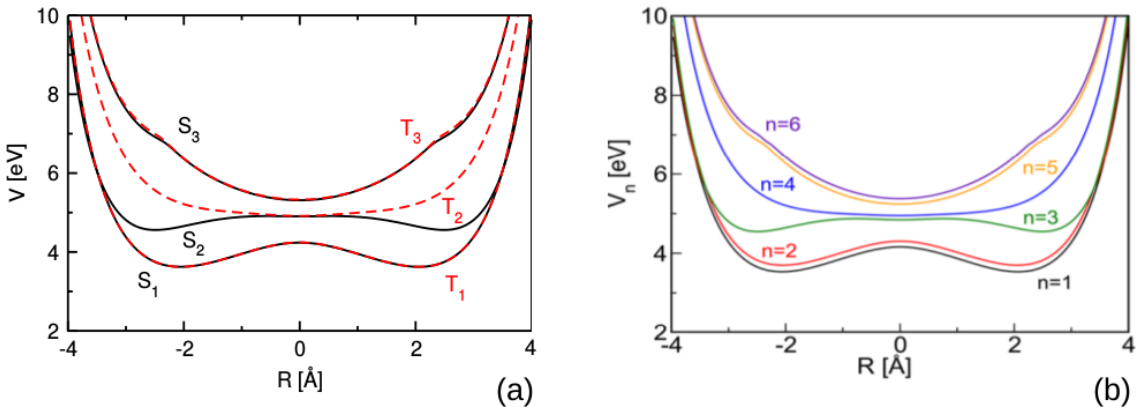

Figure 2.3: Potential energy curves of the ESM model for (a) the uncoupled case and (b) when the singlets and triplets are coupled with a λ value of 10.28x10^{-3} eV/Å

where the charge numbers are again set to $Z_1 = Z_2 = Z = 1$. All th electron-nuclei and electron-electron interactions are cut-off with *error functions* (erf) and contain the three screening parameters R_c, R_e and R_f.

Since one of the objectives of this thesis is to manipulate the singlet-triplet transitions, to monitor the spin transitions, the coupling term is introduced heuristically as

$$J(x, y) = \lambda(x - y) \tag{2.53}$$

where λ is a constant coupling strength-parameter and determines the time scale of the singlet-triplet transition. This is the simples antisymmetric form that allows to describe the spin-orbit coupling in a grid. The possible dependence of the coupling on the nuclear coordinate R is neglected. The coupling operator $J(x, y)$ creates new potential energy terms that couple (and mix) the Born-Oppenheimer electronic potentials. They are calculated as

$$V_{S_n,T_m}(R) = \int \mathrm{d}x\mathrm{d}y\varphi_n^S(x, y, R)J(x, y)\varphi_m^T(x, y, R) \tag{2.54}$$

where $\varphi_n^S(x, y, R)$ and $\varphi_m^T(x, y, R)$ denote the electronic eigenfunctions of the singlet and triplet symmetry, respectively.

The potential energy curves for both the uncoupled and coupled cases are represented in figure 2.3 for a given value of λ.

2.6.3 The soft-core Coulomb potential

In this thesis, we are also interested in the dynamics of the H_2^+ and HeH^{2+} molecules in the presence of a strong field so we need to use a consistent model for treating both continuum and bound electronic states in a system with a single electron and two protons.

The hydrogen molecular ion (the simplest molecule), is of fundamental interest in atomic and molecular physics. It constitutes a bound three-body Coulomb system which, in contrast to its atomic counterparts, the negative hydrogen ion and the helium atom, exhibits (if we neglect rotation) two time scales, the fast electronic motion (attosecond scale), and the vibrational motion of the nuclei (femtosecond scale). The interaction of this smallest molecule with strong femtosecond laser pulses is of particular interest, since the pulse duration is comparable to the vibrational period (14 fs for H_2^+ in the vibrational ground state). Further, from a theoretical point of view, the simple structure of H_2^+ allows for a numerical solution of the time dependent Schrödinger equation within reduced dimensionality models.

As a first approximation, we use a (1+1)D Hamiltonian to describe the H_2^+ molecule (one dimension for the electronic motion z, and the other for the internuclear distance), including the internuclear distance R and the electron separation to the center of mass z, where the electron is constrained to move in the molecular axis. For this reduced dimensional study the inter-particle interaction is modeled by a soft-core Coulomb potential. This model was first proposed to study strong field dynamics of the Hydrogen atom [208].

For the one dimensional Hydrogen model atom it reads

$$V(z) = -\frac{Q^2}{(\varepsilon^2 + z^2)^{1/2}} \tag{2.55}$$

The parameter ε is interpreted as the squared average transverse extension of the electronic wave function and it is introduced to remove the singularity at the origin. It can be fitted to some spectroscopic properties of the molecule than one may need to reproduce in the model, for instance the bond energy or the ionization potential. In addition, one can parametrize (R) as a function of the internuclear distance, thereby allowing a much better fit of the electronic curves calculated with the model with those obtained by ab initio approaches [280–283]. Since we are interested in qualitative properties, for simplicity we set the parameter to one. An important property of this potential is that at large z (electronic coordinate), it falls off like $1/z$. Consequently, it represents accurately the Coulombic electron-ion final-state interaction during atomic ionization,

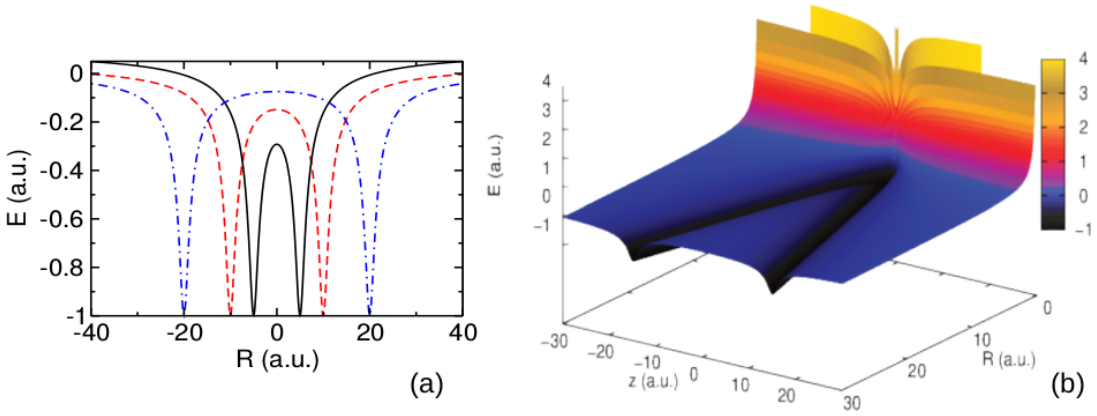

Figure 2.4: Soft core Coulmb potential (a) for different internuclear separations (R=10 a.u. in black, R=20 a.u. in dashed red and R=40 a.u. in dashed blue points) under the BO approximations and (b) the full dimensional representation

and it supports near-threshold levels that scale like Rydberg levels. Figure 2.4 shows the soft core Coulomb potential for a given internuclear separation (BO potential) and the full dimensional case.

This model has been extensively applied as a first qualitative step to analyze ionization processes in H_2^+ and high-harmonic spectra [284, 285], as well as electron-nuclear dynamics [286–289] or to treat electron correlation in He atom [290].

We also apply the soft-core coulomb potential model to study the HeH^{2+} system. This molecule is very interesting as it forms the simplest asymmetric molecule, with a single electron. There have been several experimental [291] and theoretical studies [292, 293] determining the chemical features of this very unstable molecular cation. The HeH^{2+} is highly unstable, as expected from doubly charged species. Therefore, few data is known [291]. Up to date, studies in this molecule have focused on ionization, predicting electron localization, or control of the photodissociation and photoassociation [294–296].

The HeH^{2+} is highly unstable, as expected from doubly charged species. Therefore, few data is known [291].

Again for an aligned HeH^{2+} with the He atom placed at the left of the center of mass and the H atom placed at the right of the center of mass, the $(1+1)$D Hamiltonian using a soft core Coulomb potential, is

$$\begin{aligned}\hat{H}(z,R) = &-\frac{1}{2\mu_e}-\frac{\partial^2}{\partial z^2}-\frac{1}{2\mu_e}-\frac{\partial^2}{\partial R^2}\\ &-\frac{q_e Q_{He}}{\sqrt{(z+aR)^2+\varepsilon_1^2)}}-\frac{q_e Q_H}{\sqrt{(z-pR)^2+\varepsilon_2^2)}}+\frac{Q_{He}Q_H}{R}\end{aligned} \tag{2.56}$$

where the reduced mass of the electron is $\mu_e = 1 - 1/M = 0.9999\mathrm{m}_e$ (M is the total mass of the molecule, m_e the electron mass) and $\mu = m_p m_\alpha/(m_p + m_\alpha)01478.4$ m_e (m_p is the mass of the proton and m_α is the mass of the alpha particle) is the reduced mas of the molecular frame. Here, a and p account for the relative distances of the α particle and the proton with respect to the center of mass, $a = m_p/(m_p + m_\alpha) = 0,2012$ and $p = m_\alpha/(m_p + m_\alpha) = 1 - a = 0.7988$ [296]. The smoothing parameters $\varepsilon_1, \varepsilon_2$ are adjusted to represent the ionization energy as we are working with large internuclear distances. Asymptotically, the ground state correlates with He^+(1s) and the first excited state corresponds to H(1s), therefore E(HeH^{2+},1s)=E(He^+,1s) and E(HeH^{2+},2s)=E(H,1s). Under these conditions we obtain $\varepsilon_1(He^+)$= 0.705 and ε_2(H)= 1.414.

Quantum Control Theory

Quantum Control schemes

In this chapter we focus on the theoretical aspects of different quantum control strategies. In the field of quantum control several simple schemes we proposed based on the analytical solution of the TDSE in simple systems. Despite their simplicity, generally we can classify the numerical solutions of complex models based on the solutions obtained with these schemes, and they are useful as initial approximations to use in algorithm (e.g. QOCT) approaches.

Initially, we describe two basic models (with analytic solution) of control of population dynamics: the π-pulses model based on the Rabi-formula (3.1) and the model of pulses of variable frequencies based on the Landau-Zener formula (3.2). Although we first introduce the models considering the quantum system as discrete energy levels, in our work we will always treat the system in terms of wave packets, that is, superpositions of discrete (or even continuum) levels of the molecule. As the processes we are studying occur under the strong and ultrashort limits, the uncertainty principle works against the selective excitation and the dynamics can not be described easily in terms of a reduced number of discrete levels. Therefore, we will illustrate the mechanism for electronic transitions involving nuclear wave packets.

We finally introduce two closely related models of strong field control based on manipulation of the "effective" Hamiltonian based on the change of the energy levels when a strong laser field acts that lead us to control the population transfer and influence the system dynamics: the *Light Induced Potentials* (LIPs) and the *Non Resonant Dynamic Stark Effect* (NRDSE).

3.1 π pulse mechanism

Considering the simplest model of two discrete levels coupled by a constant resonant field, the Rabi solution [297], establishes that there is a full population inversion between

the two states when the condition $\Omega_0 T = n\pi$ is fulfilled (where n is any odd number). The Rabi frequency, Ω_0, is a measure of the strength of the interaction in frequency units. It is defined by the relationship $\Omega = \frac{\mu_{12}\mathcal{E}}{\hbar}$, where μ_{12} is the dipole transition moment between the two states and $\mathcal{E}$ is the maximum amplitude of the laser. Although the Rabi formula is only valid for constant interactions (infinite duration), it can be generalized by the Area Theorem [298], which sets that the maximum population transfer is achieved if the integral $\int_0^T \Omega(t)\mathrm{d}t = n\pi$. The Area Theorem determines the transition properties between two levels due to the π type pulses, with a carrier frequency resonantly coupling the two states. However, it also establishes the minimum energy needed to produce population inversion with certainty.

Now, we focus on the description of the π model and its limitations when working in the ultrafast regime, that is, when we can not describe the system with discrete levels. We start considering wave packet transfer processes between two electronic states, or potential energy curves, $V_1(x)$ and $V_2(x)$, in the ultrashort time limit. Due to the lack of energy resolution, we will follow the dynamics in the coordinates representation (see 2.1). The Schrödinger equation of the system under the influence of a laser field, under the Born-Oppenheimer approximation, is

$$i\hbar\frac{\partial}{\partial t}\begin{matrix}\psi_1\\ \psi_2\end{matrix} = \begin{matrix}T+V_1(x) & -\mu_{12}(x)\mathcal{E}(t)\\ -\mu_{12}(x)\mathcal{E}(t) & T+V_2(t)\end{matrix}\begin{matrix}\psi_1\\ \psi_2\end{matrix} \tag{3.1}$$

where $T = -\frac{\hbar^2}{2m}\frac{\partial^2}{\partial x^2}$ is the kinetic energy operator and $\mathcal{E}(t) = A(t)\cos[\omega(t)+\varphi]$ is the laser pulse.

Within the RWA (1.2.1) we can neglect the transition probability from $V_1(x)$ to $V_2(x)$ by the spontaneous emission of a photon, and the reverse process, the transition from $V_2(x)$ to $V_1(x)$ by absorption. In addition, in the Dirac representation, we can make the unitary transformation $\psi_2(x,t) = \psi_2(x,t)e^{-i\omega(t)t}$, $\psi_1(x,t) = \psi_1(x,t)$ and the Schrödinger equation reads

$$i\hbar\frac{\partial}{\partial t}\begin{matrix}\psi_1\\ \psi_2\end{matrix} = \begin{matrix}T+U_1(x) & -\hbar\Omega(x,t)/2\\ -\hbar\Omega(x,t)/2 & T+U_2(t)\end{matrix}\begin{matrix}\psi_1\\ \psi_2\end{matrix} \tag{3.2}$$

where $\Omega(x,t) = \mu_{12}(x)\mathcal{E}(t)/\hbar$ is the Rabi frequency of the system, which depends on the spatial coordinate (it would be constant in the Frank-Condon approximation) and time (it depends only on the pulse envelope but not in the frequency). The photon energy-shifted potentials are $U_1(x) = V_1(x)$ and $U_2(x) = V_2(x) - \hbar\omega(t)$. These potentials are displaced by one photon energy, so the curves cross where the laser is in resonance.

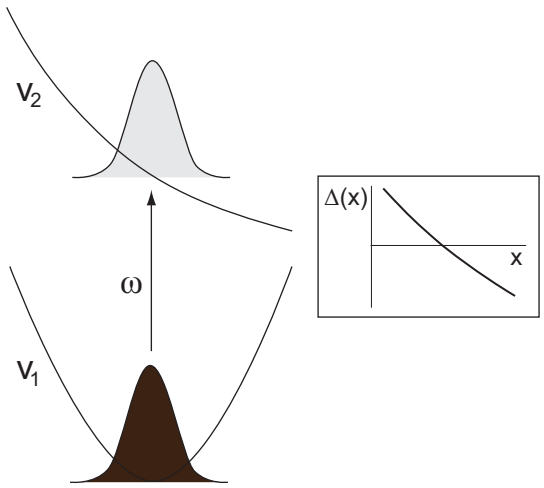

Figure 3.1: Wave function transfer between electronic states by pulses of area π [300]

In general, we will write $\psi_n(x,t)$ instead of $\psi_n(x,t)$, unless it induces confusion.

Now the point is how to maximize the population transfer from the initial $V_1(x)$ to the excited potential $V_2(x)$. One can apply the π-pulse mechanism to induce the population inversion between the electronic potentials, where the wave packet is transferred from one potential to the other, but previously some conditions must be fulfilled. Firstly, we have to assume the instantaneous excitation approximation [299], by which the wave packet is not moving during the action of the laser, so its kinetic energy is constant. In addition, from the RWA, $V_1(x)$ is in resonance with the excited potential $V_2(x)$ only for a given value coordinate x_0, as it shown in fig. 4.1.

There the head and tail of $\psi_1(x,0)$ will be out of resonance or detuned with respect to the electronic transition (fig. 4.1). Therefore, we can simplify the Schrödinger equation (3.2) by a unitary transformation to give

$$i\hbar\frac{\partial}{\partial t}\begin{matrix}\psi_1(x)\\ \psi_2(x)\end{matrix} = \begin{matrix}0 & -\hbar\Omega(t)/2\\ -\hbar\Omega(t)/2 & \Delta(x)\end{matrix}\begin{matrix}\psi_1(x)\\ \psi_2(x)\end{matrix} \tag{3.3}$$

where $\Delta(x) = U_2(x) - U_1(x)$. To simplify the notation we have assumed a constant dipole (Condon limit). This unitary transformation can only be made when the kinetic energy is constant.

So the transition probability between $U_1(x)$ and $U_2(x)$ for each x can be evaluated using a 2-level system Hamiltonian with coupling $\Omega(t)$ and detuning $\Delta(x)$. When considering pulses like $\mathcal{E}(t) = A_0\,\mathrm{sech}(t/T)$, the Hamiltonian [eq. (3.3)] has an analytic solution, that was firstly proposed by Rosen and Zener [299,301]. When the pulse ends,

the transition probability is

$$P(U_1(x) \rightarrow U_2(x)) = \sin^2(S/2)\,\mathrm{sech}^2[\pi\Delta(x)T] \tag{3.4}$$

where S is the pulse area and T the pulse duration. The pulse area is defined by [299]

$$S = \int_{-\infty}^{\infty} \mathrm{d}t\; \Omega(t\,) \tag{3.5}$$

So the global transition probability will be the probability averaged for each value of x,

$$P = \int \mathrm{d}x\;\; |\psi_1(x\,,0)|^2\, P(U_1(x\,) \rightarrow U_2(x\,),t) \tag{3.6}$$

Then, the transition probability depends on the pulse area, as in the model of two discrete levels, as well as on the detuning, which reduces the maximum possible population transfer. If we define Δ_T as the range of variation of the detuning where the wave packet is located (see fig. 4.1), then only when $T \ll \Delta_T$, $\mathrm{sech}^2(\pi\Delta(x)T) \approx 1$, and the wave packet can be completely transferred to the excited potential. This is equivalent to make the pulse width, $(\Delta\omega)_{pulse} = 1/T$, larger than the electronic absorption band, $(\Delta\omega)_{abs.sp.}$.

Additionally, the instantaneous excitation approximation must be fulfilled, which implies that the duration of the population transfer between $\psi_1(x,t)$ and $\psi_2(x,t)$, given by the inverse of the Rabi frequency, must be smaller than the characteristic time of motion of the wave packets, since the wave packets disperse and move from the Frank Condon window where the transfer takes place (see fig. 4.1).

To summarize, the conditions that have to be fulfilled for a full population transfer from $\psi_1(x,t)$ to $\psi_2(x,t)$ are

- the pulse area must be π or an odd multiple of π
- the Rabi frequency must be larger than the characteristic frequency of motion of the wave packets
- the pulse duration (T) must be smaller than the inverse of the absorption band (in units of frequency)

3.2 Landau-Zener model:variable frequency pulses

In the last section we have analyzed the population transfer between two states coupled by a π pulse in resonance with the transition. Besides the π transition, population transfer is also possible if we vary the laser frequency to cross the resonance between the states [302, 303]. Now, we consider the same system but we introduce a pulse with variable frequency, $\mathcal{E}(t) = A(t)\cos[\eta(t)]$, where $\eta(t) = \int_0^t \omega(t\,)\mathrm{d}t$. Usually, pulses where the frequency varies linearly with time are used, $\omega(t) = \omega(0) + \chi t/2$, where χ is the rate of frequency change or *chirp* [304].

Regarding wave packet transfer processes, we can follow the same description of the previous section but detuning with these chirped pulses. If the Rabi interaction frequency is larger than the inverse of the time that determines the velocity of motion of the wave packets, then eq. (3.3) is still acceptable under this context but now the detuning varies with the spatial and temporal coordinates, $\Delta(x,t) = U_2(x,t) - U_1(x) = V_2(x) - \hbar\omega(t) - V_1(x)$.

Then, for each x, assuming the Rabi frequency is roughly constant during the pulse duration (τ), the Hamiltonian is analogous to the Landau-Zener model [305]. Therefore, the transition probability reads

$$P(U_1(x) \to U_2(x), t >> \tau) = 1 - \mathrm{e}^{-\pi\frac{\Omega^2}{2\chi}} \tag{3.7}$$

From this equation, it follows that the condition required to obtain the full population transfer is

$$\Omega^2 \geq 4\chi \tag{3.8}$$

In addition, if we assume that the interaction is effective while the detuning is lower than the maximum Rabi frequency (or the Rabi frequency at the half-width of the pulse), we can define a time during which the transition is efficient [306], $t_{LZ} = \Omega(0)/\chi$. The pulse duration must be larger than this time

$$\tau > \Omega(0)/\chi \tag{3.9}$$

The same result is obtained considering the frequency bandwidth, $\Delta\omega(t) = \int_\tau \omega(t\,)\mathrm{d}t$ that must be always larger than the Rabi frequency. For a linear chirp, $\chi = \Delta\omega/\tau > \Omega(0)/\tau$, which gives the same criteria obtained before.

Therefore, considering both conditions, eq. (3.8) and eq. (3.9),

$$S = \int_{-\infty}^{\infty} \mathrm{d}t\, \Omega(t\,) \sim \Omega(0)\tau > \Omega(0)^2/\chi > 4 > \pi \tag{3.10}$$

or squaring eq. (3.9) and solving

$$\tau^2\chi > \Omega(0)^2/\chi > \pi \tag{3.11}$$

If this condition is fulfilled, in eq. (3.7) the global transition probability will be ≈ 1.

As it follows from the last inequality, in a Landau-Zener transition, the pulse area must be larger than π. Actually, the area must be much larger than π as the transition is effective just for a short period of time in which the laser frequency is close to resonance, albeit Cao [307] demonstrated that nearly total inversion can be achieved in the limit that the Area Theorem imposes.

Nowadays, pulse chirping technologies allow to manipulate the amplitude and phase of the different frequency components of the pulse to create pulses of almost arbitrary shape. Usually, a chirp is created by spectrally splitting in a prism a fixed frequency pulse of minimum uncertainty (called *transformed limited pulse*), introducing delays between the different components (by changing the optical path or using the dispersive properties of a medium) and put them again together in another prism. Thus, the properties of the chirped pulse are related to the primitive pulse. If τ_{TL} is the width of the original pulse and Γ_{TL} the corresponding bandwidth , $\Gamma_{TL} \sim 1/\tau_{TL}$ (the exact relationship depends on the pulse shape by the Fourier transform). The same bandwidth will be used to transform the frequencies. However, the relation between $\Gamma = \Gamma_{TL}$ and τ is not that simple, as the pulse shape now depends on the chirp χ. When both the pulse of minimum width is Gaussian (i.e. the envelope has Gaussian shape), and the chirp is linear, then by the Fourier transform we obtain [308],

$$\Gamma_{TL}^2 = (1 + \chi^2\tau^4)/\tau^2 \tag{3.12}$$

where χ is in $(\text{time})^{-2}$ units. We can express the chirp also in the frequency space, obtaining

$$\tau^2 = (1 + \chi\,^2\Gamma_{TL}^4)/\Gamma_{TL}^2 \tag{3.13}$$

where χ is in$(\text{time})^2$ units. These two magnitudes are related by

$$\chi = \chi\,\Gamma_{TL}^4(1 + \chi\,^2\Gamma_{TL}^4)^{-1} \tag{3.14}$$

These relations indicate that the chirp depends on the original pulse width and the stretching that occurs during the phase modulation. When $\tau \gg \tau_{TL}$ it is easy to demonstrate that $\chi \approx 1/\tau\,\tau_{TL}$. Moreover, during the conversion of frequencies the total energy of the pulse is typically conserved, so $\Omega = \Omega_{TL}\sqrt{\tau_{TL}/\tau}$ and the relationship between the areas is

$$\frac{S}{S_{TL}} \sim \frac{\Omega\,\tau}{\Omega_{TL}\tau_{TL}} = \sqrt{\frac{\tau}{\tau_{TL}}} \tag{3.15}$$

Regarding the population transfer with chirped pulses, when working with wave packets the frequency range of the chirp must be larger than the maximum detuning, $\Delta_T \sim \chi\tau$. Generally this can be achieved by a transformation of frequencies of a transformed-limited pulse. The width of the pulse must be $\tau_{TL} \ll 1/\Delta_T$. The two conditions to be imposed to the pulse parameters are: $\Omega_{TL}^2 \cdot \tau_{TL}^2 > \pi$ y $\tau/\tau_{TL} \geq S_{TL}^2 = \Omega_{TL}^2 \cdot \tau_{TL}^2$.

To summarize, the sufficient conditions to assure full wave packet transfer are:

1. The pulse width of the transformed limited pulse must be as short as possible, $\tau_{TL} < 1/\Delta_T$, typically in the femtosecond scale.

2. The intensity much be as large as possible, in particular $\Omega_{TL} > \Delta_T$, but not so large to avoid multiphotonic transitions.

3. The stretching of the pulse must be as large as possible, thus $\tau \gg \tau_{TL}$. Nevertheless, the chirped pulse duration must be smaller than the time scale of the motion of the wave packet, so the instantaneous excitation approximation is fulfilled.

However, it is important to notice that the instantaneous excitation approximation can not be purely applied, as in the vertical transition not all the components of the wave packet are transferred at the same time to the excited potential. Depending on the chirp value and sign, the highest energy (negative chirp) or the lowest energy components (positive chirp) will be transferred before. Therefore, the transition induces a variation on the kinetic moment of the excited wave packet, implying a deformation of the wave packet [309]. Although this fact is not essentially detrimental to the complete transfer, it must be analyzed with more detail. In fig. 4.2 we show the most relevant elements of the problem.

When negative chirped pulses are employed, the Raman Stokes transition competes with the absorption. As the wave packet is moving in $U_2(x)$, it can return (vibrationally

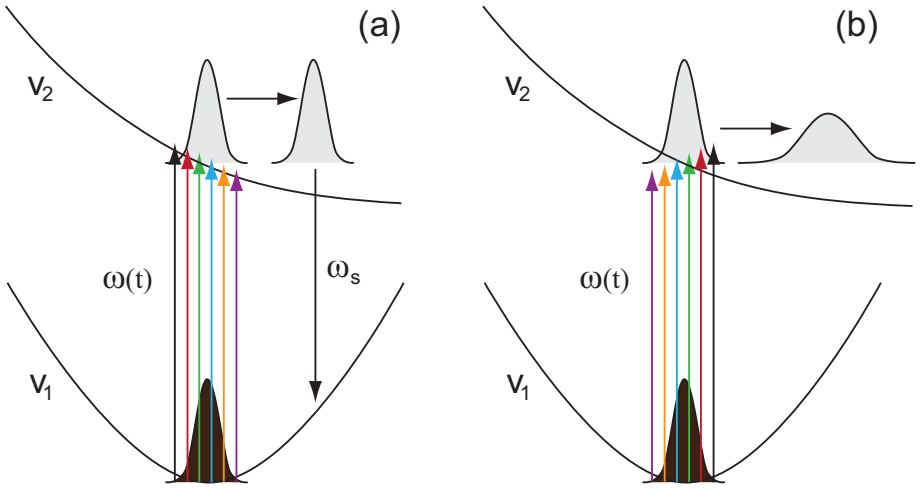

Figure 3.2: Wave packet transfer between electronic states by chirped pulses, in the limit of instantaneous excitation. With a negative chirp (a) the dispersion of the wave packet is minimum, but it could return initial potential by a Raman Stokes effect when $\omega(t) \approx \omega_s$. With a positive chirp (b) this effect is decoupled, but the wave packet dispersion is maximum [300].

excited) to the initial potential by stimulated emission, thus creating an effect of pump-dump with only one pulse [310] which implies the already mentioned Raman Stokes mechanism. Conversely, when positive chirps are used, the stimulated emission is uncoupled, so when the wave packet moves, it does not return to the initial potential, even if the pulse area is an odd multiple of π. Moreover, the dispersion of the wave packet is maximum, as the higher energy components are excited at the end [311].

3.3 Strong fields: control strategies based on the dynamic Stark effect

With the development of ultrafast and ultrastrong laser pulses many non-linear processes in molecules have been observed and controlled experimentally [17, 312]. Aside from enabling multi-photon excitation pathways, a strong field induces large Stark shifts that can deeply alter the structure of the electronic potentials [99, 313, 314, 314, 315].

Previously we have analyzed the ultrashort time limit, where the population transfer is more conveniently described in terms of wave packets in the coordinate representation. In this section, we will work with intense laser fields, in the high energy limit, where non linear effects have to be considered. The population transfer is again treated by wave packet propagation, as the energy is the conjugate variable of time in the uncertainty

principle. However, the models we used to describe the π and chirped pulses are not useful anymore. As the transition to vibrational levels now becomes important, we do not represent the system in terms of the electronic potentials of the isolated molecule, since they do not provide straightforwardly the most relevant information of the system dynamics. We turn back to the adiabatic representation (1.2.2) to understand the evolution of the system, and to make it simpler we will assume the RWA (1.2.1). Based on these equations, we will demonstrate how an intense laser field modifies substantially the molecular potentials, due to a strong dynamic Stark effect (or Autler-Townes splitting when the laser frequency is resonant to the electronic transitions [316]). In this situation, the dressed states are called *Light induced potentials* (LIPs) but instead of probability amplitudes we will work with adiabatic wave packets.

Herein, the basic elements to analyze the system dynamics are explained. We will illustrate the theoretical model for the simplest system, described by two electronic states coupled by a laser field in the adiabatic approximation. We finally set forth some of the most outstanding phenomena related to the application of strong laser fields.

3.3.1 The nonresonant dynamic Stark effect: Light Induced Potentials

The Stark effect is the shift of the energy levels due to the presence of an external electric field. Several textbooks discuss the Stark effect produced by a static field [317, 318].

The dynamic Stark effect is the quasi static shift in energy levels due to the application of optical fields. The effect is in several ways similar to the static Stark effect. There are some important differences between the static and dynamic Stark effect. In an oscillating field, there are no stationary states so it is not useful to work with static levels. However, under appropriate conditions [319], the idea of a quasi static level becomes applicable and the levels behave as if they feel a static field: the eigenstates do not follow the instantaneous electric field, but instead they react only to the intensity of the pulse envelope.

The field strengths achievable with a static electric field are much smaller than the field strengths of laser pulses, so with the advent of modern ultrafast lasers [1], which can easily exceed intensities of a TW/cm^2, the dynamic Stark effect can be applied on rapid time scales and with energies comparable to those of many quantum systems in the absence of the field. As a result, the dynamic Stark effect due to nonresonant laser fields has become an increasingly important part of atomic, molecular, and optical physics.

There are different situations with oscillating fields depending on the field strengths and frequencies. If the field oscillates slowly, the states adiabatically follow the instantaneous electric field. If the driving field is in or near resonance with a pair of quantum levels, population transfer will occur and the levels may split as in the Rabi effect. Our focus is on the nonresonant case, which is of special interest in molecular dynamics due to its generality.

The control mechanism based on nonresonant dynamic Stark effect (NRDSE) was first proposed by Sussman *et al.* [320] and it is particularly useful for quantum control [15] because ultrafast laser pulses can easily exceed atomic field strengths of 10^9 V/cm, opening the possibility of the dynamic Stark effect being highly nonperturbative and being so on femtosecond timescales.

The NRDSE scheme is a simple but very general procedure for transferring the time dependent control exerted by the field on one part of the Hamiltonian, where dipole moments are non-zero, into energy control that affects the desired region of the spectra, where the dipole couplings are symmetry forbidden.

In this section, we explain how we could base the control mechanism solely on the effects of the nonresonant dynamic Stark effect. First, we start from the Schrödinger equation in the RWA [eq. (1.21)] and we define the diabatic wave functions ψ_1^d and ψ_2^d. The real adiabatic representation would be the one that completely diagonalizes the global Hamiltonian of the Schrödinger equation, but it is impossible to solve analytically. So, usually just the potential matrix is diagonalized including the laser coupling. The Schrödinger equation is

$$-\frac{\hbar}{i}\frac{\partial}{\partial t}\begin{matrix}\psi_1^d\\ \psi_2^d\end{matrix} = \overbrace{\begin{pmatrix} \hat{T}+V_1(x) & -\mu_{12}(x)\mathcal{E}_0(t)/2 \\ -\mu_{12}(x)\mathcal{E}_0(t)/2 & \hat{T}+V_2(x) \end{pmatrix}}^{\hat{H}^d} \begin{matrix}\psi_1\\ \psi_2\end{matrix} \tag{3.16}$$

where $V_2(x) = V_2(x) - \hbar\omega$.

We can simplify the notation and write

$$-\frac{i}{\hbar}\left(\dot{\psi}_1^d\,,\dot{\psi}_2^d\right)^\dagger = \left(\hat{K}+\hat{V}+\hat{W}(t)\right)\left(\psi_1^d\,,\psi_2^d\right)^\dagger$$

$\hat{K}$ is the matrix of the kinetic energy operator, which is diagonal; $\hat{V}$ is the potential energy matrix, diagonal as well, and $\hat{W}(t)$ is the coupling matrix, non diagonal and $\left(\psi_1^d,\psi_2^d\right)^\dagger$ is the vector of wave functions in the diabatic representation. Now, a $\hat{R}(x,t)$

matrix is chosen such that

$$\hat{R}^{-1}(x,t)\left(V(x)+\hat{W}(t)\right)\hat{R}(x,t)=\hat{U}(x,t)$$

is a diagonal matrix. For two coupled potentials $\hat{R}(x,t)$ can be obtained analytically.

The Schrödinger equation can be written as

$$-\frac{i}{\hbar}\left(\dot{\psi}_+^A\ ,\dot{\psi}_-^A\right)^\dagger=\left(\hat{R}^{-1}(x,t)\hat{T}\hat{R}(x,t)+\hat{U}(x,t)\right)\left(\psi_+^A\ ,\psi_-^A\right)^\dagger-\frac{i}{\hbar}\hat{R}^{-1}(x,t)\dot{\hat{R}}(x,t)\left(\psi_+^A,\psi_-^A\right)^\dagger$$

where $\left(\psi_+^A\ ,\psi_-^A\right)^\dagger=\hat{R}^{-1}(x,t)\left(\psi_1^d\ ,\psi_2^d\right)^\dagger$ are the wave functions in the adiabatic representation. Usually the problem is simplified considering that $\hat{R}(x,t)$ weakly depends on the x coordinate and on time, therefore $\hat{R}^{-1}(x,t)\hat{T}\hat{R}(x,t)\approx\hat{T}$ can be considered diagonal and in addition, the non-adiabatic coupling term is neglected.

But we always have to be cautious with respect to this last assumption, as the non-adiabatic coupling could be important around the avoided crossings of the potentials [321,322]. Within the previous approximations, the simplified Schrödinger equation is

$$i\hbar\frac{\partial}{\partial t}\begin{array}{c}\psi_+^A\\ \psi_-^A\end{array}=\begin{array}{ccc}T+U_+^{LIP}(x,t) & 0 & \psi_+^A\\ 0 & T+U_-^{LIP}(x,t) & \psi_-^A\end{array}\tag{3.17}$$

which is diagonal. The adiabatic wave packets evolve in the light induced potentials $U_\alpha^{LIP}(x,t)$. Using a constant laser (CW laser), $U_\alpha^{LIP}(x,t)$ can be calculated analytically:

$$U_\pm^{LIP}(x,t)=\frac{1}{2}\left[V_1(x)+V_2(x)\right]\pm\frac{1}{2}\sqrt{\Delta(x)^2+\Omega^2}\tag{3.18}$$

where $\Delta(x)=V_1(x)-V_2(x)-\hbar\omega$ is the detuning between the potentials and the laser frequency and $\frac{1}{2}\left[V_1(x)+V_2(x)\right]$ is the average potential.

If the initial state runs into a wave packet localized in one adiabatic state, U_+^{LIP} for instance, then, the initial state in the adiabatic representation will be $\left(\psi_+^A(0)\ ,\psi_-^A(0)\right)^\dagger=\left(\psi_1^d(0)\ ,0\right)^\dagger$. In this situation, according to eq. (3.17) we just need to follow the dynamics of this wave packet in the $U_+^{LIP}(x,t)$ potential, which initially coincides with $U_1(x)$. The wave packet dynamics will depend essentially on the topology of one potential modified by light.

Turning back to eq. (3.18), if the Rabi frequency of the transition is much smaller than the energy difference between the potentials, meaning $\Delta(x)\gg\Omega$ (except around resonance, x_c, where $\Delta(x)_c=0$ and the two potentials cross), then $U_-(x<x_c)\approx U_1(x)-\Omega^2/4\Delta(x)$ and $U_-(x>x_c)\approx U_2(x)-\Omega^2/4\Delta(x)$. We use the same approxima-

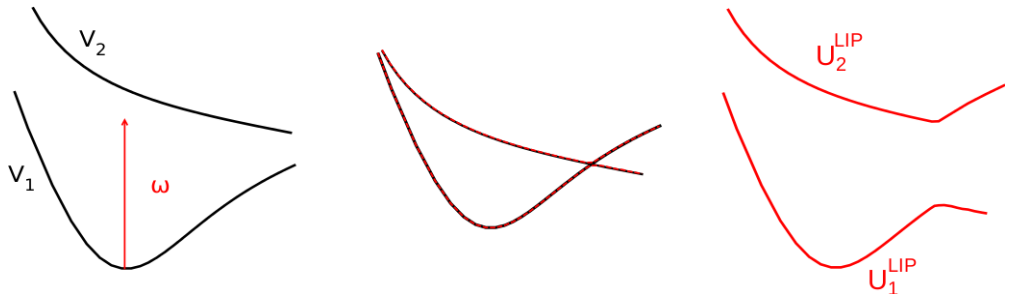

Figure 3.3: Diabatic potentials (left) and adiabatic light induced potentiial curves (right). When coupling a bound with a dissociative potential by means of strong laser field, the new LIPs experience desestabilization, U_1^{LIP} (bond softening), or stabilization, U_2^{LIP} (bond hardening)

tion for $U_+(x)$ but changing the signs and the potentials on both sides of x_c. In this way, the laser light modifies the potentials due to the electronic repulsion (Stark effect), generating the LIPs. These potentials have different shape at each side of the resonance x_c, and additionally the structure can be altered depending on the Rabi frequency. In particular, around x_c an avoided crossing is produced, when the potentials get energetically separated by a quantity equal to Ω. The Rabi frequency must be intense enough so the adiabatic approximation is valid. Otherwise, the avoided crossing is not wide enough and the wave packet in $U_-(x < x_c)$ would be transferred to $U_+(x > x_c)$ by so called non adiabatic couplings, by which the wave packet would remain always in $U_1(x)$.

Figure 4.3 shows two molecular potentials in the absence of radiation: the ground potential $V_1(x)$ and a dissociative excited potential, $V_2(x)$. On the right side, one can appreciate the LIPs structure when a laser is acting, for a constant dipole moment, μ_{12}. Due to the different shapes of the potentials, $V_1(x)$ and $V_2(x)$, the detuning $\Delta(x)$ depends on x, thus the induced Stark effect also depends on the internuclear distance. An intense laser field modifies $V_1(x)$ decreasing the energy of the dissociation barrier, thus reducing the bonding energy of the molecule (*bond softening*). On the other hand, $V_2(x)$ presents now a potential minimum allowing with bounded vibrational states. Both phenomena have been experimentally observed by spectroscopic techniques [98,200]. As a very interesting example of a dynamic based on these LIPs, we refer to the APLIP method (*Adiabadic Passage by Light Induced Potentials*) [101]. This method has been extensively studied in our group [321,323–325] and used, for example to selectively invert the electronic population of different electronic states.

3.3.2 The nonresonant dynamic Stark effect: controlling spin-orbit transitions

The physical mechanism underlying the control of the spin coupling via the NRDSE can be understood by considering just a two-level system with one singlet (S) and one triplet (T) state, coupled via V_{ST}. The energy of these states can be Stark-shifted by a nonresonant electromagnetic field with envelope $\mathcal{E}$ [109].

For a given field frequency, the dynamic polarizabilities for the singlet and triplet states are $\alpha_j(\omega)$ $(j = S, T)$, where the frequency dependence is omitted in the following. We can assign the zero point of energy to the field-free singlet energy, thus the Hamiltonian of the system results in

$$\hat{H} = \begin{matrix} -\alpha_S \mathcal{E}(t)^2/2 & V_{ST} \\ V_{ST} & \Delta(0) - \alpha_T \mathcal{E}(t)^2/2 \end{matrix} \tag{3.19}$$

where $\Delta(0)$ is the energy difference between the states in the absence of the field. Shifting the energies by a suitable unitary transformation,

$$\hat{H} = \begin{matrix} 0 & V_{ST} \\ V_{ST} & \Delta(\mathcal{E}) \end{matrix} \tag{3.20}$$

where $\Delta(\mathcal{E}) = \Delta(0) - (\alpha_T - \alpha_S)\mathcal{E}^2(t)/2$.

Now, we can use the Rabi formula (3.1) to predict the spin-coupling dynamics. If the system is initially in the singlet state and assuming a constant envelope $\mathcal{E}$, the population in the triplet is

$$P_T = \left(\frac{V_{ST}}{\Omega_e}\right)^2 \sin^2 \Omega_e t \tag{3.21}$$

where $\Omega_e = \sqrt{V_{ST} + \Delta(\mathcal{E})^2}$.

Following this formula, we can create a laser-controlled spin switch whenever the dynamic polarizabilities of the singlet and the triplet states are different, $\alpha_S = \alpha_T$. As an example, fig. 4.4 shows a cases of shifted levels to induce the spin-locking or spin-switching just by an appropriate choice of the amplitude and frequency of the laser field. The scenario is the ESM model previously described (see sec. 2.6.2) and we include the first two pairs of singlet and triplets (V_1^S, V_1^T, V_2^S and V_2^T). For instance, if $\Delta(0) \ll |V_{ST}|$ (as in the ESM model, starting in V_1^S where the ground singlet and triplet states are degenerated and $\Delta(0) = 0$), a substantial spin transfer will occur at $\tau_{ST} = \pi/2V_{ST}$. This spin-mixing dynamics can be locked while a laser pulse acts if we

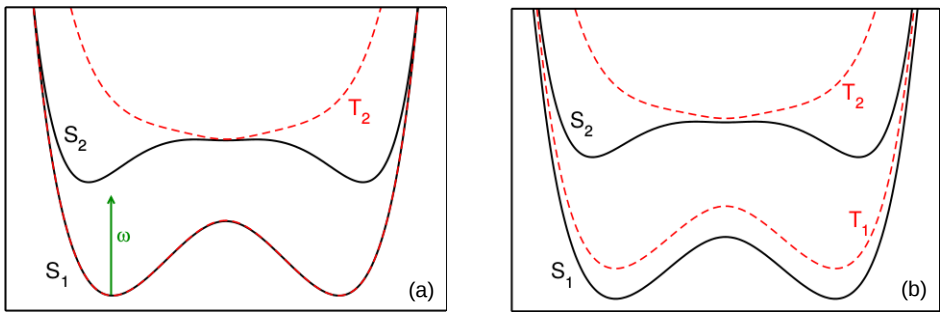

Figure 3.4: Extended Shin-Metiu model potential energy curves. (a) In the abscence of a laser field, $\Delta(0) << V_{S_1,T_1}$ and there will be spin transfer at $\tau_{ST} = \pi/2V_{S_1,T_1}$. (b) Under the effect of a strong laser field with, for example, a frequency below the resonant transition between S_1 and S_2 (other non-resosnant frequencies can be chosen), we make $\Delta(\mathcal{E}) >> V_{ST}$ and thus the spin switching can be locked.

make $\Delta(\mathcal{E}) >> V_{ST}$. On the other hand, if $\Delta(0) >> |V_{ST}|$ (as in the ESM starting in V_2^S) full population transfer can be induced by making $\Delta(\mathcal{E}) = 0$. Besides, the dynamic polarizabilities depend on the laser pulse frequency as well. Additionally, the two-level theory can be used to propose alternative quantum control scenarios [109].

We can extend directly the effective 2-level Hamiltonian to the nuclear Hamiltonian in the Born-Oppenheimer approximation. Disregarding the population absorption we obtain

$$\begin{aligned} \hat{H} &= -\tfrac{1}{2m}\tfrac{\mathrm{d}^2}{\mathrm{d}R^2}\hat{I} \\ &+ \begin{matrix} V_1^S(R) - \alpha_S(R,\omega)\mathcal{E}(t)^2/2 & V_{S_1,T_1}(R) \\ V_{S_1,T_1}(R) & V_1^T(R) - \alpha_T(R,\omega)\mathcal{E}(t)^2/2 \end{matrix} \end{aligned} \tag{3.22}$$

where $\hat{I}$ is the 2 X 2 unitary matrix.

Since this mechanism is a very simple scheme to control the system dynamics just playing with the field frequencies and strengths, it can be applied to many other scenarios to successfully control the evolution of the system. However, for strong fields and beyond the Born-Oppenheimer approximation (i.e. considering the coupled nuclear-electronic system), eq. (3.22) may not give quantitative results. In the first place because it is not easy to evaluate the dynamic polarizabilities $\alpha_j(R,\omega)$, and secondly, because usually the multi-photon absorption to excited states and ionization can not be neglected.

Quantum Control algorithms

The development of new laser devices and the technology of pulse shaping that affords a relatively simple manipulation of light, has opened up the field of laser control of chemical reactions, until then dominated only by theorists [5, 6, 9, 78, 326]. Whereas, in experiment optimal pulses are optimized through a learning-loop setup, from a theoretical point of view, different control schemes have been introduced. As a general strategy, the interaction of a system with an external field, in our case a laser field, is tailored such that a transition from an initial state $|\Psi_i\rangle$ at a time t_i to a final state $|\Psi_f\rangle$ (or target state) at a time t_f is induced. In achieving this goal, one might distinguish global and local control schemes. Both methods assume the complete knowledge of the system Hamiltonian and essentially use time propagation to optimize the fields. In the first case, the most commonly used technique is quantum optimal control theory (QOCT) [5, 9, 326, 327]. This technique uses a variational principle and an iterative process of forward and backwards propagations to construct a field which guides the wave function optimally towards the predefined target wave function. The control fields are constructed employing information on the entire dynamics from time t_i to time t_f. The nature of the iterative optimization shows many similarities with the commonly used experimental learning algorithm approach [62, 65]. However, its numerical implementation is computationally very expensive, due to the multiple propagations. Local control schemes (LCT) [11, 12] move away from the picture of a global target. Instead, a control field is calculated as a function of the instantaneous dynamics of the system at each time step. In LCT the field is calculated on the fly and therefore is obtained at the same time as the control with one single forward propagation. We want to note that there exist similarities between monotonically convergent algorithms for OCT and LCT: in some cases, the solution of the OCT equations using Krotov's scheme yields the LCT equations. This relationship has been elucidated by Salomon and Turinici [175].

In this thesis, we use operators to control electronic transfer after implementing the

local control algorithm. Now, we will present in some detail the characteristics and equations related to this theory.

4.1 Quantum Optimal Control Theory

In the optimal control approach, the quantum control problem can be formulated as a problem of seeking a set of admissible controls satisfying the system dynamic equations and simultaneously minimizing a cost functional. The cost functional may be different according to the practical requirements of the quantum control problem, such as minimizing the control time [328, 329], the control energy [330, 331], the error between the final state and target state, or a combination of these conditions.

The standard version of OCT is based on the assumption that a molecular state, the target state ϕ_t , is attainable by a laser driven molecular wave function $|\psi(t)\rangle$ at time T. In other words, the overlap expression $|\langle\phi_T|\psi(T)\rangle|^2$ is equal to unity [61, 62]. To determine the optimal laser pulse, which drives the system to its predefined target state, one considers the overlap to be a functional of the field strength $\mathcal{E}(t)$. A maximum value of this functional should be obtained by the optimal pulse. To this end, OCT is formulated as a task which maximizes the functional with the constraint that the field strength has a finite value.

4.1.1 Deriving Quantum Optimal Control Equations

The aim is to find the field that maximizes the functional $J = \langle\psi(T)|\hat{P}|\psi(T)\rangle$, where $\hat{P}$ is a projector operator, $\hat{P} = |\phi_t\rangle\langle\phi_t|$, such that $J = P_{if}$ is the transition probability to go from $\psi(0) = \psi_i$ at initial time to ϕ_t at final time. The same derivation is valid if $\hat{P}$ is any positive semidefinite operator ($\langle\psi(T)|\hat{P}|\psi(T)\rangle \geq 0$ for any ψ). At the same time, the use of very strong laser pulses must be penalized, as the strong pulses break the validity of most approximate Hamiltonian descriptions, and the equations need to be explicitly dependent on the field.

Variational calculus can be used to find the extremes of the functional

$$J = \langle\psi(T)|\hat{P}|\psi(T)\rangle - \frac{1}{\alpha}\int \frac{|\mathcal{E}(t)|^2}{s(t)}\mathrm{d}t \tag{4.1}$$

The functional is composed of two elements, the first term $\langle\psi(T)|\hat{P}|\psi(T)\rangle$ specifies the yield, that is the overlap with the target state ϕ_t on the expectation value of the hermitian operator $\hat{P}$.

The second term in J penalizes the electric field fluence. The weight factor α, also know as the penalty factor, allows for flexibility in choosing the relative importance of the physical objectve and fluence. The shape function $s(t)$ was first applied into OCT by ref. [332], introducing a time dependence of the penalty factor α, which means that for different times different intensities will be allowed. It avoids abruptly changing fields and sets a minimum for the pulse bandwidth. The envelope function$s(t)$ switches on and off smoothly, thus imprinting this property on the optimized field.

One can vary $\psi(T)$ and $\mathcal{E}(t)$, therefore we can write

$$J + \delta J = \langle \psi(T) + \delta\psi(T)|\hat{P}|\psi(T) + \delta\psi(T)\rangle - \frac{1}{\alpha}\int \frac{|\mathcal{E}(t) + \delta\mathcal{E}(t)|^2}{s(t)}\mathrm{d}t \tag{4.2}$$

Considering just first order variations of the wave function $\psi(T)$ and $\mathcal{E}(t)$,

$$\delta J = \langle \delta\psi(T)|\hat{P}|\psi(T)\rangle + \langle \psi(T)|\hat{P}|\delta\psi(T)\rangle - \frac{2}{\alpha}\int \frac{\mathcal{E}(t)}{s(t)}\delta\mathcal{E}(t)\mathrm{d}t \tag{4.3}$$

As the first two terms are complex conjugates, the last equation results in

$$\delta J = 2\mathrm{Re}\big[\langle \psi(T)|\hat{P}|\delta\psi(T)\rangle\big] - \frac{2}{\alpha}\int \frac{\mathcal{E}(t)}{s(t)}\delta\mathcal{E}(t)\mathrm{d}t \tag{4.4}$$

In order to find a maximum (extreme) of $\delta J/\delta\mathcal{E}(t)$ one needs to know how $\delta\psi(T)$ depends on $\delta\mathcal{E}(t)$. In most derivations of the quantum OCT equations one uses Lagrange multipliers to consider both functions independent. The maximization of J is constrained by the dynamical equation for ψ, which is the TDSE. The quantum dynamics of the system, including the variations, must follow the equation

$$\dot{\psi}(t) + (\dot{\delta\psi})(t) = -i\big[\hat{H}(t) - \mu\delta\mathcal{E}(t)\big](\psi(t) + \delta\psi(t)) \tag{4.5}$$

But we are just considering first order variations, thus

$$(\dot{\delta\psi})(t) = -i\hat{H}(t)\delta\psi(t) + i\mu\delta\mathcal{E}(t)\psi(t) \tag{4.6}$$

This is a non-homogeneus TDSE that conects $\delta\psi(t)$ with $\delta\mathcal{E}(t)$ at all times, and in particular, at final time, as required in eq. (4.4).

Solving the non-homegeneous first order differential equation one gets

$$\delta\psi(t) = \hat{U}(t, 0; \mathcal{E})\delta\psi(0) + i\int_0^t \hat{U}(t, t\,; \mathcal{E}(t\,))\mu\delta\mathcal{E}(t\,)\psi(t\,)\mathrm{d}t \tag{4.7}$$

In this last equation $\delta\psi(0) = 0$ since the initial state does not change, then at final

time

$$\delta\psi(t) = i\int_0^T \hat{U}(T,t\,;\mathcal{E}(t\,))\mu\delta\mathcal{E}(t\,)\psi(t\,)\mathrm{d}t \tag{4.8}$$

Substituing eq. (4.8) in eq. (4.4) we obtain

$$\delta J = \int_0^T \mathrm{d}t\,\big\{2\mathrm{Re}[\langle\psi(T)|\hat{P}\hat{U}(T,t\,;\mathcal{E})\mu\delta\mathcal{E}(t\,)|\psi(t\,)\rangle\,] - \frac{2}{\alpha s(t\,)}\mathcal{E}(t\,)\delta\mathcal{E}(t\,)\big\} \tag{4.9}$$

Since $\delta\mathcal{E}(t)$ is real and given a complex function z, $\mathrm{Re}(iz) = -\Im(z)$, thus

$$\delta J = -2\int_0^T \mathrm{d}t\,\big\{\Im\big[\langle\psi(T)|\hat{P}\hat{U}(T,t\,;\mathcal{E})\mu|\psi(t\,)\rangle\big] + \frac{1}{\alpha s(t\,)}\mathcal{E}(t\,)\big\}\mathrm{t} \tag{4.10}$$

Defining an instantaneous gradient $\mathrm{d}J_t/\mathrm{d}\mathcal{E}(t)$ such that

$$\delta J = \int_0^T \frac{\mathrm{d}J_t}{\mathrm{d}\mathcal{E}(t)}\delta\mathcal{E}(t)\mathrm{d}t \tag{4.11}$$

where

$$\frac{\mathrm{d}J_t}{\mathrm{d}\mathcal{E}(t)} = -2\big\{\Im\big[\langle\psi(T)|\hat{P}\hat{U}(T,t;\mathcal{E})\mu|\psi(t)\rangle\big] + \frac{1}{\alpha s(t)}\mathcal{E}(t)\big\} \tag{4.12}$$

Making $\mathrm{d}J_t/\mathrm{d}\mathcal{E}(t) = 0$ at each time t, we find the maximum of the functional. This equation is obeyed by the optimal field. We obtain

$$\Im\big[\langle\psi(T)|\hat{P}\hat{U}(T,t;\mathcal{E}_{OC}(t))\mu|\psi(t)\rangle\big] + \frac{1}{\alpha s(t)}\mathcal{E}_{OC}(t) = 0 \tag{4.13}$$

Which gives us

$$\mathcal{E}_{OC}(t) = -\alpha s(t)\Im\big[\langle\psi(T)|\hat{P}\hat{U}(T,t;\mathcal{E}_{OC}(t))\mu|\psi(t)\rangle\big] \tag{4.14}$$

or

$$\mathcal{E}_{OC}(t) = -\alpha s(t)\Im\big[\langle\psi(T)|\hat{P}\hat{U}(T,t;\mathcal{E}_{OC}(t))\mu\hat{U}(t,0;\mathcal{E}_{OC}(t))|\psi(0)\rangle\big] \tag{4.15}$$

This is an implicit equation: $\mathcal{E}_{OC}(t)$ depends on $\hat{U}(T,t;\mathcal{E}_{OC}(t))$ which itself depends on $\mathcal{E}_{OC}(t)$. In particular, knowing $\mathcal{E}_{OC}(t)$ requires knowledge of the whole history of the dynamics, from the past to the present [via $\hat{U}(t,0;\mathcal{E}_{OC}(t))$] and from the future to the present [via $\hat{U}(T,t;\mathcal{E}_{OC}(t))$]. To solve the non-linear equation one needs iterative

procedures. Notice that, had we not included the quadratic penalty form of the field in the functional, the gradient [eq. (4.12)] would not be an explicit function of the field.

Now, if we define the performance function

$$\chi(T) = \hat{P}\psi(T) \tag{4.16}$$

then

$$\langle\psi(T)|\hat{P}\hat{U}(T,t;\mathcal{E}_{OC}) = \langle\chi(T)|\hat{U}(T,t;\mathcal{E}_{OC}) = \langle\chi(t)| \tag{4.17}$$

The function χ can be only evaluated at the end of the dynamics and then one propagates it backwards in time with the optimal field, which can be written as

$$\mathcal{E}_{OC}(t) = -\alpha s(t)\Im\big[\langle\chi(T)|\mu|\psi(T)\rangle\big] \tag{4.18}$$

This is the quantum OCT equation for the optimal field. Also eq. (4.12) can be written in terms of the χ function

$$\frac{\mathrm{d}J_t}{\mathrm{d}\mathcal{E}(t)} = -2\big\{\Im\big[\langle\chi(t)|\mu|\psi(t)\rangle\big] + \frac{1}{\alpha s(t)}\mathcal{E}(t)\big\} \tag{4.19}$$

4.1.2 Finding the optimal control pulses

As noticed, eq. (4.18) [or the equivalent form (4.15)] are implicit equations that can only be solved by iterative procedures. The two most common algorithms that solve the optimal control equations are described. In the following, $\mathcal{E}^{(k)}(t)$ and $\mathcal{E}^{(k+1)}(t)$ are two consecutives steps of the iterative procedure. To start the algorithm an initial guess field is needed $\mathcal{E}^{(k=0)}(t)$. On the other hand, one must impose convergence conditions, in order to end the algorithm at a certain time, for instance

$$\int_0^T \mathrm{d}t \frac{\big[\mathcal{E}^{(k+1)}(t) - \mathcal{E}^{(k)}(t)\big]^2}{s(t)} \leq T_\kappa \qquad \text{or} \qquad J^{(k+1)} - J^{(k)} \leq \kappa \tag{4.20}$$

where κ (κ) are predetermined criteria for convergence.

To simplify notation and use eq. (4.18), $\psi^{(\kappa)}(t)$ will be the wave function obtained by propagating with $\hat{U}\big(t,0;\mathcal{E}^{(\kappa)}(t)\big)$ and likewise $\chi^{(\kappa)}(t)$ to the performance function obtained by proagating with $\hat{U}\big(T,t;\mathcal{E}^{(\kappa)}(t)\big)$.

The gradient method

In this algorithm eq. (4.18) is taken as the gradient of J_t with respect to $\mathcal{E}(t)$ [113, 333, 334]. It is based on choosing a field on step $\kappa+1$ as the field on step κ plus a contribution along the gradient obtained with the same κ field

$$\frac{\mathrm{d}J_t}{\mathrm{d}\mathcal{E}(t)} = -2\Big\{\Im\big[\langle\chi^{(\kappa)}|\mu|\psi(t^{(\kappa)})\rangle\big] + \frac{1}{\alpha s(t)}\mathcal{E}(t)\Big\} \tag{4.21}$$

Then

$$\mathcal{E}^{(\kappa+1)}(t) = \mathcal{E}^{(\kappa)}(t) + \beta\frac{\mathrm{d}J_t^{(\kappa)}}{\mathrm{d}\mathcal{E}(t)} \tag{4.22}$$

Where β is a positive constant determined by linear procedure that minimizes $J^{(\kappa+1)} = J[\mathcal{E}_\beta^{(\kappa+1)}(t)]$. By this choice and at least for a certain range of β, it is fulfilled that $J^{(\kappa+1)} \geq J^{(\kappa)}$.

The Krotov method

The previous approach has one central disadvantage linked to the use of a gradient. The gradient method is prone to get stuck in the local minima of search space and the convergence rate is rather slow. For this reason a global iterative procedure was developed, termed Krotov method [335–337]. This scheme uses an immediate feedback and converges quadratically [117]. This algorithm is based on using as the optimal field at step $\kappa + 1$

$$\mathcal{E}^{(\kappa+1)}(t) = -\alpha s(t)\Im\big[\langle\chi^{(\kappa)}(t)|\mu|\psi^{(\kappa+1)}(t)\rangle\big] \tag{4.23}$$

This equation is very similar to eq. (4.18) but one has to notice that while $\chi^{(\kappa)}(t)$ is propagated using the field obtained at the previous step (the one that is known at all times), $\psi^{(\kappa+1)}(t)$ is propagated with the new field. This implies inmediate feedback. Obviosly, some numerical approximation must be done at some point, since $\mathcal{E}^{(\kappa+1)}(t)$ is unknown. However, one can force $\mathcal{E}^{(\kappa+1)}(0) = \mathcal{E}^{(\kappa)}(0)$ and then use this value, together with $\chi^{(\kappa)}(t)$ to calculate, via eq. (4.23), $\mathcal{E}^{(\kappa+1)}(\Delta t)$ and so on. The inmediate feedback will work better the smaller Δt is. This method guarantees $J^{(\kappa+1)} \geq J^{(\kappa)}$ and there is no need for any linear search. It is important to say that in this rapidly convergent scheme it is impossible to parameterize the field. Instead the electric field is changed freely at each point of time by the algorithm as it proceeds.

A comparison between the two methods can be found in ref. [116].

4.2 Local Control Theory

From a computational point of view Local Control Theory (LCT) is an open loop algorithm which takes into account the system's response at a certain time to construct a suitable laser pulse, to be subsequently fed to the system Hamiltonian, thereby monotonically varying a pre-defined objective functional. The control Hamiltonian is updated at each interval. Thus it constructs a feed-forward open-loop mechanism. During the propagation the algorithm stops once the objective is achieved or the preset threshold is attained. The resulting pulse is then analyzed and introduced in the experiment. Within the LCT framework one can also decide on the shape of the pulse envelope, or impose a bound on the fluency of the laser pulse, which simplifies the analysis. The fact that the control fields are chosen upon a simple objective of increasing/decreasing a certain target functional offers a physically intuitive interpretation. Besides, the set of equations used to obtain the control field are local in time, making it readily implementable within the dynamical framework(both for quantum and mixed quantum-classical treatments).

4.2.1 Deriving local control equations

The starting point is the TDSE of state $|\psi(x,t)\rangle$ evolving in time under the Hamiltonian $\hat{H}(t)$ given as $\hat{H}_0 + W(x,t)$.

$$i\hbar\frac{\partial}{\partial t}|\psi(x,t)\rangle = \hat{H}(t)|\psi(x,t)\rangle = (\hat{H}_0 + W(x,t))|\psi(x,t)\rangle \tag{4.24}$$

The unperturbed system is described by the Hamiltonian $\hat{H}_0$ and the time dependent perturbation is the coupling with the laser field, $W(x,t) = -\mu(x)\mathcal{E}(t)$.

In Local Control we want to find the field $\mathcal{E}_{lc}(t)$ that satisfies at all times

$$\frac{\partial P_{0t}}{\partial t} = \frac{\mathrm{d}}{\mathrm{d}t}|\langle\phi_t|\hat{U}(T,0;\mathcal{E}_{lc}(t))|\psi(t)\rangle|^2 = \frac{\mathrm{d}}{\mathrm{d}t}\langle\psi(t)|\hat{P}|\psi(t)\rangle \geq 0 \tag{4.25}$$

Since in LC, the operator $\hat{P}$ does not need to be positive semi-definite, we can generalize the discussion so that LC is any procedure that seeks a monotonic increase or decrease in time of any observable $\hat{O}$ of interest in the dynamics, such as a transfer probability or a property like the energy of the system $\langle H_0\rangle$.

Therefore one shall find the field $\mathcal{E}_{lc}(t)$ that satisfies

$$\frac{\partial}{\partial t}\langle\psi(t)|\hat{O}|\psi(t)\rangle \gtrless 0 \tag{4.26}$$

The time derivative of the expectation value follows from the time derivative of

the ket, $\frac{\partial}{\partial t}|\psi\rangle = -i\hat{H}|\psi\rangle$ and that of the bra $\frac{\partial}{\partial t}\langle\psi| = i\langle\psi|\hat{H}$ (which is the complex conjugate). Thus

$$\frac{\partial}{\partial t}\langle\psi(t)|\hat{O}|\psi(t)\rangle = i\langle\psi(t)|\hat{H}\hat{O}|\psi(t)\rangle - i\langle\psi(t)|\hat{O}\hat{H}|\psi(t)\rangle \tag{4.27}$$

which can be written in terms of the commutator $\left[\hat{O},\hat{H}\right] = \hat{O}\hat{H} - \hat{H}\hat{O}$

$$\frac{\partial}{\partial t}\langle\psi(t)|\hat{O}|\psi(t)\rangle = -i\langle\psi(t)|\left[\hat{O},\hat{H}\right]|\psi(t)\rangle \tag{4.28}$$

It is useful to write eq. (4.27) in the equivalent way

$$\frac{\partial}{\partial t}\langle\psi(t)|\hat{O}|\psi(t)\rangle = -2\mathrm{Re}\big(\langle\psi(t)|\hat{O}\hat{H}|\psi(t)\rangle = 2\Im\big(\langle\psi(t)|\hat{O}\hat{H}|\psi(t)\rangle\big) \tag{4.29}$$

As the expectation value is a real number despite the presence of the imaginary unit, the local control field can be chosen strictly real.

Since $\hat{H}(t) = \hat{H}_0 - \mu\mathcal{E}(t)$, separating the contributions of the two parts of the Hamiltonian in eq. (4.28) we obtain

$$\begin{aligned}\frac{\partial}{\partial t}\langle\psi(t)|\hat{O}|\psi(t)\rangle = -i\langle\psi(t)|\left[\hat{O},\hat{H}_0\right]|\psi(t)\rangle + i\mathcal{E}(t)\langle\psi(t)|\left[\hat{O},\mu\right]|\psi(t)\rangle \\ = h(t) + \mathcal{E}(t)g(t)\end{aligned} \tag{4.30}$$

where both $h(t)$ and $g(t)$, as expectation values, are real functions of time.

It is important to note that the second term in the latter equation contains the interaction $W(z,t)$ and thus the electric field. Clearly, if $\left[\hat{A},\mu\right] = 0$ no control is possible or at least we will not obtain any explicit dependence of the objective with the local control field. On the other hand, in cases where $\hat{H}_0$ commutes with the observable $\hat{O}$, i.e., $\left[\hat{A},\hat{H}_0\right] = 0$, and the observable is not explicitly time dependent, the control is simple and hints the possibility to influence the temporal change of the expectation value of $\hat{O}$ by a properly chosen external field. From eq. (4.30) it is easy to impose $\partial\langle A(t)\rangle/\partial t \geq 0$ (or ≤ 0). It suffices to make $\mathcal{E}(t)g(t) \geq 0$, or

$$\mathcal{E}_{lc}(t) = f(t)g(t) = if(t)\langle\psi(t)|\left[\hat{O},\mu\right]|\psi(t)\rangle = -2f(t)\Im\big(\langle\psi(t)|\hat{O}\mu|\psi(t)\rangle\big) \tag{4.31}$$

with $f(t) \geq 0$, since then $\partial\langle A(t)\rangle/\partial t = f(t)g(t)^2$ (for $\partial\langle A(t)\rangle/\partial t \leq 0$ we just need to

choose $f(t) \leq 0$). If $g(t) = \left[\hat{A}, \hat{\mu}\right] = 0$ (or the imaginary part of $\left\langle \psi(t)|\hat{O}\mu|\psi(t)\right\rangle$ is zero) the rate of change will be zero as well, provided $h(t) = 0$. If the last condition is not met, we would not know if that term could cause a drop in $\langle A(t)\rangle$. For this reason, in general, local control procedures are only defined for operators $\hat{A}$ such that $\left[\hat{A}, \hat{H}_0\right] = 0$.

The choice of the electric field which ensures the monotonicity condition is not unique. Also, through the proper choice of the temporal function $f(t)$, one can regulate the overall intensity and duration of the pulse.

Equations (4.30) and (4.31) constitute the main equations in the local control algorithm which will be solved on the discretized time interval by previously mentioned feed-forward method. To find a LC pulse we just need to adjust the pulse instantaneously to the value of the wave function. Examining eq. (4.31) more closely,

$$\mathcal{E}_{lc}(t) = -2f(t)\Im\left(\left\langle \psi(0)|\hat{U}(0,t;\mathcal{E}_{lc}(t))\hat{O}\mu\hat{U}(t,0;\mathcal{E}_{lc}(t))|\psi(0)\right\rangle\right) \tag{4.32}$$

The idea is that in order to get $\mathcal{E}_{lc}(t)$ we first need to know $\mathcal{E}_{lc}(t)$. But fixing $\mathcal{E}_{lc}(0)$ is enough to get $\mathcal{E}_{lc}(t)$ by solving the equations with a numerical discretization procedure (for example discretization on a grid and Split-Operator method).

Since LC requires a fast adjustment of the field $\mathcal{E}_{lc}(t)$ to the wave function, it is important to be careful with respect of the choice of Δt, which must be short enough to get sensible results from the local control equations.

One can also be overambitious and try to force $\left\langle \psi(t)|\hat{0}|\psi(t)\right\rangle$ to follow a given trajectory $a(t)$. Following eq. (4.30) this is equivalent to demand

$$\mathcal{E}(t)g(t) = \frac{\partial}{\partial t}a(t) \tag{4.33}$$

again assuming $h(t) = 0$. This is usually called *tracking* in the literature [120, 152]. Tracking is hard to achieve because whenever $g(t) = 0$ and $\frac{\partial}{\partial t}a(t) = 0$, there is no easy way to know a priori (without previously writing the field) what trajectories $a(t)$ are possible.

In this work, two different operators $\hat{O}$ were chosen to achieve local control over a single electron dynamics. The first strategy was to slow down the electron, thus reducing the energy of the system. Secondly, we induced population transfer, thus forcing a monotonic increase in P_{0t} over time by projecting the population on a desired target state.

4.2.2 Slowing the electron

Our goal will be to decrease the energy of the electron to induce electron photoassociation. A sufficient condition to reduce the energy of the system upon the interaction with an external field is that the expectation value of $\hat{H}_0$ decreases as a function of time or, equivalently, that its time derivative (the energy rate) is less than zero,

$$\frac{\partial}{\partial t}\langle \hat{H}_0 \rangle = \frac{\partial}{\partial t}\big\langle \psi(t)|\hat{H}_0|\psi(t)\big\rangle < 0 \tag{4.34}$$

The rate expression is evaluated employing the time dependent Schrödinger equation as

$$\frac{\partial}{\partial t}\langle \hat{H}_0 \rangle = i\left\langle [\hat{H}(t), \hat{H}_0] \right\rangle = i\mathcal{E}(t)\left\langle [-\hat{\mu}, \hat{T}] \right\rangle = \mathcal{E}(t)\frac{1}{i2m}\left\langle \left(\frac{\partial^2 \hat{\mu}}{\partial z^2} + 2\frac{\partial \hat{\mu}}{\partial z}\frac{\partial}{\partial z} \right\rangle \right. \tag{4.35}$$

If the field is chosen as

$$\mathcal{E}(t) = \lambda \frac{i}{2m}\left\langle \frac{\partial^2 \mu}{\partial z^2} + 2\frac{\partial \mu}{\partial z}\frac{\partial}{\partial z} \right\rangle \tag{4.36}$$

with λ being a negative number, then eq. (4.34) is fulfilled automatically. In the special case of a linear dipole moment, i.e., $\mu = qz$ (with q being a constant), eq. (4.35) takes the simple form

$$\frac{\partial}{\partial t}\langle H_0 \rangle = \mathcal{E}(t)\frac{q}{m}\langle \hat{p} \rangle \tag{4.37}$$

where $\hat{p}$ is the momentum operator, and the control field [eq. (4.36)] is proportional to the expectation value of the momentum [138, 139, 338]:

$$\mathcal{E}_{lc}(t) = \lambda f(t)\langle \hat{p} \rangle \tag{4.38}$$

where $f(t)$ is an envelope function.

This equation indicates that the field must oppose the momentum of the electron, and the faster the electron goes, the stronger $\mathcal{E}_{lc}(t)$ must be in order to stop the particle.

Population transfer

Another expression for the field is obtained if the objective is to increase the population in a target eigenstate $|\phi_T\rangle$ of H_0 [156, 339]. Defining the projector $P_T = |\phi_T\rangle\langle\phi_T|$, the rate of population transfer into the target state is

$$\frac{\partial}{\partial t}\langle P_T\rangle = i\langle[H(t), P_T]\rangle = i\mathcal{E}(t)\langle[-\mu, P_T]\rangle = \mathcal{E}(t)2\Im\left\{\left\langle\psi(t)|\mu|\phi_T\right\rangle\left\langle\phi_T|\psi(t)\right\rangle\right\} \quad (4.39)$$

where $\Im$ denotes the imaginary part. Here, the control field which steadily increases the target state population is

$$\mathcal{E}(t) = \lambda f(t)\Im\left\{\left\langle\psi(t)|\mu|\phi_T\right\rangle\left\langle\phi_T|\psi(t)\right\rangle\right\} \quad (4.40)$$

with λ chosen to be positive and $f(t)$ an envelope function. From this expression it is obvious that some overlap between the wave packet $|\psi(t)\rangle$ and the target state $|\phi_T\rangle$ is needed initially, otherwise the field remains zero at all times. This problem is overcome by artificially populating the target state at initial time with some small fraction of the total population. It is, however, important to note that this is only necessary to start the numerical algorithm and has no important consequences in the local control field finally obtained.

The local control field is telling us about how the field must be in order to force a monotonic increase of $P_T = |\phi_T\rangle\langle\phi_T|$ over time. Unfortunately, comparing with OCT, the local control field is almost never the optimal field, but one can improve the final yield with an optimized field version. Nevertheless, local control theory is much faster and computationally affordable than Optimal Control.

Results

Results

5.1 Control of spin-orbit transitions in ion strings via nonresonant strong laser pulses

In this chapter we focus on the description of controlling the spin state of the wave function.

Only a few schemes have been proposed in the literature to optically control spin transitions by means of strong laser pulses [187, 340]. In previous works of our group, different strategies were also suggested to control the spin transfer by means of nonresonant strong laser pulses [109–112]. The aim is now to explore the limits of the validity of these schemes and the quest of possible corrections, including new effects that can not be observed under the Born-Oppenheimer approximation. To describe the electron dynamics and the spin-orbit transitions (singlet-triplet transitions) we first motivate an extended version of the Shin-Metiu model (the ESM model) (2.6.2) where the coupling is introduced heuristically. This model allows us to study the effects of ionization and the breakdown of the Born-Oppenheimer approximation.

In the article entitled: "*Quantum wave packet dynamics in spin-coupled vibronic states*" (*J. Phys. Chem. A*, **116**, *11427-11433*, 2012) the nonresonant dynamic Stark effect (NRDSE) is used to decouple the singlet-triplet transition and therefore dynamically lock the spin state in the adiabatic limit and in the full ESM model (vibronic wave packets). The work presents the model Hamiltonian and its Born-Oppenheimer limit, giving detail about the procedure used to include the singlet-triplet coupling in a phenomenological way. The potential energy curves in the uncoupled and coupled cases were calculated as well as the potential coupling matrix elements and the transition dipole moments.

We compare the results obtained under the Born-Oppenheimer approximation using different number of electronic states (the dynamics of nuclear wave packets modelm

DNWP) with those obtained from the full ESM model (vibronic wave packets). In the absence of a laser field, full population transfer is achieved at both levels of calculation, which means that the DNWP approach gives the correct dynamical results. Under the effect of a nonresonant strong laser field, the population is efficiently maintained within the manifold of singlet states. Including more electronic states in the model, only increases the dispersion of the population among different singlet states, although the overall population of the triplet states slightly varies. When performing the calculations in the full ESM model, this effect increased and the predominant dynamical process was multiphoton absorption leading to ionization. However, the triplet states were not populated essentially.

In "*Manipulating the singlet-triplet transition in ion strings by nonresonant dynamic Stark effect*" (*Theor. Chem. Acc.*, **132**, *1359*, 2013), the ESM model was employed to influence the spin-orbit transitions by means of strong laser fields as in the precedent work. In this case, we worked under the Born-Oppenheimer approximation including different number of electronic states and couplings (DNWP approach). The nonresonant dynamic Stark effect was again applied to avoid a singlet-triplet transition, whilst to force a spin transfer a combination of a chirped and a transformed limited pulses were used. We explored different pulse parameters (nonresonant frequencies and intensities) and chose the optimal values that provided the best results in locking the singlet-triplet transition. We compared these results to those obtained when more electronic states were included. Once again the need of using strong fields led to multiphoton ladder climbing as the main constraint to the strong-field control of spin transitions.

In the work "*The time-scale of non linear events driven by strong fields: can one control the spin coupling before ionization runs over?*" (*J. Phys. B: At. Mol. Opt. Phys.*, **47**, *124027*, 2014) the relation between spin-coupling and the ionization rate was investigated to identify the conditions for the efficient control of the spin-orbit coupling via the nonresonant dynamic Stark effect while suppressing the ionization in the ESM Hamiltonian.

To guide the study, a simple analytical two-level Hamiltonian was proposed (with one singlet and one triplet), the 2-PSI model, which includes the effective ionization rate Γ. This model was used as a guide to find suitable regimes or ranges of parameters where one can achieve the control of spin coupling in a more complex system. By defining a maximum threshold for the triplet population we obtained a minimum for the Stark shift and thus a threshold value for the field intensity. In order to find the conditions under which the time scale of ionization is smaller than the time scale of spin transfer, we used a simple but very general equation for the ionization as a function of the field. Armed

with these formulas, we finally found an expression which relates the characteristic times of the spin transfer and that of ionization in the presence of a laser field, making then possible to privilege one process versus the other. The parameters of the 2-PSI model were then fitted in the 3D ESM Hamiltonian. The analytical results estimated for the optimal values of spin coupling versus electric field strength are useful to establish an efficient quantum control of spin transitions before the ionization dominates. Thus, we can influence the competing processes of spin-transitions and ionization within certain limits. In this case, for relatively weak spin couplings and control field intensities, we could achieve efficient spin locking in an initial singlet state.

5.1.1 Quantum wave packet dynamics in spin-coupled vibronic states

Falge, M., Engel, V., Lein, M., Vindel-Zandbergen, P., Chang, B.Y. and Sola, I.R., *J. Phys. Chem. A*, **116**, *11427-11433* (2012)

THE JOURNAL OF PHYSICAL CHEMISTRY A

Article

pubs.acs.org/JPCA

Quantum Wave-Packet Dynamics in Spin-Coupled Vibronic States

Mirjam Falge,[†] Volker Engel,[†] Manfred Lein,[‡] Patricia Vindel-Zandbergen,[§] Bo Y. Chang,[∥] and Ignacio R. Sola*[,§]

[†]Institut für Physikalische und Theoretische Chemie and Röntgen Research Center for Complex Material Systems Campus Nord, Universität Würzburg, Emil-Fischer-Straße 42, 97074 Würzburg, Germany

[‡]Institut für Theoretische Physik, Leibniz Universität Hannover, Appelstraße 2, 30167 Hannover, Germany

[§]Departamento de Quimica Fisica, Universidad Complutense, 28040 Madrid, Spain

[∥]School of Chemistry (BK21), Seoul National University, Seoul 151-747, Republic of Korea

ABSTRACT: Extending the Shin−Metiu two-electron Hamiltonian, we construct a new Hamiltonian with effective singlet−triplet couplings. The Born−Oppenheimer electronic potentials and couplings are obtained for different parameters, and the laser-free dynamics is calculated with the full Hamiltonian and in the adiabatic limit. We compare the dynamics of the system using nuclear wave packets for different numbers of Born−Oppenheimer potentials and vibronic wave packets on a full 3-dimensional (two electron coordinates plus one nuclear coordinate) grid. Using strong fields, we show that it is possible to dynamically lock the spin state of the system by decoupling the singlet−triplet transition via a nonresonant dynamic Stark effect in the adiabatic limit. Although a similar spin-locking mechanism is observed in the dynamics of vibronic wave packets, multiphoton ionization cannot be neglected leading to the breakdown of the control scheme.

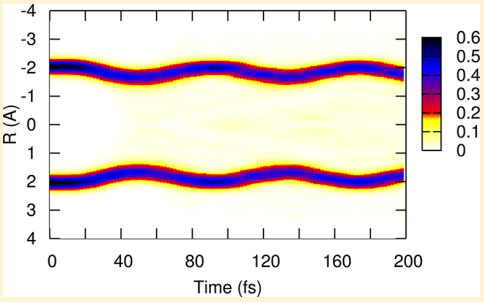

INTRODUCTION

The application of femtosecond laser pulses proved to be very useful in inducing, characterizing and controlling molecular processes as in, e.g., unimolecular reactions.[1] The concept of a nuclear wave packet was paramount in constructing theoretical models that guided the experiments and provided the grounds for the design of quantum control schemes.[2−6] Despite its great explanatory capabilities, the dynamics of nuclear wave packets (DNWP) generally fails to account for important physical processes in two limits: at high excitation and in strong fields. Then the breakdown of the Born−Oppenheimer approximation (BOA) and the role of electron dynamics, specially of ionization processes, must be considered carefully.

Recently, the development of phase-stabilized subfemtosecond pulses[7] or train of pulses[8] has led to the emerging field of attophysics.[9,10] Many theoretical challenges lie ahead in understanding the key dynamical aspects of the laser-driven electrons, particularly when the single-active electron approximation is not valid, that is, for highly correlated electronic motion. We note that a large part of the attosecond schemes, such as streaking, requires the presence of a strong infrared field. In this work we are interested in exploring the limit of validity of the nuclear wave packet approach when using strong pulses.

The solution of the Schrödinger equation of coupled electron−nuclear motion is far too demanding. Therefore, models of reduced dimensionality have been employed extensively to describe multiphoton processes occurring in strong laser fields see, e.g., refs 11−15. Shin and Metiu introduced a useful one-dimensional model for charge-transfer processes in solids.[16,17] Within their approach, the electron−nucleus interactions are parametrized in such a way that the transition from a Born−Oppenheimer adiabatic dynamics to motions involving strong nonadiabatic couplings can be studied systematically.[18−21] The initially proposed model involved a single electron and a single nucleus moving in one dimension, but the extension to include two electrons has been presented.[22] Below, we perform another extension of the Shin−Metiu model where a coupling of singlet and triplet states is introduced heuristically. We will refer to this model as the ESM (extended Shin−Metiu) model. For the purpose of illustrating the dynamics of spin transitions, the strength of the coupling was chosen so that full singlet−triplet population transfer would occur in the range of 100 fs. The ESM model allows us to evaluate the role of *static* and *dynamic* electron correlation and the breakdown of the BOA in the presence of strong fields, by comparing the results of DNWP for the Born−Oppenheimer approximation of the ESM model, with the dynamics of *vibronic* wave packets, that is, wave packets depending on two electronic coordinates and one internuclear distance.

In this work we focus on controlling the spin state of the wave function. Only a few schemes have been proposed in the literature to optically control spin transitions (which are naturally dipole forbidden) by means of strong laser pulses. For instance, Hübner et al. have numerically applied ultrashort π-pulses to induce spin

Special Issue: Jörn Manz Festschrift

Received: July 3, 2012
Revised: August 30, 2012
Published: September 4, 2012

   dx.doi.org/10.1021/jp306566x | *J. Phys. Chem. A* 2012, 116, 11427−11433

changes,[23−26] whereas Manz et al. used a combination of IR and UV pulses.[27,28] The properties of strong fields were fully used in the nonresonant dynamic Stark effect (NRDSE) scheme.[29−35] Strong fields generate large Stark shifts that strongly change the spectrum of the electronic states. If localized couplings such as conical intersections or spin−orbit couplings exist between the electronic states, by choosing fields with the appropriate intensity, one can displace the positions and energies where these transitions occur. Without changing the electronic state or even strongly modifying the vibrational energy, it is therefore possible to force the initial wave function to avoid (or visit) these regions at a given time, thus changing the rate of those processes. In the ESM model this implies using field intensities of the order of a TW/cm^2 or higher.

In this work we show how the NRDSE allows us to lock the spin transition in the DNWP even when the dimension of the basis of electronic states in the Born−Oppenheimer approximation increases. The same principles apply to the dynamics of vibronic wave packets. However, multiphoton ionization cannot be avoided and is the predominant dynamical process. Ultimately, a better understanding of the dynamics of vibronic wave packets will certainly motivate the emergence of newer control schemes. This work, essentially, sets up the first stage, where a control scheme motivated by the physics of nuclear wave packets, fails to control the system when ionization is not neglected.

The remainder of the paper is organized as follows. In section II we describe the ESM Hamiltonian and its Born−Oppenheimer limit, detailing the procedure used to include singlet−triplet coupling in a phenomenological way. Section III gives the results of the dynamics in the absence of an external field and with the control field. We compare the results obtained within the Born−Oppenheimer approximation (DNWP) using different number of electronic states, and in the full ESM model (vibronic wave packets). Section IV contains the Conclusions.

HAMILTONIAN MODEL

Extended Shin−Metiu Model. We regard an extended version of the Shin−Metiu model[16,17] (ESM), which consists of an ion (coordinate R) and two electrons (coordinates x, y) being confined to move in a single dimension. These particles interact with each other and two additional fixed ions through screened Coulomb interactions. The particle configuration is sketched in Figure 1. There, the fixed ions are located at distances $R_1 = -5$ Å and $R_2 = 5$ Å. The Hamiltonian reads (atomic units are employed)

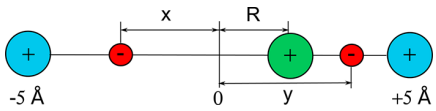

Figure 1. Particle configuration in the one-dimensional model of coupled nuclear-electronic dynamics. Two electrons and one nucleus move in the field of two extra nuclei, which are fixed at distances of ±5 Å.

$$H(x,y,R) = -\frac{1}{2}\frac{\partial^2}{\partial x^2} - \frac{1}{2}\frac{\partial^2}{\partial y^2} - \frac{1}{2m}\frac{\partial^2}{\partial R^2} + V(x,y,R) \tag{1}$$

with the nuclear mass m, which we take as the proton mass. The potential energy is given as

$$V(x,y,R) = \frac{Z_1 Z}{|R_1 - R|} + \frac{Z_2 Z}{|R_2 - R|} + \frac{\mathrm{erf}(|x-y|/R_e)}{|x-y|} - \frac{Z_1\,\mathrm{erf}(|R_1 - x|/R_f)}{|R_1 - x|} - \frac{Z_2\,\mathrm{erf}(|R_2 - x|/R_f)}{|R_2 - x|} - \frac{Z\,\mathrm{erf}(|R - x|/R_c)}{|R - x|} - \frac{Z_1\,\mathrm{erf}(|R_1 - y|/R_f)}{|R_1 - y|} - \frac{Z_2\,\mathrm{erf}(|R_2 - y|/R_f)}{|R_2 - y|} - \frac{Z\,\mathrm{erf}(|R - y|/R_c)}{|R - y|} \tag{2}$$

where in the numerical calculation, the charge numbers are set to $Z_1 = Z_2 = Z = 1$. The electron−nuclei and electron−electron interactions are parametrized by error functions (erf) and contain the three screening parameters R_c, R_e, and R_f. They are taken as equal and are assigned numerical values of 1.5 Å in our numerical calculations. The total time-dependent wave function of the two-electron, one-nucleus system is

$$\phi(q,t) = \psi(x,y,R,t)\, s(1,2) \tag{3}$$

where $\psi(x,y,R,t)$ is the time-dependent spatial part and $s(1,2)$ denotes the spin function, respectively. Because of exchange symmetry, the spatial wave function is either symmetric ($\psi^+(x,y,R,t)$, singlet (S)) or antisymmetric ($\psi^-(x,y,R,t)$, triplet (T)) with respect to electron exchange. As long as there is no coupling between the two symmetry species, the time evolution of the wave functions is given as

$$\psi^{\pm}(x,y,R,t) = \mathrm{e}^{-\mathrm{i}Ht}\psi^{\pm}(x,y,R,t=0) \tag{4}$$

so that, starting with an symmetric/antisymmetric wave function, the symmetry is strictly conserved as a function of time.

To monitor spin-flip transitions, we introduce a coupling between the two symmetry manifolds and write the Hamiltonian for the total system as

$$\mathbf{H} = \begin{pmatrix} H(x,y,R) & J(x,y) \\ J(x,y) & H(x,y,R) \end{pmatrix} \tag{5}$$

In order that the symmetry in the two components of the wave function is conserved, the coupling operator $J(x,y)$ has to be antisymmetric with respect to electron exchange. As a simple function which fulfills this property we choose

$$J(x,y) = \lambda(x - y) \tag{6}$$

where λ is here taken as a constant coupling strength-parameter. For simplicity, we neglect the possible dependence of the coupling on the nuclear coordinate R.

Electronic Structure and Potential Curves. We first study the electronic structure of the model system by solving the electronic Schrödinger equation for fixed nuclear positions R, which, in the uncoupled case, reads

$$H_{\mathrm{el}}(x,y,R)\, \varphi_n^{\mathrm{M}}(x,y,R) = V_n^{\mathrm{M}}(R)\, \varphi_n^{\mathrm{M}}(x,y,R) \tag{7}$$

where M = S or M = T, respectively, and $H_{\mathrm{el}}(x,y,R)$ denotes the electronic Hamilton operator:

$$H_{\mathrm{el}}(x,y,R) = -\frac{1}{2}\frac{\partial^2}{\partial x^2} - \frac{1}{2}\frac{\partial^2}{\partial y^2} + V(x,y,R) \tag{8}$$

dx.doi.org/10.1021/jp306566x | J. Phys. Chem. A 2012, 116, 11427−11433

The functions $V_n^M(R)$ $(n = 1, 2, ...)$ denote the respective potential energy curves. In the coupled problem, we have:

$$\begin{pmatrix} H_{el}(x,y,R) & J(x,y) \\ J(x,y) & H_{el}(x,y,R) \end{pmatrix} \begin{pmatrix} \varphi_n^+(x,y,R) \\ \varphi_n^-(x,y,R) \end{pmatrix} = V_n(R) \begin{pmatrix} \varphi_n^+(x,y,R) \\ \varphi_n^-(x,y,R) \end{pmatrix} \quad (9)$$

The potentials and electronic wave functions in each case are calculated by complex-time propagation.[36] Because the total wave function contains a symmetric and antisymmetric component and is no longer of pure singlet or triplet character, we denote the two components as $\varphi_n^{\pm}(x,y,R)$, respectively. In Figure 2, we show the two sets of potentials obtained in the case

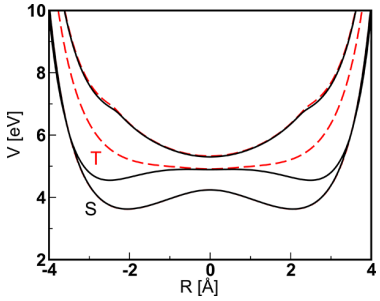

Figure 2. Potential curves $V_n^M(R)$ for the lowest three electronic quantum numbers n in the singlet (M = S, solid lines) and in the triplet (M = T, dashed lines) states. Notice that T_1 and T_3 practically coincide with S_1 and S_3, so that they cannot be distinguished from the corresponding singlets in the figure.

of zero coupling and for quantum numbers n = 1, 2, and 3. The curves within the same symmetry are well separated in energy, suggesting that a nuclear dynamics can properly be described within the adiabatic approach of the Born−Oppenheimer approximation.

The ground-state potentials of the two symmetries are nearly identical whereas larger differences occur in the first excited state, except for the region around the symmetry point $R = 0$. This can be rationalized by analysis of the electronic wave functions. In the ground state, the electronic probability density is attached to the left and right fixed nuclei with vanishing density at the symmetry line with $x = y$. These densities are almost identical for both symmetries. In the excited state, however, fixing the nuclear distance to $R = 2$ Å, density builds up at the symmetry line in the singlet density, which then differs essentially from the triplet density, the latter being zero for $x = y$ by definition. It is only around the configuration where the nucleus is located at $R = 0$, that the two electron densities again resemble each other. We note that the near degeneracy of the singlet and triplet lowest energy states is related to the present choice of the model parameters and the linear configuration of our model, which does not allow for exchange contributions from occupied orbitals located at larger negative and positive distances, R. Introducing a coupling, as specified above, results in a splitting of the potential curves. An example is given in Figure 3, which contains potentials obtained for a coupling parameter $\lambda = 10.28 \times 10^{-3}$ eV/Å.

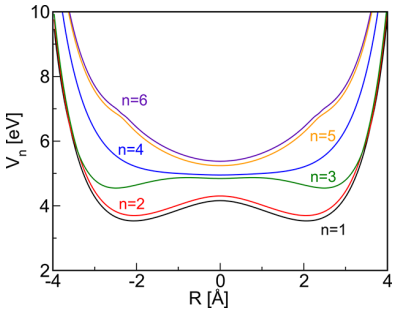

Figure 3. Potential curves $V_n(R)$ for the lowest six electronic quantum numbers n and a coupling parameter of $\lambda = 10.28 \times 10^{-3}$ eV/Å.

The different electronic states are coupled by matrix elements of the form

$$V_{S_n,T_m}(R) = \int dx\, dy\, \varphi_n^S(x,y,R)\, J(x,y)\, \varphi_m^T(x,y,R) \quad (10)$$

These couplings are displayed in Figure 4 for a coupling parameter of $\lambda = 1.028 \times 10^{-3}$ eV/Å. Note that they directly scale

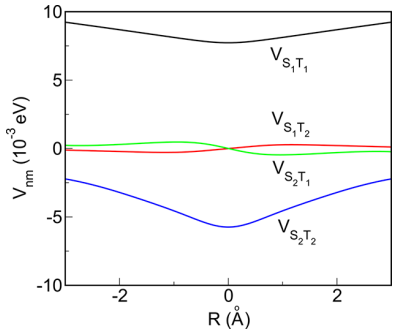

Figure 4. Potential coupling matrix elements.

with λ. They are symmetric/antisymmetric with respect to the configuration at $R = 0$. The strongest couplings exist between states with equal quantum numbers in the two manifolds. In the case these numbers are different, the extra node on one or the other wave function leads to a reduced coupling and also sign changes. The choice of λ determines the strength of the coupling and therefore the time scale of the singlet−triplet transition. As shown in the results in section III, this leads to full singlet−triplet transfer in roughly 100 fs. This choice allows control with an external field.

When an electric field interacts with the system, the coupled electronic states approach also needs the transition dipole-moments. They are defined as (M = S, T)

$$\mu_{M_n,M_m}(R) = \int dx\, dy\, \varphi_n^M(x,y,R)\, (-x - y)\, \varphi_m^M(x,y,R) \quad (11)$$

In Figure 5, we compare these transition dipole moments with those determined with the electronic wave functions of the coupled problem, i.e.:

$$\mu_{n,m}(R) = \int dx\, dy\, \varphi_n^-(x,y,R)\, (-x - y)\, \varphi_m^-(x,y,R) + \int dx\, dy\, \varphi_n^+(x,y,R)\, (-x - y)\, \varphi_m^+(x,y,R) \quad (12)$$

dx.doi.org/10.1021/jp306566x | J. Phys. Chem. A 2012, 116, 11427−11433

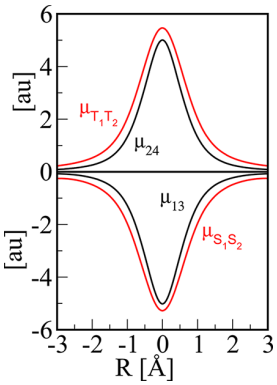

Figure 5. Transition dipole moments μ_{nm} between the spin-coupled states compared to those calculated by employing the noncoupled triplet and singlet electronic wave functions ($\mu_{M_nM_m}$).

These elements are strongest for the symmetric configuration and of opposite sign for the two spin manifolds. The weak mixing of the states of different symmetry does not change the values essentially, as is the case for the potential energy curves; see Figure 3. Note that our system is charged and thus the dipole moments are not translationally invariant. We calculated them in the coordinate system illustrated in Figure 1.

Hamiltonian for the DNWP Approach. Assuming the Born−Oppenheimer approximation, it is possible to simulate the dynamics of the singlet−triplet population transfer by means of nuclear wave packets. To observe the effects of a strong nonresonant field on the spin-coupling dynamics, one needs to include in the Hamiltonian at least one excited singlet and one excited triplet state for a symmetrical setting where the strongly coupled lowest-energy states can experience Stark-shifts, thus changing the dynamics. This is what we call the minimal symmetric set (MSS) model.

In the MSS model, the nuclear dynamics Hamiltonian in the presence of the control field $\varepsilon_c(t)$ is

$$\mathbf{H}^{\text{eff}} = -\frac{1}{2m}\frac{\mathrm{d}^2}{\mathrm{d}R^2}\mathbf{I} + \begin{pmatrix} V_1^S(R) & -\mu_{S_1,S_2}(R)\,\varepsilon_c(t) & V_{S_1,T_1}(R) & V_{S_1,T_2}(R) \\ -\mu_{S_1,S_2}(R)\,\varepsilon_c(t) & V_2^S(R) & V_{S_2,T_1}(R) & V_{S_2,T_2}(R) \\ V_{T_1,S_1}(R) & V_{T_1,S_2}(R) & V_1^T(R) & -\mu_{T_1,T_2}(R)\,\varepsilon_c(t) \\ V_{T_2,S_1}(R) & V_{T_2,S_2}(R) & -\mu_{T_1,T_2}(R)\,\varepsilon_c(t) & V_2^T(R) \end{pmatrix} \tag{13}$$

where **I** is the 4 × 4 unit matrix and the potentials and couplings are those obtained in the Born−Oppenheimer approximation of the ESM model as explained in section II.B. In the numerical calculations we use "square" laser pulses with fast ramps of $\sin^2(\pi(t-t_0)/\tau_s)$ form. The switching on/off time is set to τ_s = 25 fs.

The extension of the model to include a more complete set of electronic states is straightforward. One only needs to include in eq 13 all the relevant potentials $V_j^S(R)$, $V_j^T(R)$ and couplings $\mu_{S_iS_j}(R)$, $\mu_{T_iT_j}(R)$, $V_{S_iT_j}(R)$, calculated in section II.B. In addition to the MSS we have considered a model including the 6 lowest singlet and triplet states (LSS). These 12 Born−Oppenheimer states span the energy range of any 3-photon process starting in S_1 for the laser frequency used in the numerical results.

DYNAMICS

Field-Free Dynamics. The quantum dynamics in the full vibronic calculation is governed by the time-dependent Schrödinger equation (TDSE) containing the Hamiltonian of eq 1 with solutions $\psi(x,y,R,t)$. We solve the TDSE on a 3D grid of 256 × 256 × 256 points using the split-operator[37] with Fast-Fourier transform technique to evaluate the effect of the kinetic energy operator.[38] On the spatial grid, the electron coordinates vary from −15 to +15 Å whereas the nuclear coordinate varies from −4 to +4 Å. Absorbing barriers at the grid boundaries were used to take into account ionization and dissociation. With respect to the DNWP, the TDSE is governed by the Hamiltonian of eq 13 (or a similar one, based on the LSS model). The numerical solution is also obtained using the split-operator technique in the nuclear grid of 256 points defined between R = −4 and R = +4 Å.

To compare the exact calculation with the DNWP approach, we calculate populations as (M = S, T)

$$P_n^M(t) = \int \mathrm{d}R\ |\langle\varphi_n^M(x,y,R)|\psi(x,y,R,t)\rangle_{xy}|^2 \tag{14}$$

In other words, we first project the total wave function on the electronic eigenfunctions of the uncoupled system and calculate the norm of the such obtained nuclear component. We start with an illustration of the field-free dynamics and regard the singlet−triplet population transfer choosing an initial wave packet, which is the vibronic ground state of the S_1 state. This state most strongly couples to the T_1 state so that for $\lambda = 1.028 \times 10^{-3}$ eV/Å, a complete transfer of population takes place in approximately 120 fs, following basically the behavior of a resonant two-level system.

This is illustrated in Figure 6, which compares the populations obtained from the fully coupled calculation ($P_n(t)$) with those

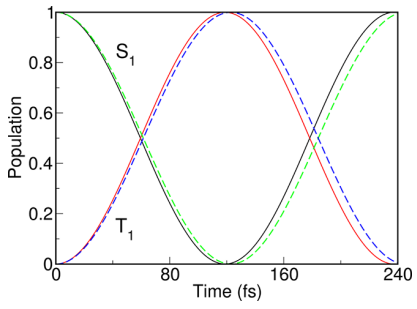

Figure 6. S−T population transfer. Shown are curves obtained within the complete electron−nuclear calculation (straight lines) and within the approach employing coupled electronic states (dashed lines).

dx.doi.org/10.1021/jp306566x | J. Phys. Chem. A 2012, 116, 11427−11433

from the DNWP approach ($P_m^M(t)$) calculated using only the lowest energy singlet and triplet states. It is seen that the spin-transition dynamics is very similar, which means that the DNWP approach gives the correct dynamical results for the example regarded. Similar results would be obtained for different values of λ, varying only the period of the Rabi flopping between the singlet and triplet states.

Nuclear Wave Packet Dynamics in External Fields. We have seen that in the absence of an external field the population is rapidly transferred from the singlet to the triplet state. To manipulate the spin transition, the control pulse must be switched fast enough. Additionally, because the transition dipole moment in the Franck–Condon region is relatively small, we need strong pulses. However, multiphoton absorption to other singlet states must be avoided. The mechanism of decoupling the singlet–triplet transition relies on second-order nonresonant processes.[33,34] Thus, the laser frequency should be chosen to maximize the differences in the dynamic polarizabilities of S_1 and T_1. This is accomplished by choosing ω close to the $T_1 \rightarrow T_2$ Franck–Condon transition, which is relatively separated from the $S_1 \rightarrow S_2$ Franck–Condon transition. Using this guide, one can numerically estimate the necessary pulse peak amplitude ε_0 and carrier frequency ω. As a very rough estimate, for a constant field ε_0, one needs the energy of the nonlinear interaction with the field (the Stark shift), $\alpha\varepsilon_0^2$, to be at least of the order of $V_{S_1T_1}$ $\sim$ 0.01 eV. For $|\mu_{S_iS_j}| \sim 1$ au, assuming the dynamic polarizability is of the order of $\alpha \sim \mu^2 \sim 1$, we obtain $\varepsilon_0 \sim 0.02$ au.

In Figure 7 we show the population dynamics using a single control pulse ε_c for both the MSS and LSS models. By numerical

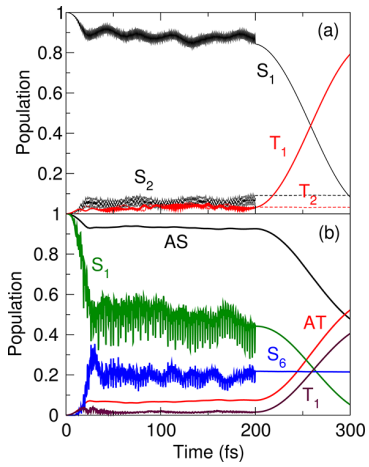

Figure 7. Electronic states population dynamics in the (a) MSS and (b) LSS models, with laser intensity 10.1 TW/cm^2 and $\hbar\omega$ = 1.63 eV. AS and AT denote the total singlet and triplet populations, respectively.

sampling we obtained best results in the LSS model with pulse parameters ε_0 = 0.017 au (implying a peak intensity I_0 of 10.1 TW/cm^2) and $\hbar\omega$ = 1.63 eV, although there is some flexibility in the choice of pulse frequencies in different intervals. With weaker pulses, the time-averaged population of the triplet state increases and the spin state does not remain constant. With stronger pulses the small Rabi oscillations observed in the MSS results (Figure 7a) can be totally suppressed. However, in the LSS model the time-averaged population in the excited singlet states considerably increases and leads to singlet–triplet transitions among the excited states. The pulse duration is arbitrarily set as 200 fs to display more clearly the effect of spin locking. However, this pulse parameter can be adjusted freely.

As observed, during the action of the laser, the population is efficiently maintained within the singlet states manifold. However, when more electronic states are included in the model (as in the LSS versus the MSS) the overall population of the triplet states increases a little, but more importantly, part of the population is excited to different singlet states. Despite using nonresonant pulses, it is difficult to avoid multiphoton absorption, but the absorption leads to a steady population. No Rabi flopping or nuclear wave packet dynamics is observed.

In Figure 8 we show the evolution of the nuclear probability density of all the singlet states. Although the potentials shown in

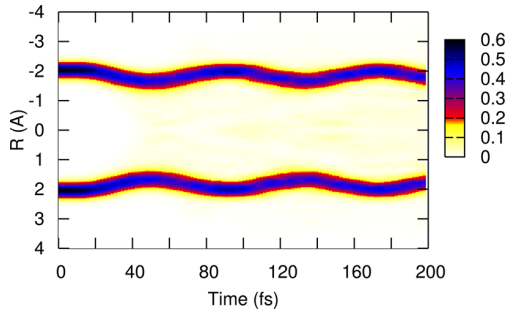

Figure 8. Nuclear probability density for all the singlet states in the LSS model with I_0 = 10.1 TW/cm^2 and $\hbar\omega$ = 1.63 eV.

Figure 2 have very different equilibrium geometries for the different singlet states, so that one could expect the spread of the nuclear density over all the energy available configuration space, the nuclear wave packet dynamics is mostly confined to the bottom of the potential energy in V_1^S, a signature that the dynamics is still mainly adiabatic.[33,34] The population dynamics in Figure 7 nicely documents that, as long as the control-field is active, the singlet population can be kept constant in the average whereas afterward, the S–T population transfer becomes effective.

Laser-Driven Vibronic Wave Packet Dynamics. We now regard the interaction of the control field $\varepsilon_c(t)$ used in the LSS model with the coupled electron–nuclear system. The Hamiltonian then is of the form

$$H_w(x,y,R,t) = H(x,y,R) + (x + y)\cdot\varepsilon_c(t) \qquad (15)$$

where $H(x,y,R)$ is the Hamiltonian from eq 1. For comparison with the DNWP approach, we calculate the populations as defined in eq 14, which are shown in Figure 9 for the singlet states

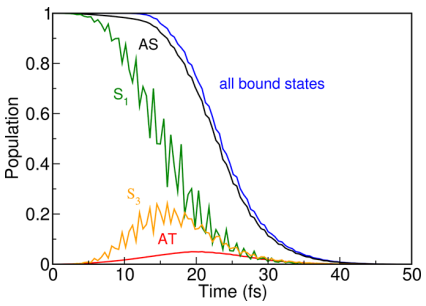

Figure 9. Population dynamics in the coupled nuclear-electron system that is subject to the control field derived within the LSS model. The population in different singlet states is shown, as indicated. Also included is the total singlet (AS) and triplet (AT) and also the total bound-state population.

dx.doi.org/10.1021/jp306566x | J. Phys. Chem. A 2012, 116, 11427–11433

S_1 and S_3. The initial decay of the S_1 state is similar to the one obtained within the LSS model (Figure 7). Also, as in the LSS approach, the triplet states are not populated essentially. This can be seen from the total triplet population (AT), which is also included in the figure. Thus, for short interaction times, both approaches give similar results.

For longer times, a different behavior evolves from the coupled electron−nuclear treatment. There, very quickly, the total bound-state population decreases to zero, meaning that the control field induces complete ionization within 40 fs. Thus an efficient ladder climbing takes place that cannot occur in the DNWP approach that incorporates a limited set of electronic states and no ionization continuum.

Although multiphoton ionization quickly undermines the purpose of controlling the spin state, the process occurs essentially in the Franck−Condon region. This can be readily observed by following the dynamics of the nuclear density of the vibronic wave packets in Figure 10. This density is determined from the

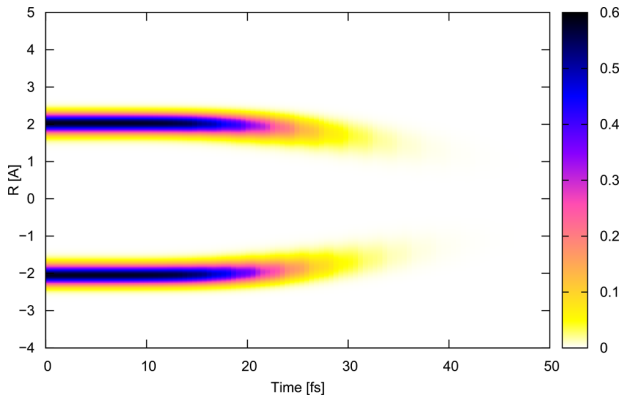

Figure 10. Nuclear probability density for all the singlet states obtained from the dynamics of vibronic wave packets using a pulse with I_0 = 10.1 TW/cm^2 and $\hbar\omega$ = 1.63 eV.

bound state fraction of the wave function. Because upon ionization the electronic density moves into the asymptotic region, the density approaches zero for longer times.

The ionization takes place with the nuclei in the initial equilibrium geometry. On the other hand, the control pulse $\varepsilon_c(t)$ is still successfully avoiding spin transitions, as revealed by the average electronic spin angular momentum, $S_{av}(t) = (\langle\psi|S^2|\psi\rangle)^{1/2}/\langle\psi|\psi\rangle = (2P_T/(P_T + P_S))^{1/2}$. In Figure 11 we show

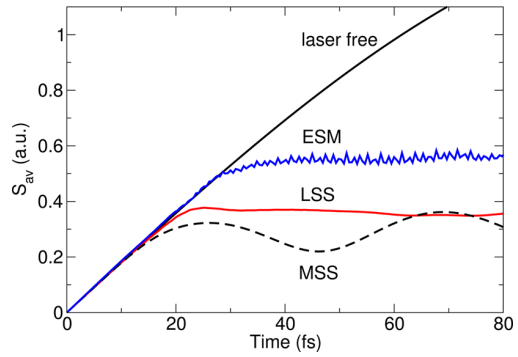

Figure 11. Average electronic spin angular momentum in the absence of the external field, and using a pulse with I_0 = 10.1 TW/cm^2 and $\hbar\omega$ = 1.63 eV for the different models.

how S_{av} behaves for the different models used in this work. Starting from the singlet state, S_{av} = 0, the electronic angular momentum reaches $\sqrt{2}$ in the triplet state, in the absence of the external field. Via NRDSE S_{av} can be efficiently "locked" with a small contamination of triplet character. For a given field strength ε_0 the locking is more effective (S_{av} is more steady) in the LSS than in the MSS, because the polarizabilities are larger when more electronic states are included in the calculation. Increasing the number of triplet electronic states (all of them are included in the ESM model) only makes S_{av} a bit larger, as the number of triplet states to which the population can flow increases.

SUMMARY AND CONCLUSIONS

In this work we have extended the two-electron Shin−Metiu model to include singlet−triplet couplings in addition to nonadiabatic couplings. We have obtained electronic bound states and their couplings in the adiabatic limit of the model. The model is flexible enough to incorporate dynamic and static electron correlation effects and is thus an excellent starting point to study strong field dynamics of vibronic (two electron plus nuclear) wave packets. This allowed us to test the limit of validity of certain control strategies motivated by the Born−Oppenheimer dynamics.

In particular, we have applied a strong-field laser control scheme based on the nonresonant dynamic Stark effect. Including different numbers of electronic states in the Born−Oppenheimer approximation we were able to show efficient spin-locking, that is, dynamics such that the spin state could remain effectively unchanged during the laser action despite the strong singlet−triplet coupling. Due to the relatively weak dipole couplings, the scheme relied on using quite strong pulses, slightly detuned from electronic resonances. The results were sufficiently satisfactory given the constraints of the models.

The same principles of efficient spin-locking were observed to apply in the dynamics of vibronic wave packets. However, fast multiphoton ionization in the Franck−Condon region could not be avoided and is in fact the predominant dynamical process. Thus the NRDSE scheme, which is a control mechanism based on the dynamics of nuclear wave packets, fails to work when the scheme is applied to vibronic wave packets. We believe that a better understanding of the dynamics of vibronic wave packets is a necessary step to motivate new strong-field control schemes that may presumably overcome strong-field ionization. The extended Shin−Metiu model is a flexible but demanding arena where these schemes can be tested and put to work.

The ESM model assumes that both the electrons and the ions are aligned with respect to the laser field. The consequences of directly treating a full 9D model are difficult to assess as it is obviously numerically too demanding to perform the required calculations. However, it could be interesting to simply inspect the role of the alignment of the system with respect to the field. As the NRDSE scheme relies only on the peak intensity, for an extended string or solid or for a gas of heavy molecules whose rotational periods are orders of magnitude larger than the duration of the applied fields (where rotation could be neglected), the expected effect would be that the molecules or regions of the solid aligned with respect to the field would "freeze" the spin components, whereas other molecules or regions would show spin dynamics. On the contrary, for molecules with fast rotational periods one could in principle expect adiabatic alignment of the molecules, although light-induced conical intersections could affect the alignment and thus the degree of control.[39]

dx.doi.org/10.1021/jp306566x | J. Phys. Chem. A 2012, 116, 11427−11433

AUTHOR INFORMATION

Corresponding Author

*E-mail: isola@quim.ucm.es.

Notes

The authors declare no competing financial interest.

ACKNOWLEDGMENTS

M.F. acknowledges financial support by the State of Bavaria (Bayerisches Eliteförderungsgesetz). M.L. thanks the Deutsche Forschungsgemeinschaft for funding the Centre for Quantum Engineering and Space-Time Research (QUEST). I. R. S. and P. V. acknowledge support from the Dirección General de Investigación of Spain under Project No. CTQ2008-06760. B. Y. C. thanks the Basic Science Research Program by the National Research Foundation of Korea grant (2010-0005643). This project was supported by the COST-action CM0702 (Chemistry with Ultrashort Pulses and Free-Electron Lasers).

REFERENCES

(1) Zewail, A. H. *Angew. Chem., Int. Ed.* **2000**, *39*, 2586.
(2) Tannor, D. J.; Kosloff, R.; Rice, S. A. *J. Chem. Phys.* **1986**, *85*, 5805.
(3) Peirce, A.; Dahleh, M.; Rabitz, H. *Phys. Rev. A* **1988**, *37*, 4950.
(4) Kosloff, R.; Rice, S. A.; Gaspard, P.; Tersigni, S.; Tannor, D. J. *Chem. Phys.* **1989**, *139*, 201.
(5) Daniel, C.; Full, J.; González, L.; Lupulescu, C.; Manz, J.; Merli, A.; Vajda, Å .; Wöste, L. *Science* **2003**, *299*, 536.
(6) Engel, V.; Meier, C.; Tannor, D. J. *Adv. Chem. Phys.* **2009**, *141*, 29.
(7) Hentschel, M.; et al. *Nature* **2001**, *414*, 509.
(8) Paul, P. M.; et al. *Science* **2001**, *292*, 1689.
(9) Ivanov, M. Y.; Kienberger, R.; Scrinzi, A.; Villenueve, D. M. *J. Phys. B: At., Mol. Opt. Phys.* **2006**, *39*, R1.
(10) Krausz, F.; Ivanov, M. *Rev. Mod. Phys.* **2009**, *81*, 163.
(11) Chelkowski, S.; Zuo, T.; Atabek, O.; Bandrauk, A. D. *Phys. Rev. A* **1995**, *52*, 2977.
(12) Zuo, T.; Bandrauk, A. D.; Corkum, P. B. *Chem. Phys. Lett.* **1996**, *259*, 313.
(13) Chelkowski, S.; Foisy, C.; Bandrauk, A. D. *Phys. Rev. A* **1996**, *57*, 1176.
(14) Lein, M.; Gross, E.; Kreibich, T.; Engel, V. *Phys. Rev. A* **2002**, *65*, 033403.
(15) Jhala, C.; Lein, M. *Phys. Rev. A* **2010**, *81*, 063421.
(16) Shin, S.; Metiu, H. *J. Chem. Phys.* **1995**, *102*, 9285.
(17) Shin, S.; Metiu, H. *J. Phys. Chem.* **1996**, *100*, 7867.
(18) Erdmann, M.; Marquetand, P.; Engel, V. *J. Chem. Phys.* **2003**, *119*, 672.
(19) Erdmann, M.; Engel, V. *J. Chem. Phys.* **2004**, *120*, 158.
(20) Erdmann, M.; Baumann, S.; Gräfe, S.; Engel, V. *Euro. Phys. J. D* **2004**, *30*, 327.
(21) Gräfe, S.; Engel, V. *Chem. Phys.* **2006**, *329*, 118.
(22) Erdmann, M.; Gross, E. K. U.; Engel, V. *J. Chem. Phys.* **2004**, *121*, 9666.
(23) Gómez-Abal, R.; Hübner, W. *Phys. Rev. B* **2002**, *65*, 195114.
(24) Gómez-Abal, R.; Hübner, W. *J. Phys.: Condens. Matter* **2003**, *15*, S709.
(25) Gómez-Abal, R.; Ney, O.; Satitkovitchai, K.; Hübner, W. *Phys. Rev. Lett.* **2004**, *92*, 227402.
(26) Satitkovitchai, K.; Pavlyukh, Y.; Hübner, W. *Phys. Rev. B* **2005**, *72*, 045116.
(27) Korolkov, M. V.; Schmidt, B. *Chem. Phys. Lett.* **2002**, *361*, 432.
(28) Korolkov, M. V.; Manz, J. *J. Chem. Phys.* **2004**, *120*, 11522.
(29) Sussman, B. J.; Ivanov, M.-Y.; Stolow, A. *Phys. Rev. A* **2005**, *71*, 051401(R).
(30) Sussman, B. J.; Underwood, J. G.; Lausten, R.; Ivanov, M.-Y.; Stolow, A. *Phys. Rev. A* **2006**, *73*, 053403.
(31) Sussman, B. J.; Townsend, D.; Ivanov, M.-Y.; Stolow, A. *Science* **2006**, *314*, 278.
(32) Sola, I. R.; González-Vázquez, J.; Santamaria, J.; Malinovsky, V. S. *Phys. Rev. A* **2006**, *74*, 043418.
(33) González-Vázquez, J.; Sola, I. R.; Santamaria, J.; Malinovsky, V. S. *Chem. Phys. Lett.* **2006**, *431*, 231.
(34) González-Vázquez, J.; Sola, I. R.; Santamaria, J.; Malinovsky, V. S. *J. Chem. Phys.* **2006**, *125*, 124315.
(35) González-Vázquez, J.; Sola, I. R.; Santamaria, J.; Malinovsky, V. S. *J. Phys. Chem. A* **2007**, *111*, 2670.
(36) Kosloff, R.; Tal-Ezer, H. *Chem. Phys. Lett.* **1986**, *127*, 223.
(37) Feit, M. D.; Fleck, J. A., Jr.; Steiger, A. *J. Comput. Phys.* **1982**, *47*, 412.
(38) Kosloff, R. *J. Phys. Chem.* **1988**, *92*, 2087.
(39) Halasz, G. J.; Sindelka, M.; Moiseyev, N.; Cederbaum, L.; Vibok, A. *J. Phys. Chem. A* **2012**, *116*, 2636.

5.1.2 Manipulating the singlet-triplet transition in ion strings by nonresonant dynamic Stark effect

Vindel-Zandbergen, P., Falge, M., Chang, B.Y., Engel, V. and Sola, I.R., *J. Theor. Chem. Acc.*, **132**, *1359* (2013)

Theor Chem Acc (2013) 132:1359
DOI 10.1007/s00214-013-1359-3

REGULAR ARTICLE

Manipulating the singlet–triplet transition in ion strings by nonresonant dynamic Stark effect

Patricia Vindel-Zandbergen · Mirjam Falge · Bo Y. Chang · Volker Engel · Ignacio R. Sola

Received: 30 October 2012 / Accepted: 7 March 2013 / Published online: 20 April 2013

Abstract Using strong laser pulses, we show that it is possible to control the spin state in a model system based on a two-electron extension with spin couplings of the Shin–Metiu Hamiltonian, truncated to account for the lowest electronic energy states. We consider two different models depending on the number of electronic states included in the calculation. The initial electronic state determines when the spin state is stable or not in the absence of an external field. In the latter case, by nonresonant dynamic Stark effect, we show that it is possible to avoid spin transitions with strong fields, using different pulse frequencies. This effective spin locking requires minimizing absorption to excited singlets as well as decoupling the singlet and triplet electronic states. In the first case, we show that it is possible to force the spin transition by a combination of two pulses, a chirped pulse and a transform limited pulse, where the time-delay must be chosen to maximize spin switching on a different electronic state. Our results show that forcing the spin switching is a more difficult goal than avoiding it and that this goal becomes highly restricted when many electronic pathways or multi-photon processes are available.

Keywords Dynamic Stark effect · Wave-packet dynamics · Quantum control

Published as part of the special collection of articles derived from the 8th Congress on Electronic Structure: Principles and Applications (ESPA 2012).

P. Vindel-Zandbergen · I. R. Sola (✉)
Departamento de Quimica Fisica, Universidad Complutense, 28040 Madrid, Spain
e-mail: ignacio@tchiko.quim.ucm.es

M. Falge · V. Engel
Institut für Physikalische und Theoretische Chemie and Röntgen Research Center for Complex Material Systems, Universität Würzburg, Campus Nord, Emil-Fischer-Str. 42, 97074 Würzburg, Germany

B. Y. Chang
School of Chemistry (BK21), Seoul National University, Seoul 151-747, Republic of Korea

1 Introduction

Laser control of quantum processes is an active arena particularly in the application of femtosecond laser pulses to quantum-state excitation and unimolecular reactions [1–3]. Successful laser control experiments have been reported in an increasing variety of physical systems, including complex chemical and biological processes [1, 2].

Addressing the dynamics of complex systems, the mechanism of the optical control is often understood from the spectral features of the pulses [4] (albeit with important caveats [5]), implying correlations between the pulse frequencies and the Hamiltonian resonances, with relative phases of the spectrum adding important dynamical information concerning the cross-talk of the resonances [6]. However, this picture is no longer valid when strong fields are used. Nonresonant effects may then completely shift or distort the Hamiltonian spectrum, which is no longer independent of the pulse spectrum [7–13]. It is possible to base the control mechanism solely on the effects of the nonresonant dynamic Stark effect (NRDSE) [14–18]. This strategy is particularly useful when the aim of the control problem is to "disconnect" an undesired transition [16, 17]. The NRDSE is behind many interesting control scenarios involving molecular alignment [19–26], the control of photodissociation reactions [14, 15, 27–29], or the control

of singlet–triplet transitions [16–18], which is also the motivation of this work.

The spin–orbit coupling is a relativistic effect that mainly affects the Hamiltonian of systems with heavy nuclei [30]. In molecules, the spin–orbit transition is one of the main sources that causes the breakdown of the Born–Oppenheimer approximation in the dynamics of excited states, inducing intersystem crossing (ISC) and altering the spectroscopy and photodissociation of molecules and the relaxation rates in complex biological systems [31, 32]. Although in not heavy atoms, the mass is often invoked as a reason to neglect the ISC processes, simulations of the dynamics of polyatomic molecules with light atoms have shown that the effect of ISC must be taken into account in many occasions [33–35]. In solids, the spin coupling between different states can be used to create states of mixed multiplicity and to prepare optical spin switches [36–39]. These are important in spintronics [40] and may have potential application as quantum information storage or quantum information processing devices [41].

Rather than using a realistic Hamiltonian for a particular system, in this work we use the very generic Shin–Metiu (SM) Hamiltonian that models charge transfer processes in some matrix environments [42–47]. The original SM model is conveniently extended to include two electron processes with singlet–triplet couplings [48, 49]. This extended Shin–Metiu (ESM) model is particularly interesting because one can treat electron and nuclear processes at the same level, without invoking the Born–Oppenheimer approximation. Recently, we have shown that in the dynamics of the ESM with strong fields, ionization is important and it is in fact the dominant process [49]. In this work, however, we neglect ionization and use the adiabatic states (electronic potential curves) obtained from the electronic Hamiltonian of the ESM in the Born–Oppenheimer approximation to simulate the dynamics of the nuclear coordinates under the influence of laser pulses and singlet–triplet couplings. For this reason, in Sect. 2 we study the ESM and give the different electronic potentials and couplings. We also show the spin-coupling dynamics of the system starting from different initial states.

The goal of the study is to survey the extent to which optical control of the singlet–triplet transfer is possible, either by adiabatically "freezing" the spin populations by means of a laser, such that the rate of spin transfer is substantially reduced, or by forcing the spin transition when this is negligible. The control of these processes is based either on a pump–dump pulse sequence or on the NRDSE scheme, whose principles are briefly reviewed for the system of study in Sect. 3. Preliminary results have shown that the NRDSE scheme can induce spin freezing, although ionization takes over the system in <50 fs. In this work, we study in detail the processes of both spin locking and spin switching. Two models of different complexity (involving different number of electronic states and couplings) are introduced. In Sect. 4, we analyze spin locking for both models, outlining the different roles of the pulse parameters, and in Sect. 5, we study the more difficult process of spin-state switching. Finally, Sect. 6 is the summary and conclusions.

2 Hamiltonian model and field-free dynamics

The electronic potentials and dipole couplings are obtained from the Born–Oppenheimer limit of an extended version of the Shin–Metiu model (ESM), including spin couplings. The ESM consists of an ion (coordinate R) and two electrons (coordinates x, y) confined to move in a single dimension, interacting with each other and two additional fixed ions through screened Coulomb interactions. Because of exchange symmetry, the spatial wave function is either symmetric ($\psi^S(x, y, R, t)$, singlet (S)) or anti-symmetric ($\psi^T(x, y, R, t)$, triplet (T)) with respect to electron exchange. Details are given in ref. [49].

The spin uncoupled Born–Oppenheimer potential energy curves and electronic wave functions are obtained by imaginary time propagation of an electronic wave function of singlet/triplet symmetry $\psi^M(x, y, t;R)$ ($M = S, T$) at fixed nuclear position R

$$\psi^M(x, y, t; R) = e^{-H_{\mathrm{el}}t}\psi^M(x, y, t = 0; R) \tag{1}$$

with the electronic Hamiltonian operator

$$H_{\mathrm{el}}(x, y, R) = -\frac{1}{2}\frac{\partial^2}{\partial x^2} - \frac{1}{2}\frac{\partial^2}{\partial y^2} + V(x, y, R) \tag{2}$$

for different values of R. In the absence of spin coupling in the electronic Hamiltonian, the wave function symmetry is conserved. For long times, t, $\psi^M(x, y, t;R)$ converges to the ground state $\varphi_1^M(x, y, R)$ of the respective symmetry and the norm of the wave function decreases as $N(t) = e^{-2V_1(R)t}$. After the ground state is determined, the next higher eigenstate $\varphi_2^M(x, y, R)$ is obtained by another imaginary time propagation starting from an initial state where the ground state is projected out:

$$\begin{aligned}\tilde{\psi}^M(x, y, t = 0; R) &= \psi^M(x, y, t \\ &= 0; R) - \left\langle \psi^M(x, y, t = 0; R) \middle| \varphi_1^M(x, y, R) \right\rangle \\ &\cdot \varphi_1^M(x, y, R).\end{aligned} \tag{3}$$

Higher eigenstates are calculated successively using the same scheme. In this way, the basis of Born–Oppenheimer electronic states $\{\varphi_j^M(x, y, R)\}$ and their respective potential curves $V_j^M(R)$ are obtained. Dipole and spin couplings are evaluated with respect to these electronic basis as well.

To monitor spin transitions, we introduce in a heuristic way a spin-coupling term of the form

$$J(x,y) = \lambda(x-y), \tag{4}$$

where the coupling strength-parameter is chosen as $\lambda = 1.028 \times 10^{-3}$ eV/Å. For simplicity, we neglect the possible dependence of the coupling on the nuclear coordinate R. $J(x, y)$ creates new potential energy terms that couple (and mix) the Born–Oppenheimer electronic potentials. They are obtained from

$$V_{S_n,T_m}(R) = \int \mathrm{d}x\,\mathrm{d}y\,\varphi_n^S(x,y,R)J(x,y)\varphi_m^T(x,y,R). \tag{5}$$

where φ_n^S and φ_m^T denote the electronic eigenfunctions of singlet and triplet symmetry, respectively. To monitor laser-driven dynamics, we calculate the transition dipole moments

$$\mu_{M_n,M_m}(R) = \int \mathrm{d}x\,\mathrm{d}y\,\varphi_n^M(x,y,R)(-x-y)\varphi_m^M(x,y,R). \tag{6}$$

where $M = S$ or T.

In Fig. 1, we show the first electronic singlet and triplet potentials obtained from the ESM Hamiltonian for a particular choice of parameters (screening parameters $R_c = R_e = R_f = 1.5$ Å and charge numbers $Z_1 = Z_2 = Z = 1$ for the ESM Hamiltonian, see ref. [49]), neglecting the spin-coupling terms. The general feature of these potentials is that the singlet and triplet states come on pairs, showing either a double-well structure or a single equilibrium geometry at $R = 0$. Because the two electrons tend to be at opposite sides of the central ion (that is, each facing a different end-ion), the exchange symmetry of the electronic wave function does not lead to substantial energy differences between the singlet and the triplet wave functions. Thus, the singlet–triplet transfer due to the V_{S_j,T_j} terms (for $j = 1$, 3, etc.) is expected to be large. However, V_2^S and V_2^T (V_5^S and V_5^T as well, for higher energies) have a different structure near the equilibrium geometry and the spin-coupling mechanism is not efficient for any reasonable value of λ.

In addition to the spin coupling, nonadiabatic coupling terms could have been included. The energy separation between the singlet curves (and between the triplet curves as well) makes internal conversion processes very unlikely, as shown in the numerical results obtained solving the full vibronic Hamiltonian [49]. Thus, we neglect their contribution in the present work.

In Fig. 2, we show the population dynamics starting either from V_1^S or from V_2^S in the absence of any external field. We solve the time-dependent Schrödinger equation for the nuclear motion in two electronic states (S_j and T_j, for j either 1 or 2),

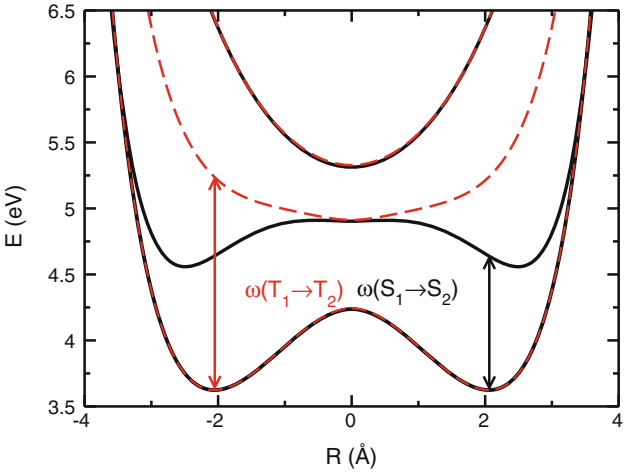

Fig. 1 Potential *curves* for the lowest three electronic states with singlet ($M = S$, *solid lines*) and triplet ($M = T$, *dashed lines*) symmetries. Notice that T_1 and T_3 practically coincide with S_1 and S_3, while S_2 and T_2 have different equilibrium geometries. Also shown in the *figure* are the frequencies for the Franck–Condon resonant transition between $S_1 \rightarrow S_2$ and $T_1 \rightarrow T_2$

$$i\frac{\partial}{\partial t}\begin{pmatrix}\psi_j^S\\ \psi_j^T\end{pmatrix} = -\frac{1}{2m}\frac{d^2}{\mathrm{d}R^2}\begin{pmatrix}\psi_j^S\\ \psi_j^T\end{pmatrix} + \begin{pmatrix}V_j^S(R) & V_{S_j,T_j}(R)\\ V_{S_j,T_j}(R) & V_j^T(R)\end{pmatrix}\begin{pmatrix}\psi_j^S\\ \psi_j^T\end{pmatrix} \tag{7}$$

using the split-operator with fast Fourier transform technique. In Eq. (7), m is the mass of a proton.

For the choice of the coupling parameter λ, we observe full singlet–triplet switching in a period $T \sim 120$ fs starting in V_1^S, and practically no triplet contamination starting from V_2^S (the maximum population in T_2 is 3×10^{-5}). The goal of this work is to design optical processes to avoid the spin

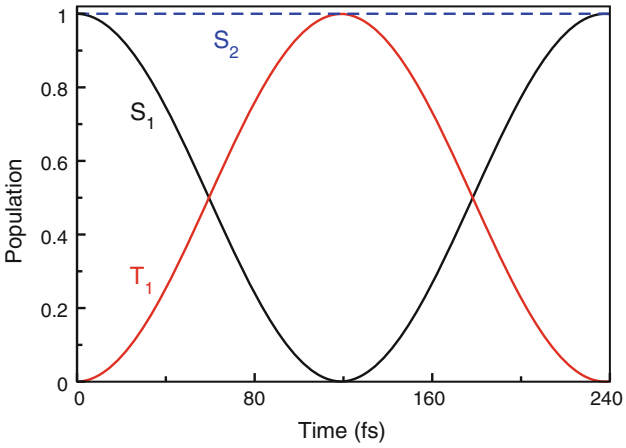

Fig. 2 Singlet triplet population transfer in the absence of an external field. In *solid lines*, we show the population of S_1 and T_1 when the dynamics starts in S_1. In *dashed line,* we show the population of S_2 when the dynamics starts from this excited state. In this case, the population in T_2 remains practically zero and it is not shown

dynamics from V_1^S (that is, to induce *spin locking*) and to force it starting from V_2^S (that is, to induce *spin switching*). To that end, we will use the NRDSE or a pump–dump scheme.

3 The NRDSE scheme

In order to understand the physical mechanism underlying the control of the spin coupling via the NRDSE, it is enough to consider the simplest polarizable two-level system with one singlet (S) and one triplet (T) state, coupled via V_{ST}, whose energy can be Stark shifted by a nonresonant electromagnetic field with envelope $\mathcal{E}(t)$ [50]. Suppose that for a given field frequency, the dynamic polarizabilities for the singlet and triplet states are $\alpha_j(\omega)$ ($j = S, T$, we will often omit the frequency dependence in the following). Then choosing the field-free singlet energy as the zero point of energy, the effective Hamiltonian for the system is

$$\mathsf{H} = \begin{pmatrix} -\alpha_S \mathcal{E}(t)^2/2 & V_{ST} \\ V_{ST} & \Delta(0) - \alpha_T \mathcal{E}(t)^2/2 \end{pmatrix} \tag{8}$$

where $\Delta(0)$ is the energy difference between the states in the absence of the field. One can choose an instantaneous zero point of energy that includes the Stark-shift contribution to the singlet energy, making the Hamiltonian

$$\mathsf{H} = \begin{pmatrix} 0 & V_{ST} \\ V_{ST} & \Delta(\mathcal{E}) \end{pmatrix} \tag{9}$$

where $\Delta(\mathcal{E}) = \Delta(0) - (\alpha_T - \alpha_S)\mathcal{E}^2(t)/2$. The Rabi formula can then be used to predict the spin-coupling dynamics. Suppose the system is initially in the singlet state, assuming for simplicity a constant envelope $\mathcal{E}$, the population in the triplet will be

$$P_T = \left(\frac{V_{ST}}{\Omega_e}\right)^2 \sin^2 \Omega_e t \tag{10}$$

where $\Omega_e = \sqrt{V_{ST}^2 + \Delta(\mathcal{E})^2}$. For instance, if $\Delta(0) \ll |V_{ST}|$ (as in the ESM model, starting in V_1^S where $\Delta(0) = 0$), substantial spin transfer will occur at $\tau_{ST} = \pi / 2V_{ST}$. This spin-mixing dynamics can be halted while a laser pulse acts if $\Delta(\mathcal{E}) \gg V_{ST}$. Conversely, if $\Delta(0) \gg V_{ST}$ (as in the ESM starting in V_2^S) full population transfer can be induced by making $\Delta(\mathcal{E}) = 0$ and timing the pulse duration exactly as $\tau_e = \pi/2\Omega_e$. Thus, a laser-controlled spin switch can be created whenever the dynamic polarizability of the singlet state is different from that of the triplet state, $\alpha_S \neq \alpha_T$. Moreover, the dynamic polarizabilities depend on the pulse frequency ω as well. Additionally, the two-level theory can be used to propose alternative (more robust) quantum control scenarios [50].

The extension of the effective 2-level Hamiltonian to the nuclear Hamiltonian in the Born–Oppenheimer approximation is straightforward. Neglecting population absorption one can obtain [51]

$$\mathsf{H} = -\frac{1}{2m}\frac{d^2}{dR^2}\mathsf{I} + \begin{pmatrix} V_1^S(R) - \alpha_S(R,\omega)\mathcal{E}(t)^2/2 & V_{S_1,T_1}(R) \\ V_{S_1,T_1}(R) & V_1^T(R) - \alpha_T(R,\omega)\mathcal{E}(t)^2/2 \end{pmatrix} \tag{11}$$

Since $V_{S_1,T_1}(R)$ is almost constant (and small) around the equilibrium geometries of the V_1^S potential and $V_1^S(R) \approx V_1^T(R)$, in the absence of the field, the population dynamics is practically that of a two-level system, where the singlet–triplet population transfer does not lead to wave-packet dynamics. This prediction explains the excellent agreement between the population dynamics in Fig. 2 and the result of applying the Rabi formula. For strong fields, however, Eq. (11) does not give quantitative results. Firstly, because it is difficult to evaluate the dynamic polarizabilities $\alpha_j(R, \omega)$, and secondly, because multi-photon absorption to excited states usually cannot be neglected. Therefore, in the following results, we solve the time-dependent Schrödinger equation including different sets of electronic states.

Within the Born–Oppenheimer approximation, the nuclear dynamics Hamiltonian in the presence of the control field $\epsilon_c(t)$, is

$$\mathsf{H}^{\text{eff}} = -\frac{1}{2m}\frac{\mathrm{d}^2}{\mathrm{d}R^2}\mathsf{I} + \begin{pmatrix} V_1^S & -\mu_{S_1,S_2}\epsilon_c(t) & V_{S_1,T_1} & V_{S_1,T_2} \\ -\mu_{S_1,S_2}\epsilon_c(t) & V_2^S & V_{S_2,T_1} & V_{S_2,T_2} \\ V_{T_1,S_1} & V_{T_1,S_2} & V_1^T & -\mu_{T_1,T_2}\epsilon_c(t) \\ V_{T_2,S_1} & V_{T_2,S_2} & -\mu_{T_1,T_2}\epsilon_c(t) & V_2^T \end{pmatrix} \tag{12}$$

where I is the 4×4 unit matrix. In Eq. (12), we have restricted the Born–Oppenheimer expansion to the minimal symmetric set (MSS) of electronic states that can represent the dynamics of the system under the influence of an external field that controls the singlet–triplet transition. In the numerical calculations, we use "square" laser pulses with fast ramps of $\sin^2(\pi(t - t_0)/\tau_s)$ form. The switching on/off time is set to $\tau_s = 25$ fs.

The extension of the model to include a more complete set of electronic states is straightforward. In addition to the MSS, we have considered a model including the 6 lowest singlet and triplet states (LSS). These 12 Born–Oppenheimer states span the energy range of any 3-photon process starting in S_1 for all laser frequencies used in this work. It should be noted though that the ESM model favors fast multi-photon excitation from the initial state to the ionization continuum [49]. The ionization process is not considered in this work. However, as pointed out in [49], the ionization process does not affect considerably the spin

dynamics and some observables such as the averaged spin angular momentum of the system, hint that the controlled process is still acting on the small population surviving ionization.

4 Spin-state locking

4.1 Dynamics using the MSS model

The results with the MSS model can be used as proof-of-principles for the optical control of the singlet–triplet transition. The initial state is the ground vibrational eigenstate of S_1, which is an even function with maximum probability on both potential wells. As an example, in Fig. 3, we show the population dynamics in the four electronic states using a single control pulse ϵ_c with different parameters that give best results over different frequency intervals. The overall duration of the pulse is set to 200 fs to display more clearly the effect of spin locking.

We have found robust solutions in the space of parameters for a broad range of peak intensities and frequencies. Although strong pulses are needed to overcome the small transition dipole, the results are not very sensitive to the peak intensity. In general, for larger peak amplitude ϵ_0 the

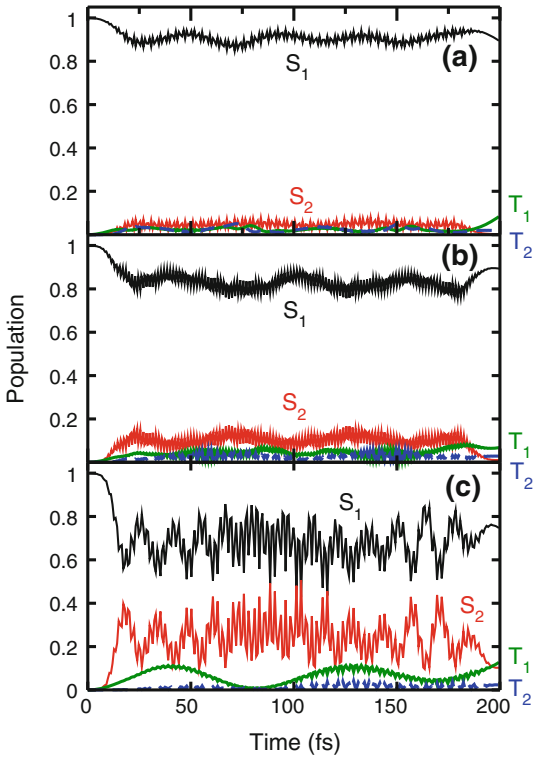

Fig. 3 Electronic states population dynamics in the MSS model with different pulse frequencies and intensities: **a** with $\hbar\omega = 1.63$ eV and $I_0 = 10.1$ TW/cm^2, **b** with $\hbar\omega = 1.41$ eV and $I_0 = 10.1$ TW/cm^2 and **c** with $\hbar\omega = 0.87$ eV and $I_0 = 8.95$ TW/cm^2

population is more evenly spread between the singlet potentials with smaller excitation of the triplet states.

The frequency must be chosen detuned from the $S_1 \rightarrow S_2$ resonance ($\hbar\omega(S_1 \rightarrow S_2) \approx 1$ eV), defined in the initial Franck–Condon region, to avoid absorption to a different state. In the example of Fig. 3a, $\hbar\omega = 1.68$ eV is slightly above the resonance between T_1 and T_2 ($\hbar\omega(T_1 \rightarrow T_2) \approx 1.6$ eV) and thus clearly blue shifted with respect to $\omega(S_1 \rightarrow S_2)$. Therefore, we expect a larger positive Stark-shift on V_1^T than in V_1^S, allowing the effective decoupling of these potentials with $\epsilon_0 = 0.017$ a.u. or larger (implying a peak intensity I_0 of 10.1 TW/cm^2).

Other frequency intervals can be chosen: If ω is between $\omega(S_1 \rightarrow S_2)$ and $\omega(T_1 \rightarrow T_2)$ the dynamic Stark-shift should be positive in V_2^S but negative in V_1^T. Weaker fields could then decouple the electronic states. However, it is more difficult to avoid populating the V_2^S potential. For the results in Fig. 3b, we use $\hbar\omega = 1.39$ eV and the same peak intensity ($I_0 = 10.1$ TW/cm^2).

With $\omega < (\omega(S_1 \rightarrow S_2), \omega(T_1 \rightarrow T_2))$ both V_2^S and V_1^T experience a negative Stark-shift (larger in V_1^S) that give similar results as those shown in case (a). However, multi-photon excitation to S_2 becomes resonant and as a result, more population is excited to S_2. The different shapes of the potentials induce nuclear motion that shows up in some Rabi oscillations between the electronic populations in S_1 and S_2. In Fig. 3c, for $\hbar\omega = 0.84$ eV, we have slightly reduced the pulse intensity to $I_0 = 8.95$ TW/cm^2.

4.2 Dynamics in the LSS model

When considering a larger set of electronic states, the control of the process becomes more complex. On one hand, the different electronic states normally *add* to the polarizabilities, increasing the effect of the Stark effect: weaker pulses could in principle be used. On the other hand, one has to care about many possible resonances $(\omega(S_1 \rightarrow S_j), \omega(S_j \rightarrow S_k))$ that lead to absorption and multi-photon ladder climbing of electronic states. Given the intensities required to decouple the singlet–triplet transition, the second effect is clearly more dominant than the first one, making the spin-state locking quite more challenging in the LSS model than in the MSS model.

In Fig. 4, we analyze the time-averaged populations in the triplets and excited singlets (all except S_1) as a function of the pulse frequency and intensity

$$\langle P_T \rangle = \frac{1}{\tau_l} \sum_{j=1}^{6} \int_0^{\tau_l} \left\langle \psi_j^T(t) | \psi_j^T(t) \right\rangle \mathrm{d}t$$
$$\langle P_{ES} \rangle = \frac{1}{\tau_l} \sum_{j>1}^{6} \int_0^{\tau_l} \left\langle \psi_j^S(t) | \psi_j^S(t) \right\rangle \mathrm{d}t \qquad (13)$$

where $\tau_l = 200$ fs is the pulse duration. The goal of decoupling the $S_1 \rightarrow T_1$ transition involves minimizing $\langle P_T \rangle$ (avoiding the singlet–triplet transition) and $\langle P_{ES} \rangle$ (avoiding the absorption to other electronic states). Whereas with stronger pulses, $\langle P_T \rangle$ is small for all the range of frequencies explored in this work, $\langle P_{ES} \rangle$ is particularly large at lower frequencies, obviously around $\omega(S_1 \rightarrow S_2)$, but also very much until $\omega > \omega(T_1 \rightarrow T_2)$. Disregarding vibrational excitation, the LSS model includes all singlet states that can be accessed by three photons at $\hbar\omega \sim 1.7$ eV.

In Fig. 5, we show the population dynamics for three different cases. For the three frequency windows $\omega < \omega(S_1 \rightarrow S_2)$ (smaller), $\omega(S_1 \rightarrow S_2) \leq \omega \leq \omega(T_1 \rightarrow T_2)$ (intermediate) and $\omega > \omega(T_1 \rightarrow T_2)$ (larger), we have chosen ω and ϵ_0 such that both $\langle P_T \rangle$ and $\langle P_{ES} \rangle$ are minimized. This gives $\hbar\omega = 0.87$ eV, $I_0 = 7.9$ TW/cm^2; $\hbar\omega = 1.41$ eV, $I_0 = 5.0$ TW/cm^2; and $\hbar\omega = 1.63$ eV, $I_0 = 10.1$ TW/cm^2, respectively.

In general, for all frequencies below the $S_1 \rightarrow S_2$ resonance at the pulse intensities needed for spin locking, there is always substantial absorption to excited singlet states. For the best results shown in Fig. 5, the population in the singlets is mostly steady at 0.9 (although there is some slow decay into the triplets) but the population is widely spread between S_1, S_2 and S_3. The ladder climbing excitation mechanism is very efficient in the ESM model.

As discussed in Sect. 3, the NRDSE mechanism is more efficient using intermediate frequencies. Thus, spin locking can be achieved with less intense pulses. To minimize absorption to S_3, the frequency must be smaller than 1.42 eV. However, 3-photon excitation to S_5 cannot be avoided. In the best results shown in Fig. 5, 90 % of the population is kept on the singlet states, but there is a clear beating between population in S_1 and S_5. Within the constraints of the LSS model, best results are obtained for larger frequencies. Here, part of the population goes to S_6.

In Fig. 6, we show the evolution of the nuclear probability density of all the singlet states for smaller and intermediate frequencies (the results for larger frequencies are very similar to those for intermediate frequencies). In the first case, the nuclear wave packet spreads and becomes mostly delocalized (although some coherent vibrational motion can be observed). This is mainly because the geometry of S_3 (with a single minima) is very different from that of S_1 and S_2. Surprisingly, very little singlet–triplet transfer is observed in the population of the different excited singlet states. When the laser is turned off only a small fraction of the population undergoes singlet–triplet conversion.

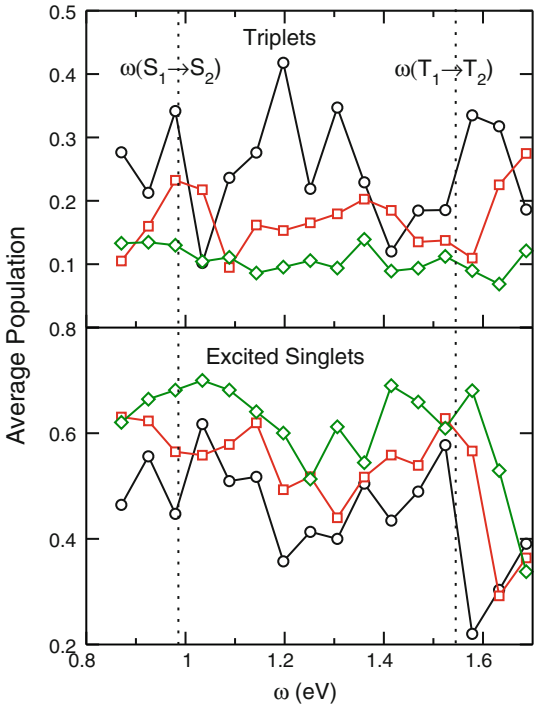

Fig. 4 Time-averaged population in all the triplet and all excited singlet states as a function of pulse frequency and intensity, for peak intensities (in TW/cm^2) of 5.0 (*circles*), 7.9 (*squares*) and 10.1 (*diamonds*). The vertical lines represent the frequencies at which the $S_1 \rightarrow S_2$ and $T_1 \rightarrow T_2$ Franck–Condon transitions are resonant at the equilibrium geometry

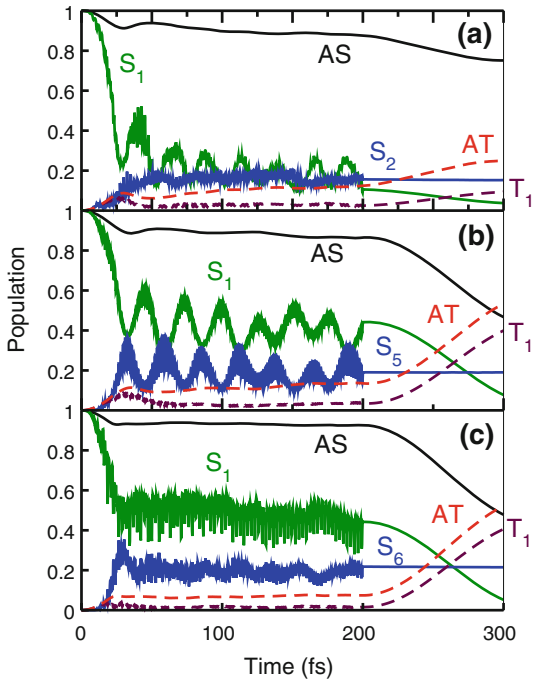

Fig. 5 Electronic states population dynamics in the LSS model with best pulse parameters in the three frequencies ranges. **a** with $\hbar\omega = 0.87$ eV $< \hbar\omega(S_1 \rightarrow S_2)$, **b** with $\hbar\omega(S_1 \rightarrow S_2) \leq \hbar\omega = 1.41$ eV $\leq \hbar\omega(T_1 \rightarrow T_2)$ and **c** with $\hbar\omega = 1.63$ eV $> \hbar\omega(T_1 \rightarrow T_2)$. Other parameters are given in the text. *AS* stands for the population of all singlet states and *AT* for the population of all the triplet states

For intermediate and larger frequencies, the nuclear wave-packet dynamics is still mostly confined to the bottom of the potential energy in V_1^S and much singlet–triplet conversion is observed when the laser is turned off.

5 Spin-state switching dynamics

As discussed in Sect. 2, almost all electronic singlet states practically overlap with the triplet states, so that the spin-transfer dynamics is very efficient. For the lowest energy potentials, only in S_2, there is no singlet–triplet transition. Following the NRDSE recipe (Sect. 3), in order to transfer the population from S_2 to T_2, one first needs to force a near-degeneracy of the two electronic states by Stark shifting the states using a strong nonresonant pulse. The electronic structure of the singlets around S_2 is quite different from that of the triplets around T_2 (S_2 is closer to S_1 while T_2 is closer to T_3), so that in principle the dynamic polarizabilities can be quite different and the NRDSE can be applied. However, the energy difference between the states at the equilibrium configuration of S_2 is approximately 1 eV, while the transition electronic dipoles are relatively small, making it impossible to compensate the energy difference by Stark-shift using any reasonably strong laser pulse. Thus, the singlet–triplet transfer cannot be indirectly induced by a single control pulse.

Instead of applying the NRDSE, in this work, we design an alternative dump–pump strategy that requires two pulses controlling the time-delay between them. The idea is sketched in Fig. 7. First, we apply a dump pulse that moves the population from S_2 to S_1. Then, we wait for the efficient singlet–triplet transfer between S_1 and T_1. Finally, a pump pulse is applied to transfer the population from T_1 to T_2. In the following, we present the results obtained within the MSS model.

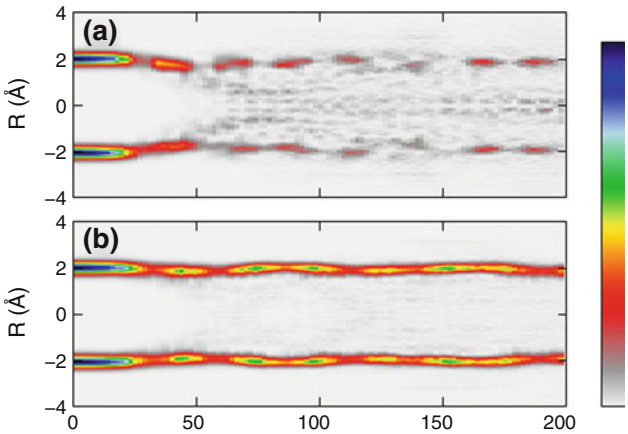

Fig. 6 Nuclear probability density for all the singlet states in the LSS model with **a** $\hbar\omega = 0.87$ eV and $I_0 = 7.9$ TW/cm^2 and **b** $\hbar\omega = 1.41$ eV and $I_0 = 5.0$ TW/cm^2

A typical result with approximately optimized pulse parameters is shown in Fig. 8. Here, we have chosen a negatively first chirped pulse with intensity $I_0 = 5.9$ TW/cm^2, duration $\tau_l = 90$ fs and frequency $\omega(t) = \omega_0 + \beta(t - t_0)/2$, where $\hbar\omega_0 = 1.15$ eV, $\hbar\beta = -0.0136$ eV/fs and t_0 is the center of the pulse. The transformed-limited second pulse has $I_0 = 0.9$ TW/cm^2, $\tau_l = 40$ fs and $\hbar\omega_0 = 1.52$ eV. The parameters of the first pulse are optimized to achieve maximal population transfer (approx 90 %) in a reasonably short time. Since the equilibrium geometry of S_2 and S_1 is very similar, it is difficult to disentangle the optical Rabi flopping between S_2 and S_1 from the spin Rabi flopping between S_1 and T_1. To avoid the $S_1 \rightarrow S_2$ back-transition, one needs to use chirped pulses. We chose a negative chirp, but it is possible to use positively chirped pulses as well. Since the $S_2 \rightarrow S_1$ Franck–Condon transition is at lower energies than the $S_2 \rightarrow S_3$ transition, at first look the choice of a positive chirp would seem a better option to minimize absorption into highly excited singlet states. For the MSS model, however, the results are slightly better for the negatively chirped pulses.

On the other hand, the equilibrium geometry of T_1 is very different from that of T_2. The time-delay between the pulses, $\tau_d = 110$ fs, is chosen to facilitate maximal singlet–triplet conversion between S_1 and T_1. For the second pulse, one can use a transformed-limited pulse because the wave packet in T_2 moves away from the Franck–Condon window and naturally deactivates the probability of stimulated emission. The parameters of the second pulse are chosen to maximize the yield of the $T_1 \rightarrow T_2$ transition in a very short time.

In Fig. 9, we show a contour plot of the time evolution of the nuclear probability densities of singlet and triplet spin character, separately. During the $S_2 \rightarrow S_1$ stimulated

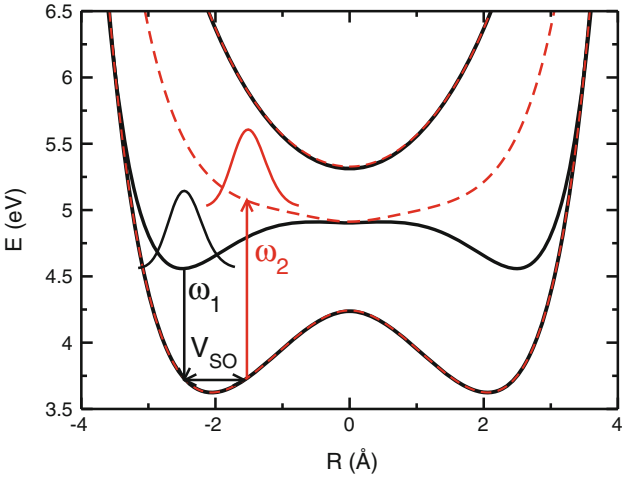

Fig. 7 Scheme of the dump–pump strategy used to induce spin switching between S_2 and T_2. We show the potential energy *curves* and the wave packets after the different stages of the process

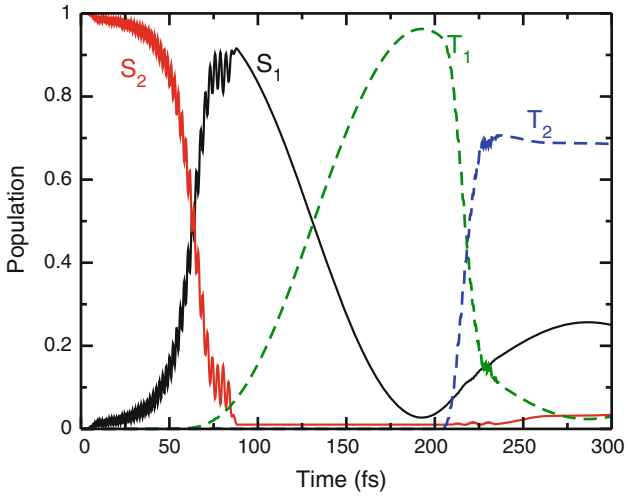

Fig. 8 Electronic states population dynamics in the MSS model applying the dump–pump scheme to induce singlet–triplet transfer from S_2 to T_2. The pulse parameters are given in the text

emission and the $S_1 \rightarrow T_1$ spin transfer, the singlet nuclear wave packet remains basically in the same region (around $R = \pm 2.5$ Å). The triplet nuclear wave packet appears at later states and moves toward $R = 0$, where the minima of T_2 is located.

Unfortunately, it is not possible to achieve similar results with the LSS model, regardless of the sign of chirp. The main problem is that in the Franck–Condon region the transition dipole between S_1 and S_2 is much smaller (a factor of 100 times smaller) than the transition dipole between S_2 and S_3 or between S_1 and S_5 or S_6. As a consequence, the dump pulse must be very strong and the transition competes with two- and three-photon absorption to other excited states, similarly at what happened when using low frequencies to lock the population in S_1. For the optimal parameters used above, a population of only 0.06

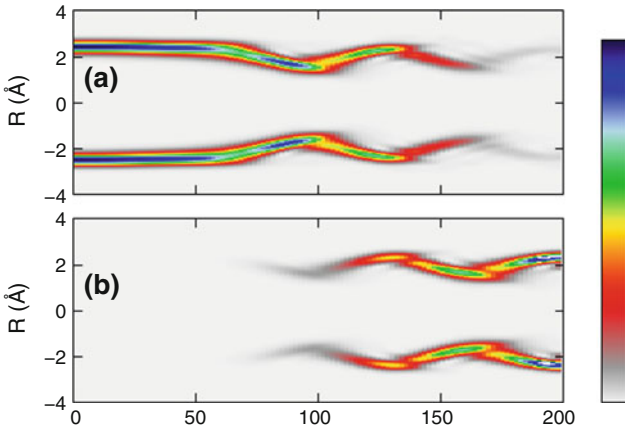

Fig. 9 Nuclear probability density in the spin-switching process for **a** all the singlet and **b** all the triplet states. The laser parameters are given in the text

arrives to T_2 at the end of the process, while singlet–triplet transitions between several excited states account for a total 22 % of population in the triplet states.

6 Summary and conclusions

In this work, we analyzed in detail the role of different laser parameters in the control of the singlet–triplet transition by means of the NRDSE. Following previous work [49], we used the ESM model to obtain the electronic potentials, dipole couplings and singlet–triplet couplings. Depending on the number of potentials included in the calculation, we defined two approximate models: the minimal MSS model and the larger LSS model. Multiphoton ionization and internal conversion were not taken into account. The time-dependent Schrödinger equation for the nuclear motion was then solved for these models starting from different electronic states in order to force spin locking when the laser-free dynamics implied full singlet-triplet conversion, or spin switching, when the laser-free dynamics conserved the spin state.

Certainly, the 3-D 5-particle collinear ESM Hamiltonian implies strong restrictions on the motion of the electrons and ion which show in the potentials and couplings. In particular, the singlet and triplet electronic states tend to have very similar energies, facilitating fast ISC processes. On the other hand, the model favors multiphoton ladder-type ionization, making strong-field control rather difficult. Still, we believe that the ESM is sufficiently flexible to allow the interplay of very different processes which can be analyzed to great detail, making the model an excellent numerical "laboratory" to test different control scenarios.

In this work, we focused on finding appropriate laser strategies and tuning the laser parameters in conditions where there is strong competence between different nonlinear processes, albeit disregarding ionization. Although appropriate laser parameters for spin switching were difficult to find even in the MSS model and were not found in the LSS model, spin locking was shown to be possible for different frequency windows. The smallness of the dipole couplings in the Franck–Condon region required the use of very strong pulses, which drove population to excited singlet states and thus opened new routes for spin transitions from the excited singlet to excited triplet states. Forcing a balance between two goals, minimizing the population in the triplet states and the population in the excited singlet states, was found to be a good strategy to identify control pulse frequencies and intensities that would maximally decouple the initial singlet state from the triplet states while at the same time they minimize the disturbance on the system.

Although previous work [49] showed that multi-photon ionization is the fastest process in the ESM model under the pulse intensities used in this work, the results also showed that ionization occurred mainly in the Franck–Condon window and did not affect the spin dynamics. In particular, the NRDSE was shown to maintain the control on the spin populations of the remaining (nonionized) parts of the system. Given that the full vibronic dynamics requires considerable computation time, the strategy used in this work also paves the way to identifying the best control scenarios when ionization is taken into account. We expect that this control strategy will be effective when the required laser intensity is smaller, for instance in weaker spin-coupling conditions.

Acknowledgments We thank Manfred Lein for general discussions at different stages of this work. I. R. S. and P. V. acknowledge support from the Dirección General de Investigación of Spain under Project No. CTQ2008-06760. B. Y. C. thanks the Basic Science Research Program by the National Research Foundation of Korea grant (2010-0005643). M. F. and V. E. acknowledge financial support by the State of Bavaria (Bayerisches Eliteförderungsgesetz) and by the DFG within the FOR1809. This project was supported by the COST-action CM0702 (Chemistry with Ultrashort Pulses and Free-Electron Lasers).

References

1. Rice SA, Zhao M (2000) Optical control of molecular dynamics. Wiley-Interscience, New York
2. Brixner T, Pfeifer T, Gerber G, Wollenhaupt M, Baumert T (2005) Chap 9: Optimal control of atomic, molecular and electron dynamics with tailored femtosecond laser pulses. In: Hannaford P (ed) Femtosecond laser spectroscopy. Springer, New York, pp 225–266
3. Brumer P, Shapiro M (2012) Quantum control of molecular processes. Wiley-VCH, New York
4. Silberberg Y (2009) Quantum coherent control for nonlinear spectroscopy and microscopy. Annu Rev Phys Chem 60:277–292
5. Geremia GM, Zhu W, Rabitz H (2000) Incorporating physical implementation concerns into closed loop quantum control experiments. J Chem Phys 113:10841–10848
6. Brixner T, Kiefer B, Gerber G (2001) Problem complexity in femtosecond quantum control. Chem Phys 267:241–246
7. Bartels R, Backus S, Zeek E, Misoguti L, Vdovin G, Christov IP, Murnane MM, Kapteyn HC (2000) Shaped-pulse optimization of coherent emission of high-harmonic soft X-rays. Nature 406:164–166
8. Levis RJ, Menkir GM, Rabitz H (2001) Selective bond dissociation and rearrangement with optimally tailored strong-field laser pulses. Science 292:709–713
9. Yuan JM, George TF (1978) Semiclassical theory of unimolecular dissociation induced by a laser field. J Chem Phys 68:3040–3052
10. Bandrauk AD, Sink ML (1981) Photodissociation in intense laser fields: predissociation analogy. J Chem Phys 74:1110–1117
11. Allendorf SW, Szoke A (1991) High-intensity multiphoton ionization of H_2. Phys Rev A 44:518–534
12. Guisti-Suzor A, Mies FH, DiMauro LF, Charron E, Yang B (1995) Dynamics of H^{2+} in intense laser fields. J Phys B 28:309–339
13. Frasinski LJ, Posthumus JH, Plumridge J, Codling K, Taday PF, Langley AJ (1999) Manipulation of bond hardening in H_2^+ by chirping of intense femtosecond laser pulses. Phys Rev Lett 83:3625–3628
14. Sussman BJ, Ivanov MY, Stolow A (2005) Nonperturbative quantum control via the nonresonant dynamic Stark effect. Phys Rev A 71:051401(R)
15. Sussman BJ, Townsend D, Ivanov MY, Stolow A (2006) Dynamic Stark control of photochemical processes. Science 314:278–281
16. González-Vázquez J, Sola IR, Santamaria J, Malinovsky VS (2006) Quantum control of spinorbit coupling by dynamic Stark-shifts induced by laser fields. Chem Phys Lett 431:231–235
17. González-Vázquez J, Sola IR, Santamaria J, Malinovsky VS (2006) Optical control of the singlet–triplet transition in Rb2. J Chem Phys 125:124315
18. González-Vázquez J, Sola IR, Santamaria J, Malinovsky VS (2007) Vibrationally state-selective spinorbit transfer with strong nonresonant pulses. J Phys Chem A 111:2670–2678
19. Friedrich B, Herschbach D (1995) alignment and trapping of molecules in intense laser fields. Phys Rev Lett 74:4623–4626
20. Seideman T (1995) Rotational excitation and molecular alignment in intense laser fields. J Chem Phys 103:7887–7896
21. Ortigoso J, Rodriguez M, Gupta M, Friedrich B (1999) Time evolution of pendular states created by the interaction of molecular polarizability with a pulsed nonresonant laser field. J Chem Phys 110:3870–3875
22. Stapelfeldt H, Seideman T (2003) Colloquium: aligning molecules with strong laser pulses. Rev Mod Phys 75:543–557
23. Leibscher M, Averbukh IS, Rabitz H (2003) Molecular alignment by trains of short laser pulses. Phys Rev Lett 90:2130011–2130014
24. Suzuki T, Sugawara Y, Minemoto S, Sakai H (2008) Optimal control of nonadiabatic alignment of rotationally cold N_2 molecules with the feedback of degree of alignment. Phys Rev Lett 100:033603
25. Bisgaard CZ, Clarkin OJ, Wu GR, Lee AMD, Gessner O, Hayden CC, Stolow A (2009) Time-resolved molecular frame dynamics of fixed-in-space CS2 molecules. Science 323:1464–1468
26. Sussman BJ, Underwood JG, Lausten R, Ivanov MY, Stolow A (2006) Quantum control via the dynamic Stark effect: application to switched rotational wave packets and molecular axis alignment. Phys Rev A 73:053403
27. Chang BY, Choi H, Shin S, Lee S, Sola IR (2009) Ultrafast photodissociation assisted by strong nonresonant Stark effect: the straddling control pulse. J Mod Opt 56:811–821
28. Chang BY, Shin S, Santamaria J, Sola IR (2009) Bond breaking in light-induced potentials. J Chem Phys 130:124320
29. Chang BY, Shin S, Sola IR (2009) Further aspects on the control of photodissociation in light-induced potentials. J Chem Phys 131:204314
30. McQuarrie DA, Simon JD (1997) Physical chemistry. University Science Books, Sausalito
31. Hare PM, Crespo-Hernández CE, Kohler B (2007) Internal conversion to the electronic ground state occurs via two distinct pathways for pyrimidine bases in aqueous solution. Proc Natl Acad Sci USA 104:435–440
32. Kwo WM, Ma C, Phillips DL (2008) A doorway state leads to photostability or triplet photodamage in thymine DNA. J Am Chem Soc 130:5131–5139
33. Etinski M, Fleig T, Marian CM (2009) Intersystem crossing and characterization of dark states in the pyrimidine nucleobases uracil, thymine, and 1-methylthymine. J Phys Chem A 113:11809–11816
34. Parker DSN, Minns RS, Penfold TJ, Worth GA, Fielding HH (2009) Ultrafast dynamics of the S1 excited state of benzene. Chem Phys Lett 469:43

35. Richter M, Marquetand P, González-Vázquez J, Sola I, González L (2012) Femtosecond intersystem crossing in the DNA nucleobase cytosine. J Phys Chem Lett 3:3090
36. Gómez-Abal R, Hübner W (2002) Simple model for laser-induced electron dynamics. Phys Rev B 65:195114
37. Gómez-Abal R, Hübner W (2003) The role of spinorbit coupling in optically induced ultrafast magnetic dynamics. J Phys Condens Mater 15:S709–S722
38. Gómez-Abal R, Ney O, Satitkovitchai K, Hübner W (2004) All-optical subpicosecond magnetic switching in NiO(001). Phys Rev Lett 92:227402
39. Satitkovitchai K, Pavlyukh Y, Hübner W (2005) Ab initio study of spin–orbit coupling effects on the low-lying excited states of NiO. Phys Rev B 72:045116
40. Zutic I, Das Sarma S (2004) Spintronics: fundamentals and applications. Rev Mod Phys 76:323–410
41. Bouwmeester D, Ekert A, Zeilinger A (2000) The physics of quantum information. Springer, New York
42. Shin S, Metiu H (1995) Nonadiabatic effects on the charge transfer rate constant: a numerical study of a simple model system. J Chem Phys 102:9285–9295
43. Shin S, Metiu H (1996) Multiple time scale quantum wavepacket propagation:electro nnuclear dynamics. J Phys Chem 100:7867–7872
44. Erdmann M, Marquetand P, Engel V (2003) Combined electronic and nuclear dynamics in a simple model system. J Chem Phys 119:672–679
45. Erdmann M, Engel V (2004) Combined electronic and nuclear dynamics in a simple model system II spectroscopic transitions. J Chem Phys 120:158
46. Erdmann M, Baumann S, Gräfe S, Engel V (2004) Electronic predissociation: a model study. Eur Phys J D 30:327–333
47. Gräfe S, Engel V (2006) Local control theory applied to coupled electronic and nuclear motion. Chem Phys 329:118
48. Erdmann M, Gross EKU, Engel V (2004) Time-dependent electron localization functions for coupled nuclear-electronic motion. J Chem Phys 121:9666–9670
49. Falge M, Engel V, Lein M, Vindel-Zandbergen P, Chang BY, Sola IR (2012) Quantum wave-packet dynamics in spin-coupled vibronic states. J Phys Chem A 116:11427. doi:10.1021/jp306566x
50. Sola IR, González-Vázquez J, Malinovsky VS (2006) Optical control of a spin switch in the weak spin–orbit coupling limit. Phys Rev A 74:043418
51. Sussman BJ (2011) Five ways to the nonresonant dynamic Stark effect. Am J Phys 79:477–484

5.1.3 The time-scale of nonlinear events driven by strong fields: Can one control the spin-coupling before ionization runs over?

Falge, M., Vindel-Zandbergen, Engel, V., Lein, M., Chang, B.Y. and Sola, I.R., *J. Phys. B*, **47**, *124027* (2014)

The time-scale of nonlinear events driven by strong fields: can one control the spin coupling before ionization runs over?

2014 J. Phys. B: At. Mol. Opt. Phys. 47 124027

(http://iopscience.iop.org/0953-4075/47/12/124027)

IOP Publishing Journal of Physics B: Atomic, Molecular and Optical Physics
J. Phys. B: At. Mol. Opt. Phys. **47** (2014) 124027 (6pp) doi:10.1088/0953-4075/47/12/124027

The time-scale of nonlinear events driven by strong fields: can one control the spin coupling before ionization runs over?

Mirjam Falge[1], Patricia Vindel-Zandbergen[2], Volker Engel[1], Manfred Lein[3], Bo Y Chang[4] and Ignacio R Sola[2]

[1] Universität Würzburg, Institut für Physikalische und Theoretische Chemie, Campus Nord, Emil-Fischer-Str. 42, D-97074 Würzburg, Germany
[2] Departamento de Quimica Fisica, Universidad Complutense, E-28040 Madrid, Spain
[3] Leibniz Universität Hannover, Institut für Theoretische Physik, Appelstraße 2, D-30167 Hannover, Germany
[4] School of Chemistry (BK21), Seoul National University, Seoul 151-747, Korea

E-mail: voen@phys-chemie.uni-wuerzburg.de and isola@quim.ucm.es

Received 18 December 2013, revised 24 February 2014
Accepted for publication 27 February 2014
Published 10 June 2014

Abstract

An initially populated spin state of an ion chain interacting with an external field can decay via spin coupling or via ionization. Using a simple two-level Hamiltonian we investigate the relation between spin-coupling and ionization rate and identify conditions for an efficient spin-control via a non-resonant Stark effect by suppressing ionization. The results are confirmed in solving the time-dependent Schrödinger equation for the interaction of a laser field with a spin-coupled model system where two electrons and a nucleus move in a collinear configuration. It is thus shown, that quantum control of intersystem crossing can indeed be effective if the intensity of the external field and the accompanying Stark-shift is adjusted properly to the spin-coupling strength.

Keywords: ionization, spin-control, non-adiabatic dynamics

(Some figures may appear in colour only in the online journal)

1. Introduction

With the development of ultrafast and ultrastrong laser pulses, many nonlinear processes in molecules have been observed and controlled experimentally [1, 2]. Aside from enabling multi-photon excitation pathways, a strong field induces large Stark shifts that can deeply alter the structure of the electronic potentials [3–7]. These effects have been used to induce molecular alignment [8–14], to assist selective population transfer between vibronic states [15–20], to control photodissociation reactions [21–25], modify the rate of photochemical processes [26–29] or even change the bond length of molecules [30–34].

We are interested in the control of spin transitions via a particular optical control strategy, based on the nonresonant dynamic Stark effect (NRDSE) [21, 22]. By Stark shifting the electronic spectra in the presence of a strong nonresonant field, one can force the decoupling of the singlet and triplet states on a system with otherwise fast intersystem crossing. However, the presence of strong fields triggers many other (unwanted) nonlinear processes, in particular multi-photon absorption to excited singlet (and triplet) states and, more importantly, multi-photon ionization. In this work we characterize the conditions required to control the spin transition on a time-scale shorter than the onset of ionization. In particular, we show under what intensities one observes a change from Stark-shift driven (i.e. controlled) to ionization driven dynamics, setting limits for the maximum values of the spin couplings under which the system is controllable via an NRDSE process.

The accurate calculation of the rate of ionization under strong fields, beyond perturbation theory, is a difficult enterprise that, nonetheless, has become quite important

with the birth of attosecond physics [2]. For two-electron systems, grid-based propagation schemes using regularized soft-core Coulomb potentials [35–37] in few dimensions (for instance, one dimension per electron) provide a reasonable ground for the evaluation of dynamical processes where both multi-photon and tunnelling ionization can occur. In previous work we have studied the interplay between nonlinear field processes, coupled electron and nuclear motion and singlet–triplet transitions. We have developed the extended Shin–Metiu model (ESM) [47] based on the original Hamiltonian introduced by Shin and Metiu to study charge transfer processes in solids with screened Coulomb potentials [38–45]. The ESM model is a dynamical model incorporating three degrees of freedom (3D) for a proton and two collinear electrons moving between two fixed ions, allowing transitions between the singlet and triplet components of the electronic wave function. Although much flexibility exists in the choice of parameters, for symmetrical couplings between all particles (equal charges and screenings) the ESM favours symmetrical arrangements where the moving ion is placed in between both fixed ions and each electron is in between one fixed ion and the central ion. When the separation between the fixed ions is large, e.g. $R = R_2 - R_1 \geqslant 10$ Å, two nuclear equilibrium geometries exist. In this regard, a molecular analogue of the present ESM structure conceivably looks more like an isomeric system rather than a diatomic molecule.

In this work we do not incorporate effects associated with the rotational degree of freedoms. An off-resonant field creates an angle-dependent potential so that, in general, the angular motion should be included in a theoretical description [46]. In neglecting rotations we adopt the reasonable approximation that the latter are too slow in comparison with the relevant time-scales (of ST-transitions and ionization, respectively) which here are in the femtosecond regime for the large coupling case. It is thus reasonable to treat the nuclear frame as frozen with respect to the rotational motion. Otherwise one can consider the ESM model as a prototype for systems with limited rotation.

In addition, because of the large separation between the two electrons in average, the energies of the here relevant singlet and triplet states are almost degenerate, especially around the equilibrium geometries. Since the electronic wave functions come on pairs of symmetric (singlet) and antisymmetric (triplet) states under exchange of electron coordinates, z_1 and z_2, any extra term in the Hamiltonian that is an odd function of $z_1 - z_2$ acts as a very effective source of spin coupling between the near degenerate states. The spin coupling is then essentially that of a two-level problem.

In our former work [47, 48], we tuned the parameters of the ESM Hamiltonian to force spin switching from the ground electronic singlet state to a degenerate electronic triplet state in 120 fs. We then showed that it is possible to control the spin transition, locking the spin populations, while at the same time minimizing multi-photon absorption [48]. However, by solving the time-dependent Schrödinger equation (TDSE) on a 3D grid we also found that the rate of ionization is much faster than the natural (laser-free) duration of the spin transition, making the whole NRDSE scheme finally ineffective [47]. In this work we analyse the conditions that are required to turn around this conclusion. The solution of the TDSE with the ESM Hamiltonian involves cumbersome numerical calculations that do not permit an easy evaluation of the interplay of different Hamiltonian parameters, particularly when they lead to opposite effects that are important in controlling the dynamics. In section 2 we build a minimal Hamiltonian for a two-level system with polarizable spin states (Stark effect), intramolecular spin couplings and effective ionization. From this so-called 2-PSI Hamiltonian we obtain analytical expressions for the time-scales of ionization and spin transfer, using a simple model for the ionization as a function of the field amplitude. We show under what conditions, that is, for what spin-coupling strengths, it is possible to decouple the spin transition before the onset of ionization. In section 3 we use the numerical calculations from the ESM dynamics to fit the parameters of the 2-PSI model in order to obtain reasonable estimates of the ionization rates within the framework of the simple model. The analytical expressions are then used as a guide to find the laser intensities for a given spin coupling that allow the spin states to be decoupled before substantial ionization occurs. The actual test of whether control is possible is then carried out in section 4 using the fully numerical ESM model for different coupling strengths. Finally, section 5 contains the conclusions.

2. The 2-PSI model

In order to understand the control of the spin transfer via the nonresonant Stark effect and the role of the ionization, we first propose a simple two-level Hamiltonian which includes the effect of Stark shifts on a singlet (α_S) and a triplet (α_T) state coupled to each other via a spin interaction term V_{ST}. This model is the same as used in [48] but we include here an effective ionization rate Γ that we regard, for simplification, equal for the singlet and triplet states

$$\mathsf{H}_{\text{eff}} = \begin{pmatrix} -\mathrm{i}\Gamma(\epsilon) & V_{ST} \\ V_{ST} & \Delta(\epsilon) - \mathrm{i}\Gamma(\epsilon) \end{pmatrix} \tag{1}$$

where the energy difference in the presence of field ϵ is

$$\Delta(\epsilon) = \Delta(0) - (\alpha_T - \alpha_S)\epsilon^2/2 \tag{2}$$

and we will make $\Delta(0) = 0$ as in the ESM, where the ground singlet and triplet states are degenerate. Atomic units will be used throughout unless otherwise stated. To simplify the notation we write $\alpha = |\alpha_T - \alpha_S|$.

The characteristic time for the spin transfer in the absence of the field is defined by

$$\tau_{ST} = \frac{\pi}{2V_{ST}}. \tag{3}$$

In the presence of an external field, assuming for simplicity a constant envelope ϵ, integrating the TDSE for the above Hamiltonian (equation (1)) gives for the triplet population:

$$P_T(t) = \mathrm{e}^{-\Gamma t}\left(\frac{V_{ST}}{\Omega_e}\right)^2 \sin^2 \Omega_e t \tag{4}$$

with $\Omega_e = \sqrt{V_{ST}^2 + \Delta(\epsilon)^2}$, and we assumed that initially, only the singlet state is populated, i.e. $P_s(t = 0) = 1$. The latter can

be depopulated via ionization and spin transfer. The NRDSE gives a prescription to avoid the spin transfer: use a field strong enough that $\Delta(\epsilon) \gg V_{\rm ST}$.

For instance, defining a maximum threshold value for the triplet population, P_T^m, provides, via equation (4), the minimum (threshold) for the Stark shift, Δ_m. Let us first neglect ionization. From

$$P_T^m = \frac{V_{\rm ST}^2}{V_{\rm ST}^2 + \Delta_m^2} \tag{5}$$

we obtain

$$\Delta_m = V_{\rm ST}\sqrt{\frac{1-P_T^m}{P_T^m}} = V_{\rm ST}\chi^{1/2} \tag{6}$$

where

$$\chi = P_S^m/P_T^m \tag{7}$$

is the relative singlet to triplet conversion at the threshold, when the singlet population is the minimum allowed. Clearly, the control is possible as long as the polarizabilities of the singlet and triplet states are different enough, $\alpha > 0$. Since the Stark-shift is a quadratic effect in the field, the threshold value for the field intensity is, from equation (2)

$$\epsilon_m^2 = \frac{2V_{\rm ST}\chi^{1/2}}{\alpha}. \tag{8}$$

Additionally, the field changes the time-scale of the spin transfer. If we define τ_e as the first time the triplet population is maximal, for large χ ($\Delta_m \gg V_{\rm ST}$) one obtains

$$\tau_e = \frac{\pi}{2}\Omega_e^{-1} \approx \frac{\pi}{2}\frac{1}{\Delta_m} = \chi^{-1/2}\tau_{\rm ST}. \tag{9}$$

Now we go back to the ionization problem. The goal of the control is to avoid losing population from the singlet state neither from a spin transition nor from ionization. Given the above Hamiltonian (equation (1)) the task is difficult, as a strong field is needed to avoid spin transfer while the strong field immediately induces ionization via $\Gamma(\epsilon)$. The key here is to find under which conditions the time-scale of the ionization is much slower than the time-scale of the spin transfer, such that one can maintain the population in the initial state in the presence of the field for a time longer than $\tau_{\rm ST}$.

We use here a simple but very general equation for the ionization as a function of the field

$$\Gamma = C\epsilon_m^n. \tag{10}$$

In a strong field approximation the parameter n can be related to the field frequency (twice the number of photons required to reach ionization). We simply regard equation (10) as an empirical model. Under this view the model is in fact quite general and roughly reproduces the ionization rate in the ESM Hamiltonian at short times, as we will show in the next section. Thus, the parameters of equation (10) for the PSI-model will be obtained by fitting the results of the numerical simulations using the ESM Hamiltonian. The model allows a simple relation between the time-scale of ionization and the field amplitude. Defining the characteristic time of ionization as the lifetime $\tau_{\rm ion} = \ln 2\,\Gamma^{-1}$, and inserting the threshold field given by equation (8) for a fixed χ we obtain

$$\tau_{\rm ion} = \frac{\ln 2}{C}\left(\frac{\alpha}{2V_{\rm ST}\chi^{1/2}}\right)^{n/2}. \tag{11}$$

The relation between the characteristic times of the spin transfer and ionization is

$$\frac{\tau_{\rm ST}}{\tau_{\rm ion}} = \frac{\pi C}{2\ln 2}\left(\frac{2}{\alpha}\right)^{n/2}\chi^{n/4}V_{\rm ST}^{(n-2)/2} = K\chi^{n/4}V_{\rm ST}^{(n-2)/2} \tag{12}$$

where K depends only on the non-spin-coupled part of the Hamiltonian that gives the spectra of the singlets and triplets and the ionization potentials (fixed for a certain set of parameters in the ESM model, for instance) and is thus approximately independent of $V_{\rm ST}$. Although one can change the value of K by playing with different pulse frequencies (thus changing the dynamic polarizability difference α) for the ESM model we have found that it is clearly larger than 1 ($K \sim 40$).[5]

The same result with an extra $\chi^{-1/2}$ factor is obtained by comparing $\tau_{\rm ion}$ with the time-scale for the spin transfer in the presence of the field

$$\frac{\tau_e}{\tau_{\rm ion}} = K\chi^{(n-2)/4}V_{\rm ST}^{(n-2)/2} \tag{13}$$

Clearly if $n = 2$, then $\tau_{\rm ST}/\tau_{\rm ion} = K\chi^{1/2}$, and the time-scales for ionization and spin transfer will be fixed by the non-spin-coupled part of the Hamiltonian. With $K \gg 1$ this makes ionization the dominant process. However, for values of n different than 2, it will be possible to privilege one process versus the other. We will show in the next section that for the ESM with symmetric parameters, $n > 2$. Thus the spin transfer can be controlled before the onset of ionization in the regime of weak spin couplings or small $V_{\rm ST}$.

3. Fitting the 2-PSI parameters with the ESM model: the ionization rate

Following the simple 2-PSI model, the most relevant parameter to determine if one can control the spin transfer by a quadratic field effect (the Stark shift) before the ionization takes place, is the exponent n that measures the dependence of the ionization rate on the field, which will depend on the Hamiltonian model.

We now turn to the full ESM Hamiltonian. The ESM couples the singlet manifold (symmetric wave functions) with the triplet manifold (antisymmetric wave functions). In matrix form:

$$\mathbf{H}_{\rm ESM} = \begin{pmatrix} H(z_1, z_2, Z) & \lambda(z_1 - z_2) \\ \lambda(z_1 - z_2) & H(z_1, z_2, Z). \end{pmatrix} \tag{14}$$

The coupling is chosen as the simplest antisymmetric form with the spin-coupling strength given by λ. The diagonal part is the 3D Hamiltonian for the collinear motion of two electrons (z_1 and z_2) and one proton (Z) with mass m

$$H(z_1, z_2, Z) = -\frac{1}{2}\frac{\partial^2}{\partial z_1^2} - \frac{1}{2}\frac{\partial^2}{\partial z_2^2} - \frac{1}{2m}\frac{\partial^2}{\partial Z^2} + V(z_1, z_2, Z) \tag{15}$$

under an effective (screened) Coulomb type potential $V(z_1, z_2, Z)$. In what follows, we vary λ. As a reference value, we use the coupling strength $\lambda_0 = 1.028 \times 10^{-3}$ eV Å^{-1}

[5] Using $\hbar\omega = 1.63$ eV and $\mathcal{I}_0 = 10.1$ TW cm^{-2} (in au 0.06 and 0.017, respectively) we observe $\tau_{\rm ion} = 22$ fs and $\tau_{\rm ST} = 120$ fs. On the other hand, the singlet to triplet ratio is $\chi \sim 10$ (as a rough estimation) and $n = 2.6$. With these results we obtain $K \sim 40$ au.

that was recently tested to control the spin-transfer dynamics [47, 48]. For this choice of parameters we observed $\tau_{ST,0} = 120$ fs. Here and in the following, a subindex '0' refers to results obtained with this set of parameters.

In order to fit the parameters of the 2-PSI model we solve the TDSE on a 3D grid with the ESM Hamiltonian [47, 48] using the split operator with fast Fourier transform [49, 50]. The spatial grid for the nuclear coordinate ranges from −4 to +4 Å, whereas the spatial grid for the electron coordinates is divided into an inner region ($|x|$ and $|y| \leqslant 10$ Å) and an outer region ($|x|$ or $|y| > 10$ Å) where the wavefunction is damped by an absorbing boundary. Assuming that ionization is effective in the outer region, the non-ionized population corresponds to the norm of the wavefunction in the inner region.

Since we are interested only in the rate of ionization as a function of the field, the spin coupling is set to zero ($\lambda = 0$) in these simulations in order to avoid spin transfer. The envelope of the electric field is a $\sin^2$-function which rises from time $t = 0$ to 50 au (1.21 fs) to its maximum and is then kept constant at the latter value. The remaining, non-ionized population $P_{ni}(t)$, which corresponds to $P_S(t)$ in the 2-PSI model, was calculated for different values of the field amplitude ϵ sampled over more than one order of magnitude at a frequency $\omega = 0.06$ au. The frequency was chosen following the analysis of [48] where efficient control of the spin-transition was observed for frequencies below and above some possible one-photon electronic resonances in a simplified ESM Hamiltonian obtained by truncating the electronic basis to the first six Born–Oppenheimer states, disregarding ionization and non-adiabatic transitions. Then $\ln(P_{ni}) \approx -\Gamma t$ was linearly fitted to obtain the rate of ionization Γ. Figure 1(a) shows that the linear fit is reasonably good as soon as ionization sets in, i.e., when the wave packet leaves the edges of the 3D grid.

In figure 1(b) we show the results of fitting Γ to the field amplitude ϵ in logarithmic scale (because we are only interested in the slope of the curves, the arguments of the logarithms are the rates in fs^{-1} and field strengths in au, respectively). With amplitudes ranging approximately from 0.002 to 0.030 au the behaviour is approximately linear with an exponent of $n = 2.6$. Deviations occur for lower intensities i.e. longer ionization times because the simple 2-PSI model fails to take into account the dependence of the rate with the ion's motion. However, the exponential model still provides a reasonable estimate. Power-law dependencies of the ion signal on the laser intensity with exponents between one and two are familiar from 1+1 photon resonance enhanced multi-photon ionization as studied, e.g., in the case of the NO molecule, see [51] and references therein.

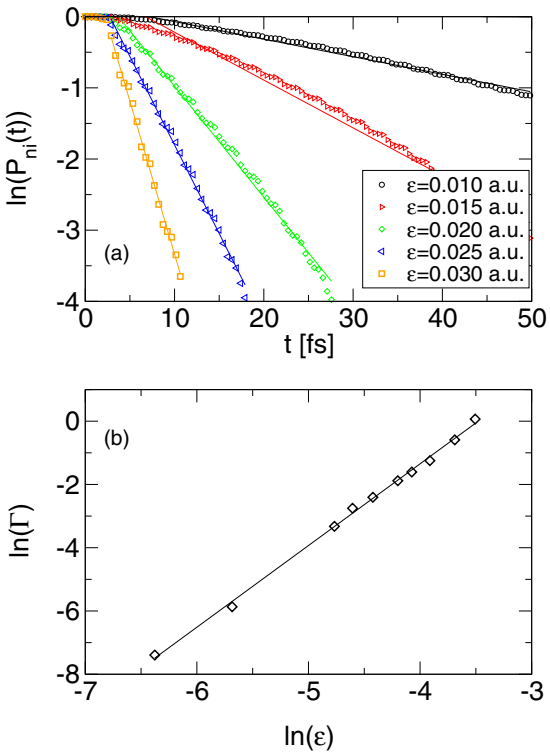

Figure 1. (a) Logarithmic decay of the remaining (non-ionized) population $\ln(P_{ni})$ as a function of time, for different pulse amplitudes ϵ from 0.01 to 0.03 au and $\omega = 0.06$ au. The solid lines show the best linear fits at short times up to 100 fs. (b) Logarithmic fit of the population decay due to ionization with respect to the field amplitude giving a slope of $n = 2.6$.

4. Control of spin transfer before the onset of ionization

As shown in the previous section, Γ can be fitted with the form given by equation (10) with an exponent close to but larger than 2. Thus, one expects that τ_{ST} may become smaller than τ_{ion} for weak V_{ST}. However, the small departure from the quadratic dependence implies that large changes in V_{ST} (or correspondingly τ_{ST}) will be needed to observe a shift from ionization driven to Stark-shift driven dynamics, where the spin transfer is controlled before ionization takes over.

For instance, taking the results of [47] as a reference, with $\epsilon_0 = 0.017$ au we obtained $\chi \sim 10$ (this is a rough estimation, since due to the fast ionization it is difficult to assess the decoupling between the spin states) and $\tau_{ion,0} \sim 22$ fs, which is about six times shorter than $\tau_{ST,0}$. With $n = 2.6$, in order to make $\tau_{ion} \sim \tau_{ST}$ while keeping χ, we would need to work with a Hamiltonian with a much weaker coupling V_{ST}

$$\frac{V_{ST}}{V_{ST,0}} = \left(\frac{\tau_{ST}}{\tau_{ion}}\frac{\tau_{ion,0}}{\tau_{ST,0}}\right)^{2/(n-2)} \approx \left(\frac{\tau_{ion,0}}{\tau_{ST,0}}\right)^{2/(n-2)} \approx \left(\frac{1}{6}\right)^{2/(n-2)} \approx \frac{1}{390}. \quad (16)$$

Thus, only when the spin coupling is roughly 400 times weaker than the reference result it is possible to avoid the spin transition before substantial ionization occurs working with fields of an amplitude an order of magnitude weaker. In fact, as equation (9) shows, it will be possible to observe the effect on the spin decoupling before, since τ_e can be easily 3–10 times shorter than τ_{ST}.

In figure 2 we show how the probability of ionization and the average spin angular momentum $S_{av} = \sqrt{2P_T}$ vary as a function of the scaled time (t/τ_{ST}) for different choices of the spin coupling, here written as different multiples of the reference time for the spin transition, $\tau_{ST,0}$. In the absence

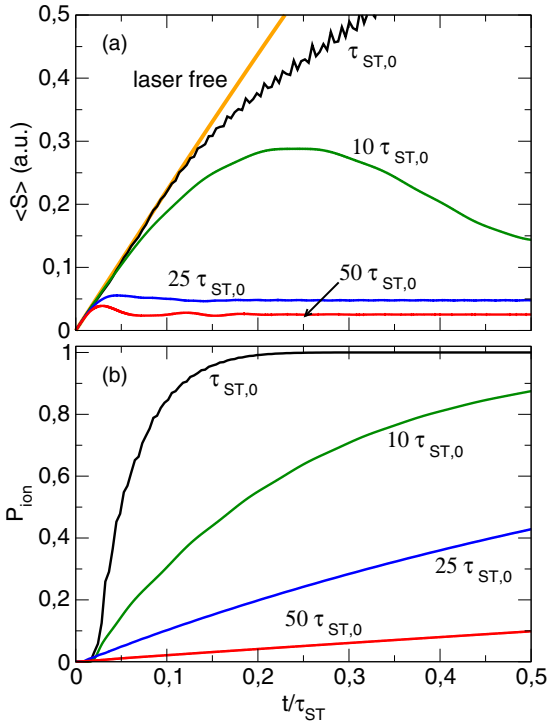

Figure 2. Triplet state population (a) and probability of ionization (b) as a function of the time scaled with respect to the spin-flipping time (t/τ_{ST}) for different spin-coupling strengths, given as multiples of a reference inverse strength $\tau_{ST,0}$. The results are obtained from the numerical solution of the TDSE for the ESM-model and show that for $\tau_{ST} \sim 25\tau_{ST,0}$ it is already possible to control the spin transition before significant ionization occurs.

of an external control field, S_{av} rises to $\sqrt{2}$ (not shown in the figure) while in the strong coupling case, S_{av} reaches a plateau of ∼0.6. The curve shows many oscillations due to numerical instabilities, as practically all population ionizes and therefore P_{ni} get close to zero after $t \sim 0.2\,\tau_{ST,0} = 24$ fs. With a coupling ten times weaker ($\tau_{ST} = 10\,\tau_{ST,0}$), using a field $\epsilon = 0.005\,37$ au $\approx 1/\sqrt{10} \times \epsilon_0$ the ionization dominates (>50%) before τ_{ST}. However, as the relation of singlet to triplet state population is $\chi \sim 10$ and $\tau_e \sim \tau_{ion}$ one can observe the first attenuated coherent oscillation of S_{av} before ionization takes over the system. For even weaker couplings one can clearly observe the process of spin locking with minor ionization (<20%) at times smaller or even of the order of τ_{ST}. For instance, with $\tau_{ST} = 25\,\tau_{ST,0}$ we have used $\epsilon = 0.0034$ au $\approx 1/\sqrt{25} \times \epsilon_0$ while for $\tau_{ST} = 50\,\tau_{ST,0}$ we used $\epsilon = 0.0024$ au $\approx 1/\sqrt{50} \times \epsilon_0$. These results show that for a coupling strength of $V_{ST} \leqslant 1/25 \times V_{ST,0}$ efficient spin locking can be achieved before significant ionization occurs. The rough guess given by equation (16) underestimates the coupling strength required for an efficient control, but gives the right order of magnitude for convenient parameters.

5. Summary and conclusion

In this work we show that spin locking with the help of external electric fields can, in principle, be achieved under certain conditions. We first analyse ionization and control of spin transfer via the nonresonant dynamic Stark effect (NRDSE) scheme in a very simple, but general, two-level approximation of a non-resonantly driven system with strong internuclear (singlet–triplet) couplings. It is found that the key feature that determines if optical spin-control is possible or not is the dependence of the ionization rate on the control field amplitude. In a simple empirical model this dependence can be approximated as a power law with the exponent deciding if ionization or control is the predominant process for a given set of parameters.

The 2-PSI model reduces the electronic active states to the ground manifold (the singlet and triplet quasi-degenerate states) and lacks any nuclear dynamics. However, it can be used as a guide to find suitable regimes or ranges of parameters where one can achieve the control of spin coupling in more complex systems. This requires the fitting of the parameters of the model with respect to the dynamics of the complex system that is being approximated.

As a numerical study, in this work we have investigated the control of the spin state in a coupled two-electron-nucleus motion under a strong field, namely the ESM Hamiltonian. It was found that the analytical estimates for the optimal values of spin coupling versus electric field strength are useful to establish an efficient quantum control of spin transitions before ionization is effective. Thus the competing processes of spin-transitions and ionization can, within certain limits, be influenced. In particular, for relatively weak spin couplings and control field intensities we could achieve efficient spin locking in an initial singlet state.

It has to be noted that our conclusions rest on the particular model (the ESM Hamiltonian) that we employ in the calculation. However, the coupled electron-nuclei model contains many essential ingredients for the description of the dynamics of molecules in laser fields. For example, it incorporates not only the ST-coupling but also the influence of vibrational motion on the accompanying transitions being important in, e.g., biradicals which exhibit crucial ST-interactions [52]. Also, with respect to the electronic structure, the entire manifold of singlet- and triplet-states is included [47]. Within the ESM model it is possible, by a proper choice of parameters, to increase the density of electronic states which, nevertheless, is enough in the present study to allow a very efficient ionization.

Indeed, one may claim that the ESM Hamiltonian poses very challenging conditions for the control of the spin state. Namely, one observes one-photon resonant enhanced ionization and, on the other hand, the spin coupling is very effective, as the singlet and triplet states are resonant or quasi-resonant for most nuclear geometries. Hence the nuclear dynamics does not reduce the efficiency of the singlet–triplet transition, as would be expected in other systems.

Although we emphasize the model character of the present study, we are confident that our main point, namely that it is possible to control the ST-transitions in the presence of ionization, is still valid if the dynamics of the system is more complicated. When the number of nuclear degrees of freedom or electronic states is increased, the spin-flip time is modified and the field parameters have to be adjusted accordingly to

achieve a successful control. To prove the general controllability of spin-coupling, much more elaborate studies will be necessary.

Acknowledgments

This work was supported by the NRF grant funded by the Korean government (2007-0056343) and the International cooperation program managed by the NRF of Korea (no. 2013K2A1A2054518), the Basic Science Research program funded by MEST (2010-0005143), the MICINN project CTQ2012-36184, and the European COST Action CM0702. MF and VE acknowledge financial support by the DFG within the FOR 1809. ML acknowledges financial support from the Centre for Quantum Engineering and Space-Time Research (QUEST).

References

[1] Silberberg Y 2009 *Annu. Rev. Phys. Chem.* **60** 277
[2] Krausz F and Ivanov M 2009 *Rev. Mod. Phys.* **81** 163
[3] Yuan J M and George T F 1978 *J. Chem. Phys.* **68** 3040
[4] Bandrauk A D and Sink M L 1981 *J. Chem. Phys.* **74** 1110
[5] Allendorf S W and Szoke A 1991 *Phys. Rev.* A **44** 518
[6] Guisti-Suzor A, Mies F H, DiMauro L F, Charron E and Yang B 1995 *J. Phys. B: At. Mol. Opt. Phys.* **28** 309
[7] Frasinski L J, Posthumus J H, Plumridge J, Codling K, Taday P F and Langley A J 1999 *Phys. Rev. Lett.* **83** 3625
[8] Friedrich B and Herschbach D 1995 *Phys. Rev. Lett.* **74** 4623
[9] Seideman T 1995 *J. Chem. Phys.* **103** 7887
[10] Ortigoso J, Rodriguez M, Gupta M and Friedrich B 1999 *J. Chem. Phys.* **110** 3870
[11] Stapelfeldt H and Seideman T 2003 *Rev. Mod. Phys.* **75** 543
[12] Leibscher M, Averbukh I S and Rabitz H 2003 *Phys. Rev. Lett.* **90** 213001
[13] Suzuki T, Sugawara Y, Minemoto S and Sakai H 2008 *Phys. Rev. Lett.* **100** 033603
[14] Bisgaard C Z, Clarkin O J, Wu G R, Lee A M D, Gessner O, Hayden C C and Stolow A 2009 *Science* **323** 1464
[15] Garraway B and Suominen K-A 1998 *Phys. Rev. Lett.* **80** 932
[16] Sola I R, Santamaria J and Malinovsky V 2000 *Phys. Rev.* A **61** 043413
[17] Kallush S and Band Y 2000 *Phys. Rev.* A **61** 041401
[18] Sola I R, Chang B Y, Santamaria J, Malinovsky V and Krause J 2000 *Phys. Rev. Lett.* **85** 4241
[19] Wollenhaupt M and Baumert T 2011 *Faraday Discuss. Chem. Soc.* **153** 9
[20] Bayer T, Braun H, Sarpe C, Siemering R, von den Hoff P, de Vivie-Riedle R, Baumert T and Wollenhaupt M 2013 *Phys. Rev. Lett.* **110** 123003
[21] Sussman B J, Ivanov M Y and Stolow A 2005 *Phys. Rev.* A **71** 051401
[22] Sussman B J, Townsend D, Ivanov M Y and Stolow A 2006 *Science* **314** 278
[23] Chang B Y, Choi H, Shin S, Lee S and Sola I R 2009 *J. Mod. Opt.* **56** 811
[24] Chang B Y, Shin S, Santamaria J and Sola I R 2009 *J. Chem. Phys.* **130** 124320
[25] Chang B Y, Shin S and Sola I R 2009 *J. Chem. Phys.* **131** 204314
[26] González-Vázquez J, Sola I R, Santamaria J and Malinovsky V S 2006 *Chem. Phys. Lett.* **431** 231
[27] González-Vázquez J, Sola I R, Santamaria J and Malinovsky V S 2006 *J. Chem. Phys.* **125** 124315
[28] González-Vázquez J, Sola I R, Santamaria J and Malinovsky V S 2007 *J. Phys. Chem.* A **111** 2670
[29] González-Vázquez J, González L, Sola I R and Santamaria J 2009 *J. Chem. Phys.* **131** 104302
[30] Chang B Y, Rabitz H and Sola I R 2003 *Phys. Rev.* A **82** 063414
[31] Sola I R, Chang B Y and Rabitz H 2003 *J. Chem. Phys.* **119** 10653
[32] Chang B Y, Shin S and Sola I R 2010 *Phys. Rev.* A **82** 063414
[33] Sola I R, Shin S and Chang B Y 2011 *J. Chem. Phys.* **134** 104301
[34] Chang B Y, Shin S, Palacios A, Martin F and Sola I R 2013 *Chem. Phys. Chem.* **14** 1405
[35] Javanainen J, Eberly J and Su Q 1988 *Phys. Rev.* A **38** 3430
[36] Su Q and Eberly J 1991 *Phys. Rev.* A **44** 5997
[37] Kulander K C, Mies F H and Schafer K J 1996 *Phys. Rev.* A **53** 2562
[38] Shin S and Metiu H 1995 *J. Chem. Phys.* **102** 9285
[39] Shin S and Metiu H 1996 *J. Phys. Chem.* **100** 7867
[40] Erdmann M, Marquetand P and Engel V 2003 *J. Chem. Phys.* **119** 672
[41] Erdmann M and Engel V 2004 *J. Chem. Phys.* **120** 158
[42] Gräfe S and Engel V 2006 *Chem. Phys.* **329** 118
[43] Erdmann M, Gross E K U and Engel V 2004 *J. Chem. Phys.* **121** 9666
[44] Falge M, Engel V and Gräfe S 2011 *J. Chem. Phys.* **134** 184307
[45] Falge M, Engel V and Gräfe S 2012 *J. Phys. Chem. Lett.* **3** 2617
[46] Sindelka M, Moiseyev N and Cederbaum L S 2011 *J. Phys. B: At. Mol. Opt. Phys.* **44** 045603
[47] Falge M, Engel V, Lein M, Vindel-Zandbergen P, Chang B Y and Sola I R 2012 *J. Phys. Chem.* A **116** 11427
[48] Vindel-Zandbergen P, Falge M, Chang B Y, Engel V and Sola I R 2013 *Theor. Chem. Acc.* **132** 1359
[49] Feit M D, Fleck J A Jr and Steiger A 1982 *J. Comput. Phys.* **47** 412
[50] Kosloff R 1988 *J. Phys. Chem.* **92** 2087
[51] Jacobs D C, Madix R J and Zare R N 1986 *J. Chem. Phys.* **85** 5469
[52] Bonačić-Koutecký V, Koutecký J and Michl J 1987 *Angew. Chem. Int. Edn Engl.* **26** 170

5.2 Control of electron transfer between separated nuclei

In this chapter we study the simulation and control of the electron transfer in the femto- and attosecond scale by intense laser pulses using the Local Control Theory (4.2). The control of the electron processes is a challenge due to the velocity at which the electron moves and disperses, particularly when the electron ionizes.

The work "*Local Control approach to ultrafast electron transfer*" (*Chem. Phys.*, 2016, *In press*), focuses on the control of a process involving reversible quantum transitions between bound and ionized states (continuum) which is an essential ingredient in attophysics. That is, the aim is to maximize the probability that an electron, after being transported through the continuum, can be retrapped as it returns to the core. The electron transfer process was studied in the H_2^+ (symmetric system) and HeH^{2+} (asymmetric system) molecules, both modeled by a soft core Coulomb potential (2.6.3) and working under the Born-Oppenheimer approximation in one spatial dimension.

Two different local control formulations were employed to increase the yield of photoassociation of the electron with the desired nuclei using eq. (4.38) and eq. (4.40). In the first approach the aim is to decrease the energy of the electron after being excited to the continumm as it crosses the target nucleus. In the second approach, the objective is to increase th population in a target state, that is, the eigenfunction of the desired nuclei. In both situations the control mechanism is based on impulsive de-excitation and occurs in the attosecond regime. The results demonstrate that by applying local control theory one can in principle design laser pulses which lead to efficient electron transfer to a target nucleus. The first approach was found to be more efficient, but in any case, the mechanism is an impulsive retrapping induced by a strongly peaked field when the electron is crossing the target nucleus. However, in any situation, in all cases, the ionization process is always competing with the electron retrapping. We also found that the efficiency of photoassociation is reduced at larger internuclear distances, for larger initial electron kinetic energies and when the amplitude of the laser control fields is decreased artificially. It was also demonstrated that the nuclear motion did not affect the efficiency of the processes.

Although the work shows that the laser control of long range electron transfer via the continuum is in principle possible, the required attosecond pulses are in general so short and intense that are currently not achievable experimentally.

In the work entitled "*Slow electron transfer between separated nuclei*" (*In prepara-*

tion), the process of electron transfer is based on a tunneling mechanism and occurs in the femtosecond time scale. As in the previous work, the scenario is the H_2^+ molecule and we consider large internuclear separations. Initially the photoassociation with the target proton is achieved by means of local control fields at different distances using eq. (4.40). Using Husimi distribution functions, it is found that the transfer is mediated by a tunneling mechanism. A scheme was proposed, where tunneling and thus electron transfer, occurs between the first excited localized states. We demonstrated that analytical pulses led to the same final results, so local control theory is not be needed when tunneling is the sole mechanism of the electron transfer. Under these conditions, ionization was completely avoided and almost 100 % of population transfer to the target proton was achieved. However, this method failed when larger internuclear distances were considered, as the tunneling time increases exponentially and one needs to selectively excite the electron to Rydberg states even closer to the continuum, a process that is difficult by itself.

The time scale of the slow electron transfer mechanism is of the order or larger than typical vibrational periods. The fixed nuclei approximation is just valid as long as the electronic processes occur much faster than the nuclear motion. Thus, the effect of including the nuclear motion was also analyzed using the same pulses as in the 1D results. As expected, the yield of the process decreased, although some population transfer was achieved and ionization was also avoided. Furthermore, the effect of the initial nuclear kinetic energy was studied in two different ways: by adding an initial momentum (positive and negative) and by varying the width of the nuclear wave function. In the first situation, we found that for small negative momenta, the yield of photoassociation increased, but for higher values and positive momenta the electron transfer decreased. This effect was also affected by the population loss by ionization. The effect was explained by considering the potential energy curves of the excited states where the tunneling occurs and the average of the internuclear distance with the initial kinetic energy.

The femtosecond transfer based on tunneling promises higher yields if the nuclei are not too far apart, but the results are sensitive to model dimensionality and nuclear motion and are more difficult to extrapolate to other molecular processes.

5.2.1 Local Control approach to ultrafast electron transfer

Vindel-Zandbergen, P., Meier, C. and Sola, I.R, *Chem. Phys.* (*In press*)

Chemical Physics xxx (2016) xxx–xxx

Contents lists available at ScienceDirect

Chemical Physics

journal homepage: www.elsevier.com/locate/chemphys

Local control approach to ultrafast electron transfer

Patricia Vindel-Zandbergen [a], Christoph Meier [b], Ignacio R. Sola [a,*]

[a] Departamento de Química Física, Universidad Complutense, 28040 Madrid, Spain
[b] Laboratoire Colisions, Agrégats et Reactivité, UMR 5589, IRSAMC, Université Paul Sabatier, 31062 Toulouse, France

ARTICLE INFO

Article history:
Available online xxxx

Keywords:
Electron transfer
Quantum control
Attosecond pulses
Local control theory

ABSTRACT

We study ultrafast electron transfer between separated nuclei using local control theory. By imposing electron ionization and electron transport through the continuum, different local control formulations are used to increase the yield of retrapping the electron at the desired nuclei. The control mechanism is based on impulsive de-excitation. Both symmetric and asymmetric nuclear arrangements are analyzed, as well as the role of the nuclear motion.

1. Introduction

In recent years, advances in laser technology enabled the production of sub-femtosecond (*i.e. attosecond*) pulses, with frequencies in the UV regime, paving the way to the development of a new scientific domain, called Attosecond Physics [1,2]. These pulses are so short that ionization or Auger processes can be in principle resolved in real time; alternatively, their bandwidths are large enough that several electronic states can be coherently excited at the same time. Currently, attophysics techniques are mainly used as a spectroscopic tool, to unravel ultrafast molecular (or condensed phase) processes, by means of *e.g.* pump–probe techniques.

One can observe several analogies with the field of Femtochemistry [3], where the pump–probe scheme was successfully used to resolve the nuclear dynamics. After monitoring the motion of nuclei, a natural step forward was to attempt to control the nuclear dynamics [4], which was proposed both in the time and energy (frequency) domain. In the first case, the control can be seen as the search for an external, often phase-modulated field, $\mathcal{E}(t)$, such that a transition from the initial state $|\psi_i\rangle$ to a predefined target state $|\psi_f\rangle$ at a time t_f is induced and typically maximized. The target state can imply the preparation of a new chemical species, for instance, through the fragmentation of a particular bond.

In achieving this goal, one may distinguish two different strategies, optimal control theory [5] (OCT) and local control theory [6] (LCT). In OCT, the control fields are constructed employing information on the entire dynamics from time t_i to time t_f, whereas in LCT, the field is determined instantaneously, taking the system's response into account. Different local control schemes have found many applications in molecular physics [7–23].

The main purpose of this work is to apply local control techniques to attosecond processes, involving the motion of electrons. The control of the electron processes is a challenge due to the velocity at which the electron moves and disperses, particularly when the electron ionizes. However, attosecond pulses can be seen as the ideal tools, acting very locally in time and offering wide bandwidth to span both continuum and bound states. Presently, the experimental techniques that allow to modulate attosecond pulses are not yet developed. However, the theoretical anticipation is timely, as it helps determining the physical resources that might be necessary in order to exert this control.

Within this scientific context, our goal is to control the electron transfer between two separated protons, mainly aided by local control methods. This elementary process can constitute an important step toward the control of many chemical reactions involving charge rearrangement. In this work the electron transfer is not mediated by nuclear motion. Hence, it relies on fast processes through the ionization continuum. The essential step involves the photoassociation of the electron colliding with the target proton. In some respects, this work complements studies of photoassociation between neutral atoms in slow collision [24,25].

One ultimate motivation is to determine the laser resources necessary to enhance the yield of reversible quantum transitions between bound states and ionized states, which is an essential ingredient in attophysics [1,2]. Our work should be regarded as a tentative step towards that goal as we use simplified models where the electron is treated in a single dimension.

The paper is organized as follows. In Section 2 we introduce the model Hamiltonian and describe the numerical methods applied to interpret the control mechanisms. In Section 3 we investigate under which conditions one can maximize electron transfer

* Corresponding author.
E-mail address: isola@quim.ucm.es (I.R. Sola).

http://dx.doi.org/10.1016/j.chemphys.2016.04.015
0301-0104/

between two protons largely separated within the framework of local control theory. We consider impulsive ultrafast processes that occur in few femtoseconds. We also analyze the effect of the nuclear dynamics onto the yields. Finally, Section 4 is the conclusions.

2. Numerical methods

We need to use a consistent model for treating both continuum and bound electronic states in a system with a single electron and two nuclei. As a first approximation, we use a 1-D Hamiltonian, where the electron is constrained to move in the molecular axis z driven by a linearly polarized external field, $\mathcal{E}(t)$. Neglecting small mass polarization terms, the Hamiltonian in the length gauge is (atomic units are used throughout unless otherwise stated)

$$H = -\frac{1}{2}\frac{\mathrm{d}^2}{\mathrm{d}z^2} + V(z,R) + z\mathcal{E}(t) \tag{1}$$

For this reduced dimensional study the internuclear distance R is fixed and the electron-nuclei potential is modeled by a soft-core Coulomb potential [26]

$$V(z,R) = -\frac{Q_1}{\sqrt{\left((z+aR)^2+\varepsilon_1^2\right)}} - \frac{Q_2}{\sqrt{\left((z-bR)^2+\varepsilon_2^2\right)}} + \frac{Q_1Q_2}{R} \tag{2}$$

where Q_i are the nuclear charges ($Q_{He}=2$ and $Q_H=1$ a.u.), a and b account for the relative distances of the nuclei with respect to the center of mass, and ε_i are smoothing parameters. In the case of H_2^+, $a=p=1/2$ whereas for *e.g.* HeH^{2+}, $a=m_p/(m_p+m_\alpha)=0,2012$ and $b=m_\alpha/(m_p+m_\alpha)=1-a=0.7988$ [27]. The smoothing parameters were chosen as $\varepsilon_1=\varepsilon_2=1$ for H_2^+ and $\varepsilon_1(\mathrm{He})=0.705$, $\varepsilon_2(\mathrm{H})=1.414$ for HeH^{2+}.

This model has been extensively applied as a first qualitative step to analyze ionization processes in H_2^+ and high-harmonic spectra [28,29], as well as electron-nuclear dynamics [30–33]. One can easily extend the calculation to include the nuclear motion by removing the constraint in R and by adding the internuclear kinetic energy, as explained later. For the laser-controlled dynamics shown in this work, the 2-D calculations give quantitatively the same results as the 1-D model. Initially, we assume a fixed nuclei approximation, where an hydrogen atom and a proton, or the He and H nuclei, are largely separated. Two different ways to achieve electron transfer applying LCT are considered. In the first one, the objective is mathematically expressed as the population in a target state $|\psi_f\rangle$, constructed as a wave function localized at the nuclei where we want the electron to be recaptured.

Defining the projector $P_T=|\psi_f\rangle\langle\psi_f|$, the rate of population transfer into the target state is

$$\begin{aligned}\frac{\mathrm{d}}{\mathrm{d}t}\langle P_T\rangle &= i\langle[H(t),P_T]\rangle = i\mathcal{E}(t)\langle[-\mu,P_T]\rangle \\ &= \mathcal{E}(t)2\Im\{\langle\Psi(t)|\mu|\psi_f\rangle\langle\psi_f|\Psi(t)\rangle\}\end{aligned} \tag{3}$$

Hence, a control field of the form

$$\mathcal{E}(t) = \lambda\Im\left[\langle\Psi(t)|\mu|\psi_f\rangle\langle\psi_f|\Psi(t)\rangle\right] \tag{4}$$

where $\Im$ stands for the imaginary part and $\Psi(t)$ is the wave function of the system, guarantees monotonic increase in time of population in the target state [34,35].

In the second LC protocol, we minimize the energy of the electron once it moves out in the ionization continuum, such that the electron can be stopped and retrapped in the further nuclei. A sufficient condition to reduce the energy of the system upon the interaction with an external field is that the expectation value of H_0 (the Hamiltonian in the absence of the external field) decreases as a function of time or, equivalently, that its time derivative (the energy rate) is lower than zero. Using the time dependent Schrödinger equation (TDSE) the rate is evaluated as

$$\begin{aligned}\frac{\mathrm{d}}{\mathrm{d}t}\langle H_0\rangle &= i\langle[H(t),H_0]\rangle = i\mathcal{E}(t)\langle[-\mu,T]\rangle \\ &= \mathcal{E}(t)\frac{1}{i2m}\left\langle\left(\frac{\mathrm{d}^2\mu}{\mathrm{d}z^2}+2\frac{\mathrm{d}\mu}{\mathrm{d}z}\frac{\mathrm{d}}{\mathrm{d}z}\right)\right\rangle\end{aligned} \tag{5}$$

In the special case of a linear dipole moment, i.e., $\mu=qz$ (with q being a constant), Eq. (5) takes the simple form

$$\frac{\mathrm{d}}{\mathrm{d}t}\langle H_0\rangle = \mathcal{E}(t)\frac{q}{m}\langle p\rangle \tag{6}$$

Hence, one can reduce the energy of the system choosing a field proportional to the expectation value of the momentum [36–38],

$$\mathcal{E}(t) = \lambda f(t)\langle\Psi(t)|p|\Psi(t)\rangle \tag{7}$$

with $\lambda<0$.

In both cases λ enters as a free parameter that measures the strength of the laser interaction. λ is found numerically by trial and error. In Eq. (7) we include a positive sine square envelope function $f(t)$ that forces a time-delay in the action of the control field, to avoid minimizing the energy before the electron has time to fly over the outer nuclei.

In the homonuclear (symmetrical) system, one has to take superpositions of the ground and the first excited electronic states of the Hamiltonian in order to construct the initial and target localized states,

$$\psi_{L_1/R_1} = (\psi_1 \pm \psi_2) \tag{8}$$

where ψ_{L_1} is the lowest energy wave function localized at the left proton (left potential well) of Eq. (2) and ψ_{R_1} is the target wave function localized at the right potential well.

In general, in our simulations we assume that the initial state is already excited, that is, ψ_L is multiplied by an exponential factor that gives an initial momemtum in the positive direction

$$\Psi(z,0) = \psi_{L_1}(z)\mathrm{e}^{ik_e z} \tag{9}$$

In addition, to initiate the LCT approach one needs a small "seed" of population in the right potential well (the target state), which we fix as $\approx 0.3\%$. Once the local control field is found, this "seeded" population is no longer needed, and the simulations shown in the results imply 100% population in the ground (localized) state at initial time.

The numerical results are obtained by solving the TDSE with the Split-Operator method [39–41] with time steps of $\Delta t=0.01$ a.u. A grid of 256 points spanning from $z=-80$ to $z=80$ a.u. is used for the electronic coordinate. Imaginary ("optical") potentials [42,43] absorb the outgoing wave functions avoiding reflection on the grid boundaries and allowing to measure the ionization probability. The eigenstates $\psi_{1,2}$ from Eq. (8) are computed using the Fourier Grid Hamiltonian method [44]. The dynamical mechanism of the transfer is studied by analyzing the approximate phase-space representation of the wave functions at different times, using the Husimi transformation [45].

Finally, to study the role of the nuclear motion in the control of the electron transfer, 1 + 1D calculations were performed using the full Hamiltonian of Eq. (1) including the nuclear kinetic term. The initial wave packet is then the product of the electronic wave function times a nuclear Gaussian wave packet $\psi_{\mathrm{nuc}}(R)$, centered at the left nuclei.

In this case, we use a grid of 1024 points ranging from $R=0.1$ to $R=150$ a.u. for the nuclear coordinate and 256 points from $z=-80$ to $z=80$ for the electronic coordinate.

Please cite this article in press as: P. Vindel-Zandbergen et al., Chem. Phys. (2016), http://dx.doi.org/10.1016/j.chemphys.2016.04.015

3. Fast electron transfer

3.1. Impulsive mechanism after fast electron ionization

We first consider electron transfer in the symmetrical system, between an Hydrogen atom and a proton.

In general, the yields of the LCT control process are very small unless higher momentum is given to the electron at initial time. Here we study the solutions that are obtained when the initial kinetic energy is larger than the ionization energy, so that the electron moves from one nuclei to the other through the continuum. The role of the LCT pulse is then to maximize the probability of retrapping the electron at the desired (right) nucleus.

We first apply the LCT approach based on the projection operator for fixed internuclear distance. As typical parameters we use $R = 20$ a.u. and an initial momentum of $k_e = 1.25$ a.u., that is ~ 0.1 a.u. above the ionization threshold, which guarantees almost complete ionization. Moving freely, the electron takes about ~ 0.4 fs to reach the outer nucleus. Certainly the retrapping mechanism requires an impulsive action, which must be provided by the control field. Hence we chose k_e to be as small as possible without compromising the first ionization step. Best results were obtained with $\lambda = 25$ in Eq. (4).

Fig. 1 shows the population dynamics, partitioned into the left and right domains, under the local control field, shown in the inset, for a propagation time of $t_f = 4$ fs,

$$P_R(t) = |\langle \Psi(z,t)|\Psi(z,t)\rangle_{z\in R}|^2 \tag{10}$$

where R is $(0, L/2)$ (with L the grid size) for the right domain.

Also shown is the optimization yield, measured as the overlap of the wave function with the target state,

$$P_{R_1}(t) = |\langle \psi_{R_1}|\Psi(z,t)\rangle|^2 \tag{11}$$

Finally, P_T is the norm of the wave function remaining in the grid, such that $P_{\rm ion} = (1 - P_T)$ provides asymptotically (at large time) the ionization probability. Several features can be extracted from the results: the probability of ionization is essentially unity given the initial kinetic energy of the electron; the local control pulse is mainly a spike with a maximum peak amplitude of $\mathcal{E}_{max} = -1.1$ a.u. and 0.15 fs duration, that allows photoassociation of the electron in the right well, with an efficiency around $\sim 10\%$. However, there are some features of the pulse before and after the spike (some modulation) that are necessary for the final yield to raise significantly.

Similar results were obtained for larger internuclear distances. For an internuclear distance of $R = 40$ a.u., the laser main spike has a peak amplitude of about $\mathcal{E}_{max} = -0.9$ a.u., 0.1 fs duration and is centered at $t = 3.5$ fs. In this case, there is another important spike that slightly increases as well the population on the target nucleus ($\mathcal{E}_{max} = -0.5$ a.u. and 0.2 fs duration) at $t = 1.8$ fs. The yields are typically slightly smaller as the electron wave packet is more spread and the electron probability around the target state becomes smaller.

One striking feature of the pulse is the strong peak around $t = 0.8$ fs. To analyze its importance with respect to the total ionization $P_{\rm ion} = (1 - P_T)$ and with respect to the control objective P_R or P_{R_1} (as defined by Eqs. (10) and (11) respectively), we perform test calculations using the control field, but with the maximum peak amplitude ($\mathcal{E}_{max}$) cut by a threshold value $\mathcal{E}^{tr}$.

The results are shown in Fig. 2, which contains a direct comparison of $P_{\rm ion}$, P_R and P_{R_1}, obtained without and with cut-off, the latter denoted by $P^{tr}_{\rm ion}$, P^{tr}_R and $P^{tr}_{R_1}$. As major result one finds that the control objective, P_R and P_{R_1}, strongly relies on this feature in the control field. On the other hand, the total ionization probability is almost unaltered by this peak.

3.2. Impulsive transfer by pump plus local control de-excitation

In the previous section, the LCT control mechanism was influenced by the choice of the initial wave function, where we imparted a momentum to the electron enough to have almost full ionization. Here we provide results supporting ultrafast electron transfer obtained from LCT under different settings. In particular, we use an ultrashort pump pulse to generate the ionization and we use the LCT approach based on slowing the momentum (that is, a local control field proportional to $\langle p(t)\rangle$). An essential ingredient of this pump plus local control (P + LC) implementation is to start the LCT algorithm after some delay with respect to the pump pulse. This is regulated by the envelope sine square function $f(t)$, which is switched on at $t = 0.25$ fs. Now, the target wave function is just employed as a tool to measure the fraction of the electron wave packet recaptured in the ground state of the right proton (11), since it is not included in the LCT algorithm.

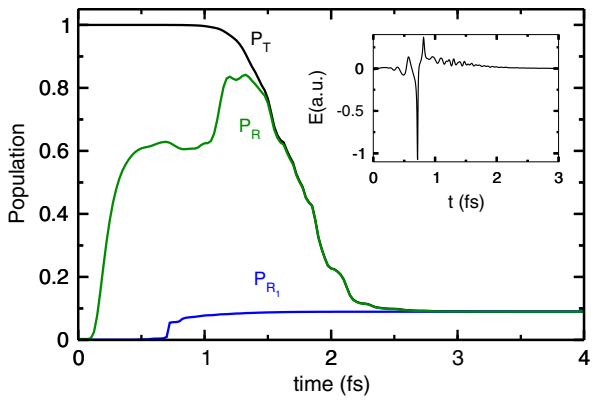

Fig. 1. Population dynamics and laser control field (inset) for electron transfer between two protons separated 20 a.u. We show the norm of the wave function remaining in the grid P_T (so $1 - P_T$ is a rough measure of the ionization probability), the overall electron probability in $z > 0$ (P_R) and the population in the target state P_{R_1}, which is approximately the probability of retrapping the electron in the right proton.

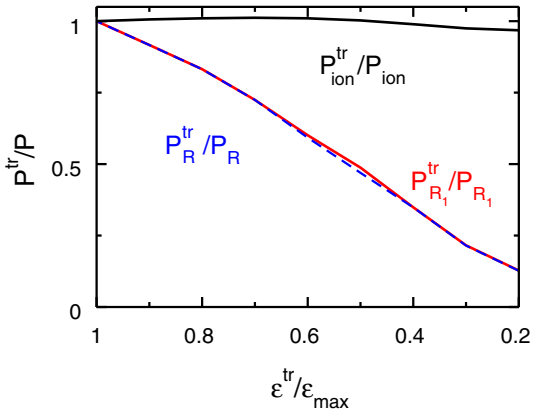

Fig. 2. Sensitivity of the yield of ionization $P_{\rm ion} = 1 - P_T$, electron transfer P_R and state-selective electron transfer P_{R_1} to the peak amplitude of the local control field. We show the ratio of the probabilities obtained using the truncated field with those obtained using the LC field, where the truncated field is obtained by cutting the peak amplitude of the LC field, $\epsilon_{\rm max}$. The calculations were obtained for a fixed internuclear distance of $R = 20$ a.u.

Please cite this article in press as: P. Vindel-Zandbergen et al., Chem. Phys. (2016), http://dx.doi.org/10.1016/j.chemphys.2016.04.015

As a representative example, we show results for an internuclear distance of 20 a.u. Ultrafast ionization is achieved by means of a sine squared half-cycle 500 as pulse (total duration) with a peak amplitude of 0.35 a.u. The effect of the pump pulse is similar to that obtained by imparting an initial momentum to the electron. Here we use $k_e = 0$ in the initial wave function. Best results are obtained with $\lambda = 0.6$ for a total propagation time of $t_f = 6$ fs.

Fig. 3 shows the approximate yield of ionization $P_{\text{ion}}(t) = 1 - P_T(t)$ when one applies only the pump pulse (P) and when both the pump and the local control field are used (P + LC). In the latter case, we also show the yield $P_{R_1}(t)$. The pump pulse is responsible for 95% probability of ionization. The control pulse achieves 50% of electron transfer, measured as the final probability localized on the right well, $P_R(t = \infty)$. The energy de-excitation induced by this LCT approach is such that it slightly reduces the efficiency of the pump pulse in inducing the ionization (that is, there remains a larger population in $P_L(t = \infty)$), but a larger probability (around 40%) is found on the lowest excited state localized on the right proton. This effect can be controlled by the time-delay of the LC. However, a larger time-delay reduces the yield of electron transfer on the right proton, so a tradeoff must be found.

The control mechanism of the photoassociation is again impulsive and the electron retrapping occurs in ~ 3 fs. The LC pulse consists of an intensive peak acting when the electron is crossing the right proton which induces photoassociation by decreasing the electron energy. Comparing the results obtained by this approach with those obtained with Eq. (3) (the LC field as a function of the projection operator) we observe that in both cases the dynamics follows an impulsive mechanism, but the local control pulse is simpler and typically less intense and yet gives higher electron transfer efficiencies than in the former case. The LCT approach based on Eq. (4) (field proportional to the average momentum) directly favors the impulsive strategy, such that the local solutions work better.

To explain the proposed impulsive mechanism, we plot in Fig. 4 the Husimi distributions obtained from the wave function at different times, using the same local control field as the results of Fig. 3. During the electron transfer, the momentum distribution is always positive, with a mean kinetic energy above the ionization potential. Due to the initial momentum given to the electron, the wave function quickly spreads. The first laser spike projects part of this wide wave function on the right proton around $t_3 \sim 0.5$ fs. The subsequent slight modulations allow for a small slow down of the electron distribution and a small probability of retrapping (see at $t_4 \sim 1.0$ and $t_5 \sim 1.7$ fs) although after the first spike the electron mainly ionizes with relatively large kinetic energy.

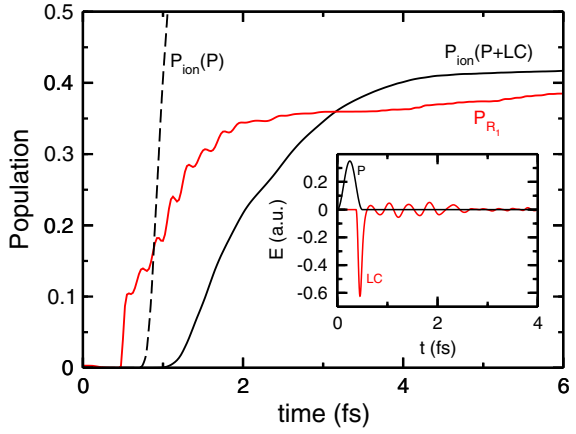

Fig. 3. Population dynamics and laser control field (in the inset) for electron transfer between two protons separated 20 a.u. when the laser control field is proportional to the expectation value of the momentum. $P_{\text{ion}}(P)$ represents the ionization probability when an attosecond laser pulse (P in the inset) is applied to excite the electron and $P_{\text{ion}}(P + LC)$ results from the action of the laser control field (LC in the inset).

This mechanism is also valid for longer distances with similar results. For an internuclear distance of $R = 40$ a.u. we achieve $\sim 30\%$ photoassociation with a pump pulse of $t = 250$ as duration and a peak amplitude of 0.3 a.u. and a local control pulse with $\lambda = 114$ for a total propagation time of $t_f = 4$ fs.

3.3. Asymmetries: the HeH^{2+} system

Here we analyze the results of electron transfer from the Hydrogen atom to an alpha particle (He^{2+}), where the electron moves from left to right, and from He^+ to the proton (right to left). Because the system is asymmetric, the initial (localized) wave functions are eigenstates of the electronic Hamiltonian (1). As the best results for the symmetric case where obtained using the "pump plus laser control" scheme, this strategy is also employed to achieve electron transfer in the HeH^{2+} molecule. As a representative example, we show results for an internuclear distance of 20 a.u.

Fig. 5 shows for both cases the yield of ionization when just the pump pulse (P) is applied ($P_{\text{ion}}(t) = 1 - P_T(t)$) and when both the pump and control fields are acting (P + LC), as well as the projection into the lowest energy eigenstates localized on either the Helium nucleus (P_{He}) or the Hydrogen nucleus (P_{H}). In both cases, the pump pulse achieves around 60% of ionization. When we ionize the H atom the pump pulse is a sine square 500 as pulse with a peak amplitude of 0.3 a.u. To ionize the electron from He^+, the pump pulse is a sine square pulse with a total duration of 1 fs and a significantly larger peak amplitude of 1.0 a.u. Once again, we add some delay between the pump and local control pulses, regulated by the envelope functions $f(t)$, which are switched on at $t = 0.25$ fs and at $t = 0.5$ fs, respectively. From H to He^{2+} the control pulse reduces the yield of ionization to a 10% and achieves 50% of electron retrapping. Hence the efficiency of the trapping mechanism is very high, larger than 80%. These results are obtained with $\lambda = 1.5$ for a total propagation time of 8 fs. When we transfer the electron from He^+ to the proton, the yield of ionization remains the same, but the probability of retrapping the electron at the proton is smaller ($\sim 15\%$). Best results are obtained with $\lambda = 0.5$ for the local control pulse, and a total propagation time of 3 fs. Because stronger pump pulses are needed to ionize He^+ than H, the electron typically travels with larger kinetic energy (*i.e.* faster) through the continuum from right to left and it is more difficult to retrap the electron, as expected. This is more clearly observed when the initial state is prepared by adding an initial (negative) momentum to the lowest state localized in He^+.

In any case, the impulsive mechanism with the laser field proportional to the expectation value of the momentum provides larger yields of electron transfer than those obtained by the projection on a localized target state, and require less intense pulses. (Using the projector operator, peak amplitudes ~ 6 a.u. are typically required in the control fields.) The same procedure can be applied when the nuclei are separated by larger internuclear distances yielding slightly smaller yet qualitatively similar results.

3.4. The role of the nuclear motion

We have performed $1 + 1$D calculations including the nuclear motion on the results of ultrafast electron transfer, applying the same local control pulses (or pump plus LC pulses) obtained from the 1D studies.

As expected by the ultrafast nature of the impulsive mechanism, the frozen nuclei approximation gives excellent results,

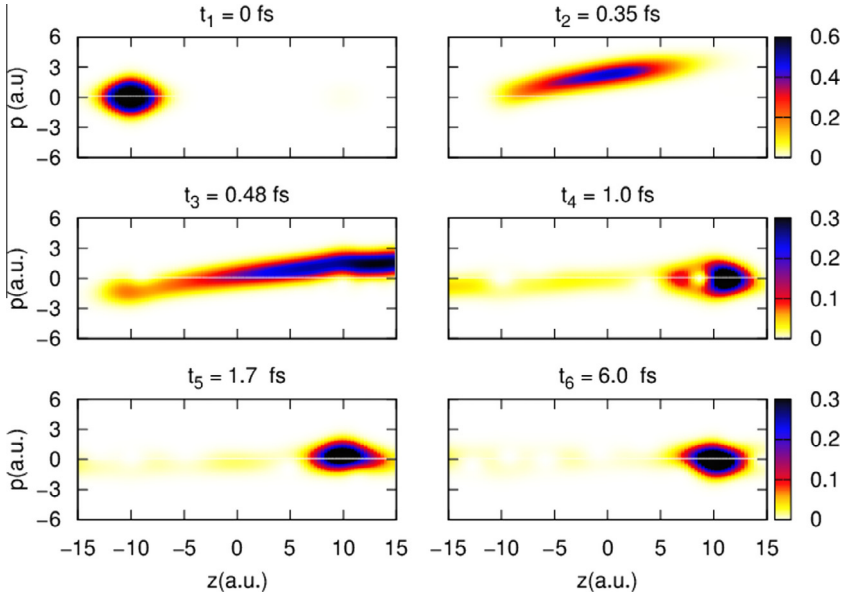

Fig. 4. Electron transfer mechanism revealed by the Husimi distributions of the electron wave function, shown at different times.

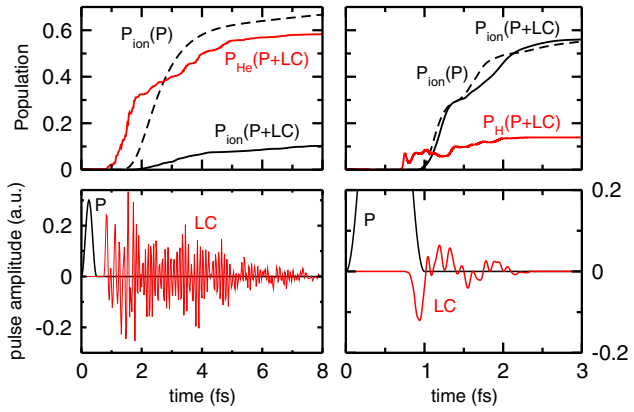

Fig. 5. Population dynamics and laser control fields for the electron transfer between H and He^{2+} (left panels) and He^{+} and a proton (right panels). We use a laser control field proportional to the expectation value of the momemtum. $P_{ion}(P)$ represents the ionization probability when an attosecond laser pulse (P) is applied to excite the electron and $P_{ion}(P+LC)$ results from the action of the laser control field (LC). P_{He} and P_{H} give the populations on the lowest electronic state of each nuclei.

and the dynamics remains unchanged when the initial nuclear kinetic energy for the internuclear motion (given either by a net momentum or induced by a highly localized initial Gaussian packet) is of the order of the initial electron kinetic energy. Unrealistic kinetic energies (larger than 0.2 a.u.) are needed to observe changes of the order of 0.2% in the yields.

4. Summary and conclusions

We have used local control theory to study the possibility of long-range ultrafast electron transfer between nuclei separated by large distances such that the transfer has effectively to proceed through the continuum. As a consequence, the electronic wave packet suffers extensive spreading, which yields a control by external laser pulses extremely difficult. Despite this challenging situation, we found that by applying local control theory one can conceive electric fields which lead to efficient electron transfer to a target nucleus. However, in any situation, the objective of electron retrapping is always in competition with ionization. As for the initial excitation, two approaches have been explored: one is to apply a momentum boost to the electron wave packet to provide sufficient energy to be promoted into the continuum, the other is to apply an attosecond laser pulse to the initially bound system. In both cases, the excitation is followed by the control pulse, which induced retrapping. Again, two possibilities have been studied, one based on a projection to a bound, localized target state, the other based on minimization of the mean momentum after a well-chosen delay. The latter approach was found to be more efficient. In any case, the mechanism is an impulsive retrapping induced by a strongly peaked field, occurring at the moment when the electronic wave packet has a large overlap with the target nucleus.

The efficiency of retrapping the electron (reducing the ionization) decreases at larger internuclear distances or when the kinetic energy of the electron is larger or when we artificially reduce the amplitude of the electric field, but qualitatively the same impulsive mechanism is observed. The nuclear kinetic energy plays no significant role at the timescales considered in this work. On the other hand, for asymmetric electron transfer (*e.g.* in HeH^{2+}) stronger modulations are observed in the local fields and persisting for longer times, in particular when one aims at retrapping at the nuclei with more positive charge, that is, with a larger attractive basin.

Despite the fact the obtained attosecond pulses are currently not achievable in the laboratory, our study shows that a laser control of long range electron transfer via the continuum is in principle possible. The presented calculations treat the electronic dynamics in one spatial dimension using soft-core Coulomb potentials, however, the impulsive mechanism can be expected to work in full dimensionality as well. In this case, spreading that occurs in all dimensions might be more difficult to overcome by the control. In addition, if the electron comes off one proton with angular momentum then the photoassociation could involve additional challenges. But on the other hand, the true Coulomb potential might be more efficient to attract the moving electron, potentially leading to efficient trapping. It is thus very interesting to extend the presented methodology to full dimensionality, without invoking the soft core potential approximation.

Please cite this article in press as: P. Vindel-Zandbergen et al., Chem. Phys. (2016), http://dx.doi.org/10.1016/j.chemphys.2016.04.015

Conflict of interest

The authors have declared no conflict of interest.

Acknowledgments

Financial support from the MICINN (Project CTQ2012-36184 and CTQ2015-65033) and the COST-action (Grant No. CM1204, XLIC), as well as the computational facilities by CALMIP, Toulouse, are gratefully acknowledged.

References

[1] M.F. Kling, M.J. Vrakking, Annu. Rev. Phys. Chem. 59 (1) (2008) 463.
[2] F. Krausz, M. Ivanov, Rev. Mod. Phys. 81 (1) (2009) 163.
[3] A.H. Zewail, Angew. Chem. Int. Ed. 39 (15) (2000) 2586.
[4] M. Shapiro, P. Brumer, References, in: Quantum Control of Molecular Processes, Wiley-VCH Verlag GmbH & Co. KGaA, 2011, p. 513.
[5] A.P. Peirce, M.A. Dahleh, H. Rabitz, Phys. Rev. A 37 (12) (1988) 4950.
[6] D.J. Tannor, R. Kosloff, A. Bartana, Faraday Discuss. 113 (1999) 365.
[7] M. Sugawara, Chem. Phys. Lett. 358 (3–4) (2002) 290.
[8] Y. Ohtsuki, H. Kono, Y. Fujimura, J. Chem. Phys. 109 (21) (1998) 9318.
[9] Y. Ohtsuki, Y. Yahata, H. Kono, Y. Fujimura, Chem. Phys. Lett. 287 (5–6) (1998) 627.
[10] M. Sugawara, S. Yoshizawa, S. Yabushita, Chem. Phys. Lett. 350 (3–4) (2001) 253.
[11] M. Sugawara, J. Chem. Phys. 118 (15) (2003) 6784.
[12] M. Sugawara, Y. Fujimura, J. Chem. Phys. 101 (8) (1994) 6586.
[13] G. Katz, M.A. Ratner, R. Kosloff, Phys. Rev. Lett. 98 (20) (2007) 203006.
[14] Y. Chen, P. Gross, V. Ramakrishna, H. Rabitz, K. Mease, J. Chem. Phys. 102 (20) (1995) 8001.
[15] M. Sugawara, Y. Fujimura, Chem. Phys. 196 (1) (1995) 113.
[16] M. Sugawara, Y. Fujimura, J. Chem. Phys. 100 (8) (1994) 5646.
[17] Y. Watanabe, H. Umeda, Y. Ohtsuki, H. Kono, Y. Fujimura, Chem. Phys. 217 (2) (1997) 317.
[18] K. Hoki, Y. Ohtsuki, H. Kono, Y. Fujimura, J. Phys. Chem. A 103 (32) (1999) 6301.
[19] K. Hoki, Y. Ohtsuki, Y. Fujimura, J. Chem. Phys. 114 (4) (2001) 1575.
[20] Y. Fujimura, L. González, K. Hoki, J. Manz, Y. Ohtsuki, Chem. Phys. Lett. 306 (1) (1999) 1.
[21] P. Marquetand, V. Engel, J. Chem. Phys. 127 (8) (2007) 084115.
[22] P. Marquetand, C. Meier, V. Engel, J. Chem. Phys. 123 (20) (2005) 204320.
[23] V. Engel, C. Meier, D.J. Tannor, Local Control Theory: Recent Applications to Energy and Particle Transfer Processes in Molecules, vol. 141, John Wiley & Sons Inc, 2009. pp. 29–101.
[24] C.P. Koch, J.P. Palao, R. Kosloff, Phys. Rev. A 70 (2004) 013402.
[25] C.P. Koch, R. Kosloff, F. Masnou-Seeuws, Phys. Rev. A 73 (2006) 043409.
[26] J. Javanainen, J.H. Eberly, Q. Su, Phys. Rev. A 38 (7) (1988) 3430.
[27] B.Y. Chang, S. Shin, J. Santamaria, I.R. Sola, Chem. Phys. 442 (2014) 18.
[28] Q. Su, J.H. Eberly, Phys. Rev. A 44 (1991) 5997.
[29] K.C. Kulander, F.H. Mies, K.J. Schafer, Phys. Rev. A 53 (1996) 2562.
[30] B.Y. Chang, S. Shin, A. Palacios, F. Martín, I.R. Sola, J. Phys. B 48 (4) (2015) 043001.
[31] B.Y. Chang, S. Shin, A. Palacios, F. Martín, I.R. Sola, J. Chem. Phys. 139 (8) (2013) 184306.
[32] T. Bredtmann, S. Chelkowski, A.D. Bandrauk, Phys. Rev. A 84 (2011) 021401.
[33] C. Lefebvre, H.Z. Lu, S. Chelkowski, A.D. Bandrauk, Phys. Rev. A 89 (2014) 023403.
[34] S. Gräfe, M. Erdmann, V. Engel, Phys. Rev. A 72 (2005) 013404.
[35] R. Kritzer, C. Meier, V. Engel, Chem. Phys. Lett. 477 (1–3) (2009) 75.
[36] S. Gräfe, P. Marquetand, V. Engel, N.E. Henriksen, K.B. Mller, Chem. Phys. Lett. 398 (1–3) (2004) 180.
[37] S. Gräfe, C. Meier, V. Engel, J. Chem. Phys. 122 (18) (2005) 184103.
[38] P. Marquetand, S. Gräfe, D. Scheidel, V. Engel, J. Chem. Phys. 124 (5) (2006) 054325.
[39] M. Feit, J. Fleck Jr., A. Steiger, J. Comp. Phys. 47 (3) (1982) 412.
[40] M.D. Feit, J. Chem. Phys. 78 (1) (1983) 301.
[41] M.D. Feit, J.A. Fleck, J. Chem. Phys. 80 (6) (1984) 2578.
[42] D. Macias, S. Brouard, J. Muga, Chem. Phys. Lett. 228 (6) (1994) 672.
[43] J. Palao, J. Muga, Chem. Phys. Lett. 292 (1) (1998) 1.
[44] C.C. Marston, G.G. Balint-Kurti, J. Chem. Phys. 91 (6) (1989) 3571.
[45] K. Husimi, Proc. Phys. Math. Soc. Jpn 22 (1940) 264.

5.2.2 Slow electron transfer between separated nuclei

Vindel-Zandbergen, P., Meier, C. and Sola, I.R, (*In preparation*)

Vindel-Zandbergen, P., Meier, C. and Sola, I.R, *Chem. Phys.* (*In press*)

Slow electron transfer between separated protons

I. INTRODUCTION

The paper is organized as follows. In section II we introduce the model Hamiltonian and describe the numerical methods applied to interpret the control mechanism. In section III we find the control mechanism that imply slow electron transfer between two protons largely separated via tunneling, taking hundreds of femtoseconds. In section IV we study the role of the nuclear motion in the control of the electron transfer under this timescale. Finally, section V is the conclusions.

II. NUMERICAL METHODS

We need to use a consistent model for treating both continuum and bound electronic states in a system with a single electron and two protons. As a first approximation, we use a 1 + 1D Hamiltonian, including the internuclear distance R and the electron separation to the center of mass z, where the electron is constrained to move in the molecular axis. For this reduced dimensional study the inter-particle interaction is modeled by a soft-core Coulomb potential [**?**]. In the presence of a linearly polarized external field, $\mathcal{E}(t)$, and neglecting small mass polarization terms, the Hamiltonian in the length gauge is (atomic units are used throughout unless otherwise stated)

$$H = -\frac{1}{2}\frac{\partial^2}{\partial z^2} - \frac{1}{M}\frac{\partial^2}{\partial R^2} + V(z,R) - z\mathcal{E}(t) \qquad (1)$$

where M is the mass of the proton, with the soft-core Coulomb potential

$$V(z,R) = -\frac{1}{\sqrt{1+(z-R/2)^2}} - \frac{1}{\sqrt{1+(z+R/2)^2}} + \frac{1}{R} \qquad (2)$$

This model has been extensively applied as a first qualitative step to analyze ionization processes in H_2^+ and high-harmonic spectra [**?** **?**], as well as electron-nuclear dynamics[**?** **?** **?** **?**].

Initially, we assume a fixed nuclei approximation, where an hydrogen atom and a proton are largely separated. In Section III we select results for fixed internuclear distances of 10 and 20 a.u. We achieve electron transfer applying LCT. The objective is mathematically expressed as the population in a target state $|\psi_f\rangle$[**?** **?**] , constructed as a wave function localized at the proton where we want the electron to be recaptured. Therefore, the control field depends on the projection on a target state

$$\mathcal{E}(t) = \lambda\Im\big[\langle\Psi(t)|\mu|\psi_f\rangle\langle\psi_f|\Psi(t)\rangle\big] \qquad (3)$$

where $\Im$ stands for the imaginary part and $\Psi(t)$ is the wave function of the system.

Here λ enters as a free parameter that measures the strength of the laser interaction. λ must be found numerically

In finding the local control field with Eq.(3), the projection operator $P_t = |\psi_{R_1}\rangle\langle\psi_{R_1}|$ must commute with the Hamiltonian of the system[**?**]. Therefore, the target wave function must be an eigenfunction of the Hamiltonian. However, if the separation of the protons is not large enough, the localized wave functions are not true eigenstates, as the tunneling time cannot be neglected. One way to solve this problem is to add a very small static field component, $\mathcal{E}_{DC}$, to break the symmetry of the Hamiltonian, such that the effective potential is tilted, $V_{\text{tilted}}(z) = V(z) + z\mathcal{E}_{DC}$. Then the target and the initial states are the ground or first excited electronic wave functions of the Hamiltonian with the DC component localized at the desired proton. The initial state is ψ_L localized at the left potential well and ψ_R is the target state at the right potential well.

By making $\mathcal{E}_{DC}$ small enough, the tilted potential has no significant impact on the search of the local control field for large internuclear distances ($R \geq 20$ a.u.). However, the DC component is an essential ingredient in the control of electron localization at smaller proton separations.

In our simulations, the initial state is created by exciting the H_2^+ molecule, that is, ψ_L is multiplied by an exponential factor that gives an initial momentum in the positive direction

$$\Psi(z,0) = \psi_{L_1}(z)\mathrm{e}^{ik_e z} \qquad (4)$$

In addition, to initiate the LCT approach one needs a small "seed" of population in the right potential well (the target state), which we fix as $\approx 0.3\%$. Once the local control field is found this "seeded" population is no longer needed, and the simulations shown in the results imply 100% population in the ground (localized) state at initial time.

Numerical results are obtained by solving the TDSE with the Split-Operator method [**?** **?** **?**] with time steps ranging from $\Delta t = 0.1$ to 0.01 a.u. depending on the simulation. A grid of 1024 points spanning from $z = -80$ to $z = 80$ a.u. is used for the electronic coordinate. Imaginary ("optical") potentials [**?** **?**] absorb the outgoing wave functions avoiding reflection on the grid boundaries and allowing to measure the ionization probability. The eigenstates $\psi_{L,R}$ are computed using the Fourier Grid Hamiltonian method [**?**]. The dynamical mechanism of the transfer is studied by analyzing the approximate phase-space representation of the wave functions at different times, using the Husimi transformation [**?**].

Finally, to study the role of the nuclear motion in the control of the electron transfer, 1 + 1D calculations were

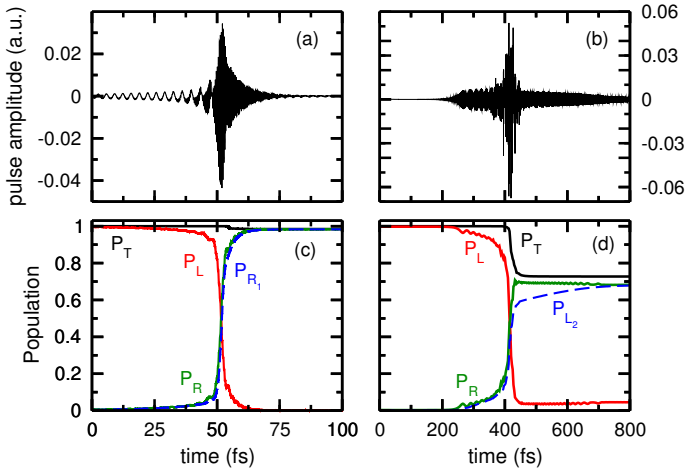

FIG. 1: Laser control fields and population dynamics for an internuclear distance of 10 [(a) and (c)] and 20 a.u.[(b) and (d)], when tunneling is the mechanism responsible for electron transfer.

performed using the full Hamiltonian of Eq.(1). The initial wave packet is the product of the electronic wave function times a nuclear Gaussian wave packet $\psi_{\rm nuc}(R)$, centered at the left nuclei. Now, we use a grid of 1024 points ranging from $R = 0.1$ to $R = 150$ a.u. for the nuclear coordinate and 256 points from $z = -80$ to $z = 80$ a.u. for the electronic coordinate.

III. SLOW ELECTRON TRANSFER

The tunneling mechanism

We first study electron transfer when the electron stars with a small momentum. The initial wave function, localized at the left potential, has an initial momentum of $k_e = 0.001$ a.u. [see Eq.(4)]. Under these conditions, best results are obtained for nuclei separated less than 20 a.u. The results of a typical LCT calculation are shown in Fig.

We have used the LCT approach based on the projection operator on a target wave function that is the lowest energy eigenfunction localized on the right well of a "tilted" potential. The calculations were performed using a static field of $\mathcal{E}_{DC} = -5{\cdot}10^{-3}$ a.u. and $\mathcal{E}_{DC} = -2{\cdot}10^{-5}$ a.u. Best results were obtained with $\lambda = 0.2$ for $R = 10$ a.u. and $\lambda = 2.8$ for $R = 20$ a.u. in Eq.(3).

Fig.1(a) and (b) show the optimal field for $R = 10$ and $R = 20$ a.u. and (c) and (d) panels represent the population dynamics partitioned into the left and right domains

$$P_D(t) = |\langle \Psi(z,t)|\Psi(z,t)\rangle_{z\in D}|^2 \qquad (5)$$

where D is $(-L/2, 0)$ or $(0, L/2)$ (with L the grid size) for the left and right domains, respectively. Also shown is the optimization yield, measured as the overlap of the wave function with the target state,

$$P_{R_1}(t) = |\langle \psi_{R_1}|\Psi(z,t)\rangle|^2 \qquad (6)$$

As observed, for $R = 10$ a.u., complete electron transfer is achieved with $\sim 0.08\%$ population remaining in the left potential well. The final population in the right potential well is completely localized in the target state, $P_{R_1}/P_R = 1$, an there is no population loss due to ionization. For $R = 20$ a.u., again the electron transfer is almost complete, with $\sim 6\%$ population in the left Hydrogen. The final population is localized in the target state, $P_{R_1}/P_R = 0.99$, while the remaining population (less than 30%) is lost as ionization.

To interpret the mechanism under the electron transfer process, it is interesting to observe that the average energy of the electron never exceeds the energy of the internal barrier between the two protons in the soft-core Coulomb potential, $V(0, R = 10)$ and $V(0, R = 20)$ [Eq.(2)]. In addition, at these internuclear distances, the tunneling times between localized states in one well to the other are within the time-scales of the control process. A rough calculation for $R = 20$ a.u. gives $t_1 \approx 3$ ps for population inversion between the ground localized states ψ_{L_1} and ψ_{R_1}, and $t_2 \approx 250$ fs for population inversion between the first excited localized states in each well, ψ_{L_2} and ψ_{R_2}. For $R = 10$ a.u., the population inversion between ψ_{L_1} and ψ_{R_1} is $t_1 \approx 100$ fs. For the soft-core model other excited states have energies above the Coulomb barrier. Roughly we propose the following mechanism as the key process governing the electron transfer: First, as a net positive momentum is given to the electron initially, the electron finds itself distributed between the excited states of the left Hydrogen with energies below the continuum. The electron transfer occurs by tunnelling. Finally the control laser field decreases the energy of the electron in the right basin.

To help visualizing the process we use the Husimi transformation. Fig.2 shows the Husimi plots of the electron wave function at the time the electron transfer is happening for $R = 20$ a.u. As observed, the momentum distribution is localized around zero and does not change, implying that the electron is not reaching the continuum while it moves to the right potential well. These distributions correspond to a tunneling mechanism, where the electron density starts to "disappear" from the left Hydrogen atom and is transferred to the proton on the right.

Since tunneling is the main mechanism behind the electron transfer, in the following the mechanism is imposed on the dynamics by finding biased control fields.

Using the mechanism proposed before, the idea is to use two laser pulses tuned to the first electronic transition, time delayed by t_2, the time it takes to tunnel in the first excited localized states. This is a "four-states" scheme where only the localized ground states (ψ_{L_1} and ψ_{R_1}) and first excited states (ψ_{L_2} and ψ_{R_2}) participate

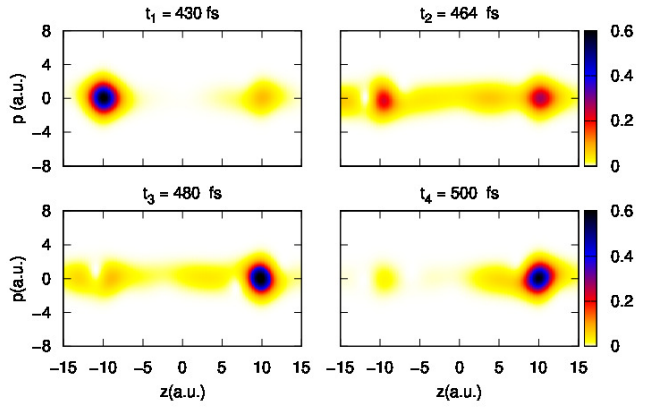

FIG. 2: Husimi functions for different times when the electron is being transferred from the left Hydrogen atom to the proton on the right for an internuclear distance of $R = 20$ a.u

in the dynamics. In this control scenario we have used $k_e = 0$. Fig.3(a) and (b) show the laser pulses and the population dynamics. The first laser pulse that produces population inversion from ψ_{L_1} to ψ_{L_2} is equivalent to a π pulse of $\sim$ 20 fs duration, 0.02 a.u. pulse amplitude and $\omega = 0.39$ a.u. The second laser pulse that de-excites the electron from ψ_{R_2} to ψ_{R_1} is also a π pulse of $\sim$ 10 fs duration, 0.02 a.u. pulse amplitude and $\omega = 0.39$ a.u. The yield of population inversion for the second pulse is only slightly lower than 1. Using this scheme, one can completely avoid ionization ($\approx 2\%$). In fig.4 we observe the propagation of the electronic wave packet, that shows the mechanism of the "four-states" scheme.

For $R = 10$ a.u. the mechanism is even simpler. Since tunneling time is $t_1 = 100$ fs, starting from the localized state at the left Hydrogen, we just need to propagate enough time and the electron is completely transferred to the right potential well, without the action of an external laser field.

In summary, electron transfer between protons that are separated by moderately large distances is possible by means of a slow transfer process, where tunneling below the internal barrier is the predominant mechanism. Tunneling can be made the sole mechanism responsible for the process. In this case, however, local control theory is not required, as analytical pulses, or even no external field, can lead to the same final results. The tunneling mechanism can not be used effectively when the internuclear distance increases, as the tunneling time increases exponentially and one needs to selectively excite the electron to Rydberg states ever closer to the continuum, a process that is difficult by itself. In addition, as we show in the next section, the nuclear dynamics acts as a very strong perturbation source that affects the yield of the process.

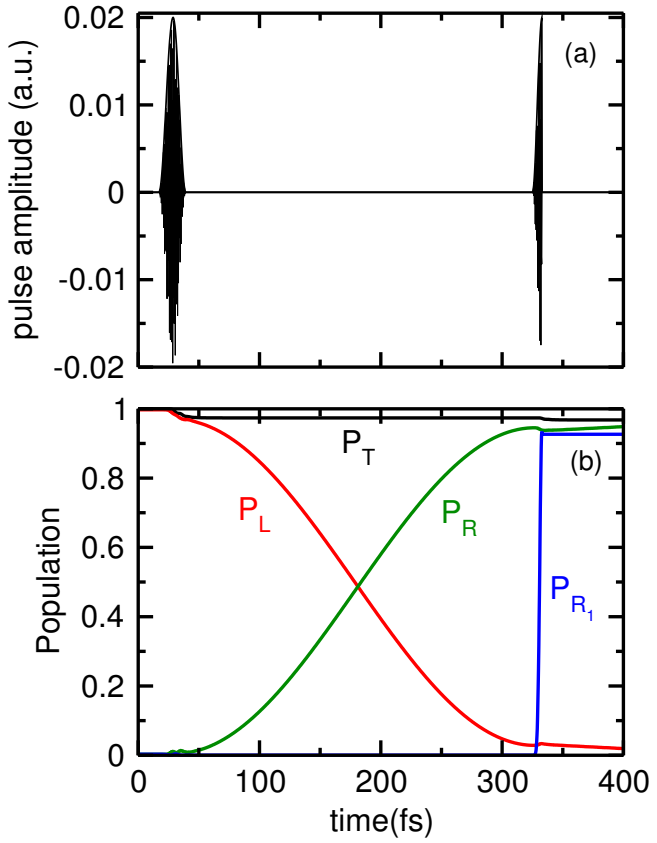

FIG. 3: Population dynamics and analytic laser field of the "four-states" scheme

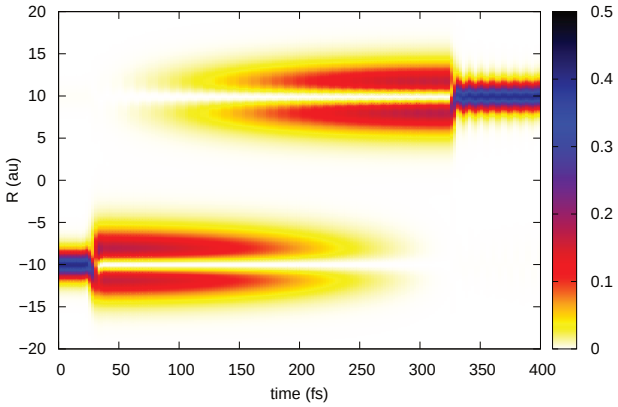

FIG. 4: Wave packet propagation in the "four-states" scheme

The role of the nuclear motion

The fixed nuclei approximation is valid as long as the electronic processes occur in a time-scale much faster than that of the nuclear motion. In the slow electron transfer mechanism, the transfer times are of the order or larger than typical vibrational periods. Here, we ana-

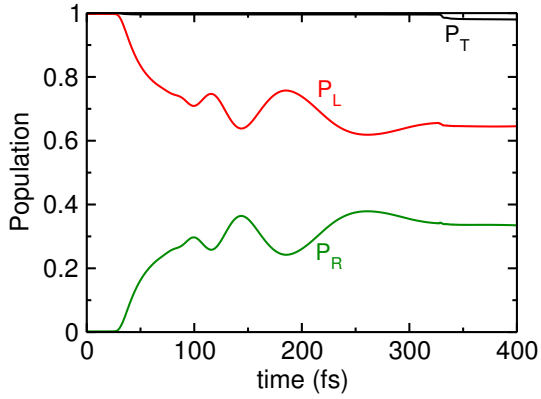

Fig.4

FIG. 5: Population dynamics of a 2-D calculation with no initial nuclear kinetic energy when the analytic laser control field is acting

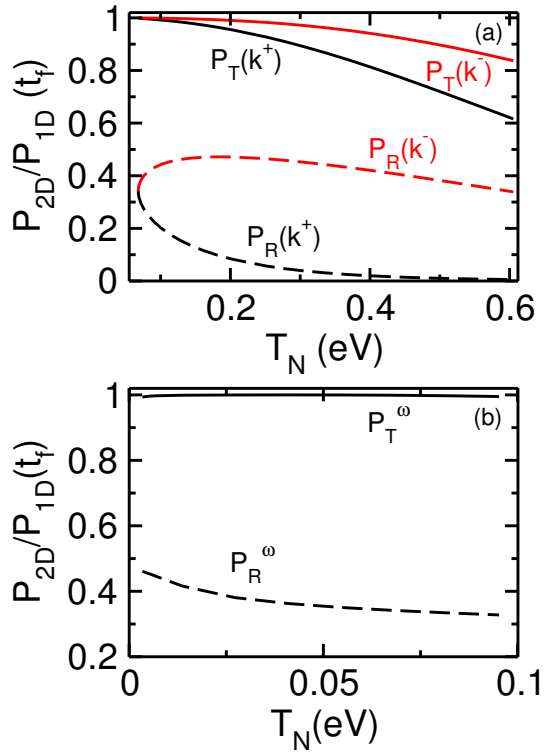

FIG. 6: Variation of total and right well remaining population at t_f with the initial nuclear kinetic energy (a) depending on the initial momentum given to the nuclei, positive (k_n^+) and negative (k_n^-) (b) as a function of the initial width of the nuclear wave function

lyze how the nuclear motion affects the yield of the process. We use the optimal pulses found in the fixed-nuclei LCT approach, as well as the analytic pulses of the "four-state" scheme and apply them on a full 2-D (or (1+1D)) calculation considering different initial nuclear wave functions. The effect of the initial nuclear kinetic energy is considered in two different ways: by studying the effect

FIG. 7: Wave packet at different times for a 2-D propagation

of the width of the Gaussian nuclear wave function and by adding a net momentum in the positive or negative direction. However, we do not directly apply the LCT approach to the $(1+1)$D TDSE.

As a representative example, fig.5 shows the effect of the nuclear motion over the population dynamics for $R = 20$ a.u., when the analytic pulses of the 1-D "four-states" scenario are used in a 2-D calculation and no initial kinetic energy is given to the nuclei. Although some population transfer is achieved and ionization is also avoided, the effect of the nuclear motion completely influences the photoassociation process. Now, only $\sim 30\%$ population remains at the right Hydrogen and the electron transfer mainly occurs in the first 150 fs, but the transfer mechanism is the same as in the 1-D situation. As we can see in fig.7 the 2-D wave packet initially spreads along the internuclear coordinate ($t_1 = 20$ fs). Then, the first laser pulse excites the electron to the excited state ($t_1 = 40$ fs) in the left Hydrogen (negative z values). Now, the tunneling time is lower since the wave function is moving to lower internuclear distances, and the population transfer mainly finishes at $t_3 = 60$ fs. Between $t_4 = 325$ fs and $t_5 = 330$ fs the population inversion occurs from the excited and ground state in the right nucleus, when the second laser pulse is acting. Finally, at $t_6 = 400$ we obtain the wave packet at the end of the propagation, with the electron population distributed in the two potential wells and spread along the internuclear distance, but mainly around $R = 20$ a.u.

Fig.6 shows the effect of the nuclear motion as the ratio between the 2-D and the 1-D results for the yield of the process $P_R(\infty)$ (the probability of being localized at the right proton at final time) as well as for the remaining (not ionized) population $P_T(\infty)$. In Fig.6(a) we fix the initial width of the nuclear Gaussian wave packet at $\sigma = 0.31$ a.u. and we consider the effect of positive or negative nuclear momentum. In fig.6(b) the net momentum is zero and only the width of the initial Gaussian wave packet is changed. As a first insight, one can observe the yield of population transfer decreases to $\sim 30\%$ when no initial momentum is given to the nuclei, but the total population remains as in the 1-D calculations.

Also, we can notice differences in the variation of the final population depending on the sign of the initial nuclear momentum. The total population decreases as the initial kinetic energy increases for both positive and negative momenta, but the degree of population loss is bigger in the positive case. As well, we can appreciate this behaviour in the population transfer to the right potential well for positive values of the nuclear momentum. However, when considering the negative case, initially there is an increase in the electron transfer to the right proton for small initial kinetic energies of the nuclei. Then,

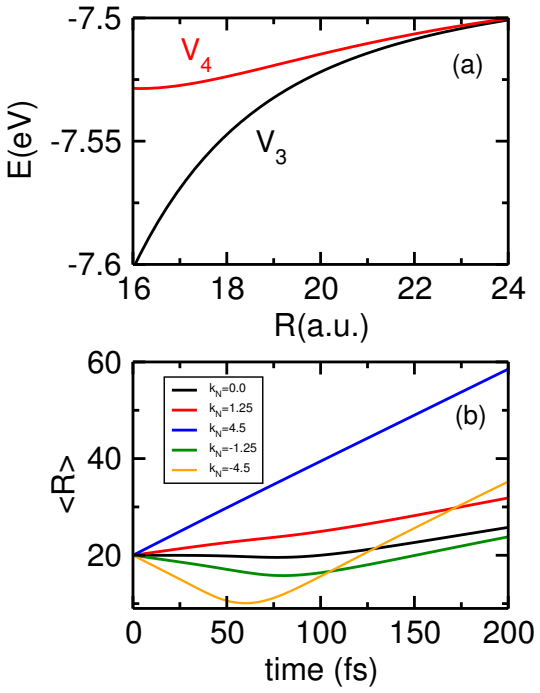

FIG. 8: (a)Potential energy curves of the second and third excited states around R=20 a.u. (b)Variation of the average of the internuclear distance for different values of the initial nuclear momenta. For negative values, the nuclei initially approach until a minimum value of $< R >$ when they collide and then the internuclear distance increases. For positive values of k_N, the nuclei always separate. The gradient of the variation of $< R >$ is greater as k_N is larger.

the yield decreases but not as drastically as for positive values.

These results can be explained by considering the potential energy curves of the second and third excited states where the tunneling is happening [fig.**??** (a)] and the variation of the average of the internuclear distance with the initial nuclear kinetic energy [fig.**??** (b)]. When we apply a negative momentum, the nuclei start to get closer, so the tunneling time decreases, therefore, initially the electron transfer increases. But, from kinetic values larger than ~ 0.15 eV the electron transfer remains constant, regardless of the increase of the initial nuclear momentum. The decrease of the population in the right potential is due to the total population loss by ionization.

When considering positive values of the initial momentum, as the nuclei separate, the energy difference between the excited states decreases and the tunneling time increases, lowering the population transfer, finally even avoiding photoassociation.

Fig.**??**(c) shows the overlap between the projections over the nuclear coordinate of the wave functions corresponding the second (ψ_3) and third (ψ_4) excited states. For high negative values of the initial nuclear momentum, the overlap drops to ~ 0.4 during the first 50 fs that coincides with the decreasing of the mean value of the internuclear distance, and then it reaches again the maximum value, as $< R >$ enlarges. As the initial nuclear momentum increases, the overlap is bigger, corresponding again with the variation of the expectation values of R. Regarding the nuclear potential energy curves around $R = 20$ a.u. [fig.**??**(a)], for lower values of the internuclear distance, the energy difference between states increases, so the overlap between the second and third excited states must decrease. On the other hand, as we move to larger values of R, the energy difference becomes nearly zero, so the excited states are now degenerated states and the overlap between them is close to 1.

Resuming, for negative values of the initial nuclear momentum, the population transfer increases as the nuclei approximate. The internuclear distance decreases so the energy difference between the excited states increases and the tunneling time diminishes. Positive values of initial kinetic energies, imply a rise of the internuclear distance as the nuclear are separating, so the energy difference between the excited states is reduced. The tunneling time increases so the population transfer is lower. This effect is more significant as the initial nuclear kinetic energy is bigger. Regarding the effect of the initial width of the nuclear wave packet, we can observe the total population remains constant but the population transfer increases as we move to lower values of initial kinetic energy. Therefore, highly localized nuclear wave packets (small widths) favour the electron transfer.

IV. CONCLUSIONS AND OUTLOOK

In this work, we have successfully controlled the electron transfer in the H_2^+ molecule with the electron initially localized in one the Hydrogen nuclei, by means of intense and ultrashort laser fields. We worked with a highly simplified Hamiltonian and a soft-core Coulomb potential was used to represent the system, for qualitatively understanding the nature of the process.

We have applied Local Control Theory (LCT) to obtain laser control pulses that lead us to population transfer and electron localization.

The photoassociation is induced by means of tunneling, which corresponds with a slow electron transfer, and the local control field depends on the projection on a target state. This mechanism gave rise to highly acceptable results.

Moreover, the effect of the nuclear motion was also evaluated. Despite we have demonstrated the nuclei motion influences the electron transfer, we still achieved some degree of control over the photoassociation, with satisfactory yields, however the effect of the initial nuclear kinetic energy results more important.

This model can also be extended to simulate the behavior and control the electron transfer in other molecules. (*add conclusions and outlooks*)

[1] J. Javanainen, J. H. Eberly, and Q. Su, "Numerical simulations of multiphoton ionization and above-threshold electron spectra," *Phys. Rev. A*, vol. 38, pp. 3430–3446, Oct. 1988.

[2] Q. Su and J. H. Eberly, "Model atom for multiphoton physics," *Phys. Rev. A*, vol. 44, pp. 5997–6008, Nov 1991.

[3] K. C. Kulander, F. H. Mies, and K. J. Schafer, "Model for studies of laser-induced nonlinear processes in molecules," *Phys. Rev. A*, vol. 53, pp. 2562–2570, Apr 1996.

[4] B. Y. Chang, S. Shin, A. Palacios, F. Martín, and I. R. Sola, "Oscillating molecular dipoles require strongly correlated electronic and nuclear motion," *J. Phys. B*, vol. 48, no. 4, p. 043001, 2015.

[5] B. Y. Chang, S. Shin, A. Palacios, F. Martín, and I. R. Sola, "Ultrafast coherent control of giant oscillating molecular dipoles in the presence of static electric fields," *J. Chem. Phys.*, vol. 139, no. 8, p. 184306, 2013.

[6] T. Bredtmann, S. Chelkowski, and A. D. Bandrauk, "Monitoring attosecond dynamics of coherent electron-nuclear wave packets by molecular high-order-harmonic generation," *Phys. Rev. A*, vol. 84, p. 021401, Aug 2011.

[7] C. Lefebvre, H. Z. Lu, S. Chelkowski, and A. D. Bandrauk, "Electron-nuclear dynamics of the one-electron nonlinear polyatomic molecule H_3^{2+} in ultrashort intense laser pulses," *Phys. Rev. A*, vol. 89, p. 023403, Feb 2014.

[8] S. Gräfe, M. Erdmann, and V. Engel, "Population transfer in the multiphoton excitation of molecules," *Phys. Rev. A*, vol. 72, p. 013404, Jul 2005.

[9] R. Kritzer, C. Meier, and V. Engel, "Local control of population transfer in molecules under fluctuating perturbations," *Chemical Physics Letters*, vol. 477, no. 13, pp. 75 – 79, 2009.

[10] V. Engel, C. Meier, and D. Tannor, *Local Conttrol Theory: Recent Applications to Energy and Particle Transfer Processes in Molecules*, vol. 141, pp. 29–101. John Wiley & Sons, Inc., Feb 2009.

[11] M. Feit, J. Fleck Jr., and A. Steiger, "Solution of the schrödinger equation by a spectral method," *J. Comp. Phys.*, vol. 47, pp. 412–433, Sept. 1982.

[12] M. D. Feit, "Solution of the schro hdinger equation by a spectral method II: (vibrational energy levels of triatomic molecules)," *J. Chem. Phys.*, vol. 78, no. 1, p. 301, 1983.

[13] M. D. Feit and J. A. Fleck, "Wave packet dynamics and chaos in the Hénon-Heiles system," *J. Chem. Phys.*, vol. 80, pp. 2578–2584, Mar. 1984.

[14] D. Macias, S. Brouard, and J. Muga, "Optimization of absorbing potentials," *Chem. Phys. Lett.*, vol. 228, pp. 672–677, Oct. 1994.

[15] J. Palao and J. Muga, "A simple construction procedure of absorbing potentials," *Chem. Phys. Lett.*, vol. 292, pp. 1–6, July 1998.

[16] C. C. Marston and G. G. Balint @ PKurti, "The fourier grid hamiltonian method for bound state eigenvalues and eigenfunctions," *J. Chem. Phys.*, vol. 91, pp. 3571–3576, Sept. 1989.

[17] K. Husimi, "Some formal properties of the density matrix," *Proc. Phys. Math. Soc. Jpn*, vol. 22, pp. 264–314, 1940.

Conclusions

Summary and conclusions

6.1 Summary

In this thesis we have theoretically demonstrated the posibility of controlling the electron and nuclear dynamics excited by intense ultrashort pulses in different scenarios. We join quantum control techniques with femto and attosecond processes working in highly simplified potential models representing the systems under study to follow the combined nuclear and electron dynamics. These simple models allowed us to understand the nature of the processes, its controllability and the validity of the usual approximations.

The first main idea was to influence the singlet and triplet transitions in ion strings, using the extended Shin-Metiu (ESM) model. Within this model system it is possible to characterize the coupled motion of the nucleus and the electron simultaneously. The spin-orbit coupling was introduced heuristically to allow transitions between the singlet and triplet components of the wave function. The underlying mechanism controlling the dynamics was the Non Resonant Dynamic Stark effect. A strong field can change the energy spectra of the singlet and triplet states, independently. Therefore, just by playing with field frequencies and strengths, one can find the optimal parameters to successfully control the evolution of the system and avoid or induce a spin transition. A more complete description of this scheme and the model is discussed in section 3.3.2 and 2.6.2.

We first address the decoupling of the singlet-triplet transition in the adiabatic limit (including different sets of singlet and triplet states) and in the full ESM model (dynamics of vibronic wave packets). In the absence of a laser field full population transfer is achieved at both levels of calculation. Under the effect of a nonresonant strong laser field, the energy of the states is shifted and the population is efficiently maintained within the manifold of the singlet states. Including all electronic states in the model (full ESM model), only increases the dispersion of the population among different singlet states

and the predominant effect is multiphoton absorption leading to ionization. However, the triplet states are not populated essentially. Additionally, different pulse parameters were tested working under the Born-Oppenheimer approximation in the ESM model to choose the optimal values that provided the best results in locking the singlet-triplet transition. Besides, a spin trasnfer is forced by a combination of a chirped and a transformed limited pulse. Finally, in order to identify the conditions for the effcient control of the spin-orbit transitions, the realationship between the spin coupling and the ionization rate was investigated in a simple analytical two-level Hamiltonian. For a more detailed explanation of these results see sec. 5.1.

Right after, we continue describing the simulation and control of the electron transfer in the femto- and attosecond scale by intense laser pulses using the Local Control Theory (see sec. 4.2). The basic idea behind this algorithm is to choose a control field in order to ensure an increase or decrease of the expectation value of an observable during a certain period of time where the external field is acting. Using a soft core Coulomb potential to describe the system (H_2^+) and working under the Born.Oppenheimer approximation the aim was to excite the electron initially localized in one nucleus and then retrap it in the other atom. Two different formulations of this theory were used. In the first one, the laser field depends on the expectation value of the momentum of the electron and the aim is to decrease the energy of the system. In the second one, the laser field depends on the projection of the wave function in a target state (the lowest eigenstate of the target nucleus). Depending on the time scale of the electron transfer two different mechanisms were found. In the femtosecond domain, tunneling is the predominant mechanism where the electron never overcomes the internal barrier between the nuclei, whereas in the attosecond scale the electron transfer occurs by an implusive mechanism (the electron reaches the continuum and then is retrapped in the target nucleus). We also tested the validity of the "fixed nuclei" results and how the initial kinetic energy affects the electron transfer, by applying the laser control fields that emerge from 1D calculations on a full 2D (1+1D) calculation. For a detailed discussion of these resutls see sec. 5.2.

6.2 Conclusions and outlooks

The main objecive of this thesis is the merging of two emerging research areas, Quantum Control and ultrafast physics (femto and attosecond processes). We applied different control methods to various physical processes of current importance involving both

electron and nuclear dynamics. In the following we report the fundamental conclusions we can extract form this work:

- Including different number of electronic states in the Born-Oppenheimer approximation, we have applied a strong field laser control scheme based on NRDSE to influence the spin-orbit transitions

- We have analyzed in detail the role of different laser parameters in the control of singlet-triplet transitions in conditions where there is strong competence between different non-linear processes. The appropiate parameters fos spin switching were diffucult to find but we showed efficient spin-locking despite the strong singlet-triplet coupling for different frequency windows.

- The same principles of efficient spin-locking were observed to apply in the dynamics of vibronic wave packets, however, multi-photon ionization is the predominant dynamical process, thus the NRDSE scheme fails to work when it is applied to the coupled electron-nuclear system.

- However, we have shown that the competing processes of spin-transitions and ionization can be influenced and it is possible to establish an efficient quantum control of spin transitions before ionization is effective.

- It was found in a very simple two-level approximation model that the key feauture that determines if optical spin control is possible or not is the dependence of the ionization rate on the control field amplitude

- The extended two-electron Shin-Metiu model is an excellent starting point to study strong field dynamics of vibronic wave packets, allowing us to test the limit of validity of certain control strategies defined in the Born-Oppenheimer basis.

- A better understanding of the dynamics of vibronic wave packets is a necessary step to motivate new strong-field control schemes that may presumably overcome multiphoton ionization or tunneling ionization.

- We found that applying Local Control Theory one can concieve electric fields which lead to efficient electron transfer to a target nucleus, even in the callenging situation when the transfer proceeds through the continuum when the electron retrapping is always in competition with ionization and the electronic wave packet suffers extensive spreading.

- Highly simplified Hamiltonians have shown to be very useful for qualitatively understanding the nature of the processes under study
- We have studied two different mechanisms of electron transfer depending on the time scale of the electron dynamics. In the attosecond regime we found the photoassociations is an impulsive process, where the electron is excited to the continuum and then is retrapped by an intense peak attosecond pulse. In the femtosecond scale the eletron transfer occurs by a tunneling mechnism.
- Electron transfer through the ionization continuum demands strong requirements in terms of frequency, intensity and timing on attosecond pulses to maximize the probability of re-trapping the electron at the desired core, clearly exceeding current capabilities. On the other hand the efficiency is less model dependent.
- Femtosecond transfer based on tunneling, however, promises higher yields if the nuclei are not too far apart, but the results are sensitive to model dimensionality and nuclear motion and are more difficult to extrapolate to other molecular processes.
- In the femtosecond transfer we have found that analytical pulses lead to same final results as the local control pulses, thus LCT is not requiered when tunneling is the sole mechanism of electron transfer.
- Although we can not yet assess whether the control of electron transfer or other electron processes should be better exerted in the atto or in the femto regime, the results show that it is still too early to retire Femtochemistry from the race.

References

Bibliography

[1] A. H. Zewail, Angew. Chem. Int. Ed. 39 (15) (2000) 2586–2631.

[2] M. F. Kling, M. J. Vrakking, Annu. Rev. Phys. Chem. 59 (1) (2008) 463–492.

[3] F. Krausz, M. Ivanov, Rev. Mod. Phys. 81 (1) (2009) 163–234.

[4] M. Shapiro, P. Brumer, References, in: Quantum Control of Molecular Processes, Wiley-VCH Verlag GmbH & Co. KGaA, 2011, pp. 513–535.

[5] D. J. Tannor, S. A. Rice, J. Chem. Phys. 83 (10) (1985) 5013–5018.

[6] D. J. Tannor, R. Kosloff, S. A. Rice, J. Chem. Phys. 85 (10) (1986) 5805–5820.

[7] P. Brumer, M. Shapiro, Chem. Phys. Lett. 126 (6) (1986) 541 – 546.

[8] P. Brumer, M. Shapiro, Faraday Discuss. Chem. Soc. 82 (1986) 177–185.

[9] A. P. Peirce, M. A. Dahleh, H. Rabitz, Phys. Rev. A 37 (12) (1988) 4950–4964.

[10] R. Kosloff, S. Rice, P. Gaspard, S. Tersigni, D. Tannor, Chem. Phys. 139 (1) (1989) 201–220.

[11] D. J. Tannor, R. Kosloff, A. Bartana, Faraday Discuss. 113 (0) (1999) 365–383.

[12] V. Engel, C. Meier, D. Tannor, Local Control Theory: Recent Applications to Energy and Particle Transfer Processes in Molecules, Vol. 141, John Wiley & Sons, Inc., 2009, pp. 29 – 101.

[13] M. Erdmann, P. Marquetand, V. Engel, J. Chem. Phys. 119 (2) (2003) 672.

[14] M. Erdmann, V. Engel, J. Chem. Phys. 120 (1) (2004) 158.

[15] B. J. Sussman, D. Townsend, M. Y. Ivanov, A. Stolow, Science 314 (5797) (2006) 278–281.

[16] H. Rabitz, R. de Vivie-Riedle, M. Motzkus, K. Kompa, Science 288 (5467) (2000) 824–828.

[17] F. Krausz, M. Ivanov, Rev. Mod. Phys. 81 (1) (2009) 163.

[18] A. H. Zewail, Science 242 (4886) (1988) 1645–1653.

[19] M. Dantus, R. M. Bowman, A. H. Zewail, Nature 343 (1990) 737–739.

[20] T. Baumert, M. Grosser, R. Thalweiser, G. Gerber, Phys. Rev. Lett. 67 (1991) 3753–3756.

[21] T. Baumert, B. Bühler, R. Thalweiser, G. Gerber, Phys. Rev. Lett. 64 (1990) 733–736.

[22] R. Huebener, Electrons in Action: Roads to Modern Computers and Electronics, Wiley-VCH Verlag, Weinheim, 2005.

[23] F. Krausz, M. Ivanov, Rev. Mod. Phys. 81 (1) (2009) 163.

[24] A. Baltuska, T. Udem, M. Uiberacker, E. Goulielmakis, C. Gohle, R. Holzwarth, V. S. Yakivlev, A. Scrinzi, Hänsch, F. Krausz, Nature 421 (2003) 611–615.

[25] P. Agostini, F. Fabre, G. Mainfray, G. Petite, N. K. Rahman, Phys. Rev. Lett. 42 (1979) 1127–1130.

[26] A. McPherson, G. Gibson, H. Jara, U. Johann, T. S. Luk, I. A. McIntyre, K. Boyer, C. K. Rhodes, J. Opt. Soc. Am. B 4 (4) (1987) 595–601.

[27] M. Ferray, A. L'Huillier, X. Li, L. Lompre, G. Mainfray, C. Manus, J. Phys. B 21 (3) (1988) L31.

[28] X. F. Li, A. L'Huillier, M. Ferray, L. A. Lompré, G. Mainfray, Phys. Rev. A 39 (1989) 5751–5761.

[29] J. L. Krause, K. J. Schafer, K. C. Kulander, Phys. Rev. A 45 (1992) 4998–5010.

[30] A. L'Huillier, M. Lewenstein, P. Salières, P. Balcou, M. Y. Ivanov, J. Larsson, C. G. Wahlström, Phys. Rev. A 48 (1993) R3433–R3436.

[31] K. J. Schafer, B. Yang, L. F. DiMauro, K. C. Kulander, Phys. Rev. Lett. 70 (1993) 1599–1602.

[32] P. B. Corkum, Phys. Rev. Lett. 71 (1993) 1994–1997.

[33] R. Trebino, K. W. DeLong, D. N. Fittinghoff, J. N. Sweetser, M. A. Krumbgel, B. A. Richman, D. J. Kane, Rev. Sci. Instrum. 68 (9) (1997) 3277–3295.

[34] Y. Mairesse, F. Quéré, Phys. Rev. A 71 (2005) 011401.

[35] P. M. Paul, E. S. Toma, P. Breger, G. Mullot, F. Augé, P. Balcou, H. G. Muller, P. Agostini, Science 292 (5522) (2001) 1689–1692.

[36] P. Agostini, L. DiMauro, Rep. Prog. Phys. 67 (6) (2004) 813.

[37] M. Hentschel, R. Kienberger, C. Spielmann, G. A. Reider, N. Milosevic, T. Brabec, P. Corkum, U. Heinzmann, M. Drescher, F. Krausz, Nature 414 (2001) 509–513.

[38] T. Remetter, P. Johnsson, J. Mauritsson, K. Varju, Y. Ni, F. Lepine, E. Gustafsson, M. Kling, J. Khan, R. Lopez-Martens, K. J. Schafer, M. J. J. Vrakking, A. L/'Huillier, Nat. Phys. 2 (2006) 323–326.

[39] M. Drescher, M. Hentschel, R. Kienberger, M. Uiberacker, V. Yakovlev, A. Scrinzi, T. Westerwalbesloh, U. Kleineberg, U. Heinzmann, F. Krausz, Nature 419 (2002) 803–807.

[40] J. Itatani, J. Levesque, D. Zeidler, H. Niikura, H. Pepin, J. C. Kieffer, P. B. Corkum, D. M. Villeneuve, Nature 432 (2004) 867–871.

[41] G. Sansone, F. Kelkensberg, J. F. Pérez-Torres, F. Morales, M. F. Kling, W. Siu, O. Ghafur, P. Johnsson, M. Swoboda, E. Benedetti, F. Ferrari, F. Lne, J. L. Sanz-Vicario, S. Zherebtsov, I. Znakovskaya, A. L'Huillier, M. Y. Ivanov, M. Nisoli, F. Mart M. J. J. Vrakking, Nature 465 (2010) 763–766.

[42] A. L. Cavalieri, N. Muller, T. Uphues, V. S. Yakovlev, A. Baltuska, B. Horvath, B. Schmidt, L. Blumel, R. Holzwarth, S. Hendel, M. Drescher, U. Kleineberg, P. M. Echenique, R. Kienberger, F. Krausz, U. Heinzmann, Nature 449 (2007) 1029–1032.

[43] A. Schiffrin, T. Paasch-Colberg, N. Karpowicz, V. Apalkov, D. Gerster, S. Muhlbrandt, M. Korbman, M. Reichert, Joachim Schultze, S. Holzner, J. V. Barth, R. Kienberger, R. Ernstorfer, V. S. Yakovlev, M. I. Stockman, F. Krausz, Nature 493 (2007) 70–74.

[44] A. Borot, A. Malvache, X. Chen, A. Jullien, J.-P. Geindre, P. Audebert, G. Mourou, F. Quere, R. Lopez-Martens, Nat. Phys. 8 (2012) 416–421.

[45] E. F. Garman, Science 343 (6175) (2014) 1102–1108.

[46] R. J. D. Miller, Science 343 (6175) (2014) 1108–1116.

[47] F. Kelkensberg, W. Siu, J. F. Pérez-Torres, F. Morales, G. Gademann, A. Rouzée, P. Johnsson, M. Lucchini, F. Calegari, J. L. Sanz-Vicario, F. Martín, M. J. J. Vrakking, Phys. Rev. Lett. 107 (2011) 043002.

[48] W. Siu, F. Kelkensberg, G. Gademann, A. Rouzée, P. Johnsson, D. Dowek, M. Lucchini, F. Calegari, U. De Giovannini, A. Rubio, R. R. Lucchese, H. Kono, F. Lépine, M. J. J. Vrakking, Phys. Rev. A 84 (2011) 063412.

[49] P. Ranitovic, C. W. Hogle, P. Rivière, A. Palacios, X.-M. Tong, N. Toshima, A. González-Castrillo, L. Martin, F. Mart M. M. Murnane, H. Kapteyn, Proceedings of the National Academy of Sciences 111 (3) (2014) 912–917.

[50] F. Calegari, D. Ayuso, A. Trabattoni, L. Belshaw, S. De Camillis, S. Anumula, F. Frassetto, L. Poletto, A. Palacios, P. Decleva, J. B. Greenwood, F. Martín, M. Nisoli, Science 346 (6207) (2014) 336–339.

[51] E. A. McCullough, R. E. Wyatt, J. Chem. Phys. 51 (3) (1969) 1253–1254.

[52] R. E. Wyatt, J. Chem. Phys. 51 (8) (1969) 3489–3502.

[53] M. D. Feit, J. A. Fleck, J. Chem. Phys. 80 (6) (1984) 2578–2584.

[54] V. Engel, H. Metiu, R. Almeida, R. A. Marcus, A. H. Zewail, Chem. Phys. Lett. 152 (1) (1988) 1 – 7.

[55] V. Engel, H. Metiu, J. Chem. Phys. 90 (11) (1989) 6116–6128.

[56] H. Metiu, V. Engel, J. Opt. Soc. Am. B 7 (8) (1990) 1709–1726.

[57] M. Ferray, A. L'Huillier, X. F. Li, L. A. Lompre, G. Mainfray, C. Manus, J. Phys. B 21 (3) (1988) L31.

[58] U. Johann, T. S. Luk, H. Egger, C. K. Rhodes, Phys. Rev. A 34 (1986) 1084–1103.

[59] J. X. Tull, M. A. Dugan, W. S. Warren, High-resolution, ultrafast laser pulse shaping and its applications, in: W. S. Warren (Ed.), Advances in Magnetic and Optical Resonance, Vol. 20 of Advances in Magnetic and Optical Resonance, Academic Press, 1997, pp. 1 – 65.

[60] S. Chu, Nature 416 (2002) 206–210.

[61] M. Shapiro, P. Brumer, Principles of the Quantum Control of Molecular Processes, John Wiley & Sons, Inc., 2003.

[62] S. Rice, M. Zhao, Optical Control of Molecular Dynamics, Wiley,New York, 2000.

[63] K. Bergmann, H. Theuer, B. W. Shore, Rev. Mod. Phys. 70 (1998) 1003–1025.

[64] M. Shapiro, P. Brumer, Rep. Prog. Phys. 66 (6) (2003) 859.

[65] A. Assion, T. Baumert, M. Bergt, T. Brixner, B. Kiefer, V. Seyfried, M. Strehle, G. Gerber, Science 282 (5390) (1998) 919–922.

[66] A. M. Weiner, A. M. Kan'an, IEEE J. Sel. Top. Quantum Electron. 4 (2) (1998) 317–331.

[67] M. M. Wefers, K. A. Nelson, Opt. Lett. 20 (9) (1995) 1047–1049.

[68] G. M. Huang, T. J. Tarn, J. W. Clark, J. Math. Phys. 24 (11) (1983) 2608–2618.

[69] P. Ehrenfest, Z. Physik 45 (1927) 455–457.

[70] T. Baumert, J. Helbing, G. Gerber, Coherent Control With Femtosecond Laser Pulses, John Wiley & Sons, Inc., 2007, pp. 47–82.

[71] M. Wollenhaupt, T. Baumert, J. Photochem. Photobiol. A 180 (3) (2006) 248 – 255.

[72] E. D. Potter, J. L. Herek, S. Pedersen, Q. Liu, A. H. Zewail, Nature 355 (1992) 66–68.

[73] M. Machholm, N. E. Henriksen, J. Chem. Phys. 113 (18) (2000) 7838–7844.

[74] N. Elghobashi, L. González, J. Manz, J. Chem. Phys. 120 (17) (2004) 8002–8014.

[75] N. Elghobashi, P. Krause, J. Manz, M. Oppel, Phys. Chem. Chem. Phys. 5 (2003) 4806–4813.

[76] N. Elghobashi, L. González, Phys. Chem. Chem. Phys. 6 (2004) 4071–4073.

[77] T. Brixner, G. Gerber, Chem. Phys. Chem. 4 (5) (2003) 418–438.

[78] P. Brumer, M. Shapiro, Annu. Rev. Phys. Chem. 43 (1) (1992) 257–282.

[79] S. M. Park, S.-P. Lu, R. J. Gordon, J. Chem. Phys. 94 (12) (1991) 8622–8624.

[80] S.-P. Lu, S. M. Park, Y. Xie, R. J. Gordon, J. Chem. Phys. 96 (9) (1992) 6613–6620.

[81] J. A. Fissi, L. Zhu, K. Suto, G. He, R. J. Gordon, Chem. Phys. 233 (2-3) (1998) 335 – 341.

[82] V. D. Kleiman, L. Zhu, X. Li, R. J. Gordon, J. Chem. Phys. 102 (14) (1995) 5863–5866.

[83] V. D. Kleiman, L. Zhu, J. Allen, R. J. Gordon, J. Chem. Phys. 103 (24) (1995) 10800–10803.

[84] L. Zhu, K. Suto, J. A. Fiss, R. Wada, T. Seideman, R. J. Gordon, Phys. Rev. Lett. 79 (1997) 4108–4111.

[85] U. Gaubatz, P. Rudecki, M. Becker, S. Schiemann, M. Külz, K. Bergmann, Chem. Phys. Lett. 149 (5) (1988) 463 – 468.

[86] U. Gaubatz, P. Rudecki, S. Schiemann, K. Bergmann, J. Chem. Phys. 92 (9) (1990) 5363–5376.

[87] J. Oreg, F. T. Hioe, J. H. Eberly, Phys. Rev. A 29 (1984) 690–697.

[88] S. Kuhr, W. Alt, D. Schrader, M. Müller, V. Gomer, D. Meschede, Science 293 (5528) (2001) 278–280.

[89] G. K. Paramonov, V. A. Savva, Phys. Lett. A 97 (8) (1983) 340 – 342.

[90] M. Holthaus, B. Just, Phys. Rev. A 49 (1994) 1950–1960.

[91] J. Klein, F. Beil, T. Halfmann, Phys. Rev. A 78 (2008) 033416.

[92] Y.-X. Du, Z.-T. Liang, W. Huang, H. Yan, S.-L. Zhu, Phys. Rev. A 90 (2014) 023821.

[93] V. S. Malinovsky, D. J. Tannor, Phys. Rev. A 56 (6) (1997) 4929.

[94] V. S. Malinovsky, I. R. Sola, Phys. Rev. A 70 (2004) 042304.

[95] I. Thanopulos, M. Shapiro, J. Am. Chem. Soc. 127 (41) (2005) 14434–14438.

[96] G. W. Richings, G. A. Worth, J. Phys. Chem. A 116 (46) (2012) 11228–11240.

[97] A. Bandrauk, M. Sink, Chem. Phys. Lett. 57 (4) (1978) 569 – 572.

[98] A. Zavriyev, P. H. Bucksbaum, J. Squier, F. Saline, Phys. Rev. Lett. 70 (1993) 1077–1080.

[99] S. W. Allendorf, A. Szöke, Phys. Rev. A 44 (1991) 518–534.

[100] A. Giusti-Suzor, F. Mies, L. DiMauro, E. Charron, B. Yang, J. Phys. B 28 (3) (1995) 309.

[101] B. M. Garraway, K. Suominen, Phys. Rev. Lett. 80 (1998) 932–935.

[102] V. Malinovsky, J. Santamaría, I. Sola, J. Phys. Chem. A 107 (40) (2003) 8259–8270.

[103] J. González-Vázquez, I. Sola, J. Santamaría, J. Phys. Chem. A 110 (4) (2006) 1586–1593.

[104] B. Y. Chang, H. Rabitz, I. R. Sola, Phys. Rev. A 68 (3) (2003) 031402.

[105] I. R. Sola, B. Y. Chang, H. Rabitz, J. Chem. Phys. 119 (20) (2003) 10653–10657.

[106] B. Y. Chang, S. Lee, I. R. Sola, J. Chem. Phys. 121 (22) (2004) 11118–11128.

[107] B. Y. Chang, S. Lee, I. R. Sola, J. Santamaría, J. Chem. Phys. 122 (20) (2005) 204316.

[108] B. Y. Chang, S. Lee, I. R. Sola, J. Santamaría, Phys. Rev. A 73 (2006) 013404.

[109] I. R. Sola, J. González-Vázquez, V. S. Malinovsky, Phys. Rev. A 74 (2006) 043418.

[110] J. González-Vázquez, I. R. Sola, J. Santamaría, V. S. Malinovsky, J. Chem. Phys. 125 (12) (2006) 124315.

[111] J. González-Vázquez, I. R. Sola, J. Santamaría, V. S. Malinovsky, J. Phys. Chem. A 111 (14) (2007) 2670–2678.

[112] J. González-Vázquez, I. R. Sola, J. Santamaría, V. S. Malinovsky, Chem. Phys. Lett. 431 (46) (2006) 231 – 235.

[113] S. Shi, A. Woody, H. Rabitz, J. Chem. Phys. 88 (11) (1988) 6870–6883.

[114] S. Shi, H. Rabitz, J. Chem. Phys. 92 (1) (1990) 364–376.

[115] S. Shi, H. Rabitz, Comput. Phys. Commun. 63 (1-3) (1991) 71 – 83.

[116] I. Sola, J. Santamaría, , D. Tannor, J. Phys. Chem. A 102 (23) (1998) 4301–4309.

[117] W. Zhu, J. Botina, H. Rabitz, J. Chem. Phys. 108 (5) (1998) 1953–1963.

[118] M. Sugawara, Y. Fujimura, J. Chem. Phys. 101 (8) (1994) 6586–6592.

[119] Y. Ohtsuki, H. Kono, Y. Fujimura, J. Chem. Phys. 109 (21) (1998) 9318–9331.

[120] P. Gross, H. Singh, H. Rabitz, K. Mease, G. M. Huang, Phys. Rev. A 47 (6) (1993) 4593–4604.

[121] A. Bartana, R. Kosloff, D. J. Tannor, Chem. Phys. 267 (1-3) (2001) 195–207.

[122] R. J. Levis, G. M. Menkir, H. Rabitz, Science 292 (5517) (2001) 709–713.

[123] W. Jakubetz, J. Manz, H.-J. Schreier, Chem. Phys. Lett. 165 (1) (1990) 100 – 106.

[124] M. V. Korolkov, G. K. Paramonov, B. Schmidt, J. Chem. Phys. 105 (5) (1996) 1862–1879.

[125] S. Chelkowski, A. D. Bandrauk, P. B. Corkum, Phys. Rev. Lett. 65 (1990) 2355–2358.

[126] S. Chelkowski, A. D. Bandrauk, Chem. Phys. Lett. 186 (2-3) (1991) 264 – 269.

[127] S. Chelkowski, A. D. Bandrauk, J. Chem. Phys. 99 (6) (1993) 4279–4287.

[128] M. Kaluža, J. T. Muckerman, P. Gross, H. Rabitz, J. Chem. Phys. 100 (6) (1994) 4211–4228.

[129] M. Lysebo, L. Veseth, Phys. Rev. A 90 (2014) 063427.

[130] R. S. Judson, H. Rabitz, Phys. Rev. Lett. 68 (1992) 1500–1503.

[131] C. J. Bardeen, V. V. Yakovlev, K. R. Wilson, S. Carpenter, P. M. Weber, W. S. Warren, Chem. Phys. Lett. 280 (1-2) (1997) 151 – 158.

[132] A. Assion, T. Baumert, M. Bergt, T. Brixner, B. Kiefer, V. Seyfried, M. Strehle, G. Gerber, Science 282 (5390) (1998) 919–922.

[133] v. Vajda, A. Bartelt, E. C. Kaposta, T. Leisner, C. Lupulescu, S. Minemoto, P. Rosendo-Francisco, L. Wöste, Chem. Phys. 267 (1-3) (2001) 231 – 239.

[134] H. Kawashima, M. M. Wefers, K. A. Nelson, Ann. Rev. Phys. Chem. 46 (1) (1995) 627–656.

[135] R. Bartels, S. Backus, E. Zeek, L. Misoguti, G. Vdovin, I. Christov, M. Murnane, K. H.C., Nature 406 (2000) 164–166.

[136] R. Kosloff, A. D. Hammerich, D. Tannor, Phys. Rev. Lett. 69 (15) (1992) 2172–2175.

[137] A. Bartana, R. Kosloff, D. J. Tannor, J. Chem. Phys. 99 (1) (1993) 196–210.

[138] S. Gräfe, C. Meier, V. Engel, J. Chem. Phys. 122 (18) (2005) 184103.

[139] P. Marquetand, S. Gräfe, D. Scheidel, V. Engel, J. Chem. Phys. 124 (5).

[140] P. Marquetand, V. Engel, Chem. Phys. Lett. 407 (4-6) (2005) 471 – 476.

[141] S. Gräfe, P. Marquetand, V. Engel, N. E. Henriksen, K. B. Møller, Chem. Phys. Lett. 398 (1-3) (2004) 180–185.

[142] B. F. E. Curchod, T. J. Penfold, U. Rothlisberger, I. Tavernelli, Chem. Phys. Chem. 16 (10) (2015) 2127–2133.

[143] N. V. Vitanov, T. Halfmann, B. W. Shore, K. Bergmann, Phys. Chem. 52 (1) (2001) 763–809.

[144] M. Sugawara, S. Yoshizawa, S. Yabushita, Chem. Phys. Lett. 350 (3-4) (2001) 253–259.

[145] M. Sugawara, Chem. Phys. Lett. 358 (3-4) (2002) 290–297.

[146] M. Sugawara, J. Chem. Phys. 118 (15) (2003) 6784–6800.

[147] M. Sugawara, Chem. Phys. Lett. 378 (5-6) (2003) 603 – 608.

[148] M. Sugawara, Y. Fujimura, J. Chem. Phys. 100 (8) (1994) 5646 – 5655.

[149] Y. Ohtsuki, Y. Yahata, H. Kono, Y. Fujimura, Chem. Phys. Lett. 287 (5-6) (1998) 627–631.

[150] H. Umeda, Y. Fujimura, Chem. Phys. 274 (2-3) (2001) 231–241.

[151] D. J. Tannor, Introduction to quantum mechanics: a time-dependent perspective, University Science Books, Sausalito, Calif., 2007.

[152] Z.-M. Lu, H. Rabitz, Phys. Rev. A 52 (3) (1995) 1961–1967.

[153] S. E. Sklarz, D. J. Tannor, arXiv:quant-ph/0404081.

[154] S. E. Sklarz, D. J. Tannor, Chem. Phys. 322 (1-2) (2006) 87 – 97.

[155] M. Sugawara, Chem. Phys. Lett. 358 (3-4) (2002) 290 – 297.

[156] R. Kritzer, C. Meier, V. Engel, Chem. Phys. Lett. 477 (1-3) (2009) 75 – 79.

[157] S. Gräfe, M. Erdmann, V. Engel, Phys. Rev. A 72 (2005) 013404.

[158] B. F. E. Curchod, T. J. Penfold, U. Rothlisberger, I. Tavernelli, Phys. Rev. A 84 (2011) 042507.

[159] C. Meier, M.-C. Heitz, J. Chem. Phys. 123 (4) (2005) 044504.

[160] P. Marquetand, V. Engel, J. Chem. Phys. 127 (8) (2007) 084115.

[161] Y. Ohtsuki, H. Kono, Y. Fujimura, J. Chem. Phys. 109 (21) (1998) 9318 – 9331.

[162] M. Sugawara, S. Yoshizawa, S. Yabushita, Chem. Phys. Lett. 350 (3-4) (2001) 253 – 259.

[163] M. Sugawara, J. Chem. Phys. 118 (15) (2003) 6784 – 6800.

[164] M. Sugawara, Y. Fujimura, J. Chem. Phys. 101 (8) (1994) 6586 – 6592.

[165] G. Katz, M. A. Ratner, R. Kosloff, Phys. Rev. Lett. 98 (20) (2007) 203006.

[166] Y. Chen, P. Gross, V. Ramakrishna, H. Rabitz, K. Mease, J. Chem. Phys. 102 (20) (1995) 8001 – 8010.

[167] M. Sugawara, Y. Fujimura, Chem. Phys. 196 (1) (1995) 113 – 124.

[168] P. Marquetand, C. Meier, V. Engel, J. Chem. Phys. 123 (20).

[169] Y. Watanabe, H. Umeda, Y. Ohtsuki, H. Kono, Y. Fujimura, Chem. Phys. 217 (2) (1997) 317 – 323.

[170] K. Hoki, Y. Ohtsuki, H. Kono, Y. Fujimura, J. Phys. Chem. A 103 (32) (1999) 6301 – 6308.

[171] K. Hoki, Y. Ohtsuki, Y. Fujimura, J. Chem. Phys. 114 (4) (2001) 1575 – 1581.

[172] Y. Fujimura, L. González, K. Hoki, J. Manz, Y. Ohtsuki, Chem. Phys. Lett. 306 (1) (1999) 1 – 8.

[173] S. Gräfe, V. Engel, Chem. Phys. 329 (1-3) (2006) 118 – 125.

[174] V. S. Malinovsky, C. Meier, D. J. Tannor, Chem. Phys. 221 (1-2) (1997) 67 – 76.

[175] J. Salomon, G. Turinici, J. Chem. Phys. 124 (7) (2006) 074102.

[176] A. H. Zewail, Science 328 (5975) (2010) 187–193.

[177] C. Neidel, J. Klei, C.-H. Yang, A. Rouzée, M. J. J. Vrakking, K. Klünder, M. Miranda, C. L. Arnold, T. Fordell, A. L'Huillier, M. Gisselbrecht, P. Johnsson, M. P. Dinh, E. Suraud, P.-G. Reinhard, V. Despré, M. A. L. Marques, F. Lépine, Phys. Rev. Lett. 111 (2013) 033001.

[178] P. Krause, T. Klamroth, P. Saalfrank, J. Chem. Phys. 123 (7) (2005) 074105.

[179] J. C. Tremblay, T. Klamroth, P. Saalfrank, J. Chem. Phys. 129 (8) (2008) 084302.

[180] B. Mignolet, A. Gijsbertsen, M. J. J. Vrakking, R. D. Levine, F. Remacle, Phys. Chem. Chem. Phys. 13 (2011) 8331–8344.

[181] A. S. Moskalenko, A. Matos-Abiague, J. Berakdar, Phys. Rev. B 74 (2006) 161303.

[182] T. Klamroth, J. Chem. Phys. 124 (14) (2006) 144310.

[183] F. Remacle, R. D. Levine, PNAS 103 (18) (2006) 6793–6798.

[184] I. Franco, M. Shapiro, P. Brumer, J. Chem. Phys. 128 (24) (2008) 244906.

[185] K. A. Pronin, A. D. Bandrauk, Phys. Rev. B 69 (2004) 195308.

[186] S. S. Skourtis, D. N. Beratan, R. Naaman, A. Nitzan, D. H. Waldeck, Phys. Rev. Lett. 101 (2008) 238103.

[187] M. V. Korolkov, J. Manz, J. Chem. Phys. 120 (24) (2004) 11522–11531.

[188] I. Schaefer, R. Kosloff, Phys. Rev. A 86 (2012) 063417.

[189] A. Ben Haj Yedder, C. Le Bris, O. Atabek, S. Chelkowski, A. D. Bandrauk, Phys. Rev. A 69 (2004) 041802.

[190] A. D. Bandrauk, N. H. Shon, Phys. Rev. A 66 (2002) 031401.

[191] R. A. Bartels, M. M. Murnane, H. C. Kapteyn, I. Christov, H. Rabitz, Phys. Rev. A 70 (2004) 043404.

[192] C. Winterfeldt, C. Spielmann, G. Gerber, Rev. Mod. Phys. 80 (2008) 117–140.

[193] J. Solanpää, J. A. Budagosky, N. I. Shvetsov-Shilovski, A. Castro, A. Rubio, E. Räsänen, Phys. Rev. A 90 (2014) 053402.

[194] M. Wollenhaupt, A. Präkelt, C. Sarpe-Tudoran, D. Liese, T. Baumert, J. Opt. B 7 (10) (2005) S270.

[195] T. Brixner, G. Krampert, T. Pfeifer, R. Selle, G. Gerber, M. Wollenhaupt, O. Graefe, C. Horn, D. Liese, T. Baumert, Phys. Rev. Lett. 92 (2004) 208301.

[196] T. Bayer, M. Wollenhaupt, T. Baumert, J. Phys. B 41 (7) (2008) 074007.

[197] S. Gräfe, V. Engel, M. Y. Ivanov, Phys. Rev. Lett. 101 (2008) 103001.

[198] F. Martín, J. Fernández, T. Havermeier, L. Foucar, T. Weber, K. Kreidi, M. Schöffler, L. Schmidt, T. Jahnke, O. Jagutzki, A. Czasch, E. P. Benis, T. Osipov, A. L. Landers, A. Belkacem, M. H. Prior, H. Schmidt-Böcking, C. L. Cocke, R. Dörner, Science 315 (5812) (2007) 629–633.

[199] A. D. Bandrauk, Molecules in laser fields, CRC Press, 1993.

[200] P. H. Bucksbaum, A. Zavriyev, H. G. Muller, D. W. Schumacher, Phys. Rev. Lett. 64 (1990) 1883–1886.

[201] H. Niikura, F. Legare, R. Hasbani, M. Y. Ivanov, D. M. Villeneuve, P. B. Corkum, Nature 421 (2003) 826–829.

[202] A. Scrinzi, M. Y. Ivanov, R. Kienberger, D. M. Villeneuve, J. Phys. B 39 (1) (2006) R1.

[203] M. Lein, J. Phys. B 40 (16) (2007) R135.

[204] C. C. Marston, G. G. Balint-Kurti, J. Chem. Phys. 91 (6) (1989) 3571–3576.

[205] J. Fleck, J.A., J. Morris, M. Feit, Appl. phys. 10 (2) (1976) 129–160.

[206] S. Shin, H. Metiu, J. Chem. Phys. 102 (23) (1995) 9285.

[207] S. Shin, H. Metiu, J. Phys. Chem. 100 (19) (1996) 7867–7872.

[208] J. Javanainen, J. H. Eberly, Q. Su, Phys. Rev. A 38 (7) (1988) 3430 – 3446.

[209] A. Szabo, N. Ostlund, Modern Quantum Chemistry, Dover, New York, 1996.

[210] T. Helgaker, P. Jorgensen, J. Olsen, Molecular Electronic Structure Theory, Wiley & Sons, Chichester, 2000.

[211] J. Zhang, Theory and Application of Quantum Molecular Dynamics, World Scientific, Singapore, 1999.

[212] C. Cohen-Tannoudji, S. Reynaud, J. Phys. B 10 (3) (1977) 345.

[213] A. Messiah, Quantum Mechanics, North-Holland, Amsterdam, 1965.

[214] W. Domcke, D. R. Yarkony, H. Köppel (Eds.), Conical Intersections: Electronic Structure, Dynamics and Spectroscopy, Advanced Series in Physical Chemistry, World Scientific, 2004.

[215] D. McQuarrie, J. Simon, Physical Chemistry, University Science Books, Sausalito, 1997.

[216] B. Zhang, L. E. Berg, T. Hansson, Chem. Phys. Lett. 325 (5-6) (2000) 577 – 583.

[217] N. Gador, B. Zhang, R. Andersson, P. Johansson, T. Hansson, Chem. Phys. Lett. 368 (1-2) (2003) 202 – 208.

[218] B. Zhang, N. Gador, T. Hansson, Phys. Rev. Lett. 91 (2003) 173006.

[219] M. Merchán, L. Serrano-Andrés, M. Robb, L. Blancafort, J. Am. Chem. Soc. 127 (6) (2005) 1820–1825.

[220] M. A. Nielsen, I. L. Chuang, Quantum computation and quantum information, Cambridge University Press, 2000.

[221] I. Žutić, J. Fabian, S. Das Sarma, Rev. Mod. Phys. 76 (2004) 323–410.

[222] D. Bouwmeester, A. Ekert, A. Zeilinger, The physics of quantum information, Springer, New York, 2000.

[223] W. H. Press, S. Teukolsky, W. Vetterling, B. Flannery, Numerical recipes: the art of scientific computing, Cambridge University Press, Cambridge, UK; New York, 1997.

[224] R. Kosloff, J. Phys. Chem. 92 (8) (1988) 2087–2100.

[225] D. Harris, G. Engerholm, W. Gwinn, J. Chem. Phys. 43 (1965) 1515.

[226] A. Dickinson, P. Certain, J. Chem. Phys. 49 (1968) 4209.

[227] J. Lill, G. Parker, J. Light, Chem. Phys. Lett. 89 (1982) 483–489.

[228] J. Light, I. Hamilton, J. Lill, J. Chem. Phys. 82 (1985) 1400.

[229] M. D. Feit, J. A. Fleck Jr., A. Steiger, J. Comput. Phys. 47 (3) (1982) 412–433.

[230] M. Feit, J. Fleck, Appl. Opt. 20 (16) (1981) 2843–2851.

[231] J. Blatt, J. Comput. Phys. 1 (3) (1967) 382 – 396.

[232] A. Askar, A. S. Cakmak, J. Chem. Phys. 68 (6) (1978) 2794–2798.

[233] C. Leforestier, R. Bisseling, C. Cerjan, M. Feit, R. Friesner, A. Guldberg, A. Hammerich, G. Jolicard, W. Karrlein, H. Meyer, N. Lipkin, O. Roncero, R. Kosloff, J. Comput. Phys. 94 (1) (1991) 59 – 80.

[234] R. Kosloff, Ann. Rev. Phys. Chem. 45 (1) (1994) 145–178.

[235] H. Tal-Ezer, R. Kosloff, J. Chem. Phys. 81 (9) (1984) 3967–3971.

[236] T. J. Park, J. C. Light, J. Chem. Phys. 85 (10) (1986) 5870–5876.

[237] M. D. Feit, J. Chem. Phys. 78 (1) (1983) 301.

[238] D. Macías, S. Brouard, J. Muga, Chem. Phys. Lett. 228 (6).

[239] J. Palao, J. Muga, Chem. Phys. Lett. 292 (1-2) (1998) 1–6.

[240] D. Neuhauser, M. Baer, J. Chem. Phys. 91 (8) (1989) 4651–4657.

[241] D. Neuhasuer, M. Baer, J. Chem. Phys. 90 (8) (1989) 4351–4355.

[242] R. Santra, L. Cederbaum, Phys. Rep. 368 (1) (2002) 1 – 117.

[243] J. Muga, J. Palao, B. Navarro, I. Egusquiza, Phys. Rep. 395 (6) (2004) 357 – 426.

[244] N. Moiseyev, Phys. Rep. 302 (5-6) (1998) 212 – 293.

[245] Y. Sajeev, R. Santra, S. Pal, J. Chem. Phys. 123 (20) (2005) 204110.

[246] S. Feuerbacher, T. Sommerfeld, R. Santra, L. S. Cederbaum, J. Chem. Phys. 118 (14) (2003) 6188–6199.

[247] R. Kosloff, D. Kosloff, J. Comput. Phys. 63 (2) (1986) 363 – 376.

[248] A. Nissen, H. O. Karlsson, G. Kreiss, J. Chem. Phys. 133 (5) (2010) 054306.

[249] T. Seideman, W. H. Miller, J. Chem. Phys. 96 (6) (1992) 4412–4422.

[250] N. Rom, N. Lipkin, N. Moiseyev, Chem. Phys. 151 (2) (1991) 199 – 204.

[251] M. Monnerville, P. Halvick, J. Rayez, Chem. Phys. 159 (2) (1992) 227 – 234.

[252] D. I. Bondar, R. Cabrera, H. A. Rabitz, arXiv:1202.3628arXiv:1202.3628.

[253] R. Cabrera, D. I. Bondar, H. A. Rabitz, arXiv preprint arXiv:1107.5139.

[254] E. Wigner, Phys. Rev. 40 (1932) 749–759.

[255] L. Cohen, J. Math. Phys. 7 (5) (1966) 781–786.

[256] H. O. Bartelt, K. H. Brenner, A. W. Lohmann, Opt. Comm. 32 (1) (1980) 32 – 38.

[257] G. B. Lemos, R. M. Gomes, S. P. Walborn, S. Ribeiro, P. H., F. Toscano, Nat. Commun. 3 (2012) 1211.

[258] K. Husimi, Proc. Phys. Math. Soc. Jpn 22 (1940) 264–314.

[259] T. Shito, arXiv:1211.3274.

[260] G. Wallis, ZAMM - Appl. Math. Mecha. 72 (12) (1992) 684–684.

[261] A. Anderson, J. J. Halliwell, Phys. Rev. D 48 (1993) 2753–2765.

[262] W. P. Schleich, Phase Space Functions, Wiley-VCH Verlag GmbH & Co. KGaA, 2005, pp. 321–348.

[263] A. Wehrl, Rev. Mod. Phys. 50 (1978) 221–260.

[264] F. Pennini, A. Plastino, Phys. Rev. E 69 (2004) 057101.

[265] M. Janssen, Fluctuations And Localization In Mesoscopic Electron Systems, Vol. 64, World Scientific Lecture Notes in Physics, 2001.

[266] S. Chelkowski, T. Zuo, O. Atabek, A. D. Bandrauk, Phys. Rev. A 52 (4) (1995) 2977.

[267] E. Runge, E. K. U. Gross, Phys. Rev. Lett. 52 (1984) 997–1000.

[268] T. Seideman, J. Chem. Phys. 103 (18) (1995) 7887–7896.

[269] C. Horn, M. Wollenhaupt, M. Krug, T. Baumert, R. de Nalda, L. Bañares, Phys. Rev. A 73 (2006) 031401.

[270] R. Torres, R. de Nalda, J. P. Marangos, Phys. Rev. A 72 (2005) 023420.

[271] H. Stapelfeldt, T. Seideman, Rev. Mod. Phys. 75 (2003) 543–557.

[272] V. Sidis, Adv. Chem. Phys 82 (1992) 73–134.

[273] T. Pacher, L. Cederbaum, H. Köppel, Adv. Chem. Phys. 84 (1993) 293–392.

[274] S. Chelkowski, C. Foisy, A. D. Bandrauk, Phys. Rev. A 57 (1998) 1176–1185.

[275] S. Chelkowski, M. Zamojski, A. D. Bandrauk, Phys. Rev. A 63 (2001) 023409.

[276] M. Lein, T. Kreibich, E. K. U. Gross, V. Engel, Phys. Rev. A 65 (3) (2002) 033403.

[277] M. Erdmann, S. Baumann, S. Gräfe, V. Engel, Eur. Phys. J. D 30 (3) (2004) 7.

[278] S. Gräfe, V. Engel, Chem. Phys. 329 (1-3) (2006) 118–125.

[279] M. Erdmann, E. K. U. Gross, V. Engel, J. Chem. Phys. 121 (19) (2004) 9666.

[280] H. Meyer, G. Berghe, J. Phys. A 23 (7) (1990) 1323.

[281] F. M. Fernandez, J. Phys. A: Mathematical and General 24 (6) (1991) 1351.

[282] R. L. Hall, N. Saad, K. D. Sen, J. Math. Phys. 51 (2) (2010) 022107.

[283] B. Feuerstein, U. Thumm, Phys. Rev. A 67 (2003) 043405.

[284] Q. Su, J. H. Eberly, Phys. Rev. A 44 (1991) 5997 – 6008.

[285] K. C. Kulander, F. H. Mies, K. J. Schafer, Phys. Rev. A 53 (1996) 2562 – 2570.

[286] B. Y. Chang, S. Shin, A. Palacios, F. Martín, I. R. Sola, J. Phys. B 48 (4) (2015) 043001.

[287] B. Y. Chang, S. Shin, A. Palacios, F. Martín, I. R. Sola, J. Chem. Phys. 139 (8) (2013) 184306.

[288] T. Bredtmann, S. Chelkowski, A. D. Bandrauk, Phys. Rev. A 84 (2011) 021401.

[289] C. Lefebvre, H. Z. Lu, S. Chelkowski, A. D. Bandrauk, Phys. Rev. A 89 (2014) 023403.

[290] D. G. Lappas, A. Sanpera, J. Watson, K. Burnett, P. L. Knight, R. Grobe, J. H. Eberly, J. Phys. B 29 (16) (1996) L619.

[291] I. Ben-Itzhak, I. Gertner, O. Heber, B. Rosner, Phys. Rev. Lett. 71 (1993) 1347–1350.

[292] D. R. Bates, T. R. Carson, Proc. Math. Phys. Eng. Sci. 234 (1197) (1956) 207–217.

[293] A. Arthurs, R. Bond, J. Hyslop, Proc. Phys. Soc. A 70 (8) (1957) 617.

[294] K. Liu, W. Hong, P. Lu, Opt. Express 19 (21) (2011) 20279–20287.

[295] G. L. Kamta, A. D. Bandrauk, Phys. Rev. Lett. 94 (2005) 203003.

[296] B. Y. Chang, S. Shin, J. Santamaría, I. R. Sola, Chem. Phys. 442 (2014) 18 – 25.

[297] I. I. Rabi, Phys. Rev. 51 (1937) 652–654.

[298] L. Allen, J. Eberly, Optical resonance and two-level atoms, Dover, N.Y., 1987.

[299] B. Garraway, K. Suominen, Rep. Prog. Phys. 58 (4) (1995) 365.

[300] B. Chang, PhD. Thesis, Universidad Complutense de Madrid.

[301] N. Rosen, C. Zener, Phys. Rev. 40 (1932) 502–507.

[302] L. D. Landau, Physics of the Soviet Union 2 (46-51) (1932) 28.

[303] C. Zener, Proc. Math. Phys. and Eng. Sci. 137 (833) (1932) 696–702.

[304] N. V. Vitanov, B. M. Garraway, Phys. Rev. A 53 (1996) 4288–4304.

[305] B. W. Shore, The Theory of Coherent Atomic Excitation, Volume 2, Multilevel Atoms and Incoherence, 1990.

[306] I. R. Sola, V. S. Malinovsky, B. Y. Chang, J. Santamaria, K. Bergmann, Phys. Rev. A 59 (1999) 4494–4501.

[307] J. Cao, C. J. Bardeen, K. R. Wilson, Phys. Rev. Lett. 80 (1998) 1406–1409.

[308] V. Malinovsky, J. Krause, Eur. Phys. J. D 14 (2) (2001) 147–155.

[309] K. A. Suominen, B. M. Garraway, Phys. Rev. A 48 (1993) 3811–3819.

[310] S. Ruhman, R. Kosloff, J. Opt. Soc. Am. B 7 (8) (1990) 1748–1752.

[311] C. J. Bardeen, J. Che, K. R. Wilson, V. V. Yakovlev, V. A. Apkarian, C. C. Martens, R. Zadoyan, B. Kohler, M. Messina, J. Chem. Phys. 106 (20) (1997) 8486–8503.

[312] Y. Silberberg, Ann. Rev. Phys. Chem. 60 (1) (2009) 277–292.

[313] J. Yuan, T. F. George, J. Chem. Phys. 68 (7) (1978) 3040–3052.

[314] A. D. Bandrauk, M. L. Sink, J. Chem. Phys. 74 (2) (1981) 1110–1117.

[315] A. Giusti-Suzor, F. Mies, L. DiMauro, E. Charron, B. Yang, J. Phys. B 28 (3) (1995) 309.

[316] S. H. Autler, C. H. Townes, Phys. Rev. 100 (1955) 703–722.

[317] H. Friedrich, H. Friedrich, Theoretical atomic physics, Vol. 3, Springer, 2006.

[318] H. Ohanian, Principles of Quantum Mechanics, Prentice Hall, Englewood Cliffs, 1990.

[319] B. J. Sussman, Am. J. Phys. 79 (2011) 477–484.

[320] B. J. Sussman, M. Y. Ivanov, A. Stolow, Phys. Rev. A 71 (2005) 051401.

[321] B. Y. Chang, I. R. Sola, J. Santamaría, V. S. Malinovsky, J. L. Krause, J. Chem. Phys. 114 (20) (2001) 8820–8830.

[322] P. Marquetand, M. Richter, J. González-Vzquez, I. R. Sola, L. González, Faraday Discuss. 153 (2011) 261–273.

[323] I. R. Sola, J. Santamaría, V. S. Malinovsky, Phys. Rev. A 61 (4) (2000) 043413.

[324] I. R. Sola, B. Y. Chang, J. Santamaría, V. S. Malinovsky, J. L. Krause, Phys. Rev. Lett. 85 (2000) 4241–4244.

[325] J. J. Bajo, J. González-Vázquez, I. R. Sola, J. Santamaria, M. Richter, P. Marquetand, L. González, J. Phys. Chem. A 116 (11) (2012) 2800–2807.

[326] D. J. Tannor, S. A. Rice, Coherent Pulse Sequence Control of Product Formation in Chemical Reactions, John Wiley & Sons, Inc., 2007, pp. 441–523.

[327] J. Broeckhove, L. Lathouwers, Time-Dependent Quantum Molecular Dynamics, Nato Science Series B:, Springer US, 2013.

[328] N. Khaneja, R. Brockett, S. J. Glaser, Phys. Rev. A 63 (2001) 032308.

[329] D. Sugny, C. Kontz, H. R. Jauslin, Phys. Rev. A 76 (2007) 023419.

[330] D. D'Alessandro, M. Dahleh, IEEE Trans. Automat. Contr. 46 (6) (2001) 866–876.

[331] S. Grivopoulos, B. Bamieh, IEEE Trans. Automat. Contr. 53 (4) (2008) 980–992.

[332] K. Sundermann, R. de Vivie-Riedle, J. Chem. Phys. 110 (4) (1999) 1896–1904.

[333] P. Gross, D. Neuhauser, H. Rabitz, J. Chem. Phys. 96 (4) (1992) 2834–2845.

[334] S. Shi, H. Rabitz, J. Chem. Phys. 92 (5) (1990) 2927–2937.

[335] V. F. Krotov, Advances in Nonlinear Dynamics and Control: A Report from Russia, CRC Press, Boston, MA, 1993, Ch. Global Methods in Optimal Control Theory, pp. 74–121.

[336] J. Somlói, V. A. Kazakov, D. Tannor, Chem. Phys. 172 (1) (1993) 85 – 98.

[337] D. J. Tannor, V. Kazakov, V. Orlov, Time-Dependent Quantum Molecular Dynamics, Springer US, Boston, MA, 1992, Ch. Control of Photochemical Branching: Novel Procedures for Finding Optimal Pulses and Global Upper Bounds, pp. 347–360.

[338] S. Gräfe, V. Engel, Chem. Phys. Lett. 385 (1-2) (2004) 60 – 65.

[339] S. Gräfe, M. Erdmann, V. Engel, Phys. Rev. A 72 (2005) 013404.

[340] R. Gómez-Abal, O. Ney, K. Satitkovitchai, W. Hübner, Phys. Rev. Lett. 92 (2004) 227402.